John Gore

SOCIETY FOR MAGNETIC RESONANCE IMAGING
SIXTH ANNUAL MEETING
27 FEBRUARY–2 MARCH, 1988

WESTIN COPLEY PLACE
BOSTON, MASSACHUSETTS

PROGRAM AND ABSTRACTS

Organizing Committee

David D. Stark, M.D.
Chairman, Organizing Committee

R. Mark Henkelman, Ph.D.
Val M. Runge, M.D.
Chairmen, Scientific Program

Barry L. Engelstad, M.D.
Chairman, Educational Program

E. Mark Haacke, Ph.D.
Chairman, Flow Imaging Program

Jeffrey C. Weinreb, M.D.
Chairman, Evening Tutorial Program

SMRI SESSION DESIGNATIONS and LOCATIONS

Educational Sessions will be presented in the America Ballroom Center, 4th level.

The Flow Imaging Topical Program will be presented in the Staffordshire Room, third level.

PS: designates a Plenary Symposium. Plenary Symposia will be presented in the America Ballroom Cent 4th level.

P: designates a Poster Scientific Paper. Poster Papers will be presented in the America Ballroom North, 4th level.

No. 101–449: designates an Oral Scientific Paper. Oral Papers will be presented in the following order. Location information will be found on the page indicated:

No. 101–108: Sunday, February 28, 10:30 am–Noon.
ROOM: page ix.

No. 109–116: Sunday, February 28, 3:45–5:15 pm.
ROOM: page x.

No. 201–223: Monday, February 29, 10:20 am–Noon.
ROOM: page xi.

No. 224–254: Monday, February 29, 3:45–5:30 pm.
ROOM: page xii.

No. 301–325: Tuesday, March 1, 10:20 am–Noon.
ROOM: page xiii.

No. 326–346: Tuesday, March 1, 3:45–5:30 pm.
ROOM: page xiv.

No. 401–424: Wednesday, March 2, 10:20 am–Noon.
ROOM: page xv.

No. 425–449: Wednesday, March 2, 3:45–5:30 pm.
ROOM: page xvi.

W: designates Works-in-Progress Papers. Schedule to be distributed on-site.

TABLE OF CONTENTS

Special Issue: SMRI Sixth Annual Meeting—Program and Abstracts

MAGNETIC RESONANCE IMAGING

An International Journal of Basic Research & Clinical Applications in Medicine
The Official Publication of the Society for Magnetic Resonance Imaging

Editorial Offices: *Clinical Articles:* Dr. F.W. Smith, Aberdeen Royal Infirmary, Foresterhill, Aberdeen AB9 2ZB, Scotland; or *Research Articles:* Dr. J. Gore, Dept. of Diagnostic Imaging, Yale University School of Medicine, 333 Cedar St., New Haven, CT 06510, USA.

Publishing, Subscription, and Advertising Offices: Pergamon Journals, Inc., Fairview Park, Elmsford, NY 10523, USA; and Pergamon Journals Ltd. Headington Hill Hall, Oxford OX3 0BW, England.

Published Bi-monthly. Annual institutional subscription rate (1988): US$195.00; Two-year institutional subscription rate (1988/89): US$370.50; Professional subscription rate (1988): US$80.00. Prices are subject to change without notice. Members of the Society of Magnetic Resonance Imaging may order personal subscriptions at a concessional rate; details of these rates are available upon request. Notify 8 weeks in advance of address change with a copy of the subscription mailing label. *Microform subscriptions:* Information available upon request.

The Item-Fee Code for this publication is: 0730-725X/88 $3.00 + .00

Printed in the USA

PTS
FREQUENCY SYNTHESIZERS

HIGH-PERFORMANCE DIRECT SYNTHESIZERS

Accurate, stable, quiet frequencies on command, fast. For NMR, imaging, SATCOM, surveillance, ATE. Sources adapting to your needs with options. High demonstrated reliability. Thousands in use.

PTS 040

Range: 0.1-40MHz
Resolution: 0.1Hz-100KHz (opt.)
Switching: 5-20μs
Output: +3 to +13dBm: 50 ohm
Spurious Outputs: −75dB

Phase Noise: −75dBc, (0-15KHz)
Freq. St'd: Oven, TCXO, Ext.
Interface: BCD par. or GPIB
Size: 19″W, 5¼″H, 18″D
Price: $4,400.00*

Other Options:
Progr. Attenuator, 0-90db
(or 0-99dB with GPIB)
nx10MHz output 20-140MHz
or any 10MHz line (20-140)

PTS 120

Range: 90-120MHz
Resolution: 0.1Hz-100KHz (opt.)
Switching: 5-20μs
Output: +3 to +10dBm: 50 ohm
Spurious Outputs: −75dBc

Phase Noise: −75dBc, (0.5Hz-15KHz)
Freq. St'd: Oven, TCXO, Ext.
Interface: BCD par. or GPIB
Size: 19″W, 5¼″H, 18″D
Price: $4,400.00*

Other Options:
Progr. Attenuator, 0-90dB
(or 0-99dB with GPIB)
nx10MHz output 20-140MHz
or any 10 MHz line (20-140)

PTS 160

Range: 0.1-160MHz
Resolution: 0.1Hz-100KHz (opt.)
Switching: 5-20μs
Output: +3 to +13dBm: 50 ohm
Spurious Outputs: −75dB

Phase Noise: −63dBc, (0-15KHz)
Freq. St'd: Oven, TCXO, Ext.
Interface: BCD par. or GPIB
Size: 19″W, 5¼″H, 18″D
Price: $5,600.00*

Other Options:
Progr. Attenuator, 0-90dB
(or 0-99dB with GPIB)
nx10MHz output 20-140MHz
or any 10 MHz line (20-140)

PTS 250

Range: 1-250MHz
Resolution: 0.1Hz-100KHz (opt.)
Switching: 5-20μs
Output: +3 to +13dBm: 50 ohm
Spurious Outputs: −70dB

Phase Noise: −63dBc, (0-15KHz)
Freq. St'd: Oven, TCXO, Ext.
Interface: BCD par. or GPIB
Size: 19″W, 5¼″H, 18″D
Price: $6,400.00*

Other Options:
Progr. Attenuator, 0-90dB
(or 0-99dB with GPIB)
nx10MHz output 20-140MHz
or any 10 MHz line (20-140)

PTS 500

Range: 1-500MHz
Resolution: 0.1Hz-100KHz (opt.)
Switching: 5-20μs
Output: +3 to +13dBm: 50 ohm
Spurious Outputs: −70dB

Phase Noise: −63dBc, (0-15KHz)
Freq. St'd: Oven, TCXO, Ext.
Interface: BCD par. or GPIB
Size: 19″W, 5¼″H, 18″D
Price: $7,500.00*

Other Options:
Progr. Attenuator, 0-90dB
(or 0-99dB with GPIB)
nx10MHz output 20-140MHz
or any 10 MHz line (20-140)

*Prices are US only, manual & remote, (BCD), 1 Hz res. with oven std.

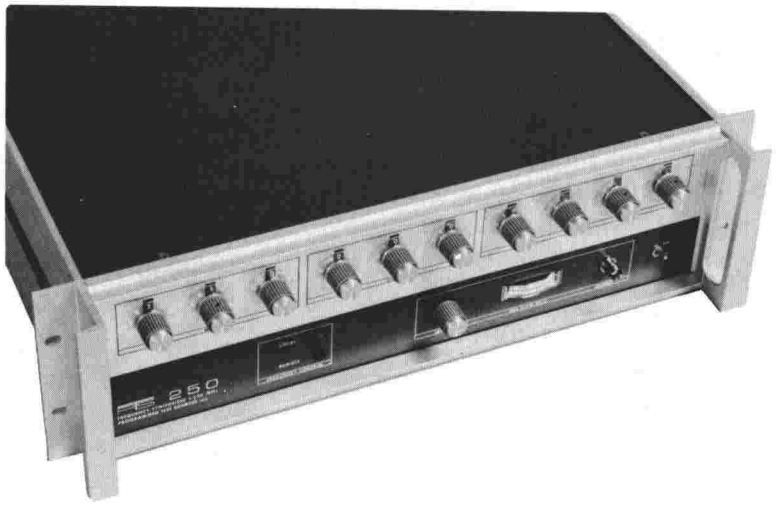

NEW
2
UNITS IN
ONE PACKAGE: A
SEPARATE SYNTHESIZER
0.1–3 MHz
(1 Hz RESOLUTION)
IS AVAILABLE IN ALL OF
OUR MODELS ONLY $600 EXTRA!

Choice of table-look-up resolution with phase—continuous switching.

PROGRAMMED TEST SOURCES, INC.
P.O. Box 517, 9 Beaver Brook Rd., Littleton, MA 01460 617-486-3008

SMRI WEEK

Friday 2/26	Saturday 2/27	Sunday 2/28	
5:00–9:00 pm General Registration America Ballroom Foyer, 4th floor	7:00 am–9:00 pm General Registration	7:00 am–6:00 pm General Registration 9:30 am–5:00 pm Technical Exhibits/ Poster Sessions	
	8:00–8:15 am EDUCATIONAL SESSION: Opening Remarks	8:00–9:30 am EDUCATIONAL SESSION: Body I	8:00–9:30 TOPICAL PROGRAM: Flow I
	8:30–10:00 am EDUCATIONAL SESSION: Basics		
	10:00–10:30 am Morning Break	9:30–10:30 am Morning Break	9:30–10:30 am Morning Break
	10:30 am–Noon EDUCATIONAL SESSION: Neuro I	10:30 am–Noon EDUCATIONAL SESSION: Body II	10:30 am–Noon TOPICAL PROGRAM: Scientific Papers No. 101–108
	Noon–1:00 pm Lunch	Noon–1:00 pm Lunch	Noon–1:30 pm Lunch
	1:00–3:00 pm EDUCATIONAL SESSION: Neuro II	1:00–3:00 pm EDUCATIONAL SESSION: Body III	1:30–3:00 pm TOPICAL PROGRAM: Flow II
	3:00–3:30 pm Afternoon Break	3:00–3:30 pm Afternoon Break	3:00–3:45 pm Afternoon Break
	3:30–5:30 pm EDUCATIONAL SESSION: Neuro III	3:30–5:30 pm EDUCATIONAL SESSION: Body IV	3:45–5:15 pm TOPICAL PROGRAM: Scientific Papers No. 109–116
			5:30–7:30 pm EVENING WORKSHOP: TUTORIAL: Physics CLINICAL REVIEW: Neuro Body

IN BRIEF

Monday 2/29	Tuesday 3/1	Wednesday 3/2
7:00 am–6:00 pm General Registration 9:30 am–5:00 pm Technical Exhibits/ Poster Sessions	7:00 am–6:00 pm General Registration 9:30 am–5:00 pm Technical Exhibits/ Poster Sessions	7:00 am–5:30 pm General Registration 9:30 am–1:00 pm Technical Exhibits/ Poster Sessions
7:45–8:00 am SCIENTIFIC SESSION: Opening Remarks	8:00–9:30 am PLENARY SYMPOSIUM: Image Contrast and Pulse Sequence Optimization	8:00–9:30 am PLENARY SYMPOSIUM: Non-Invasive MR Arthrography
8:00–9:30 am PLENARY SYMPOSIUM: Fast Imaging		
10:00–10:30 am Morning Break	9:30–10:20 am Morning Break	9:30–10:20 am Morning Break
10:30 am–Noon SCIENTIFIC SESSIONS: Scientific Papers No. 201–223 Works-in-Progress	10:20 am–Noon SCIENTIFIC SESSIONS: Scientific Papers No. 301–325 Works-in-Progress	10:20 am–Noon SCIENTIFIC SESSIONS: Scientific Papers No. 401–424 Works-in-Progress
Noon–1:30 pm Lunch	Noon–1:30 pm Lunch	Noon–1:30 pm Lunch
1:30–3:00 pm PLENARY SYMPOSIUM: Abdominal Imaging	1:30–3:00 pm PLENARY SYMPOSIUM: Quantitation of Cardiovascular Function	1:30–3:00 pm PLENARY SYMPOSIUM: Head and Spine
3:00–3:45 pm Afternoon Break	3:00–3:45 pm Afternoon Break	3:00–3:45 pm Afternoon Break
3:45–5:30 pm SCIENTIFIC SESSIONS: Scientific Papers No. 224–254	3:45–5:30 pm SCIENTIFIC SESSIONS: Scientific Papers No. 326–346	3:45–5:30 pm SCIENTIFIC SESSIONS: Scientific Papers No. 425–449
5:30–7:30 pm EVENING WORKSHOPS: TUTORIAL: Physics CLINICAL REVIEW: Neuro Pediatric	5:30–7:30 pm EVENING WORKSHOPS: CLINICAL REVIEW: Neuro/General MRI Musculoskeletal SITE PLANNING TECHNOLOGIST MTNG.	

GENERAL MEETING INFORMATION

REGISTRATION

All meeting registration will take place in the Essex Ballroom Foyer, 3rd level of the Westin Copley Place, during the following hours:

Friday, February 26	5:00 pm–9:00 pm
Saturday, February 27	7:00 am–9:00 pm
Sunday, February 28	7:00 am–6:00 pm
Monday, February 29	7:00 am–6:00 pm
Tuesday, March 1	7:00 am–6:00 pm
Wednesday, March 2	7:00 am–5:30 pm

TECHNICAL EXHIBITS

An impressive collection of leading-edge technical exhibitors will once again support the SMRI scientific program. To offer you, the attendees, maximum exposure to the manufacturers, exhibit hours have been tailored to the scientific program schedule. Please plan to visit this integral component of the annual meeting in the Essex Ballroom during th following hours:

Sunday, February 28	9:30 am–5:00 pm
Monday, February 29	9:30 am–5:00 pm
Tuesday, March 1	9:30 am–5:00 pm
Wednesday, March 2	9:30 am–1:00 pm

SOCIAL PROGRAM

The Society for Magnetic Resonance Imaging cordially invites all attendees (single day registrants must visit the Social Program Desk, registration area) to join in an evening of fellowship at the following receptions:

Opening Reception Essex Ballroom Foyer	Saturday, February 27 5:30 pm–7:30 pm
New England Clambake America Ballroom South	Tuesday, March 1 7:30 pm–10:00 pm

A Social Program Desk will be staffed in the registration area for participants wishing to attend the receptions with their spouse.

EDUCATIONAL PROGRAM

America Ballroom Center, 4th level

8:15 am	OPENING REMARKS	B. L. Engelstad
8:30–10:00 am	BASICS:	
	Physics	J. C. Gore
	Contrast	R. E. Hendrick
	Flow	W. G. Bradley
10:00–10:30 am	MORNING BREAK	Technical Exhibits
10:30 am–Noon	NEURO I:	
	Anatomy/neoplasms	M. H. Gado
	Vascular Abnormalities	I. I. Kricheff
	White Matter Diseases	K. R. Maravilla
Noon–1:00 pm	LUNCH	Technical Exhibits
1:00–3:00 pm	NEURO II:	
	Pediatric & Trauma	R. A. Zimmerman
	Iron Effects	R. I. Grossman
	Enhancements	G. M. Bydder
3:00–3:30 pm	AFTERNOON BREAK	Technical Exhibits
3:30–5:30 pm	NEURO III:	
	Cord Disease	D. O. Davis
	Disk Disease	M. T. Modic
	Head & Neck	R. B. Lufkin
	MRS	B. D. Ross

EDUCATIONAL PROGRAM

America Ballroom Center, 4th level

8:00–9:30 am	BODY I:	
	Musculoskeletal—Joints	J. M. Beltran
	Musculoskeletal—Marrow	W. A. Murphy
	Musculoskeletal—3-D	S. E. Harms
9:30–10:30 am	MORNING BREAK	Technical Exhibits
10:30 am–Noon	BODY II:	
	Vascular Artifacts	R. L. Ehman
	Cardiac MRI	C. B. Higgins
	Cardiac MRS	M. W. Weiner
Noon–1:00 pm	LUNCH	Technical Exhibits
1:00–3:00 pm	BODY III:	
	Motion Artifacts	M. L. Winkler
	Liver MRI	J. T. Ferrucci
	MRS in Oncology	R. L. Nunnally
3:00–3:30 pm	AFTERNOON BREAK	Technical Exhibits
3:30–5:30 pm	BODY IV:	
	Genitourinary MRI	P. J. Fritzsche
	Pediatric MRI	R. B Dietrich
	Practical Issues	L. R. Muroff
	Future Directions	A. R. Margulis

TOPICAL PROGRAM: FLOW IMAGING

Morning Agenda
Staffordshire Room, 3rd level

8:00–9:30 am	FLOW Imaging I:	
	Presiding: R. M. Henkelman, W. T. Dixon	
	Advanced MR Angiography	D. G. Nishimura
	Calibration Techniques for Rephasing Moving Spins	G. W. Lenz
	CSF Flow Phenomena	W. G. Bradley
9:30–10:30 am	MORNING BREAK	Technical Exhibits
10:30 am–Noon	SCIENTIFIC PAPERS	
	Presiding: R. M. Henkelman, W. T. Dixon	
	No. 101–108: Flow I	
Noon–1:30 pm	LUNCH	Technical Exhibits

Additional Topical Program and Evening Workshop information on page x.

TOPICAL PROGRAM: FLOW IMAGING continued . . .

Afternoon Agenda
Staffordshire Room, 3rd level

1:30–3:00 pm	FLOW IMAGING II: Presiding: E. M. Haacke, D. G. Nishimura	
	Applications of Inversion and Saturation Techniques	W. T. Dixon
	MRI Methods in Turbulent, Vortical and Swirl Flows	P. R. Moran
	Applications of Cardiac-Gated Fast Scan Imaging	R. J. Herfkens
3:00–3:30 pm	AFTERNOON BREAK	Technical Exhibits
3:30–5:00 pm	SCIENTIFIC PAPERS Presiding: E. M. Haacke, D. G. Nishimura	
	No. 109–116: Flow II	

EVENING WORKSHOPS

5:30–7:30 pm

Participants:

M. J. Bronskill
J. M. Cohen
K. R. Davis
P. F. Hahn
M. Iio
K. C. Johnson
J. B. Kneeland
D. T. Kopp
J. L. Lancaster
K. R. Maravilla
D. G. Mitchell
R. Peshock
C. L. Partain
T. A. Powers
B. Rosen
V. M. Runge
A. Shirkhoda
G. Shoukinas
D. Thickman
J. C. Weinreb
M. L. Winkler
M. L. Wood

CLINICAL CASE REVIEW:

C-I: Neuro, Staffordshire Room, 3rd level
C-II: Body, St. George A–B Rooms, 3rd level

A distinguished panel of MRI physicians and physicists will present and discuss their own special cases using an interactive format. Attendees of the SMRI are invited to bring their own unusual, interesting, instructive or difficult clinical cases and artifacts. These sessions provide an excellent opportunity for participants to ask questions and to see how the experts approach clinical MRI cases.

PHYSICS TUTORIAL:

T-1: Physics, St. George C–D Rooms, 3rd level

These small group sessions provide participants with an opportunity to discuss questions regarding MRI physics and instrumentation with MRI physicists. Physicians, technologists and anyone interested in gaining an increased understanding of Magnetic Resonance Imaging concepts will benefit.

SCIENTIFIC PROGRAM

7:45 am	OPENING REMARKS America Ballroom Center, 4th level	G. D. Fullerton
8:00–9:30 am	**FAST IMAGING** Presiding: 0. Nalcioglu, R. M. Henkelman America Ballroom Center, 4th level	
	Rapid Scan MRI: An Overview Contrast & Signal-to-Noise in Fast Img. Clinical Applications: 3-D Fast Imaging Role of Instant Scan Technique in Clinical MR Imaging	F. W. Wehrli E. M. Haacke V. M. Runge I. L. Pykett
9:30–10:20 am	MORNING BREAK	Technical Exhibits
10:20 am–Noon	**SCIENTIFIC PAPERS**	
	No. 201–208: Fast Imaging Presiding: R. R. Price, R. S. Hinks Staffordshire Room, 3rd level	
	No. 209–216: Joints Presiding: S. E. Harms, J. V. Crues St. George Rooms A–B, 3rd level	
	No. 217–223: Genitourinary Presiding: S. McCarthy St. George Rooms C–D, 3rd level	
	Works-in-Progress	
Noon–1:30 pm	LUNCH	Technical Exhibits
1:30–3:00 pm	**ABDOMINAL IMAGING** Presiding: M. Iio America Ballroom Center, 4th level	
	Progress in Abdominal MRI MR/CT: Eval. of Upper Abdom. Malignancy MRI on the Upper Abdomen MRI of the Abdomen and Pelvis	M. L. Wood P. F. Hahn G. M. Bydder H. Y. Kressel
3:00–3:45 pm	AFTERNOON BREAK	Technical Exhibits

Additional Scientific Program and Evening Workshop information on page xii.

SCIENTIFIC PROGRAM continued . . .

3:45–5:30 pm SCIENTIFIC PAPERS

No. 224–230: Fast Imaging Clinical
Presiding: M. L. Wood
America Ballroom Center, 4th level

No. 231–238: Imaging Techniques
Presiding: M. J. Bronskill, S. Majumdar
Staffordshire Room, 3rd level

No. 239–246: Extremities & Tumors
Presiding: D. Hahn
St. George Rooms A–B, 3rd level

No. 247–254: Gastrointestinal
Presiding: J. T. Ferrucci
St. George Rooms C-D, 3rd level

EVENING WORKSHOPS

5:30–7:30 pm

Participants:

M. J. Bronskill
J. M. Cohen
K. R. Davis
P. F. Hahn
M. Iio
K. C. Johnson
J. B. Kneeland
D. T. Kopp
J. L. Lancaster
K. R. Maravilla
D. G. Mitchell
R. Peshock
C. L. Partain
T. A. Powers
B. Rosen
V. M. Runge
A. Shirkhoda
G. Shoukinas
D. Thickman
J. C. Weinreb
M. L. Winkler
M. L. Wood

CLINICAL CASE REVIEW:

C-I: Neuro, Staffordshire Room, 3rd level
C-II: Body, St. George Rooms A–B, 3rd level

A distinguished panel of MRI physicians and physicists will present and discuss their own special cases using an interactive format. Attendees of the SMRI are invited to bring their own unusual, interesting, instructive or difficult clinical cases and artifacts. These sessions provide an excellent opportunity for participants to ask questions and to see how the experts approach clinical MRI cases.

PHYSICS TUTORIAL:

T-I: Physics, St. George Rooms C–D, 3rd level

These small group sessions provide participants with an opportunity to discuss questions regarding MRI physics and instrumentation with MRI physicists. Physicians, technologists and anyone interested in gaining an increased understanding of Magnetic Resonance Imaging concepts will benefit.

SCIENTIFIC PROGRAM

8:00–9:30 am — **IMAGE QUALITY, SEQUENCE OPTIMIZATION AND MRI HAZARDS**
Presiding: W. Pavlicek, F. G. Shellock
America Ballroom Center, 4th level

Artifacts: Limitations to MRI Quality	M. J. Bronskill
Image Contrast and Pulse Sequence Optimization	D. D. Stark
Biological Effects of MRI and Practical Aspects of Patient Management	W. Pavlicek F. G. Shellock

9:30–10:20 am — MORNING BREAK — Technical Exhibits

10:20 am–Noon — **SCIENTIFIC PAPERS**

No. 301–309: Perfusion & Flow
Presiding: C. Dumolin, A. P. Crawley
Staffordshire Room, 3rd level

No. 310–317: Head
Presiding: G. Sze
St. George Rooms A–B, 3rd level

No. 318–325: Relaxation in Tissues
Presiding: G. D. Fullerton, M. A. Foster
St. George Rooms C–D, 3rd level

Works-in-Progress

Noon–1:30 pm — LUNCH — Technical Exhibits

1:30–3:00 pm — **QUANTITATION OF CARDIOVASCULAR FUNCTION**
Presiding: C. B. Higgins
America Ballroom Center, 4th level

Principles of Blood Flow in MRI	L. Axel
MRI of the Mediastinum	D. Hahn
Cine MRI of the Heart	C. B. Higgins

3:00–3:45 pm — AFTERNOON BREAK — Technical Exhibits

Additional Scientific Program and Evening Workshop information on page xiv.

SCIENTIFIC PROGRAM continued . . .

3:45–5:30 pm SCIENTIFIC PAPERS

No. 326–333: Spectroscopy
Presiding: M. W. Weiner
St. George Rooms A–B, 3rd level

No. 334–340: Heart
Presiding: R. J. Herfkens
St. George Rooms C–D, 3rd level

No. 341–346: Pulse Sequences
Presiding: R. E. Hendrick, L. Eastwood
Staffordshire Room, 3rd level

EVENING WORKSHOPS

5:30–7:30 pm

Participants:

M. J. Bronskill
J. M. Cohen
K. R. Davis
P. F. Hahn
M. Iio
K. C. Johnson
J. B. Kneeland
D. T. Kopp
J. L. Lancaster
K. R. Maravilla
D. G. Mitchell
R. Peshock
C. L. Partain
T. A. Powers
B. Rosen
V. M. Runge
A. Shirkhoda
G. Shoukinas
D. Thickman
J. C. Weinreb
M. L. Winkler
M. L. Wood

CLINICAL CASE REVIEW:

C-I: Neuro/General MRI, Staffordshire Room, 3rd level
C-II: Musculoskeletal, St. George Rooms A–B, 3rd level

A distinguished panel of MRI physicians and physicists will present and discuss their own special cases using an interactive format. Attendees of the SMRI are invited to bring their own unusual, interesting, instructive or difficult clinical cases and artifacts. These sessions provide an excellent opportunity for participants to ask questions and to see how the experts approach clinical MRI cases.

SITE PLANNING:

St. George Rooms C–D, 3rd level

Appropriate site planning is critical to ensure successful MRI installation and operation. This workshop will address such areas as mobile vs. fixed site, equipment selection, architectural planning and other operational considerations. Individuals who are working with or planning an MRI installation will benefit from the workshop.

MRI TECHNOLOGIST ORGANIZING COMMITTEE:

7th level meeting rooms

The SMRI would like to involve MRI technologists as a more integral component of the Society. Toward this end, a special program, geared to the MRI tech, is scheduled for the 1988 SMRI Meeting. Anyone interested in participating in the content development of these sessions is invited to attend this organizational meeting.

SCIENTIFIC PROGRAM

8:00–9:30 am **NON-INVASIVE MR ARTHROGRAPHY**
Presiding: S. E. Harms, J. M. Beltran
America Ballroom Center, 4th level

MRI of the Hands and Feet	J. S. Hyde
MRI of the Temporomandibular Joint	S. E. Harms
MRI of the Knee	J. V. Crues

9:30–10:20 am MORNING BREAK — Technical Exhibits

10:20 am–Noon **SCIENTIFIC PAPERS**

No. 401–407: Spine
Presiding: E. Kanal
Staffordshire Room, 3rd level

No. 408–415: Vessels
Presiding: F. W. Wehrli
St. George Rooms A–B, 3rd level

No. 416–424: MR Operations
Presiding: P. M. Joseph, E. R. McVeigh
St. George Rooms C–D, 3rd level

Works-in-Progress

Noon–1:30 pm LUNCH — Technical Exhibits

1:30–3:00 pm **HEAD AND SPINE**
Presiding: W. G. Bradley
America Ballroom Center, 4th level

MRI of Hemmorhage	R. N. Bryan
Clinical Utilization of Gradient Refocused Imaging Sequences	K. R. Maravilla
Nasopharynx and Skull Base	A. N. Hasso
Gadolinium DTPA MRI in the Spine	J. S. Ross

3:00–3:45 pm AFTERNOON BREAK — Technical Exhibits

SCIENTIFIC PROGRAM continued . . .

3:45–5:30 pm SCIENTIFIC PAPERS

No. 425–432: Brain
Presiding: V. M. Runge
Staffordshire Room, 3rd level

No. 433–441: Contrast Agents
Presiding: J. C. Gore, M. L. Wood
St. George Rooms A–B, 3rd level

No. 442–449: Clinical Spectroscopy
Presiding: M. W. Weiner
St. George Rooms C–D, 3rd level

POSTER PAPERS

(P) POSTER SCIENTIFIC PAPERS

AVAILABLE FOR VIEWING DURING ALL EXHIBIT HOURS

AUTHORS PRESENT 1:00–1:30 PM DAILY

SUNDAY, FEBRUARY 28–WEDNESDAY, MARCH 2

AMERICA BALLROOM NORTH, 4TH LEVEL, WESTIN COPLEY PLACE

P1

DETERMINATION OF OPTIMAL CONTRAST WITHIN THE NORMAL AND PATHOLOGIC UTERUS VIA SYNTHETIC MRI

AC Duberg, S McCarthy, RC Lange
Department of Diagnostic Radiology, Yale University School of Medicine

Although somewhat general pulse sequence protocols (SE long TR, long TE) have been established for the uterus, the optimal TR,TE combination which provides best contrast among normal or pathologic tissues in an efficient time period is not known. Directly acquired images (SE 300,20; 1700,20, 40,60,80) were used to produce computed images of proton density, T_1 and T_2. Synthetic images were then generated from the computed images and operator specified scan parameters. The selected scan parameters were varied: TR from 100–3000 and a TE from 20–80. Sagittal images through the uterus were obtained in three normal reproductive age women and three women with endometrial carcinoma.

Synthetic images were very comparable in diagnostic quality to actual acquired images. In the normal women, endometrium, junctional zone, myometrium, endocervical canal and fibrous stroma could be clearly separated at SE 100,80. Similarly in women with endometrial carcinoma, the tumor could be visualized at this very short TR, long TE sequence. Relative contrast improved with increasing TR due to improved signal-to-noise, however, beyond a TR of 500 there was no significant improvement in relative contrast. Relative contrast between these tissue layers was optimal at a TE of 80, therefore not requiring longer TE's with subsequent degradation of signal-to-noise. We conclude that much shorter repetition times than are conventionally used may be useful in demonstrating normal and pathologic uterine anatomy in a shorter scan time.

P2

THE USE OF NMR IMAGING IN THE STUDY OF LACTATION IN THE GOAT

PA Fowler, MA Foster, CH Knight* & JR Mallard
Department of Bio-Medical Physics, University of Aberdeen, *Hannah Research Institute, Ayr.

Transaxial slices were obtained throughout the lactation cycle of British Saanen goats. Imaging at 0.04 Tesla used an inter-leaved IR/SR pulse sequence allowing calculation of T1 images by a 2 point method [Ti200, Tr1000 ms]. Empty mammary gland volumes were determined, by summation of the pixel areas from serial slices at 20mm intervals through the udder, and converted to litres. Imaging of phantoms, and an isolated udder, gave errors of estimated to known volumes of 6.5±5.8% [simple phantom], 10.9±6.2% [complex phantom] and 1.9±6.2% [detached udder].

For 8 weeks after first mating, goats had small udders with short T1 [<200ms] indicative of the large proportion of mammary fat pad present. On the other hand female goats mated in previous years had slightly larger udders at this time. These were fluid-filled and had longer T1 [>250ms]. During lactation, mean milk yield, estimated udder volume and T1 were linearly related. After cessation of milking, milk collection within the udder led to a 2.5 fold increase in udder volume with an associated increase in T1 to 400ms. The relationship between mammary volume, estimated by NMR imaging, and milk yield was similar to those determined by conventional techniques.

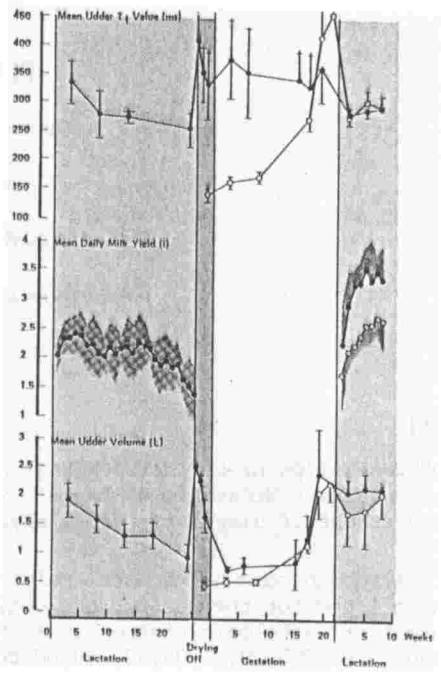

Fig.1. Udder volume, milk yield and udder T1 of goats mated for the first [O] or second time [●].

P3

TITLE SUPERPARAMAGNETIC PARTICLES AS GI-TRACT CONTRAST AGENTS: EXPERIMENTAL STUDIES IN RABBITS AT 0.02 TESLA

Authors Pekka Niemi BM, Hannu Paajanen MD, P-A Hals PhD, Minna Erkintalo BM, Martti Kormano MD
Affiliation
LEAVE THIS LINE BLANK

Abstract text

Superparamagnetic particles cause a reduction of the gut signal by a selective decrease of the T2 relaxation time ("negative contrast agent"). We have measured the relaxation rates of magnetite particles (diameter 0.5 um, Nycomed, Oslo) imbedded in agar gel at 0.02 Tesla. The test tubes containing a wide range of particle concentrations we positioned in water or oil bath, and the MR image distorsions were analysed using different pulse sequences. Finally, various concentrations of particles were administrated into 9 rabbits and abdominal MR imaging was performed at 0.02 Tesla (Acutscan, Instrumentarium). The T2 relaxation time was dramatically decreased in the test tube measurements when the concentration of particles increased from 0.01 mg/ml to 0.05 mg/ml. Significant distorsion of MR images was observed in water and oil phantom studies when the concentration of the particles increased over 0.07 mg/ml. The distorsions were more pronounced on T2-weighted images. In animal studies the lowering of the GI-tract signal down to background noise was observed even at a dose of 1 mg/kg (0.03 mg/ml) of rabbit weight. The conclusion is that ferromagnetic particles provide good negative contrast also at very low field MR system.

P4

MAGNETIC RESONANCE IMAGING OF THE PATELLOFEMORAL JOINT DURING EXTENSION AND INCREMENTAL FLEXION OF THE KNEE: A DESCRIPTION OF THE TECHNIQUE

FG Shellock and JH Mink
Section of Magnetic Resonance Imaging, Department of Diagnostic Radiology, Cedars-Sinai Medical Center, Los Angeles, CA

Although magnetic resonance imaging (MRI) has been shown to be an efficacious method for evaluating internal derangements of the knee, no prior attempt has been made to utilize this imaging modality to identify abnormalities of the patellofemoral joint related to knee flexion. According to published data using plain film and computed tomography, pathological conditions that affect the patellofemoral joint (particularly patellar tracking problems) are most apparent when the orientation of the patella to the trochlear groove can be visualized at angles of knee flexion up to 30 degrees. Therefore, our objective was to develop a technique using MRI to examine the patellofemoral joint during movement of the knee.

A special positioning device was constructed from nonferromagnetic components that enabled us to perform axial plane imaging of both knees at the following joint angles: 0 (i.e., extension), 5, 10, 15, 18, 22, 25, 28, and 32 degrees. Seven subjects were studied using T1-weighted images obtained with a 1.5 T scanner (Signa MR System, General Electric Company). The following parameters were used: TR - 500 ms, TE - 20 ms, matrix - 256 X 128, slice thickness - 5 mm, acquisition time - 1.10 min., approximate total examination time (i.e., extension to 32 degrees flexion) - 20 min. Images were displayed using both static and "dynamic" formats. Qualitative analysis of these studies indicated that normal subjects (N = 4) had patellas that were centralized in the trochlear groove throughout the range of motion studied, while patients (N = 3) with known pathology had patellas that appeared to be tilted and/or subluxed.

In conclusion, we developed a means of using MRI to examine the patellofemoral joint during extension and flexion of the knee that is reasonably fast and simple enough for implementation in a clinical setting. The diagnostic value of this MRI application for evaluating pathology of the patellofemoral joint remains to be demonstrated.

P5

MR-IMAGING IN DISORDERS OF THE FOOT AND ANKLE

F-U Oesterreich, M Heller, RP Spielmann, HH Jend, R Maas, T Knepper
Department of Radiology, University Hospital Eppendorf, Hamburg

Twenty-two patients with clinically suspected or radiologically and surgically confirmed diseases of foot and ankle were examined with MRI. The following pathomorphologic conditions gave rise to the MR investigations: osteochondritis dissecans, osteomyelitis, suspected recurrence of a surgically resected tumor, painful conditions of unknown origin and others.

In most of the patients a spin echo (SE) multiplanar pulse sequence was used to obtain T1- and T2-weighted images (TE 20ms - 200ms, TR 300ms - 2100ms). Fast field echo technique was applied in two patients (T1-weighted images: TE 14ms, TR 250ms, flip angle 80 degrees; T2-weighted images: TE 23.3ms, TR 400ms, flip angle 10 degrees).

MRI demonstrated pathomorphologic changes in all cases and moreover revealed additional informations in some patients, which could not be achieved by other diagnostic methods. Particularly, all cases of osteochondritis and osteomyelitis could be diagnosed. Tumor recurrence was excluded in three cases. Five of six patients with symptoms of pain were diagnosed to have a bursotendinitis, whereas one of them had a capillary hemangioma of the plantar surface of the foot. Furthermore, MRI was appropriate in delineating aseptic osteonecrosis of the talus and postoperative scar tissue in a patient with fibrosis of the plantar fascia who had undergone surgical treatment twice before. Integrity of the syndesmotic tibiofibular ligaments in a patient with an isolated posterior "Volkmann" triangle could be shown by means of MRI.

In contrast to CT and other diagnostic methods bones, joint capsules, tendons, ligaments and vessels can be delineated simultaneously in multidirectional slice technique. Thus MRI is superior to all other diagnostic procedures. A time-consuming stepwise diagnostic approach can often be avoided.

P6

EARLY DETECTION OF HEPATIC TUMOR BY CT/MR IN EXPERIMENTAL & CLINICAL STUDY

LC Chiu, TT Peng, R Ong, J Butler, T Trezona, P Chow
UCLA-Harbor Diagnostic Imaging Center, Torrance, California

Liver imaging using state of the art CT technique and 0.5T MRI was carried out using 16 rabbits. An anaplastic sarcoma was surgically implanted into the liver. Sequential scans were performed every other day after tumor implantation. Dynamic CT with 5mm incremental survey scan following IV bolus administration was performed. The rabbits were then rescanned every 2-5 minutes at the level of the lesions. MRI utilizing 300/16/16/128 and 2000/100/2/256 with gradient refocusing SE technique was performed. All animals were sacrificed within twelve hours of their last examination and surgical pathology correlated.

Our preliminary result indicated that the smallest size of tumor that could be consistently detected by dynamic CT is in the range of five millimeters. This is beyond the sensitivity for MRI. For lesions greater than eight millimeters, dynamic CT and MRI are equal in sensitivity. T1 and T2 weighted MRI pulse sequences are equally sensitive for lesions of this size. However, there is higher specificity and level of confidence in interpretation with the T2 WI. Although dynamic CT is the most sensitive modality, location of lesion and normal respiratory excursion can mask lesions. Delay scan can also miss lesions detected during the dynamic phase as they become isodense. Result of clinical application will also be presented.

P7

PRIMARY LIVER TUMORS: DIFFERENTIAL DIAGNOSIS BY MRI WITH HISTOPATHOLOGICAL CORRELATION

E Rummeny, DD Stark, R Weissleder, S Saini, PF Hahn, CC Compton, J Wittenberg, RA Malt, JT Ferrucci
Department of Radiology, Surgery, and Pathology, Massachusetts General Hospital, Boston, MA

To establish criteria for the differential diagnosis and staging of primary liver tumors (PLT), morphologic features, and MR tissue characteristics were evaluated in 45 patients. T1 and T2 weighted spin echo (SE), gradient recalled echo (GR), and phase contrast (PC) images were obtained at 0.6 T. Quantitative image analysis included measurement of tumor-liver contrast-to-noise ratios, tumor/liver signal intensity ratios, and calculations of proton density and relaxation times. Qualitative image analysis included comparison to CT (all cases), angiography (25 cases), and gross and microscopic pathological examination of the surgical specimen (15 cases). MR detected all 34 pathological proven lesions, while CT detected 28/34 lesions. Hepatocellular carcinoma (HCC) was always (17/17) hyperintense on T2W weighted images but had variable signal intensity on T1 weighted images due to fatty degeneration. Focal HCC often showed capsules (4/6) or fatty change (3/6) that permitted a tissue specific diagnosis, but multifocal HCC (0/11) did not. CT identified the tumor capsule only in 2/6 cases and never detected fatty degeneration of the tumor. Cholangiocarcinoma and focal nodular hyperplasia showed diagnostic morphologic features in 5/7 by MR and 4/7 by CT. Our experience suggests that MRI is more accurate than CT for detection, differential diagnosis, and preoperative staging of PLT.

P8

MRI OF FOCAL SPLENIC TUMORS

PF Hahn, R Weissleder, DD Stark, S Saini, G Elizondo, JT Ferrucci
Department of Radiology, Massachusetts General Hospital, Boston, MA

The study was undertaken to define the MR appearance of splenic tumors, including lesion and spleen tissue characteristics in thirteen cancer patients with focal splenic lesions; fifty volunteers and cancer patients without splenic abnormality served as controls. Measurements made in individuals with normal spleens show that relaxation times of tumor and splenic tissue are so similar that spin-echo MR imaging underestimates the size and extent of focal splenic disease or may miss lesions entirely. In patients with focal splenic lesions, four patterns were encountered that permit lesion detection on spin-echo MR images. Central areas of long T2 within the tumor were encountered in seven cases and corresponded histologically to liquefactive necrosis. Foci of short T1 produced by hemorrhage were responsible in three cases for lesion detection. One lesion isointense on both T1 weighted and T2 weighted pulse sequences was detected by gross splenic deformity. Two spleens emitted abnormally low signal on T2 weighted images, permitting lesion detection through natural tissue contrast. Transfusional iron overload is suspected in both of these cases. We conclude that MRI is an insensitive technique for screening the spleen for focal lesions.

P9

CLINICAL DIAGNOSIS OF SPLENIC LYMPHOMA AND METASTASES USING SUPERPARAMAGNETIC IRON OXIDE

R Weissleder, DD Stark, G Elizondo, LE Todd, PF Hahn, S Saini, J Wittenberg, JT Ferrucci.
Department of Radiology, Massachusetts General Hospital, Boston and MR Unit, University Hospital of Monterrey, N.L., Mexico

MRI has proven insensitive in the detection of splenic lymphoma using standard imaging pulse sequences. Previous animal research has suggested that enhanced MRI can increase detectability of focal and diffuse splenic lymphoma. We have extended this research to a clinical study of nine patients, 4 patients with splenic lymphoma, one patient with splenic metastases and 4 control spleens in patients without splenic abnormality. All patients received intravenous superparamagnetic iron oxide (AMI-25 Advanced Magnetics Inc, Cambridge, MA) at a dose of 20 and 40 μmol Fe/kg. At a dose of 40 μmol Fe/kg the signal intensity of normal splenic parenchyma decreased to that of background image noise. Focal tumor did not change its signal intensity and therefore appeared hyperintense relative to spleen. Diffuse lymphoma showed a smaller decrease in signal intensity than control spleens. This initial experience suggests that contrast enhanced MRI will be useful in the diagnosis of splenic disease.

P10

CLINICAL HIGH RESOLUTION MRI USING A 512^2 MATRIX SIZE

RP Spielmann, HH Jend, H Kooijman, R Maas, T Knepper, M Heller, FU Oesterreich
Department of Radiology, University Hospital, Hamburg, FRG

In high resolution MRI with reduced field of views (FOV), wrap-around artifacts can be a problem. An alternative approach to decrease pixel size is to increase the matrix size while maintaining the FOV constant.

We investigated the feasibility of clinical imaging with a 512^2 matrix in 22 patients with various disorders. MRI was performed with a 1.5 T magnet using multi-slice spin-echo sequences (TR: 350-450 ms, TE: 20 ms) as well as fast field-echo sequences. Slice-thickness was 3-5 mm, FOV 120-450 mm, fat-water shift 4-5 pixels. With 4-8 measurements, the acquisition time for the 512^2 matrix was 18-31 min.

The 512^2 matrix was used in 9 patients for sagittal mid-line sections through the head, in 3 patients for long sagittal sections through the spine, in 4 patients for coronal sections through the pelvis, and in 5 patients for sections through the joints of the knee and ankle. There was a significant improvement of resolution with the 512^2 matrix compared to the conventional 256^2 matrix. The increased resolution provided advantage in the definition of the borders of mass lesions and facilitated the detectability of small lesions. However, the decrease of the signal-to-noise ratio required a careful selection of other scan parameters affecting the resolution, such as slice thickness, FOV, and fat-water shift.

P11

IN VITRO T1 AND T2 MEASUREMENTS ON BREAST TISSUES

JC Blechinger and EL Madsen
Department of Medical Physics, University of Wisconsin-Madison

In vitro relaxation time measurements of breast tissue have been made at 22°C and 37°C on a 10 MHz spectrometer and at 40°C on a 40 MHz spectrometer. Results were then compared with histology.

Breast tissue, obtained from reduction mammoplasty was placed into specimen jars without media and transported on ice. Tissue samples were excised from the surgical specimen with clean forceps and scalpel on a Teflon board. Measurements began within three hours of surgery. T1 and T2 relaxation times were measured on a 10 MHz spectrometer equipped with a variable temperature probe and on a 40 MHz spectrometer using the Carr-Purcell-Meiboom-Gill spin-echo sequence with 255 recorded points for T2 and the inversion recovery sequence with 20 points for T1.

T1 at 10 MHz and 22°C averages 493 ms for mostly fibrous tissue and at 37°C averages 571 ms, corresponding to a slope of 5.18 ms/°C. This temperature distribution could be significant for imaging of the breast since the temperature varies from the skin surface to the chest wall, and also for possible monitoring of the temperature distribution in hyperthermia cancer treatment.

Four samples with varying histologies were measured at 10 and 40 MHz. The average T1 was 636 ms at 10 MHz and 946 ms at 40 MHz, yeilding an estimated power law fit of about frequency** 0.3.

P12

Fe/HBED ENHANCED MR OF LIVER CANCER

Y-M Tsang, M Chen, G Elizondo, D Stark, D White, B Engelstad, S Saini, J Ferrucci
Department of Radiology, Massachusetts General Hospital, Contrast Media Lab, UCSF

Fe-HBED is an hepatobiliary tissue specific MR contrast agent. We studied mammary carcinoma implanted in the liver of rats using the head coil of a 0.6T clinical MR imaging system and a spin echo TR=250 msec, TE=21 msec pulse sequence. Changes in liver signal-to-noise ratio (SNR) and the tumor-liver contrast-to-noise ratio (CNR) were correlated with in vitro measurements of tissue T1 and T2 relaxation times using a Bruker 20 MHz spectrometer. Immediately after intravenous injection of 0.2 mmol/kg Fe-HBED, liver SNR increased by 13%. However, nonspecific enhancement of tumor resulted in a decrease in CNR of 26%, apparent visually as a decrease in lesion conspicuity. At 30 minutes, selective distribution of Fe-HBED to liver tissue dominated; liver SNR was increased by 64% and tumor-liver CNR increased by 60%, manifested qualitatively as increased lesion conspicuity. In vivo enhancement of MR images correlated with in vitro enhancement of T1 relaxation.

P13

DELAYED MAGNETIC RESONANCE HEPATIC IMAGING WITH GADOLINIUM-DTPA

RC Nelson, ME Umpierrez, JL Chezmar, ME Bernardino
Emory University School of Medicine

MR imaging of the liver following the intravenous administration of Gadolinium-DTPA demonstrates maximum contrast enhancement between normal liver and focal lesions when T1-weighted imaging is performed within two minutes of the bolus. A rapid MR imaging sequence which would provide multiple slices through the entire liver within two minutes or less, with adequate signal-to-noise, has yet to be optimized. Another approach would be to perform delayed hepatic MR imaging 4 to 6 hours following Gd-DTPA, similar to the delayed hepatic CT technique using iodinated contrast agents. Delayed hepatic MR could be advantageous both in terms of improved lesion-to-liver contrast and because timing factors would be less critical. Since Gd-DTPA and iodinated contrast agents are in many ways analagous, we undertook this study to determine if there is delayed excretion of Gd-DTPA by the hepatocytes as is seen with iodinated agents. Eleven 3 to 5 kg. New Zealand white rabbits underwent MR imaging prior to and then at 4, 5, and 6 hours following the IV administration of 0.3 mM/kg of Gd-DTPA. Imaging was performed at 0.5 tesla utilizing a spin-echo sequence of TR/TE-250/20 msec. Operator defined ROI's were obtained from the liver and muscle both pre- and post-contrast. From these intensity changes the percent post-contrast enhancement was determined for each acquisition. The average percentage enhancement for liver and muscle at the various time intervals is as follows:

	IMMEDIATE(%)	4 HOURS(%)	5 HOURS(%)	6HOURS(%)
LIVER	31 ± 10	10 ± 14	10 ± 8	11 ± 8
MUSCLE	17 ± 17	2 ± 14	4 ± 13	4 ± 12

It is concluded that there is not significant hepatocyte excretion of Gd-DTPA at 4 to 6 hours post-contrast injection and that this would not be an advantageous paramagnetic contrast strategy for focal hepatic lesion detection.

P14

OPTIMAL PROTOCOL FOR MR ASSESSMENT OF RENAL MASSES

JK Raval, PM Colletti, WD Boswell, JM Halls
University of Southern California School of Medicine

Coronal plane imaging is the most time efficient way of scanning the kidneys by MR as fewer slices are required to image them in this plane. It is also a plane familiar to us from excretory urography. Our purpose was to evaluate the coronal plane with respect to: a) detection of renal masses and b) assess extent of tumor spread in the abdomen.

Twenty patients with solitary solid renal masses were scanned on an 0.5 T system during the work-up of their mass. Surgical/pathologic correlation was obtained in each case with respect to etiology of the mass and extent of spread. Thirteen patients had renal cell carcinoma, 2 had transitional cell carcinoma, 2 had non-Hodgkin lymphoma, and one each had liposarcoma, Wilms' tumor and oncocytoma. T1 weighted (TR 400-816/TE 20-26 msec) and T2 weighted (TR 2000-2316/TE 100 msec) coronal scans were obtained in all 20 patients. Additional axial or sagittal images were obtained in 16 patients.

The mass was depicted in 20/20 (100%) of patients when both T1 and T2 weighted coronal images were used. T1 weighted images detected the mass in 95% (19/20). T2 weighted images detected the mass in 90% (18/20). The abdominal extent of tumor spread was accurately delineated by MR in 80% (16/20) of patients using coronal images alone and 90% (18/20) of patients when using all available images. In summary, coronal T1 and T2 weighted sequences are the most time effective way of assessing the kidneys for masses by MRI. Other planes are useful in evaluating for abdominal extent of tumor.

P15

MAGNETIC RESONANCE STUDIES OF THE MOTION OF NATURAL MYOCARDIAL LANDMARKS

RH Klipstein, RH Mohiaddin, DN Firmin, SR Underwood, HG Bogren, RSO Rees, DB Longmore.
The National Heart and Chest Hospitals, London, UK

In many studies of myocardial motion it is assumed that contraction is directed symmetrically inwards but this assumption may be invalid. Examination of the motion of fixed endocardial points, requiring their accurate identification on end-diastolic and end-systolic images, clarifies this question. The high resolution of oblique magnetic resonance tomographic imaging permits definition of natural myocardial landmarks with freedom from the projection distortions of contrast ventriculography. Landmarks may be defined at the apex and at the junctions of each of the mitral valve leaflets with the endocardium on horizontal and vertical long axis views.

Seventeen normal subjects were imaged at end-diastole and at end-systole, using a spin-echo sequence (TE=24ms). The resolution was 128^2 pixels, the slice thickness 1cm, and the field of view 30-40cm. The vectors describing the motion of each landmark were calculated, giving the following results:

Horizontal long axis

Landmark	Mean Excursion (mm)	Direction
Apex	4	random
Septum	9	posterior
Lateral	10	posterior (14), anterior (3)

Vertical long axis

Landmark	Mean Excursion (mm)	Direction
Apex	6	superior
Inferior	7	anteroinferior
Anterior	7	anterior (15), posterior (2)

The main pattern of contraction indicated by landmark motion is compression of the cavity from base to apex with little apical movement, (though a few hearts show apical movement comparable with that of the other two landmarks). Thus the shortening of the endocardial perimeter is usually greater at the base than at the apex, rather than being uniform throughout. The small degree of movement of the apex in horizontal long axis views is remarkable since the apex is not anchored to any other structure. It implies translation of the ventricular cavity towards the apex during contraction.

P16

THE REPRODUCIBILITY OF MAGNETIC RESONANCE LV VOLUME AND EJECTION FRACTION MEASUREMENTS

RH Klipstein, SR Underwood, DN Firmin, RH Mohiaddin, HG Bogren, RSO Rees, DB Longmore
The National Heart and Chest Hospitals, London, UK

Estimation of left ventricular area and long axis length are commonly used for the calculation of volumes and ejection fractions. Their reproducibility depends on endocardial boundary definition which is subject to several sources of error including partial volume effect, noise, motion artifact and signal from stationary blood. This study establishes the reproducibility.

Oblique electrocardiographically gated spin-echo (TE=24ms) images were acquired at end diastole and end systole in 17 normal subjects. The resolution was 128^2 pixels, the slice thickness 1cm, and the field of view 30 to 40cm. An observer made five area and five length measurements on each view with presentation of images in random order. Single plane and biplane estimations of volume using the area-length formulae were made by taking n combinations (see table) of the areas and lengths. The coefficient of variation (the standard deviation of the measurements as a percentage of the mean) was calculated yielding the following results:

	Single HLA	Single VLA	Double HLA	Double VLA	Biplane
End-Diastolic volume	5.4	6.3	3.6	4.1	4.4
End-Systolic volume	7.3	9.3	4.8	6.0	6.2
Stroke volume	11.3	13.5	7.6	8.7	9.5
Ejection fraction	7.6	8.9	5.0	5.7	6.4

Volume and ejection fraction calculations are reproducible within the indicated limits. Variation in measurements using two area estimates is consistently lower, being very similar whether the areas come from the same (double HLA and VLA) or different (biplane) views. The range of observer error overlaps much of the normal range, but errors may be reduced considerably by measuring the same area twice.

P17

CARDIAC FUNCTION AND ANATOMY AFTER MUSTARD'S OPERATION FOR TRANSPOSITION OF THE GREAT ARTERIES

RSO Rees, CA Warnes, J Somerville, SR Underwood, DN Firmin, RH Klipstein, DB Longmore
The National Heart & Chest Hospitals, London, UK

Mustard's operation for transposition of the great arteries redirects the circulation at atrial level, and it has been used successfully since 1964. Many patients have now reached adult life, but ventricular function and tricuspid competence are important determinants of late morbidity. We have investigated magnetic resonance imaging in the assessment of cardiac anatomy and function in 17 adults, 9 to 20 years after operation.

The connections and anatomical relationships of the great arteries were clearly visible in all cases. Five patients had residual ventricular septal defects which, with the exception of one small defect, were easily visualised. The intra-atrial baffle was best seen in transverse slices, and the systemic venous connection showed as a relatively narrow channel lying in the posterior part of the cavity. The pulmonary venous connection was best seen in the coronal slices. Ventricular volumes were measured by summing areas in multiple contiguous sections, and the right to left ventricular stroke volume ratio was used as a measure of tricuspid regurgitation. Ejection fractions measured by radionuclide ventriculography were lower than the magnetic resonance measurements, and the correlation for the left ventricle was closer (r=0.75) than for the right (r=0.49). There was a significant difference between the mean right to left ventricular stroke volume ratio in those with Doppler echocardiographic evidence of tricuspid regurgitation (1.81) compared to those without (1.16), (normal range 0.8 to 1.2).

Magnetic resonance imaging is a useful adjunct in the post-operative follow-up of patients with Mustard's operation for transposition of the great arteries.

P18

MAGNETIC RESONANCE IMAGING OF EXPERIMENTAL AND CLINICAL PULMONARY EMBOLI

W. A. Erdman, R. M. Peshock, J. Kern, C. Chaney, B. Barker, J. Katz, R. W. Parkey
Univ. of Texas Health Science Center & Parkland Memorial Hospital, Dept. of Nuclear Medicine

Magnetic resonance imaging (0.35T) was performed in four laboratory dogs in which 15 pulmonary emboli had been created. Correlation of MR findings with angiography and autopsy was performed in each instance. Pulse sequences which displayed morphologic abnormalities (spin echo, gated TE30, 1.7mm resolution, 10 10mm contiguous slices) were compared with similar images acquired at the same levels but "rotated" to include different phases of the cardiac cycle at each level. Additionally, gradient reversal (TR50/TE9) single slice images with a 45 degree flip angle were obtained in an attempt to better visualize normal vessels.

Thirteen of the 15 emboli were visualized as linear areas of increased signal on the gated coronal spin echo sequences (average weight 208 mg). Two non-visualized emboli weighed only 14 mg each. Neither acute emboli nor 24 hour old emboli showed significant pulmonary infiltrates by chest x-ray, MRI or autopsy. However, patchy areas of increased signal within the parenchyma were shown on some of the diastolic images. These were shown to be "pseudoinfiltrates" which resolved on the systolic image frames. The gated single slice gradient reversal technique visualized the proximal pulmonary arteries as bright signal intensity. However, detail was not sufficient to evaluate peripheral vessels or to clearly identify intraluminal thrombi.

We have evaluated 8 patients suspected of having pulmonary emboli by MRI. Three patients were found to have PE (1 angiogram, 2 high probability lung scans), four patients were found to have pneumonia and/or atelectasis, 1 patient had a mediastinal mass obstructing the pulmonary artery. MR correctly identified two of the three cases of pulmonary emboli prospectively. Difficulty with mediastinal fat caused one false positive interpretation in a patient with pneumonia (angiogram negative). We conclude that gated rotational imaging was the most helpful in evaluating pulmonary emboli in both experimental animals and clinical studies. This was due to the varying degree of signal from flowing blood which enabled differentiation of vessels, emboli, and flow related "pseudoinfiltrate".

P19

STRESS FRACTURES OF THE KNEE; MRI EVALUATION

TC Lynch, J Crues, W Sheehan, L Harter, R Riu, FW Morgan
Santa Barbara Community Magnetic Resonance Center
UCLA Department of Radiology

Stress fractures have been identified as causing significant pain mimicing meniscal tears and other surgically treatable problems of the acutely injured knee. Initial plain radiographs are often unrevealing, as are arthroscopy and other traditional methods of evaluation. In this setting, focal areas of decreased signal intensity on short TE magnetic resonance images in the femoral condyles and tibial plateau have been noted. These signal abnormalities typically occur contralateral to collateral ligament tears. In order to establish their prevalence and clinical importance, we have undertaken a retrospective study of 250 consecutive MR studies in the evaluation of knee pain. Correlation with initial radiographs, arthroscopic findings and clinical course will be reported.

1. Engber WD: "Stress Fractures of the Medial Tibial Plateau", J.of Bone and Joint Surg [Am]. 1977 59:767-9.

P20

SURFACE COIL POSITIONING DEVICE FOR HIGH RESOLUTION MRI OF THE SPINE

H.H.Jend,R.Spielmann,M.Heller,R.Maas,H.J.Langkowski,F.U.Oesterreich,T.Knepper
Department of Radiology, University Hospital, Hamburg, West Germany

Imaging of the spine have become one of the most important applications of MR. The location of a pathology is not always clear on clinical grounds. This causes problems in placing high resolution surface coils in the appropriate position. Even the positioning of a coil to a well known location requires repeated image aquisition after lifting of the patient for repositioning of the coil. This is uneconomic and may be impossible at all with some patients.

To overcome these problems we have developed a positioning device. Two inflatable rubber tubes of 100 cm length and 8 cm diameter are wrapped and sealed in a flexible plastic sheet leaving a distance between them of the outer diameter of the surface coil. The surface coil is placed in the center of this canal. After positioning on the mat the patient is lifted a few cm by inflating the tubes. A survey scan is done allowing precise location of a suspected lesion. The surface coil is then positioned in the disired position by the help of a sliding scale.

Advantages of the positioning device are:

- no image degrading distance between body surface and coil. The coil will always be placed as near to the body surface as possible.
- no marginal images. The maximum resolution capability and SNR will always be at the point of interest.
- comfort and simplicity. The patient lies on soft rubber material or on an air cushion. Handling is easy and there are no complicated mechanical devices.
- low cost. It is only a fraction of what to spend for a switched array coil.

P21

CLINICAL APPLICATION OF COMBINED PROTON DENSITY/T_1-WEIGHTED IMAGING

S. Albert, N.E. Leeds, V. Malhotra
Department of Radiology, Beth Israel Medical Center, New York, N.Y.

The purpose of the study is to demonstrate and establish the clinical utilization of combined proton density/T_1-weighted imaging. The technique is based on build-up of longitudinal magnetization to its maximum and requires proton density (PD) as well as appropriate T_1-weighted images. PD images have been acquired by spin-echo (SE) pulse sequences with the shortest TE value available and $TR \geq 3T_1$. SE T_1-weighted images have been obtained with the same TE value and $TR < T_1$. A 1.5T GE SIGNA imager was employed in our experiments. The TE time used to obtain PD images was 20ms, and the repetition time was $TR \approx$ 2000-4000ms, somewhat longer than that of T_2-weighted images. Our results with volunteers and patients show the following clinical significance of the proton density/T_1-weighted approach: gain direct information concerning the distribution of protons in the detected pathology, highlight pathological changes associated with an increase in proton density, permit us to discriminate between different components within the lesions, helpful in identifying calcific zones, allow water/fat separation in specific parts of the image and show small CNS lesions with similar relaxation time to surrounding structures. The technique has been utilized successfully in inflammatory disease, metastases, demyelinating disease, etc.

P22

MR IMAGING OF BRAINSTEM TELANGIECTATIC AVMS

FR Murtagh, RC Vaum, MG Farese, LP Clarke, ML Silbiger
Department of Radiology, University of South Florida College of Medicine

Six patients ranging from age 6 months to 60 years were studied with MR for brainstem symptomatology. In each case, mixed areas of signal intensity with minimal or no mass effect were discovered in the midbrain or pons. Lengthened T2 and shortened T1 identified the areas as containing old hemorrhage. The presence of signal void areas indicated calcification or hemosiderin deposits. The characteristic pontine or midbrain location plus stability over time allowed diagnosis of telangiectatic AVM. We feel the MR appearance may be pathognomonic for this entity.

P23

Gd-DTPA: Clinical use in MR imaging of post-operative lumbar recurrent disc herniation and fibrosis.

Narang AK, Hueftle M, Williams A, Modic M, Davis DO.
G.W.U. M. C.

Gadolinium DTPA, a paramagnetic MR contrast agent is most familiarly utilized for delineation of brain and cord abnormalities. Since contrast enhanced CT may help define epidural fibrosis from recurrent herniated lumbar disc, the efficacy of GD-DTPA enhanced MRI was evaluated. Symptomatic patients with previous back surgery are being evaluated with pre and post Gd-DTPA "T1" and "T2" weighted images. Results to date (over 50 cases) suggest that this technique will be extremely helpful. Appropriate cases with examples of scar, disc and both will be presented.

P24

HIGH-FIELD MRI OF SELECTED SECONDARY DEMYELINATING DISEASES.

James B. Moore, M.D., Yvonne Reid, B.S., Abraham Pera, D.O.

Michigan State University Department of Radiology, East Lansing, Michigan 48824

MR has made a tremendous impact on the evaluation of demyelinating diseases in the central nervous system (CNS), especially the prototypical primary demyelinating disease multiple sclerosis. Secondary demyelinating diseases are less common, but MR's sensitivity to this pathology has made it an important part of the clinical evaluation of these patients. This exhibit presents the clinical and MR manifestations of several such disorders, including acute disseminated encephalomyelitis (ADEM), methotrexate/radiation leukoencephalopathy, and central pontine myelinolysis. Particular attention is directed to ADEM, with emphasis on the entire spectrum of this disease. The classic features of ADEM are described and illustrated, and two examples of a more benign variant are presented. This variant of ADEM has not been described in the past, and is characterized by many symmetric supratentorial white matter lesions that are completely asymptomatic and resolve over a period of days or weeks. This pattern contrasts with classic ADEM which has a posterior fossa predilection with larger lesions that often correlate with clinical signs.

P25

MR IMAGING AT 0,5 TESLA IN DURAL ARTERIO-VENOUS FISTULAE OF THE SPINAL CORD

F. GELBERT, E. ASSOULINE, D. REIZINE, A. BIONDI, M.C. RICHE, D. DORMONT, J.J. MERLAND

Service de Neuroradiologie, Hôpital Lariboisière, Paris

Dural arterio-venous fistulae of the spinal cord represent a type of vascular malformation probably more frequent than is generally supposed.

In most cases clinical findings consist of a severe progressive myelopathy. After treatment (endovascular or surgical approach) dramatically clinical improvement is usually observed.

MR study was performed in 7 patients with a 0.5 T CGR Magniscan. Both T1 and T2 weighted images were obtained (TR : 400ms, TE : 28ms and TR : 2000ms, TE : 60ms).

We have never detected the fistula itself but MR usually visualized the enlarged draining veins. In our study we stressed the importance of signal intensity abnormalities within the medullary conus due to chronic ischemia secondary to venous drainage impairement.

After treatment we observed a disappearaence or a significant decrease of pathological signal intensity which correlates well with clinical improvement.

P26

NEW NEEDLE FOR MR-GUIDED ASPIRATION CYTOLOGY OF BASE OF SKULL LESIONS
L Teresi, R Lufkin, E Spickler, G Duckwiler, L Layfield, W Hanafee
UCLA Medical Center, Department of Radiology.

CT-guided aspiration cytology of deep lesions plays an essential role in the workup of many skull base lesions. Since MRI is rapidly replacing CT as the imaging study of choice in this region, the ability to perform MR-guided aspiration cytology is becoming increasingly valuable.

Attempts at MR guided biopsy with conventional stainless steel needles and MR liver biopsy needles resulted in images with unacceptable artifacts for thin section high resolution MR of base of the skull. These artifacts were further exacerbated when gradient echo fast-scanning techniques were employed.

A new high nickel stainless steel needle was developed which produced markedly diminished artifacts. The position of the needle was easily recognized as a fine line of signal void super imposed over the lesion. Initial clinical results of MR guided needle aspirations in patients with skull base pathology will be presented.

P27

MRI SPECTRUM OF ASYMPTOMATIC DEGENERATIVE CHANGES.
L Teresi MD, R Lufkin MD, U Batzdorf MD, W Hanafee MD.
UCLA Medical Center, Department of Radiology.

The MR examination of the cervical spine shows anatomic detail and pathologic changes unlike any other imaging modality, but does not reveal their significance in relation to the patient's symptoms. Individuals referred for MR examinations of the larynx without symptoms referrable to the cervical spine were studied both retrospectively (35 patients) and prospectively (52 patients) over a two-year period.

Disc protrusion (herniation/bulge) was seen in 23% of patients age 45-54 and 51% of patients age greater than 64. Disc protrusions occurred in the posterior direction in 25 of 38 (6.6%) cases. Anterior protrusions were observed in a significant number of cases (21%). Posterolateral protrusions were seen in only 5 of 38 cases (13%) and occurred with greater frequency in patients greater than 64 years. Spinal cord impingement was observed in 8 of 60 (13%) of patients less than 64 years old, and in 9 of 36 (25%) of patients ages greater than 64. In the 45 to 64 age range, cord impingement occurred solely secondary to disc protrusion, whereas in the greater than 64 age group 4 of 9 (44%) cases showed cord impingement secondary to large posterior osteophytes. Cord compression was observed in 6 of 87 (7%) cases and occurred solely secondary to disc protrusion in all cases. Percent cord area reduction never exceeded 16% and averaged approximately 5%.

P28

MR IMAGING OF ACUTE SUBARACHNOID HEMORRHAGE

E Spickler, K McKenna, R Lufkin, J Frazee
UCLA Medical Center, Department of Radiology.

Using primates and humans as clinical material, subarachnoid hemorrhage was studied with the aid of MRI and CT scanning to compare the sensitivity and resolution of the two imaging methods and ultimately the ability of each to detect early subarachnoid hemorrhage.

Subarachnoid hemorrhage secondary to aneurysm rupture was studied in 5 human subjects while subarachnoid hemorrhage was induced in 3 Macaca nemstrina monkeys by withdrawing a needle previously surgically placed through the internal carotid artery. This latter method has been used reliably in this laboratory to produce hemorrhage and delayed vasopasm. CT and MR imaging were performed immediately after hemorrhage in the case of the monkeys and at frequent intervals for up to two weeks post hemorrhage. The imaging studies were compared with clinical and pathological specimens of all animals. Human clinical CT and MR images were studied to supplement those from primates.

Results Acute hemorrhage was recognized on MR imaging as an increased signal in the region of clot when compared to surrounding CSF although the clot was isodense compared with brain. This likely reflects T1 shortening due to protein binding rather than a pure paramagnetic effect.

CT is sensitive to hemoglobin protein in acute hemorrhage, but the superior resolution of MRI particularly of the basal cisterns, results in equal or better definition of acute subarachnoid hemorrhage in many cases.

P29

MR EVALUATION OF CNS PATHOLOGY DURING ENDOVASCULAR THERAPY

P Lylyk, T Lin, R Lufkin, F Vinuela, N Martin, J Frazee, J Dion, J Bentson.
UCLA Medical Center, Department of Radiology.

Thirty patients with a variety of cerebrovascular malformations, aneurysms, and tumors were studied with MR prior to or following endovasuclar therapy. T1 and T2 weighted multiplanar 2D-FT spin echo images as well as MR angiograms were obtained. Correlation was made between MR, CT, angiography, clinical examination, and surgical findings when possible.

In all groups, MR was superior to CT and angiography in the assessment of parenchymal changes associated with the lesion and/or endovasuclar therapy such as ischemia, infarction, and subacute hemorrhage. In the AVM group, MR was better able to define feeding and draining vessels than CT, however MR was inferior to angiography. In demonstration of the nidus, MR was superior to CT and had advantages in localization over angiography. Significant shunting could be detected on MR by a discrepancy in size between the feeding vessels and nidus. In AVM's, fistulas, and aneurysms, MR could assess vessel patency and recanalization better than CT, but not as well as angiography.

P30

MRI OF THE NASOPHARYNX AND FLOOR OF THE MIDDLE CRANIAL FOSSA.

L Teresi, R Lufkin, D Becker, W Hanafee.
UCLA Medical Center, Department of Radiology.

The normal MR anatomy of the nasopharynx and floor of the middle cranial fossa was analyzed by correlating MR images from normal volunteers with whole-organ cryomicrotome sections. Anatomical communications exist between the paranasopharyngeal spaces and the surface structures of the skull base. These include the intimate relationship between the eustachian tube and the pharyngobasilar fascia, the attachments of muscle of mastication and deglutition to the skull base, and foramina for vascular and nervous structures.

Fifty patients with pathology of the inferior cranial vault, nasopharynx, and related spaces were studied with MRI. MR findings were compared with clinical records, plain films, CT and pathology when available. Neoplastic invasion of the bony floor of the middle cranial fossa, as well as the vital soft-tissue structures related to it, could be demonstrated as well as or better with MR than with CT. Tumor extension could be viewed directly as a continuous mass or indirectly by marrow replacement or displacement of normal structures. Specific anatomic routes by which tumors extend from the nasopharynx to the middle cranial fossa were derived from MR findings.

The majority of tumors extend through bony foramina and fissures. Surgical strategies for providing radical, yet save tumor excision are developed from the MRI anatomy. More extensive bone and tumor removal with preservation of cranial nerves and basal vascular structures is thus made possible. Human cranial cryomicrotome sections will be correlated with MRI anatomy, surgical strategies outlined and surgical results reported based on tumor type, extent of excision, and other adjuvent therapy.

P31

MR PROJECTION ANGIOGRAPHY: APPLICATION IN PATIENTS WITH CEREBROVASCULAR DISEASE

E. Spickler, K McKenna, R. Lufkin, L. Chiu, P. Pattany, M. Mehringer, F. Vinuela, N. Martin
UCLA Medical Center, Department of Radiology.

2D-FT thick-slice projection MR images of flowing blood were produced as follows: a flow-sensitive image was obtained by suppressing within view motion using completely rephased magnetization within the view. Correction for velocity as well as acceleration and pulsatility terms was made. A standard acquisition of the same region was then subtracted from the original image to produce the final vascular image.

These techniques were used on normal volunteers as well as patients with a variety of cerbrovascular disease including arthrosclerosis, avm's and aneurysms. Comparison was made with other imaging studies such as CT, conventional agngiography, and conventional MR. MR projection angiology is capable of producing moderate resolution images on normals and patients with cerebrovascular disease that correlate well with other x-ray imaging studies.

P32

MRI OF THE PARANASAL SINUSES

L Teresi, R Lufkin, L Hoover, E. Beahm, W. Hanafee.
UCLA Medical Center, Department of Radiology.

MRI was performed on 68 patients with a variety of abnormalities of the paranasal sinuses including inflammatory disease and benign and malignant tumors. Comparison was made with clinical examination, CT or plain film imaging studies, and surgical findings when possible.

Lack of signal from air and cortical bone on T1 weighted images creates difficulty in imaging the paranasal sinuses. Fortunately all sinuses are lined with mucoperiosteum which has high signal especially when thickened. The majority of the pathological processes of the paranasal sinuses were adequately imaged using T1 weighted pulse sequences. T2 weighted sequences were occasionally useful in complex cases or for better definition in infiltrating malignant lesions or characterizing tissues in airless sinuses. Other than the single case of osteomas where x-ray studies were superior, magnetic resonance provided equal or superior information compared to the x-ray study.

P33

BIODISTRIBUTION OF SORBITOL: ^{19}F NMR IMAGING STUDIES

T Nakada*#, IL Kwee*#, BV Griffey‡, RH Griffey‡
VA Med Ctr, Martinez, CA*, Univ of Calif, Davis, CA#, Univ of New Mexico, NM‡

Sorbitol is a six carbon sugar alcohol which is synthesized in vivo from glucose by the enzymatic reaction of aldose reductase. It represents the first intermediate product of glucose in the reductive polyol pathway. Although the physiological role of the polyol pathway is not known, significant enzymatic activities are found in the brain, testis, and lens and abnormally increased activities in the polyol pathway are thought to be responsible for diabetic complications in these organs. Using ^{19}F as signal probe and 3-fluoro-3-deoxy-D-glucose (3-FDG) as metabolic probe, we have recently shown that enzymatic activities of the polyol pathway can be studied quantitatively using nuclear magnetic resonance (NMR) spectroscopy. In this study, we investigated the biodistribution of sorbitol synthesis, namely, aldose reductase activities, and organ uptake of circulating sorbitol using ^{19}F sorbitol NMR imaging technique.

Sprague-Dawley rats, 200-300g, were given a single dose of 3-FDG, 1g/kg, intravenously three hours prior to the study to obtain steady state sorbitol levels at the site of synthesis. GE CSI-4.7 System was used. The transmitter was positioned at the resonance frequency of 3-FD-sorbitol and ^{19}F images were obtained using partial saturation spin echo imaging sequences with a restoring 180^{0} pulse (TR: 600 msec, TE: 12 msec). The total time needed for data acquisition was ca. 60 min. ^{19}F images were also obtained 12 hours post 3-FDG infusion to investigate uptake of circulating sorbitol.

Significant synthesis sorbitol in the brain, eye, and testis were observed supporting previous biochemical findings of high aldose reductase activities in these organs. Images obtained 12 hours post 3-FDG infusion showed significant uptake by heart as well as urinary excretion of sorbitol into the bladder.

P34

NMR Detection of Motion Using RF Field Gradients

[1]GS Karczmar, [1,2]DB Twieg, [1]TJ Lawry, [1]GB Matson and [1]MW Weiner
[1]University of California, SF, [1]VAMCSF, and [2]Philips Medical Systems

NMR detection of motion of fluid using radio frequency field (RF) gradients is demonstrated. An inhomogeneous RF field (B_1) is applied with a phase of X (G_x) so that magnetization in each part of the sample accumulates a different phase in the YZ plane, depending on the strength of B_1 at that location. After a delay period (t_d), a rephasing RF gradient (G_{-x}) is applied to restore polarization along Z. Z magnetization is then sampled by an observe pulse sequence. The resulting signal is reduced by relaxation and molecular motion (due to diffusion, perfusion, or flow) which occur during t_d. By varying the lengths of G_x ($G_{-x} = G_x$) and t_d, the effects of molecular motion and relaxation can be distinguished.

To test this method, water was pumped through a tube along the axis of a 1 cm diameter surface coil in a 2T magnetic field. A DEPTH pulse sequence was used to detect water in a region where the B_1 gradient of the coil was 50 kHz/cm. With t_d = 0.5 sec, and G_x applied for 100 us, the signal detected from water flowing at .5 mm/sec was 30% of the signal detected from stationary water. With G_x applied for 200 us, no signal was detected from flowing water. Thus, slow flow was easily detected.

This technique offers some advantages over the use of static field (B_o) gradients to detect motion. First high B_1 gradients are readily obtainable. Second, because no eddy currents are generated, this technique may be combined with ^{31}P NMR spectroscopy to detect motion of phosphorylated metabolites (e.g. 2,3DPG in flowing blood). Alternatively, the technique may allow imaging of flow and perfusion when combined with imaging protocols.

P35

T_1 of Control and Irradiated Brains, Brain Tumors and Livers of Rats.

DJ Pizzarello, R Chandra, R Barish and U Cravioto
Department of Radiology, New York University Medical Center

We have been studying the relationship between damage to and repair of tissues other than liver to an increase in liver proton T_1 (Inv. Radiol. 21:320-324, and 652-853 1986, and MRI5 Suppl. I p 67-68, 1987);and methods of tissue sampling, T_1 measurement and data analysis used here are the same. Now we report the affect of highly localized irradiation of rat brain and a small implanted brain tumor on T_1 in brain, brain tumor and liver 1 week post irradiation. We also report T_1 values in an experiment in which implanted tumors inexplicably regressed prior to irradiation. Four thousand rads of highly collimated x-rays (6mm, diam.) were delivered to the right frontal lobe of 60-80g male rats, some with tumors implanted at that site. Groups without tumors or irradiation were controls. Mean and S.D. of T_1 of control and irradiated brain were 506 ± 7.5 and 528 ± 39 ms 1 week post irradiation. Mean and S.D. T_1 of liver in these groups were 231 ± 7.6 and 246 ± 3.2ms. None were statistically significant. In one experiment tumor was implanted and apparantly took. A week later some were killed; no tumor was found, and liver T_1 of both groups was not significantly different but longer than is usual in rats. However, the rats were sick, apparently suffering residual effects of implant. The remainder were killed 4 weeks post irradiation. No tumor was found; liver T_1 of the unirradiated group was in the usual range for rats; T_1 of the irradiated group was longer and significantly different. These animals were healthy compared to themselves at two weeks post implant, but the irradiated group was beginning to show signs of skin damage, hair loss and brain damage in the irradiated field. Preliminary results, with a larger tumor show differences between T_1 of brain, brain tumor and irradiated brain tumor. T_1 of liver lengthened in these groups.

P36

MR HEPATOBILIARY IMAGING WITH A PYRIDOXAL-5'-PHOSPHATE CHELATE

SM Rocklage, S Quay, D Worah
Salutar, Inc.

Purpose: To design, synthesize and test, in-vitro and in-vivo, novel paramagnetic manganese(II) chelates for MRI contrast enhancement. Our goal is to prepare novel manganese(II) chelates with excellent thermodynamic stability, high relaxivity, low acute toxicity and targeted biodistribution.

This study reports the first efforts to use the principle of biomimetic design in the development of in-vivo MR contrast agents. Pyridoxyl-5-phosphate is an essential enzyme for a number of important biochemical reactions, especially the transaminases found in cardiac and hepatic tissue. Since these reactions require a pyridoxyl metal centered attack on amino acids, we postulated that a metal centered, pyridoxyl phosphate chelate might be recognized by membrane transport systems for pyridoxyl-P and might thus give unique, biochemically relevant functional information in the MR diagnostic environment.

Methods: Images were acquired on a 1.5T G.E. Signa system, using a prototype 20 cm., transmit and receive saddle coil. Five mm thick, axial, multi-slice, spin-echo images were made (TR=200, TE=25). N.Z. white rabbits were anesthetized and then given doses ranging from 13 to 50 umoles/kg of Mn(DPDP) intravenously. Image collection began within 0.5 minutes and continued at 2 to 3 minute intervals for up to 60 minutes. The animal tolerated the procedure well. Images were analyzed by selecting 4 regions of interest - gallbladder, left, right and mid-liver. Mean image intensity was determined for pre- and post-injection times for all images.

Results: The ligand, dipyridoxyl diphosphate (DPDP), was prepared from pyridoxal-5-phosphate, the coenzyme vitamin B6. DPDP has been completely characterized by high-resolution NMR, elemental analysis, potentiometry and mass spectroscopy. DPDP forms 1:1 chelates with manganese(II) that are extremely water soluble (500 mM solutions) with acceptable molar relaxivity (ca. 3.5 mM-1 s-1 at 10 MHz in plasma).

Mn(DPDP) markedly enhanced the signal from liver with intensity reaching maximum or plateau at 30 minutes post-injection. The maximum post-injection signal with a dose of 13 umol/kg was 200% of pre-injection for liver and 200% for gallbladder. The hepatic vessel showed little change in signal intensity. At 60 minutes the liver and gallbladder intensities had declined to 117 and 170%.

Conclusion: Mn(DPDP) is transported into the hepatocyte in-vivo. This transport process can be visualized by MR imaging because of the dramatic relaxivity changes accompanying uptake of Mn(DPDP).

P37

RINGING ARTEFACT REDUCTION BY AN EFFICIENT LIKELIHOOD IMPROVEMENT METHOD

M. Fuderer
Philips Medical Systems, Best, Netherlands

Ringing artefacts are often visible when the time-saving reduced acquisition method is used, e.g. when scanning only the lowest 70% of the 256 data lines.

Recently, advanced reconstruction schemes have been proposed, which estimate the high-frequency data from the low spatial frequencies. These methods include ARMA (1), data extrapolation and Constrained Reconstruction (CORE) (2). These methods suppress ringing artefacts without blurring the image, but often require a lot of processing time.

Our method very efficiently estimates the high frequency data from the low-frequency data lines. In addition to the normal reconstruction, it requires practically only two extra Fourier transforms.

The high-frequency components are estimated to maximize the likelihood of the resulting MR image. This likelihood is related to the histogram of the image contrasts between adjacent pixels in the phase-encoding direction. This distribution can be modelled as a Lorentzian function, showing a maximum at zero. It reflects the occurrence frequency of flat image parts and edge contrasts. An image likelihood function can be defined and optimized for the estimated high-spatial-frequency components. This results in reduction of ringing artefacts and enhancement of edge contrast.

The results of this method on MR images of human subjects are promising. Evaluation on a 70% acquisition image show about 20% decrease of the error energy after processing. "Error energy" is defined as the total power of the difference to a 256-data-lines reference image. The elimination of visible ringing artefacts then appears almost complete.

(1) M.R. Smith et al., IEEE, vol.MI-5, No.3, P.132 (1986)
(2) E.M. Haacke, Z.P. Liang, S.H. Izen; 5th MDSP, Noordwijkerhout (1987)

P38

SELECTIONS OF PHASE ENCODINGS IN MR FLUOROSCOPY

T Tasciyan, F Farzaneh, JN Lee, RC Wright, SJ Riederer
Duke University Medical Center, Department of Radiology

In MR Fluoroscopy, images can be produced continuously at rates as high as 30/second. This is accomplished by applying a limited number N of phase encodings to a basic FLASH sequence and using a special reconstruction scheme. The encodings are applied repeatedly and the images are reconstructed by sliding a window of width N along the acquired data. Testing the method on a dynamic phantom has revealed that the motion depicted by successive reconstructed images may be in slight discrepancy with the actual movement of the phantom, the former being less smooth. To observe and smooth the character of the motion in the reconstructed images, further phantom studies have been carried out using a) different numbers of limited phase encodings; b) different distributions of phase encodings; c) different directions of motion; i.e., motion along readout vs. motion along phase encoding.

One alternative in tracking motion smoothly is to simply record a limited number of phase encodings, repeating each at an interval of N*TR, automatically updating in frequent intervals. For this case, a tradeoff exists between spatial resolution and time resolution dictated by the velocity of the phantom. The phantom used consisted of a vial 2cm in diameter and 8cm in length rolling at a velocity of 5cm/sec. The use of only 24 phase encodings along the long dimension of the vial portrayed the motion well, giving adequate spatial resolution at 12 images/sec.

Since the lower frequency phase encodings determine the crude shape of the image and hence the gross location of the phantom, another scheme updates the lower frequencies more often, sampling the encodings nonuniformly. With N limited phase encodings and K lower frequency encodings, the first reordering scheme N,K,N,K,... for N fixed and K variable gives best results when 1/3 K/N 1/2. The second reordering scheme updates at an even higher rate by recording first odd then even phase encodings: N/2odd, K/2odd, N/2even, K/2even, ... However, this distribution artifactually doubles the phantom as the sliding window can contain odd low frequency phase encodings from one position and even low frequency phase encodings from another.

Presently, the results are being extended to phantoms with different velocities.

P39

USE OF FIBEROPTIC TRANSMITTER, RECEIVER, AND CABLES FOR MR IMAGING SURFACE COILS

WS Yamanashi (1), JH Letcher, III (2), JW Frazer (3) and PD Lester (1)
(1)City of Faith Med. & Res. Ctr., Tulsa, OK; (2)U of Tulsa, Tulsa, OK; (3)UTHSC, SanAntonio, TX

The coupling of a MRI surface coil to a receiver preamplifier is normally done with either a coaxial or a twin-axial cable of predetermined impedance. The limiting factor of this approach is that the length of the cable is usually dependent upon the resonant frequency of the particular magnetic nucleus such that locating the ROI's with the coil is limited by that length. In order to obviate this problem we made use of the HFBR series opto-electric transmitters, receivers, and fiberoptic couplers. The circuit design for the transmitter consists of a three stage amplifier, a current mirror and the optic transmitter. The amplifier section amplifies the signal from the surface coil by 48 dB to give a maximum peak to peak voltage of 1 volt at the input of the current mirror. The current mirror is biased to give the necessary current to drive the optic transmitter.

P40

SERIAL MR IMAGES OF RED CELL FREE BLOOD CLOT RETRACTION
L. A. Hayman, J.J. Ford, K.H. Taber, A. Saleem and R.N. Bryan
Baylor College of Medicine, Houston, Texas

Red blood cell free platelet rich plasma was mixed with thrombin and imaged serially at 0.3, 0.5, 1.0, 1.5 and 2.4 Tesla using a Spin Density and T2 weighted spin echo pulse sequences and a gradient echo sequence. A fresh rat brain was used for comparison. The progression from an unretracted clot to an almost fully retracted clot required 4 hours. The MR images illustrate the change from a signal intensity greater than brain to a signal less than brain as the clot retracts and extrudes sera on the 1.0, 1.5 and 2.4 Tesla units. Electron micrographs at various stages of retraction demonstrate the increased density of fibrin threads as the clot retracts. The authors conclude the formation of this matrix is partially responsible for the decreased signal seen clinically in patients with acute intracranial blood.

P41

MRI BLOCH EQUATIONS WITH NONEQUILIBRIUM KINETICS
D.N. Ghosh Roy, G.T. Gullberg
University of Utah, Salt Lake City

A model of blood perfusion in the organs and the determination of certain physiological parameters based on this model are reported. The organ is considered to be a network of randomly distributed capillaries surrounded by a tissue matrix. The characterization of the perfusive flow is in terms of a hydrodynamic dispersion coefficient and a small bulk flow known as Darcy's flow. The dispersion is considered to be chiefly due to mixing at the junctions of the branching capillaries and is significiantly greater than molecular diffusion, the latter playing a minor role only across the streamlines of the unperturbed capillary flow. Dispersion and Darcy's flow are shown to be directly related to the physiological parameters of perfusion such as specific permeability and tortuosity of the bed and the porosity of the organ. Based on the statistical treatment of a porous medium, it is shown how information on the dispersion and Darcy's velocity can be used to infer certain important characteristics of perfusion.

The second part of the paper reports the solution of NMR Bloch equations with linear, nonequilibrium exchange kinetics for boundry conditions appropriate to MR Imaging. It is demonstrated that the solution does, under certain approximations, permit substantial simplifications so as to be tractable in practical situations. The MRI signal depends on the void fraction which varies dramatically with the state of the organ, allowing thereby certain limiting assumptions. These approximations are, therefore, interesting and satisfying in that they correspong to the physiological state of the organ.

P42

Mechanisms of relaxation rate enhancement from superparamagnetic contrast agents in tissues and gels.

S. Majumdar, C.F. Pope, S. Zoghbi, G. Ramirez, J.C. Gore.
Yale University School of Medicine

Superparamagnetic agents produce dramatic effects on tissue relaxation but the importance of different relaxation mechanisms is poorly understood. They give rise to susceptibility variations that induce random field gradients, and simulations and theoretical studies have previously been used [1] to relate the apparent contribution to the rate of decay of transverse magnetization to the effects of diffusion in these field gradients. The field and concentration dependences of the relaxation rates of gels doped with two such materials (AM4125 and AMI25, Advanced Magnetics, Cambridge, MA.) have been studied to evaluate these materials as contrast agents and to investigate the dominant relaxation mechanisms responsible for their effects. The spin-spin relaxation rates for both materials increased with concentration, but the spin-lattice relaxation rate for gels doped with AM4125 showed only a small correlation with concentration. The rates 1/T1 and 1/T2 at different fields indicate that in addition to diffusion, other mechanisms must contribute to the observed effects. In order to explore the field dependence and biodistribution dependence of these materials in tissue, Sprague Dawley rats were injected with different concentrations of Iron-59 labelled AM125 particles. These particles are absorbed by the reticulo-endothelial cells in the liver. The variations of liver relaxation rates with different concentrations of this material were measured from images obtained at 6.35, 63.5 and 85 MHz and from excised liver samples at 20 and 300 MHz.

[1] S. Majumdar, J.C. Gore, J. Mag. Reson., (in press).

P43

MULTISLICE CHEMICAL SHIFT IMAGING BY SLICE-SELECTION GRADIENT REVERSAL

RS Hinks, RM Quencer
Picker International and University of Miami Radiology Dept., 1115 NW 14 ST, Miami, FL

The slices of fat and water which result from a slice-selective RF pulse are physically offset from each other by the ratio of their chemical shift difference to the RF pulse bandwidth. If these slices are offset from each other by more than half a slice thickness, it is possible to selectively refocus only water (or fat) by reversing the direction of the slice selection gradient and hence reversing the relative positions of the fat and water slices.

We have developed and implemented this multislice chemical shift imaging technique at 1.5 T (Picker) with the following observations. As with other chemical shift imaging techniques, field inhomogeneity can be a limiting factor when imaging large regions. Hence, optimal results are obtained by restricting the field of view to a relatively small region, as with surface coil studies. As expected, adjustment of the first order shims to optimize homogeneity in the surface coil region greatly improves the fat/water separation. Tuning the desired resonant frequency is most reliably accomplished by simulating the scan and adjusting the center frequency while observing the magnitude of the spin echo. Increasing the frequency until the signal begins to drop off gives water as the imaging species, while decreasing the center frequency in the same manner selects fat. Note that if any frequency offsets are used, they must also be reversed between the excitation and refocusing pulses.

This technique offers several advantages over other methods of chemical shift imaging. Since only the water (or fat) signal is refocussed to form a spin echo, there is no need for acquiring multiple sequences or for post-processing. Since all of the RF pulses are slice selective, this technique is easily implemented as a multislice sequence. As well, since only the single resonance forms an echo, there is no chemical shift artifact. This allows the use of long sampling times with the associated benefits of increased signal-to-noise. Finally, the technique is widely applicable and may be used with T1 or T2-weighted scans or with virtually any sequence which uses two slice-selective RF pulses.

P44

AUTOTUNED HEMHOLTZ COILS FOR IMAGING THE CERVICAL SPINE AND PELVIS

LP Clarke, EA Bonaroti, HK Brown, FR Murtagh, ML Silbiger
Department of Radiology, University of South Florida College of Medicine

A number of surface coils were constructed for imaging the cervical spine and pelvis at an operating frequency of 42 MHZ (1 Tesla). An experimental study was performed to determine the relative importance of the following: (A) Manual tuning with capicators verses electronic tuning with varactors, (B) single coils verses Hemholtz design, (C) coils with and without distributive capicatance (i.e. Faraday Shield) and accuracy of stand alone automatic tuning mechanism using DC input to varactors. The planar and Hemholtz coils were with circular, elliptical or hybrid shape with longitudinal dimensions of 18-25 cm. The use of varactors did not influence the loaded Q of the coil or image S/N in patients or phantoms and the automatic tuning was accurate despite the range of tuning capacitance for the coil types evaluated. In most instances the Faraday Shield improved the S/N in patient measurements particularly for the pelvic area; although it reduced the unloaded Q of the coil.

P45

VARIATIONS IN T1 AND T2 DUE TO MRI CONTRAST AGENTS: EFFECT ON IMAGE CONTRAST

NA Rao (1), RE Hendrick (1), DD Stark (2)
(1) Department of Radiology, University of Colorado School of Medicine
(2) Department of Radiology, Massachusetts General Hospital

The pharmacokinetic behavior of MRI contrast agents determines the temporal variations of T1 and T2 values in tumor and normal tissues. In most cases these variations occur rapidly during the first few minutes after contrast injection. Fast scanning techniques have been suggested to make use of early contrast enhancement. However, most fast scanning techniques result in sub-optimal contrast-to-noise ratios between tumor and normal tissues. Longer acquisition times can give better contrast, but the final image is affected by the fact that T1 and T2 vary during acquisition. We have developed a model to study the effect of T1 and T2 variations during image acquisition for a given pulse sequence. Each pulse sequence repetition gives rise to an FID measurement which is a function of T1, T2 and the pulse sequence parameters. These FID measurements can be considered as scanning the image along k-space trajectories determined by the gradient fields. The variations in the FID signal due to the variations in T1 and T2 show up as modification of the data at various locations in k-space. The resultant effect on the reconstructed image can be evaluated after a 2D Fourier transform of the k-space data. Based on in-vivo and in-vitro time-dependent data within liver and liver cancer, the effect of T1 and T2 variations during image acquisition are illustrated for Gd-DTPA, Gd-DOTA and ferrite contrast agents using a variety of standard pulse sequences.

P46

AUDIO-CODED (A-C) MR IMAGING: A METHOD FOR DUAL SENSORY IMAGE PERCEPTION

W Sattin
Picker International Inc., Clinical Science Center

A method has been developed by which dynamic/functional information is encoded as audible sound rather than visual color. Audio-coding (A-C) has two advantages over visual-coding: it is a better indicator of temporal data, and humans discriminate over 1800 audible steps compared to about 128 color hues, and even less gray-levels (1).

Many imaging modalities (cine-CT, PET, MR, U/S, SPECT) are capable of providing more information than can easily be assimilated at one time. In particular, MR can provide added information for any static image, such as calculated relaxation times, in-plane flow velocity and calculated diffusion coefficients. Additionally, dynamic MR, such as cardiac cine and moving joints, contribute added functional information. Proper interpretation of this added data is difficult, and is hindered by the difficulty in attempting to communicate any more information through an already overloaded visual channel.

Most often, color-coded dynamic/functional processes are simultaneously displayed with gray-scale-encoded anatomical information. This has the disadvantage that color encoding precludes any intuitive comprehension of information; the user must learn to decode visual cues into physiological information. In A-C imaging, audio cues and visible images coalesce to create a highly intuitive method of image/data interpretation.

This technique has been used in cardiac gated, flow sensitized MR imaging. Images from sixteen positions within the R-R interval were acquired and displayed in cine mode. A region-of-interest could be located anywhere in the image plane, for example in the left ventricle to examine either aortic valve regurgitation or mitral valve stenosis. With the ROI at this position, sounds were generated which corresponded to the direction and speed of the flowing blood. Thus, the cine image display was accompanied by the audible representation of the changing blood flow. A-C MR imaging will aid the uninitiated and increase the efficiency of the experienced diagnostician.

(1) Mowbray GH and Gebhard JW, CM-936, The Johns Hopkins University (1958).

P47

DIFFERENTIAL FLOW ZEUGMATOGRAPHY*

QS Xiang, O Nalcioglu
Department of Radiological Sciences, Division of Physics and Engineering, University of California-Irvine

A new technique, named the differential flow imaging for NMR in-plane flow measurement is introduced and experimentally tested. The DFI technique acquires two successive flow influenced spin density magnitude images which reflect the dynamics of the time dependent excited spin density distribution. When obtaining the two flow influenced images, specially designed encoding gradients are applied to suppress the effect of one of the component of the velocity, say v_x. Velocity information of the other component v_y is then extracted by applying the equation of continuity in fluid mechanics to these images.

A well defined flow field was generated in a cylindrical flow phantom made by winding a teflon tubing (ID=1.32mm) on a plastic core. The flow influenced images obtained are shown in Figs.1 and 2. Tap water in the phantom flowed counterclockwise at a crosssectionally averaged speed of about 2cm/s. The large ring was the flow phantom which had been slightly distorted into oval by the y-component of flow velocity in an opposite manner in the two images. The small circles and bars correspond to stationary reference and flow perpendicular to the imaging plane. These parts are identical in the two images because of the absence of y-direction flow. Images of the y-component of the spin-flux vector $\mathbf{J}=\rho\mathbf{v}$ and the true spin density computed from Figs.1 and 2 are shown on top and bottom of Fig.3 respectively. The velocities measured by DFI agree with the expected values within the error of $\pm$5%.

Since only the magnitude images are used, this technique does not suffer from the systematic phase error in contrast to the methods based on phase measurement. On the other hand, it can be combined with the phase methods resulting in a multidimensional flow measurement in a shorter data acquisition time.

*Work supported in part by PHS Grant No. 1R01-CA41307 awarded by the NCI, DHHS.

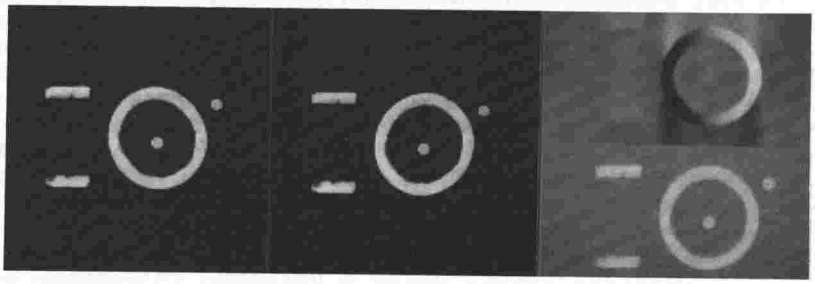

Figure 1 Figure 2 Figure 3

P48

EFFECTS OF TURBULENT FLOW ON NMR ZEUGMATOGRAPHY

O. Nalcioglu*, P. R. Moran**
*Department of Radiological Sciences, Division of Physics and Engineering, University of California-Irvine
**Department of Radiology, Bowman-Gray School of Medicine, Wake Forest University

NMR can be used in investigating various hydrodynamical properties of liquids. Recent advances in NMR imaging has made it possible to extend these studies to map out the hyrodynamical properties spatially, i.e. flow imaging. Since most flows occuring in nature are turbulent, we undertook an investigation of the effects of turbulent flow on the NMR images. The Bloch-Boltzman equation for the transverse magnetization density of an incompressible liquid is given by,

$$\partial M(\mathbf{r},t)/\partial t = [-1/T_2 - (\mathbf{v}\bullet\nabla) + D_M(\mathbf{r})\,\Delta]\, M(\mathbf{r},t) \qquad (1)$$

where T_2 is the spin-spin relaxation time, D_M molecular diffusion constant . It should be remembered that the essential characteristic of a turbulent flow is random fluctuations in time and space of all the quantities involved in the flow. This applies to the transported transverse magnetization density as well as the components of velocity. We will assume that each of the variables to comprise a mean and a turbulent fluctuation. If the flow is a steady turbulent flow, the means do not vary with time. The separation of M and $\mathbf{v}$ into a mean and a fluctuating part yields,

$$M = <M> + M'; \quad \mathbf{v} = <\mathbf{v}> + \mathbf{v}' \qquad (2)$$

where the primed quantities are the fluctuating parts with zero mean. In equation (2), $< \bullet >$ denotes the ensemble average. If one substitutes eq.(2) into eq.(1) and perform the ensemble average one obtains,

$$\partial <M>/\partial t = [-1/T_2 - (<\mathbf{v}>\bullet\nabla) + D_M\,\Delta] <M> + <(\mathbf{v}'\bullet\nabla) M'> \qquad (3)$$

We observe that the mean transverse magnetization (eq.3) obeys the same equation as the transverse magnetization (eq.1) except for the last additional term. If one is dealing with homogeneous turbulence eq. (3) can be rewritten as,

$$\partial <M>/\partial t = [-1/T_2 - (<\mathbf{v}>\bullet\nabla) + (D_M + D_T)\,\Delta]\ <M> \qquad (4)$$

where D_T is defined to be the scalar eddy diffusivity. It is clear from eq.(4) that a spin density image formed will have the flow regions attenuated by both molecular diffusion and eddy diffusivity. Since the scale of random motion of turbulence is much greater than that of the molecular motion, turbulence is many times more effective in dispersing the flowing spins. It should also be emphasized that turbulent motion is irreversible just like the molecular diffusion thus one does not have even echo rephasing in contrast to laminar flow. The attenuation of the FID signal due to turbulent liquid flow was experimentally observed by Fukuda et al..

P49

REDUCTION OF SCAN TIME IN ECHO PLANAR IMAGING

G. C. Kashmar, O. Nalcioglu
Department of Radiological Sciences, Division of Physics and Engineering, University of California-Irvine

Echo planar imaging usually requires twice as many free induction decay [FID] signals as does conventional imaging. This is due to the fact that sampling the high frequency edges of the data space at the Nyquist rate requires sampling the vertical axis twice as often as would be desirable. It has been pointed out that this problem can be resolved by the use of a theorem which states that as long as the number of data points is sufficient for Nyquist sampling, exact interpolation into a continuous bandlimited function is possible no matter where the data points are located. The theorem gives a way of calculating horizontally distorted sinc functions to be used for interpolation in the way ordinary sinc functions are used with regular spaced sampling. However, it has been reported that as deviations from regular sampling increase, signal to noise ratio (SNR) rapidly decreases. This paper studied to what extent this problem would occur in echo planar imaging. First, an algorithm was created which used the new interpolation method to produce data on Cartesian coordinates and then reconstructed an image with a two dimensional Fourier transform technique. Then the new method was compared to a "control" method which used the usual double number of FID's. The control method was a previously unpublished algorithm which uses both positively and negatively tilted echoes and utilized a corrected version of the original single large one dimensional Fourier transform. Both methods were used to make FID's from a mathematical phantom. Noise was added to these FID's and the corresponding images were reconstructed. In the absence of noise both methods provided images without any artifacts aside from truncation and roundoff errors. However, when noise was added to the simulated FID's, the interpolation method had a much lower SNR as predicted. It was observed that this noise had a characteristic texture which could be removed by the use of a correlation integral/edge detector algorithm but some noise still remained in the image.

From a plot of the image SNR versus the FID SNR for the various methods, the following conclusions can be drawn: First, with the new method, it is possible to scan at twice the speed and obtain nearly half the SNR if the interpolator/correlator is used. Secondly, averaging two sets of FID's with the interpolator/correlator is less beneficial than using the control method. Other studies were undertaken with the interpolator/correlator/edge detector method to determine the quality of more complex images and these were found to have no serious artifacts but were very noisy.

P50

MESH: A new approach to fast SE imaging
R.R. Rzedzian
Advanced NMR Systems, Inc. Woburn, MA

A new technique has been developed which can obtain spin echo (SE) images of the body at very high speeds with high resolution. The technique, called MESH (Mosaicked Echo Scan Hybrid), which can be regarded as a super-sequence of Instant scan (1), maintains the high tissue contrast of conventional SE images which can take minutes to obtain.

Instant Scan consists of a 90°-180°-[image acquire] sequence and can in a single shot acquire a complete image in 1/25th second by rapidly scanning all of k-space. If more time is available it is possible to piece together in a patchwork, or "mosaic", sectional scans of k-space carried out in 4 or more different acquisitions by MESH. In the y, or readout direction, which is scanned in 312 microseconds, assymetric gradient echoes are mosaicked to increase the coverage of k-space while in the "real time" or encoding domain, (x), interleaving or MESH-ing is performed to increase coverage. This accommodates any T2 decay over the acquisition time of 20 milliseconds. Images were obtained on an Instascan system operating at 2.0 Tesla designed and made by Advanced NMR Systems, Inc. (Woburn, MA). Four partial scans were performed during a period of suspended respiration of 18 seconds. TR was 6 seconds and TE was 24 milliseconds. The full acquisition matrix was 256 x 128 and the images have an in-plane resolution of 2.0mm with a slice thickness of 1cm.

In conclusion, it is possible to obtain high resolution SE images in a single breath hold by using MESH thereby minimizing respiratory artifacts; further with a TR time of 6 seconds, maximum T2 contrast is available in the image. Multiple slices can be obtained during the wait periods, with the exciting potential of three-dimensional scanning of the body with 2mm resolution images in a single breath hold. Finally, MESH truly allows the optimization of study times to the inherent motions of the subject while maintaining the high tissue contrast of SE.

1. R.R. Rzedzian, I.L. Pykett. Instant images of the Human Heart Using a New, Whole-Body Magnetic Resonance Imaging System. Amer. J. Roentgenology, 149 (1987) 245-250.

P51

THE USE OF CONJUGATE SYMMETRIZATION WITH 3-D VOLUME ACQUISITION
GD DeMeester, F Bearden, D Lampman, GN Holland
Picker International, NMR Division, Highland Heights, Ohio

Conjugate symmetrization allows one half of the k-space matrix to be reconstructed from the other half giving a significant savings in acquisition time, since only positive phase encoding views need be collected. In 3-D, since there are two phase encoding directions there is additional potential for using conjugate symmetry. 3-D scans with large matrices use very short TR to keep scan time manageable. With conjugate symmetrization, just over half the phase encoding views can be collected but with TR doubled which allows greater flexibility in choice of TE and sampling time, reduces demand on the gradient system allowing typically smaller field-of-view (FOV), and gives greater transverse magnetization, hence better signal-to-noise ratio.

Second, the method can prevent aliasing without increasing scan time. In the frequency encoding direction we oversample to avoid aliasing from an object that extends beyond the imaged FOV, but in the phase encode direction oversampling increases scan time; we normally choose the phase encoding axis so that that object does not extend beyond the FOV. In 3D-FT, since there are two phase encoding axes, it may not be possible to avoid aliasing in this way. Conjugate symmetry allows oversampling by collecting double the number of views, but of positive phase only. By selecting the inner views and symmetrizing, aliasing is avoided without time penalty.

Third, the technique can improve slice resolution. Often, an anisotropic data set is collected with a reduced number of data points in the slice direction. This is "slab" imaging where a thick slice is defined by selective excitation, and a number of thinner slices are described by an equal number of secondary phase encoding steps in the slice direction. Conjugate symmetrization can either increase slice resolution, or the number slices without time penalty. We can also exploit the oversampling technique to avoid artifacts that occur near the edges of the defined slab due to imperfect selective excitation.

In conclusion, conjugate symmetrization can be exploited in 3D MR imaging to overcome unique problems, and to generally enhance its usefulness.

P52

TRANSFORMATIONS PRODUCING INFORMATION ENHANCED SYNTHETIC IMAGES

JJ Sychra, V Capek, A Horowitz, M Mafee
University of Illinois at Chicago

By varying pulse sequences (PS) and their parameters, the probability of capturing additional diagnostic information in the resulting image set is increased. However, it is often difficult, and sometimes impossible, even for the trained eye to detect pathological tissue types "buried" in a large amount of image data (and noise). This dilemma of increasing information content without ability to perceive it can be solved by the development of information enhanced synthetic images. There is a large number of classes of operations on the input image data leading to synthetic images that may extract the diagnostic information from MR image data and make it distinct. These transforms convert the large input image set into a smaller and less noisy image set. Some of these transforms generate synthetic images that have tendency to contain only information not present in the other members of the resulting image set, and are consequently more perceptible and easier to distinguish from each other. While the definition of synthetic images generated by principal component or factor analyses depend on the particular case data, we will demonstrate transforms that produce information enhanced synthetic images that are comparable from case to case. The involved operation can be separated into three main categories : (1) preprocessing of original images and generation of intermediate images containing certain information extracted in a parametric form (parametric images). These operations include, for example, extraction of 2-D and 3-D texture measures. (2) combinations of nonlinear adaptive image filtering, nonlinear projections and segmentation in multi-dimensional subspaces of the pixel values. These operations include, for example, generalized principal component, factor, discriminant, compartment, and cluster analyses. (3) post-processing of the resulting images data to increase their perceptibility to the human eye. These techniques may optionally include nonlinear adaptive image filtering, local exponential histogram equalization and conditional median filtering.

Typical results illustrating the use of various techniques on MR images of brain have been obtained and mutually compared to demonstrate advantages and disadvantages of individual approaches. Suggestions for future development are formulated as well.

P53

TUMOR HETEROGENEITY AND RESPONSIVENESS TO RADIATION TREATMENTS AS REVEALED BY HIGH-RESOLUTION MRI.

F.Q.H. Ngo, R.J. Kurland,* C.A. Belfi, C. Nunez, and T.F. Meaney
Cleveland Clinic Foundation, Cleveland, OH and *Geisinger Medical Center, Danville, PA

To further evaluate the usefulness of proton NMR relaxation times (T1 and T2) for tumor prognosis following radiotherapy, we are extending our previous relaxometry study with excised tumors to in situ study using MR imaging. A GE Signa 1.5T MR scanner was employed with a whole-body coil as RF transmitter and a butterfly coil (Medical Advances, Inc.) or a GE 3-inch coil as receiver. Solid murine KHT tumor, grown in the thigh of C3H/HeN mice i.m., was imaged pairwise with a slice thickness of 3 mm and resolution of 256 by 256 pixels. T1 and T2 values were determined by IR and CPMG sequence, respectively. Our preliminary data show: 1. Good contrast can be readily achieved between tumor and surrounding muscle, bone, and fat without contrast agent. 2. Tissue heterogeneity within a tumor can be delineated by T1- or T2-weighted images; such heterogeneities which probably reflect existence of viable and necrotic tissues and localized edema were observed in unirradiated and irradiated KHT. 3. A progressing elevation of effective T2 value were seen on days 4-5 and 7-8 postirradiation with 10 Gy or 35 Gy gamma-rays (Figure). Interestingly, the T2 increase on days 4-5 was consistent with the results from excised tumors whereas the increase on days 7-8 was opposite to that found in excised tumors. The latter difference is attributed to the inability of retaining radiation-induced fluid in the tumors during excision procedures. Mapping between MRI and histologic slice of same tumor sections will be illustrated to provide the histologic basis for T2 distribution within tumors.

Supported by NCI CA 39032 of DHHS.

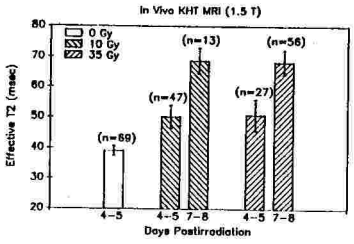

P54

TWO-SITE EXCHANGE ANALYSIS OF TRANSVERSE DECAY CURVES IN TISSUE

RV Mulkern, AR Bleier, FA Jolesz, KA Adzamli
Dept. of Radiology, Brigham and Women's Hospital, Boston MA

Although transverse magnetization decay rates in tissue may often be decomposed into a sum of two exponential functions, this has not led to a general acceptance of the two-site exchange model which predicts just such behaviour. The applicability of the model is difficult to assess largely because of the difficulty of extracting the model parameters from the experimental data. We have used the non-linear relations first proposed by McConnel (J. Chem. Phys. **28**:430, 1958), which relate the observed or apparent relaxation rates and volume fractions to the model parameters. We do not employ any of a variety of approximations used by previous workers. Since only three parameters are experimentally available from a single normalized biexponential fit and there are four independent model parameters, our calculations yield a range of model parameters which may produce a given biexponential fit. The parameters are the real volume fractions, the lifetimes of water molecules in each fraction and the transverse relaxation rates in each fraction in the absence of exchange. We also present a calculation that allows a unique evaluation of all the model parameters, using two normalized biexponential fits performed on a system in which the intrinsic relaxation rates have been changed with paramagnetic agents. The exchange rates and volume fractions are assumed to be unaffected by these agents. The experimental data used for analysis were transverse decay curves collected with a CPMG sequence on an IBM PC-10 Minispec. The biexponential fit to the data was made with a maximum likelihood method developed in this laboratory. The analysis has been applied to Mn^{++} doped whole blood (2 and 4 mM) to yield an extracellular volume fraction of 0.75 and an intracellullar lifetime of 21 ms for a water molecule, both in excellent agreement with the literature. Red and white rabbit muscle and sucrose gels treated with Gd-DPTA have also been subjected to the analysis, and we have evaluated the applicability of the two-site exchange model for these systems.

P55

^{31}P Magnetic Resonance Spectroscopy (MRS) of Normal Human Liver & Kidney

D.J. Meyerhoff, D. Rockey, G. Karczmar, M. Boska, G. Matson, and M.W. Weiner
Magnetic Resonance Unit, VA Medical Center, University of California, San Francisco

Our goal was to perform image-guided 3-dimensional localized ^{31}P MRS of human liver and kidney. Previous techniques (eg. DRESS) were critically dependent upon placement of a surface coil (S.C.) for accurate localization of the volume of interest (VOI). In contrast, the ISIS technique localizes the VOI using B_0 gradients. ISIS was modified for use with S.C. by addition of a composite pulse saturation sequence to avoid contamination of signal from outside the VOI due to T_1 smearing, which occurs during rapid pulsing. Computer simulation and phantom experiments demonstrated that spectra could be obtained without significant surface contamination. Human studies were performed on a Philips Gyroscan MRI/MRS system at 1.5 T, using a S.C. placed over the VOI. An external standard of hexamethyl phosphoroustriamide was used to optimize pulse length and quantitate molar concentrations of metabolites. The VOI was identified on the MRI image and ^{31}P MRS spectra were obtained in 10 - 30 min. Spectra from human liver, normal kidneys, and kidney transplants showed peaks for ATP, P_i, phospho-monoesters and phosphodiesters whose integrals were used for absolute quantitation. No phosphocreatine (PCr) was detected, indicating lack of contamination from surface muscle. However, absence of PCr makes it difficult to derive intracellular pH from the chemical shift of Pi. Our results demonstrate that image-guided 3-dimensional localized ^{31}P MRS spectra (ISIS) can be obtained from human liver and kidney in a clinical setting. Normal quantitative values obtained from these experiments will provide a basis to study the metabolic effects of renal and hepatic disease.

P56

In vivo ^{1}H Magnetic Resonance Studies of Leg Muscle
Narayana, P.A., Hazle, J.D., Jackson, E.D., Fotedar L.K., and Kulkarni, M.V.
The University of Texas Medical School at Houston, Department of Radiology, Houston, TX

The purpose of this work is 1) to investigate the variations of in vivo human ^{1}H MR spectra within different normal volunteers and day to day changes in the spectra on the same individual and 2) to compare two commonly used water suppression techniques to observe the resonances from tissue biochemicals. All the experiments were performed on 1.5 T SIGNA scanner. Six healthy volunteers were included in these studies. Proton spectra were obtained from the leg muscle using DRESS sequence. Water suppression was achieved either by using regular spin echo with long echo times (400-600 ms) or $1331(90^{o})$-τ-180^{o} (Sel) echo sequence with a 50 ms echo time.

The gross features exhibited by spectra with long echo times of different volunteers are similar and are reproducible. The region from resonances from the CH_2 and CH_3 groups of fatty acids dominate the 1 to 2 ppm regions. The peaks in the 3 to 3.2 ppm which arise from the $N(CH_3)$ of creatine, $N(CH_3)_3$ of choline. The resonances around 4.2 ppm arise from the lactate CH resonance. The water peak is at 4.76 ppm. The region between 5 to 6 ppm exhibits a number of resonances originating from glucose, nucleotides and unsaturated fats. The number of resonances and their relative amplitudes in the 1-2 ppm and 5-6 ppm region, however, was found to vary from normal to normal. The day to day variation of the spectra on the same normal was found to be fairly minimal. This indicates that the spectral variation observed between individuals is not due to the differences in shimming. The spectra show suprisingly large number of resonances from fatty acids. The long echo time used in these experiments enabled the acquisition of the full echo which eliminated the problems associated with the phasing of the FT spectrum.

The quality of the spectra obtained with the 1331-τ-180^{o} sequence was inferior compared to that obtained with long echo times without exception in all the six cases. Many resonances including the lactate CH and glucose were suppressed. The acquisition of half echo also poses problems with the phasing of the FT spectrum. Based on our observations, we conclude that it is preferrable to use a regular spin echo sequence with long echo time over the pulses for high resolution proton spectral studies in human muscle tissues.

P57

^{31}P COSY OF HUMAN ARM MUSCLE

Y.Ueshima,S.Yamai,T.Yamamoto,J.Hasegawa,T.Miyazaki,K.Hikida,K.Goto,N.Iriguchi,J.Takeda
Asahi Chemical Industry Co.Ltd. 221 Tanazawa,Atsugi,Kanagawa,Japan 243-02

Two-dimensional NMR spectroscopy was achieved in human arm muscle study. ^{31}P homonuclear chemical shift correlation spectroscopy(COSY) of a human arm was carried out on a 2.0 Tesla whole-body MR system Asahi Super-200. A 10 cm Alderman-Grant resonator of 34.47MHz was used. An N-type COSY sequence was applied. Sampling matrix was 1024×128, and spectral width was 2000 Hz along each axis. We chose a short repetition time (0.5sec),because ATP and ADP have short relaxation times. Signals were accumulated 32 times for each line,so the total time was approximately 35 minutes. The column axis of collected data was zero-filled to give a 1024×256 matrix. An exponential window was selected because of the short T2 of ATP and ADP. The arm muscle was kept relaxed during all the period.

The result is shown in figure 1. Diagonal peaks of Pi, PCr,γ,α and β-ATP appear clearly. α-β ATP cross peak at (16.1ppm,7.5ppm) and β-γ ATP cross peak at (16.1ppm,2.5 ppm) were recognized respectively. But α-β ADP cross peak at (7.5ppm,2.5ppm) was under the noise level.

We demonstrate two-dimensional NMR spectroscopy of human arm muscle. This investigation leads us to expect a method for observing ATP and ADP independently.

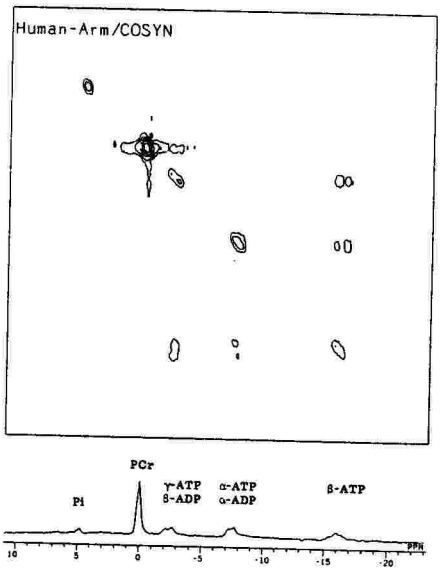

Fig. 1

PLENARY SYMPOSIA

FLOW IMAGING I

PS1

ADVANCED MR ANGIOGRAPHY

Dwight G. Nishimura
Department of Electrical Engineering, Stanford University

Over the past few years, noninvasive angiography by magnetic resonance has been an active and promising area of study in which a wide variety of methods have emerged. Generally, these methods combine flow sensitization with static material suppression and volumetric data acquisition (projection or 3-D imaging) to produce anatomic vessel images. The two main classes of flow effects – flow-dependent phase shifts resulting from gradient modulations, and so-called time-of-flight effects which depend on the spatial selectivity and timing of rf excitations – are often cited to distinguish the angiographic methods. Subtractive methods relying on flow-dependent phase shifts selectively dephase blood in one component image and rephase blood in the other component image, or, alternatively, create moderate phase shift differences in the blood signal between the two images. Time-of-flight-based methods employ either differential blood tagging or bolus tracking schemes to separate blood from surrounding static material.

With these methods, angiograms of cerebral and peripheral arteries and veins have been obtained with submillimeter resolution and in imaging times of less than ten minutes. With certain methods, both anatomical and physiological flow information are available. Coronary artery imaging presents significant challenges because of motion (both cardiac and respiratory), complex flow pathways, and undesired flow in the surrounding vessels and heart chambers.

This talk reviews, compares, and updates the status of the methods, and also discusses issues such as fast angiography, robust static material suppression, and artifacts due to irregular and higher-order flow.

PS2

CALIBRATION TECHNIQUES FOR REPHASING MOVING SPINS

GW LENZ, EM Haacke
Case Western Reserve University and University Hospitals of Cleveland

Motion of blood protons or organ movement during gradient application leads to spin dephasing and a concomitant loss of signal. With additional refocusing gradients to rephase moving spins the signal loss can be recaptured. These rephasing gradients can be simulated using a simple model taking into account gradient rise and fall times, and gradient delay times. Various optimization constraints are possible such as keeping all gradients the same amplitude to allow for high resolution, high S/N images, or to optimize for the smallest possible FOV. Sequences implemented according to theoretical solutions show remnant phase errors and necessitate calibration on a phantom. The utility of a flow phantom that produces constant velocity and accelerated flow components has been compared to a motion phantom which simulates true plug flow. Exact correlations of phase and velocity are possible with the latter phantom, and independent calibration of velocity and acceleration has been obtained. Allowing a small phase error for moving spins makes it possible to separate arteries and veins, or to measure velocity.

With short echo rephasing sequences phase effects due to higher order motion can be minimized and MR-angiography images can be obtained ungated. Projective gradient echo sequences although perfectly calibrated still suffer from severe susceptibility artifacts. This problem can be overcome with 3D volume sequences. In both techniques the optimal flip angle varies with the repeat time and blood flow velocity. Due to flow related signal enhancement, a repeat time of 100 ms and a flip angle of 40° has been shown to produce optimal C/N of flowing blood in the carotid artery at 1.5 T. Slightly lower flip angles were found optimal in the extremities.

In conclusion, calibration techniques are required when implementing flow rephasing sequences, because naive predictions may be in error if finite rise times or eddy currents are not accounted for, especially for long echo times which are clinically very important.

PS3

CSF FLOW PHENOMENA

William G. Bradley, M.D., Ph.D.
Huntington Medical Research Institutes, Pasadena, CA

Cerebrospinal fluid (CSF) is produced by the choroid plexus within the ventricles at a rate of 500 cc/day and flows through the outlet foramina of the fourth ventricle to be absorbed over the convexities by the arachnoid villi. Superimposed on this slow bulk flow is a much greater pulsatile motion due to transmitted cardiac pulsations primarily arising from the systolic expansion of the cerebral hemispheres. The to-and-fro motion of CSF through the foramen of Monro and aqueduct produces a "flow void" on spin echo images, particularly those acquired with greater T2-weighting and those acquired with thin slices using stronger gradients. On entry slices, high signal can occasionally be observed in these locations due to flow related enhancement. Such increased signal may simulate amass within the cisterns or ventricles.

Quantitation of CSF velocity requires the use of cardiac gating. Most velocity measuring techniques are derived from the original phase sensitive technique of Moran. In addition, the group at Massachusetts General Hospital has had some success quantifying flow using the "zebra stripe" technique. We have used a modification of the Moran technique developed by Feinberg, et al, to quantitate flow through the aqueduct in normal patients.

Such techniques have recently been applied to the evaluation of patients with chronic communicating hydrocephalus. Older patients with this syndrome may present with gait disturbance, dementia, and incontinence (i.e., "normal pressure hydrocephalus"). Such patients manifest a much greater flow void through ventricles due to a hyperdynamic CSF flow state. Recent work in our Laboratory by Whittemore, et al, modeling the brain with an electrical analog circuit suggests that increasing venous resistance and enlargement of the aqueduct itself may contribute to this hyperdynamic CSF flow state. Thus NPH may be primarily a disease of the cortical veins rather than of the periependymal tissues.

PS4 FLOW IMAGING II

APPLICATIONS OF INVERSION AND SATURATION TECHNIQUES

W. Thomas Dixon, Ph.D.
Emory University School of Medicine, Atlanta, Georgia 30322

Inversion or saturation of longitudinal magnetization by RF pulses introduces T1 contrast into images. When imaging moving tissues there are other interesting uses for these operations.

In some cases we want images of moving parts. Angiography is the clearest example because the motions are so large. Some methods are based on signal phase changes resulting from spins moving in a gradient; however, using inversion or saturation, it is possible to imitate conventional x-ray methods. A contrast medium is allowed to flow through the arteries into a region of interest. Images taken before and after arrival of the contrast medium are subtracted, leaving an image of vessels only. With x-rays, iodine is used for contrast; inverted or saturated blood protons are used with NMR. In this case inversion, signal negation, is preferable to saturation, signal nulling, since it provides twice the signal in the final difference image. Spins in a large region outside the ROI can be inverted all at once by a 180 pulse, or they can be inverted continuously by adiabatic fast passage as they enter the ROI, taking advantage of flow. Compared with phase-based angiography, these methods have a very limited range from labeling site to ROI since the label disappears in about T1. On the other hand, interference from veins and contralateral arteries is easily avoided.

Abdominal contents move with respiration. This brings unsaturated spins into a slice during imaging, reducing T1 contrast and smearing signal along the warp direction. Unsaturated blood flowing through a slice also spreads artifacts along the warp direction, further degrading images. Deliberate saturation of spins outside the slice restores image quality.

Moving fat in the abdominal wall deserves to be saturated, as it produces strong artifacts. This has been accomplished by inverting then waiting part of a fat T1.

PS5

MRI METHODS IN TURBULENT, VORTICAL, AND SWIRL FLOWS

Paul R. Moran
Bowman Gray School of Medicine, Department of Radiology
300 South Hawthorne Road, Winston-Salem NC 27103

In fluid dynamics, laminar streamline Poiseuille Flow is an unusual special case. Rotational fluid motions, however, are common and can be extremely stable; the possess large kinetic energy for relatively small net forward velocity (e.g., a smoke ring). Thus, even a small disturbance in flow vessels generate accelerations and pressure drops along the flow, so that the energy imparted to the fluid, downstream, is associated with rotational motions appearing as vortices. Both swirl flow (helical motion) and vortical secondary (eddies) flow are to be expected depending upon whether the vorticity-vector is along, or perpendicular to net flow, respectively. These secondary flows are relatively benign, nondissipative, and temporally coherent, but if MRI signals are phase-sensitized to motion then broad velocity distributions in local volume will generate phase-interference and NMR flow attenuation voids.

Turbulent flow, on the other hand, is highly dissipative, associated with extended pressure drops, and characterized by random, temporally incoherent short-lived vortices. However, with uncontrolled phase-sensitization, the temporal incoherence inherent to turbulence also produces strong flow voids. In observing these phenomena, it is mandatory to understand, consequently, and control MRI gradient modulations, so that turbulent, helical, and vortical flows are not "accidentally" admixed to indistinguishable strong attenuation artifact sources. In an exception to Murphy's Law, the time and distance scales easily obtained in MRI methods are matched almost ideally to those for blood-viscosity turbulent flows, and the coherent vortical and helical phenomena. Thus MRI sequences can be designed specifically to encode (or null code) all such blood flow behaviors, a measurement potential which previously has never existed as an instrumentation possibility, for liquid state flow.

PS6

CLINICAL APPLICATIONS OF CARDIAC GATED FAST SCAN IMAGING

RJ Herfkens
Department of Radiology, Magnetic Resonance Imaging Section, Duke University Medical Center

The intrinsic sensitivity of nuclear magnetic resonance to flow phenomenon has specific advantages and disadvantages in cardiovascular imaging. The recent advent of gradient refocused echoes, methods of motion artifact reduction, and velocity and excelleration compensation have combined to provide a useful method for evaluating cardiac structure and function. The combination of gradient refocused imaging techniques with cardiac gating has overcome many of the limitations of simple spin echo gated images. The addition of significant temporal resolution in a high contrast format has allowed exquisite anatomic and physiologic data to be obtained from the same examination.

The basic technique utilizes a gradient recalled echo with limited flip angle excitation. Up to four slice levels can be obtained in one acquisition. Up to 32 phases of the cardiac cycle can be obtained at each of these levels. The acquisition technique advances the phase encoding gradient with each heart beat, allowing acquisition of these slices in as little as 128 or 256 heart beats for a typical acquisition time of 3 to 4 minutes.

The high contrast tomographic presentation of data allows the calculation of a number of functional parameters. Ejection fractions have been correlated with correlation coefficients varying from .88 to .99. The ability to calculate right ventricular and left ventricular stroke volumes has allowed calculation of regurgitant fraction. The acquisition of data in the oblique plane appears to have some benefits in increasing accuracy of stroke volume measurements. Wall thickness and wall mass measurements have correlated well in animal studies and may provide a potential for following intervention such as valve replacement.

The strong relationship between flow, vortices, and turbulence allows a sensitive measure for valvular regurgitant lesions. Focal areas of decreased signal originating from a valve at the appropriate point in the cardiac cycle can localize a valvular lesion as well as provide a relative and potentially quantitative assessment of the valvular lesion. Similarly, flow changes associated with major vascular lesions such as aortic aneurysms and/or dissections can be accurately evaluated with this high contrast tomographic method.

In conclusion, rapid dynamic cardiac acquisition with gated gradient refocused echoes provides not only useful anatomic information but provides the necessary functional information for evaluating dynamic cardiac processes.

PS7 FAST IMAGING

RAPID SCAN MAGNETIC RESONANCE IMAGING: AN OVERVIEW

FW Wehrli
General Electric Medical Systems, Milwaukee, WI

The original contention that magnetic resonance would inevitably be far slower than its closest diagnostic counterpart X-Ray CT has, fortunately, not materialized. Not only is MR comparable to CT in imaging speed, there are clear indications that it might actually be faster. The finite duration of the spin lattice relaxation times, typically of the order of hundreds of milliseconds up to seconds, was by many considered an insurmountable obstacle. However, the idea to reduce the pulse flip angle, familiar to spectroscopists ever since the inception of pulse Fourier transform NMR in 1965, is equally applicable to MR imaging when combined, for example, with gradient echoes. The latter have become practical thanks to recent improvements in shimming technology. Implementations of the idea have led to rapid pulse sequences, known under a variety of acronyms like FLASH, GRASS, FISP, FAST, etc., all variants of the basic partial flip angle gradient echo technique, implemented in both 2D and 3D versions. Artifacts due to intrinsic magnetic field inhomogeneities can be shown to be corrigible by shortening the echo time appropriately such that intravoxel phase dispersion is minimal. Alternative low-flip angle techniques using true spin echoes in conjunction with forced re-equilibration will briefly be discussed.

A second class of rapid scan experiments is based on novel ways of scanning across k-space. Among these are the spiral scan techniques where the gradients are oscillated in such a way that k-space can be mapped with a few FID signals, and echo planar imaging (EPI) in which a train of echoes is generated from a single excitation whereby each echo is separately phase encoded. These techniques have more recently been shown to bear the potential to acquire image data in a fraction of a second, thereby enabling freezing physiologic motion.

While most of the novel rapid scan techniques are unlikely to supersede conventional spin echo techniques in the near future, their clinical utility as a complement to existing techniques is undisputed being demonstrated.

PS8

Contrast and Signal-to-Noise in Fast Imaging: Expectation and Reality

E. Mark Haacke and Jean A. Tkach
Case Western Reserve University

Various fast imaging methods which are proving particularly successful today include: first, steady-state free precession (SFP), low flip angle, gradient field echo sequences; and second, echo planar techniques. The methodology has been introduced by the first speaker and clinical applications are addressed by the third speaker. In this presentation, the type of contrasts available with the different techniques will be covered.

The standard control for disease discrimination is a long TR, TE spin echo sequence which has sufficient T2 weighting to reveal abnormal tissue. The gradient echoes used in SFP techniques are susceptible to local field inhomogeneities and often make very poor T2 weighted images when acquired in a single slice mode. It is shown that T2* effects can be significantly reduced using a 3D acquisition mode. The SFP signal and contrast depend delicately on T1, T2, TR, TE, flip angle and the resonant offset. The theoretical and experimental contrast for FLASH, FISP (GRASS, FAST) and CE-FAST and other techniques will be compared. Practical difficulties relating to slice profiles, inhomogeneities and motion will be covered. Although deviations from ideal conditions can cause significant contrast changes, they can be successfully predicted as well. It is recommended that rf slice profiles be designed specifically for a given TR, T1 and flip angle. The role of phase imaging will also be addressed.

The fast sequences can be used to collect images in a few seconds. They are useful for real time contrast agent studies, respiratory studies and cardiac cine mode imaging. When many slices are required or volume imaging is used, the total scan time may take as long as a multislice, multiecho SE sequence. Hence, fast imaging may be a misnomer, nevertheless, the sequences being developed have considerable flexibility for contrast enhancement.

PS9

CLINICAL APPLICATIONS OF 3-D FAST IMAGING

VM Runge
Division of Magnetic Resonance, Tufts-New England Medical Center Hospitals

The clinical potential of 3-D FAST imaging is explored on the basis of patient studies. A 3-D FLASH sequence tailored for T1 contrast was assessed in 75 clinical examinations. This included studies of the brain, spine, and extremities. Design of the imaging sequence permitted selection of TE=8-18 msec., TR=0.02-0.07 sec., slice thickness of 0.5-2.0 mm. and 32, 64, or 128 slices. Scan times varied between 3 and 15 minutes. A Mipron workstation was employed for rapid reformatting of images in any arbitrary plane desired.

The introduction of 3-D FAST imaging techniques provides potential for major advance in MR, allowing the acquisition of thin high resolution truly contiguous slices. In clinical work, it has been noted that the ability to visualize pneumocephalus, abnormal iron deposition, and cartilage is superior with 3-D FLASH when compared to conventional 2-D spin echo techniques. When TE, TR, and tip angle are properly adjusted, greater T1 contrast can be achieved on 3-D FLASH than with short TE/TR spin echo sequences. Computer algorithms allow reformatting in arbitrary planes with little loss in spatial resolution, presuming that voxel size is nearly isometric in the primary data set. Work to date has been most successful in the head and extremities. In these areas, 3-D FLASH is advocated for improved lesion localization and depiction of small abnormalities. Satisfactory examination of the spine awaits introduction of successful motion compensation techniques. The clinical potential of 3-D FISP in the head and extremities is unexplored. Much of the utility of this sequence will depend upon future tailoring of the sequence to achieve maximal T2 contrast.

Software and hardware advances have made 3-D FLASH imaging a reality. The ability to obtain very thin truly contiguous slices throughout the region of interest in a reasonable scan time may lead to displacement of 2-D T1 weighted spin echo scans. 3-D FLASH offers the combined advantages of high resolution thin section imaging with the potential for data integration and display on a routine basis of thick sections in the three orthogonal planes, easing the task of clinical interpretation by the radiologist.

ABDOMINAL IMAGING

PS10

TECHNOLOGICAL PROGRESS IN ABDOMINAL MRI

ML Wood
Tufts University and New England Medical Center, Boston, MA

Many technological advances in MRI have had more impact initially for examinations of the head or extremities than for the abdomen. The abdomen is more difficult to image, primarily because of the motion of its organs. Numerous methods have been developed for suppressing the ghosts due to periodic abdominal motion and reducing the amount of blurring in MR images. A critical evaluation of respiratory gating, reordering of phase encoding, physical restraining, breath holding, restricting the field of view, STIR, averaging, pseudo-gating, and gradient moment nulling reveals that no single method is entirely satisfactory. However, several methods can be combined advantageously. For example, physical restraining and gradient moment nulling can usually be used together. Averaging or reordering of phase encoding can be added for even greater motion artifact suppression. Depending upon further technological advances that enhance the quality of fast images, breath holding could become routine for producing the sharpest abdominal images.

Some of the progress in abdominal MRI has been overlooked, because of the persistent problem with abdominal motion. Improvements in the design of rf pulses have not only provided better slice profiles, but have also succeeded in reducing the power absorbed by the patient. Lower deposition of power has allowed the acquisition of more slices and echoes without exceeding health regulations at high field strength. Also, the transmission of circularly polarized rf has improved the uniformity of abdominal images. Another technique is half-Fourier imaging, which is useful when there is sufficient signal-to-noise. Half-Fourier imaging needs only about one-half of the time to produce an image with the same spatial resolution, which might be useful for breath hold imaging.

The successful application of new MRI technology to the abdomen has been hindered by the extensive motion of the organs. However, progress in overcoming the deleterious consequences of abdominal motion should eventually allow the new techniques to make high resolution images of the abdomen.

PS11

THE RELATIVE ROLES OF MRI AND CT IN THE EVALUATION OF UPPER ABDOMINAL MALIGNANCY

PF Hahn
Massachusetts General Hospital/Harvard Medical School

Any comparison of MR and CT for the evaluation of patients with possible malignancy must begin with a clear specification of the problem to which upper abdominal imaging is to be applied. A technique which offers detection of focal hepatic lesions with a high degree of accuracy may, for example, ultimately prove to be an inadequate staging method if extrahepatic lesions involving the pancreas, adrenal glands, kidneys, para-aortic region and spleen are overlooked. Conversely, liver imaging that offers important diagnostic clues to distinguish cavernous hemangioma from metastic disease may in some instances be preferred to a highly sensitive technique that provides little specificity. Questions of exam cost and patient throughput, operator dependence and potential hazards of the exam must be considered in defining the roles of various cross-sectional imaging modalities. Moreover, generalizations are especially hazardous as machine characteristics and pulse sequence implementation vary widely among MR facilities.

A blinded retrospective analysis has recently been reported, comparing MR at 0.6T with iodine contrast CT in 135 cases of suspected hepatic malignancy and normal volunteers. Sensitivity and specificity were analysed simultaneously, to correct for systematic under- or over-reading by the 3 experienced observers.The MR exam, consisting of a short TR/short TE T1-wtd. spin echo pulse sequence combined with a T2-wtd. pulse sequence, demonstrated a lesion in 82% of the abnormal livers, indistinguishable from the 80% detected by CT. 99% of MR exams of normal volunteers were interpreted as normal, compared to 94% of the CT. Overall, MR detected 64% lesions vs. 51% detected by CT. MR more often permitted a tissue-specific diagnosis of cavernous hemangioma vs. metastais, without need of a specifically tailored exam. In this and other studies, MR competes favorably with CT but without the possible toxicity of iodine contrast.

The major limitation of hepatic MRI is that it does not simultaneously survey the entire upper abdomen. Inferior resolution of MR images restricts sensitivity of MR for extrahepatic pathology. Moreover, GI contrast materials are available to distinguish bowel from non-bowel structures and to outline the head of the pancreas in CT; but oral contrast agents for MR are still under development. No consensus has been reached as to a preference for positive or negative contrast. Neither MR nor CT is currently effective for detecting splenic malignancy, but the advent of injectable reticuloendothelial-specific MR contrast agents may lend new importance to MR for imaging lymphomas. MR-guided biopsy techniques are in their infancy, requiring unique technology and special precautions.

PS12

MAGNETIC RESONANCE ON THE UPPER ABDOMEN.

G.M.Bydder - Hammersmith Hospital, Du Cane Road, London W12 0HS
I.R.Young - Picker International, Wembley, UK.

There are now a variety of approaches to NMR of the upper abdomen each with their advantages and disadvantages. Our own preference has been for respiratory ordered Phase Encoding (ROPE) (1), the short TI inversion recovery (STIR) sequence (2), T_2 dependent field echoes (3) and Motion Artefact Suppression (MAST).

The STIR sequence displays high sensitivity within the liver in detecting metastases although specificity needs to be established by fine needle biopsy.

The rapid T_2 sequences display lower levels of contrast than the STIR sequence but may be particularly useful in detecting hepatic iron overload.

Vascular detail is obtainable through use of the STIR sequence although separation of lesions from bowel loops remain a problem.

1. Bailes DR, Gilderdale DG, Bydder GM et al.Respiratory ordered phase encoding (ROPE): a method for reducing respiratory motion artefact in magnetic resonance imaging. J Comput Assist Tomogr 1985; 9(4):835-838.
2. Bydder GM, Young IR. MRI: Clinical use of the inversion-recovery sequence. J Comput Assist Tomogr. 1985; 9(4): 659-675.
3. Bydder GM, Payne JA, Collins AG et al.Clinical use of rapid T_2 weighted partial saturation sequences. J Comput Assist Tomogr 1987; 11(1): 17-23.

PS13

Considerable controversy exists as to the optimal technique for abdominal imaging, in terms of field strength and pulse sequence, as well as to the precise clinical role of magnetic resonance imaging in the abdomen and pelvis.

Heavily signal averaged short TR/TE pulse sequences, short TI inversion recovery sequences, long TR/TE pulse sequences with respiratory and flow compensation, as well as gradient echo pulse sequences have all been advanced as the optimal approach to magnetic resonance imaging of the abdomen. In practice, the "optimum" techinque may vary from unit to unit depending on signal to noise considerations, software availability, and practical duty cycle times.

MR is clearly a sensitive method to detect focal liver disease, yet its precise role vis-a-vis computed x-ray tomography is still unclear. This in part due to difficulties in comparing results obtained on different instruments, changes in technical approaches, and problems in providing and adequate "gold standard" for the comparison. While recent results suggest that MR compares favorably with computed tomography, further studies are required to definitively ascertain this.

Increased clinical experience with liver magnetic resonance imaging has improved our ability to characterize lesions which have been identified on MRI. Cavernous hemangiomas typically are lesions with high signal intensity on long TR/TE images. These have been successfully characterized by calculation of T2 values, and through the use of contrast to noise ratios combined with recognized morphologic features of these lesions. Focal nodular hyperplasia may also be identified on magnetic resonance images. These lesions typically appear isointense on the short TR/TE pulse sequences and may demonstrate the characteristic central scar. The signal intensity of the central scar may vary somewhat on the long TR/TE images. Experience with metastatic disease to the liver has demonstrated that the signal intensities of metastatic lesions vary considerably on the long TR/TE images. Both high signal intensity lesions and low intensity lesions may be identified. In addition, a high signal ring around metastatic foci may be commonly identified, this appears to relate to peripheral vascularity and/or edema which commonly surround these lesions.

MRI continues to demonstrate increasing utility in staging pelvic neoplasms. This is particularly true for cervical, prostate and uterine cancer. MR is also an effective tool to follow post treatment changes and to differentiate recurrent tumor from fibrosis.

IMAGE QUALITY, SEQUENCE OPTIMIZATION & MR HAZARDS

PS14

ARTIFACTS - LIMITATIONS TO MR IMAGE QUALITY

MJ Bronskill
Department of Medical Biophysics, University of Toronto

Artifacts exist in MR images in wild and prolific variety, an observation which is not surprising considering the complexity inherent in the MR imaging process. In this presentation artifacts are defined as signal intensities in an MR image which do not correspond to the true spatial distribution of tissues and tissue parameters in the plane of the patient being studied. Specifically excluded are those artifacts caused by defective components or malfunctions of the imaging system.

The original motivation for studying artifacts was twofold: i) recognition of artifacts in order to avoid image misinterpretation and ii) understanding the origins of artifacts in order to reduce or eliminate them. Initially these were separate issues with clinicians concerned primarily with the former and physicists and engineers interested mainly in the latter. A broader and more unified perspective is now emerging in which artifacts are actually the visual representations of the current limitations of MR imaging. As such, they become the focus for research and development, leading to new capabilities for MR imaging. This presentation will identify and illustrate artifacts which are current limitations to MR image quality and suggest directions for improvement.

PS15

IMAGE CONTRAST AND PULSE SEQUENCE OPTIMIZATION

DD Stark
Department of Radiology, Massachusetts General Hospital

Diagnostic images are acquired to detect disease, identify its histologic nature, and determine its extent. Screening, tissue characterization, and staging usually require different techniques, and in the case of MRI, different pulse sequences and timing parameters. The performance of diagnostic techniques for detecting pathology is quantitated as true positive and true negative fractions (TPF and TNF) which are correlated with lesion conspicuity. In turn, lesion conspicuity on magnetic resonance images can be quantitated as the difference in signal intensity between the lesion and the normal organ, scaled to random variations in pixel signal intensity or noise. This quantitative figure of merit is known as the contrast-to-noise ratio (CNR). CNR varies in a predictable way among pulse sequences but shows some variation among imaging systems and individual patients. Nevertheless, for a population of patients, CNR is the parameter to be optimized in MR imaging. Characterization of pathologic tissue can be performed using the tissue signal-to-noise ratio (SNR), tissue/tissue intensity ratios on the same image, or combining data from multiple images to derive spin density or relaxation time data. Finally, tumor staging is primarily dependent upon morphologic demonstration of tissue planes and interfaces between normal and pathologic tissues. Pulse sequence optimization for staging will vary depending on the characteristics of the tissue interfaces to be delineated. Where fatty tissue planes are the major determinant of tumor staging, T1 weighted spin echo images offer the highest SNR and greatest anatomic resolution. Where muscle is the normal tissue to be contrasted against disease, T2 weighted spin echo images or STIR is preferred.

PS16 PS17

BIOLOGICAL EFFECTS OF MRI AND PRACTICAL ASPECTS OF PATIENT MANAGEMENT.

FG Shellock, W Pavlicek*
Cedars-Sinai Medical Center, Los Angeles, CA; *Cleveland Clinic, Cleveland, Ohio

The clinical application of MRI requires a recognition and an understanding of the safe levels of exposure to the different forms of electromagnetic radiation used for this imaging technique. In addition, proper screening practices and appropriate patient management must be implemented in order to ensure that MRI does not pose any undesirable risks.

The U.S. Food and Drug Administration has recommended acceptable levels of exposure to electromagnetic fields during MRI, which are as follows: static magnetic field - whole or partial body exposures of 2 T, gradient magnetic fields - 3 T/per second, radiofrequency radiation - whole body average specific absorption rate of 0.4 W/kg. To date, no adverse biological effects have been identified for MRI devices operating at these exposure levels.

In regards to patient screening prior to MRI, potential hazards are known to exist for patients that have certain ferromagnetic metallic bioimplants. These MRI-induced hazards may result from movement, the induction of electric current, or heating. In addition, metallic bioimplants may produce unexpected artifacts that simulate pathology and can cause erroneous diagnoses. MRI is contraindicated for patients that possess any mechanically, electrically, and magnetically controlled or activated devices including pacemakers, neurostimulators, cochlear implants, bone growth stimulators, and internal infusion pumps. The risks of using MRI during pregnancy will be discussed.

Several strategies have been proposed to manage claustrophobic patients including the use of special mirrors, glasses, psychological desensitization, and sedation. Monitoring high-risk patients with equipment that is easily modified to be compatible with the MRI environment will be discussed.

QUANTITATION of CARDIOVASCULAR FUNCTION

PS18

ABSTRACT NOT AVAILABLE AT PRESS TIME

PS19

MRI OF THE MEDIASTINUM

D. Hahn
Zentrale Röntgenabteilung, Poliklinik der Universität München

MRI of the mediastinum offers many new advantages in the evaluation of mediastinal diseases. The ability of multiplanar imaging improves the detection of lymphnodes in the subcarinal space and the hilum. The exact extent of mediastinal tumors and the infiltration of many mediastinal structures as the pericardium can be better delineated.

MRI has replaced CT and angiography in the evaluation of diseases of the thoracic aorta. Especially in high risk patients with dissecting aneurysms of the aortic arch MRI is able to demonstrate the total extent of the dissection, the intimal flap and the involvement of the arch vessels and to differentiate between the true and false lumen.

Gadolinium-DTPA has offered some new chances in the evaluation of mediastinal mass lesions. Solid mass lesions always show an enhancement after i.v. application of Gd-DTPA. The inner structure of the lesion like necrotic or cystic areas can be better depicted. The use of Gd-DTPA allows a better delineation of infiltrations of the pericardium or the wall of the great vessels.

Solid tumors and malignant lymphomas of the mediastinum show a different enhancement. 75 % of the malignant tumors have a signal intensity enhancement ratio which is significantly higher than the enhancement ratio of benign lesions. Follow-up studies of malignant lymphomas using Gd-DTPA seem to be helpful in the differentiation of residual tumor tissue and fibrosis. The advantages of Gd-DTPA in mediastinal diseases are the better tissue characterization and the replacement of T 2-weighted sequences a saving of time.

PS20

CINE MAGNETIC RESONANCE IMAGING OF THE HEART

CB Higgins
Department of Radiology, University of California, San Francisco

Magnetic resonance (MR) imaging, up to the current time, has been used primarily to define anatomical abnormalities of the heart. A new technique using electrocardiographic gating, partial flip angle of the RF pulse, and gradient reversal can produce 20 to 25 msec frames at the rate of up to 32 frames per cardiac cycle (cine MRI). Analysis of the cinematic display of MR images in normal volunteers, patients with myocardial infarction or with valvular regurgitant lesions was done to quantitate changes in ventricular volumes and regional wall motion and thickening during the cardiac cycle. These cines demonstrated atrioventricular regurgitation and the severity of it was estimated by comparing stroke volumes of the two ventricles. Cine MR also demonstrated regional left ventricular dysfunction by showing loss of wall motion and thickening. Thus, cine MR permits quantitation of cardiac function.

NON-INVASIVE MR ARTHROGRAPHY

PS21

MRI OF THE HANDS AND FEET

JS Hyde, JB Kneeland, A Jesmanowicz
Department of Radiology, Medical College of Wisconsin

The following technical problems have been defined in MRI of the hand using surface or local coils. (1) Patient comfort demands a supine position with the hand extended inferiorly. Furthermore the hand must be at the side rather than across the chest or abdomen in order to minimize motional effects. (2) Additional strategies for hand immobilization are required if the highest resolution consistent with the available signal to noise (S/N) ratio is to be achieved. (3) Surface coils often are not dominantly loaded by small structures such as a finger. In this case coils of the highest possible free-space Q are required. (4) The irregular geometry of the hand and wrist requires multiple coils.

To these ends, the following coils for the upper extremities have been made: a 4 cm diam counter rotating current (CRC) coil, a finger size excite-receive saddle coil, and two excite-receive Maxwell pairs -- one for the triangular fibrocartilage, and one for the elbow. Excite-receive local coils have advantages for imaging of the hand. We favor the exclusive use of such a coil in a saddle configuration for the fingers. A one turn solenoid for the finger can yield superior images, but the awkwardness of positioning is a considerable disadvantage. Excite-receive and receive-only surface coils perform similarly for the carpal tunnel.

The Maxwell pair excite-receive elbow coil also works well for the ankle, particularly for deep structures. It seems slightly preferable to a receive-only tandem axial pair of similar dimensions. The 4 cm diameter coil has been helpful in imaging the superficial plantar nerves on the medial side of the foot and in examining the Achilles tendon as well as other tendons of the foot. Receive-only surface coils are preferred for all superficial structures of the foot (less than 2 cm from the surface).

All images thus far have been at 1.5 T (GE Signa), 3 mm slices, 256 x 256 matrix over 8 cm x 8 cm FOV. Extensive verification studies of cross-sectional anatomy using a cryomicrotome have been carried out. Numerous examples of normal anatomy and of pathology will be shown in the course of the presentation.

PS22

MRI OF THE TEMPOROMANDIBULAR JOINT

SE Harms
Department of Medical Imaging, Baylor University Medical Center, Dallas, Texas

Disorders of the temporomandibular joint (TMJ) affect up to 28% of the population. The soft tissue detail of the TMJ provided by MRI provides a clear depiction of joint anatomy for the diagnosis of most significant TMJ abnormalities.

For quality MR imaging of the TMJ, the following technical factors are necessary: surface coils, gradient magnification, and thin slice images. Most current instruments are capable of producing useful images. Methods for improving image quality include specialized bilateral TMJ coils, 3DFT multislab acquisitions, and gradient echo sequences. The technical considerations involved in planning a scan protocol are discussed.

Internal derangements of the TMJ are diagnosed by the abnormal appearance of the articulor disc. The disc can be displaced, degenerated, thickened, perforated, or distorted. Adhesions, osteophytes, and inflammatory changes can also be present. Post-operative joints can be evaluated for surgical complications such as adhesions, inflammatory change, foreign body reaction, and prosthesis breakage or dislocation. Lesions other than internal derangements can produce TMJ-like symptoms. Inflammatory disease in the TMJ in the surrounding area as well as tumors can produce TMJ-like symptoms. Clinical examples of a variety of commonly encountered clinical situations are presented.

Most TMJ patients are young, otherwise healthy individuals. Once a reliable MRI scan protocol is developed, these patients can be scanned during periods of low usage such as nights and weekends. The TMJ examination can improve MRI utilization and efficiency to reduce the overall cost per patient.

PS23

MAGNETIC RESONANCE IMAGING OF THE KNEE

Magnetic resonance imaging (MRI) is a fast, reliable and accurate non-invasive technique for evaluating soft tissue and bony injury to the knee. The normal adult meniscus contains no internal signal on T_1 and T_2 weighted images. Signal within the meniscus is the hallmark of meniscal disease by MRI. Grade 1 intrameniscal signal is irregularly marginated signal which does not abut an articular surface. Pathologically, this corresponds with early degenerative change within the meniscus. Grade 2 intrameniscus signal is linear and frequently communicates with the capsular margin of the meniscus but not with an articular margin. Grade 2 signal corresponds with an intermediate grade of degenerative change pathologically. Grades 1 and 2 meniscal signals do not correlate with arthroscopically significant tears. Grade 3 signal is prominent signal intensity within the meniscus which abuts an articular margin. Grade 3 intrameniscal signal correlates with fibrocartilaginous separations of the meniscus pathologically and with frank tears at arthroscopy. MRI may be helpful in selecting patients with meniscal tears for meniscal repair rather than menisectomy and in following patients postoperatively. Magnetic resonance imaging is excellent in detecting and characterizing acute collateral and cruciate ligament tears. A large number of intracapsular and extracapsular abnormalities around the knee which present with knee pain can also be evaluated including: free fragments, meniscal cysts, patellar chondromalacia, Baker's cysts, radiographically occult fractures and tumors. In summary magnetic resonance imaging of the knee is an exciting non-invasive diagnostic modality which can accurately evaluate soft tissue and bony disease in and around the knee and, thus, aid surgical planning.

HEAD & SPINE

PS24

MRI OF HEMORRHAGE

RN Bryan
Baylor College of Medicine Magnetic Resonance Center

The appearance of hemorrhage on MRI is more complex than CT, but also potentially more informative. With CT, the appearance of hematoma is due to variation in a single tissue component--hemeprotein concentration-- on the single CT parameter--linear attenuation coefficient. With MRI, not one, but three tissue parameters are measured- spin density, T1, and T2, and there are at least four different components of hemorrhage which affect each of these NMR parameters differently. Furthermore, there is a magnetic field dependency of some of these effects and hematomas may appear differently on different field strength instruments

In the hyperacute stage, hemorrhagic lesions appear bright on spin density, T1, and T2 weighted images on lower (approximately 0.5 T strength) systems. With higher (and possibly lower) field instruments, there may be low signal intensity (relative to brain) on T2 weighted images due to the paramagnetic-magnetic susceptibility effects of intracellular deoxyhemoglobin and the fibrin clot.

In the acute (2-4 days) stage, the hemorrhage appears isointense to bright on spin density weighted images; dark, isointense or bright on T1 weighted images; and isointense to bright on T2 weighted images. The appearance at this stage of the hemorrhage is quite variable as a number of events are simultaneously occurring, the exact timing of which will determine final signal intensity. During the late acute (4-10 days) stage of the hematoma, lesions will appear bright on spin density images; bright on T1 images; and in general, bright on T2 weighted images. The relatively unique bright appearance of hemorrhage on T1 weighted images at this stage is due to methemoglobin in extracellular fluid.

In the chronic (greater than 10 days) stage, the hemorrhage usually has two distinct components, a central area which appears bright on spin density, T1, and T2 weighted images, and a relative thin peripheral rim which appears dark on all three types of images.

Sponsored by NIH grant 5-R01-MS19056-05

PS25

CLINICAL UTILIZATION OF GRADIENT REFOCUSED IMAGING SEQUENCES

K.R. Maravilla
University of Washington School of Medicine

Gradient refocused pulse sequences or partial flip angle sequences were initially introduced to obtain images very rapidly. These sequences introduce an additional degree of complexity since image contrast depends not only on TR and TE but also on the flip angle. These sequences are also prone to a number of image artifacts that include effects due to magnetic field inhomogeneity, magnetic susceptibility changes, chemical shift effects and accentuation of flow effects.

With increased understanding and experience with partial flip angle sequences, many of these problems can be overcome or can actually be utilized to answer clinically relevant questions. Serial slice-by-slice acquisition technique enables one to obtain flow enhanced vascular imaging. Increased sensitivity for magnetic susceptibility changes can aid in the detection of hemosiderin when these changes are sometimes subtle or absent on standard T2 weighted imaging sequences. Use of gradient refocused images in the spine greatly aid in obtaining myelographic-like images of the spine in reasonably short imaging times. This presentation will focus on techniques used for gradient refocused imaging. Different clinical uses of these sequences will be illustrated.

PS26

NASOPHARYNX AND SKULL BASE
ANTON N. HASSO, M.D.

The clinical findings in patients with pathologic processes involving the nasopharynx and base of the skull do not permit precise identification of the structures involved nor of the extent of their involvement. In some cases, identification of the site of origin of a lesion is the determining factor in the differential diagnosis.

The abundant fascial planes of the nasopharynx result in exquisite MR scans of this region. Retropharyngeal adenopathy, tumor infiltration beyond the pharyngobasilar fascia and hypertrophy of lymphoid tissues are all readily seen on MR. Nasopharyngeal malignancies may demonstrate direct intracranial extention through the basal foramina and then follow the cranial nerves or vessels back into the cavernous sinus. This extension of tumors into the skull base is accurately depicted on multi-planer MR images.

Skull base lesions are usually recognized by deformities and displacements of both intra and extracranial structures. MR scans aid in making these diagnoses. In some cases, the MR signal characteristics are helpful in further illucidating the nature of the abnormality. Many nasopharynx and skull base tumors cause prolongation of both the T1 and T2 relaxation parameters. Some neoplasms contain a combination of tumor tissue, hemmorrage and/or cyst fluid with variable signal characteristics. Neurogenic tumors of the cavernous sinus have bright signals on T2 weighted images. Chondromas and chordomas are similar, but may be differentiated by their location and growth characteristics. Dermoid tumors and intraosseous cholesterol granulomas cause identifiable T1 shortening. Epidermoidomas have a multinodular appearance and cause T1 and T2 prolongation.

PS27

GADOLINIUM DTPA MR IMAGING IN THE SPINE
JS Ross
Dept. of Radiology, University Hospitals of Cleveland

Gadolinium DTPA, a paramagnetic contrast agent has been utilized to improve contrast differentiation of pathological processes, particularly on T1 weighted images. To date, the results have been very encouraging. It is efficacious in the evaluation of intramedullary neoplasms, inflammatory and demyelinating disease of the spinal cord. Neurogenic tumors, meningiomas and leptomeningeal spread of neoplasm are clearly depicted. Recent results in the evaluation of lumbar epidural fibrosis shows that there is consistent enhancement of scar facilitating differentiation from recurrent disk herniation. Intramedullary lesion enhancement occurs via passage of contrast media through alterations in the blood brain barrier with reduction in T1 and T2 relaxation times. Accumulation of contrast material also appears to occur through altered vessels in meningiomas, neuromas, leptomeningeal metastases and epidural fibrosis, presumably through "leaky" junctions or areas of intercellular gaps in the endothelium. The timing of the examination after the administration of contrast is crucial, particularly with epidural fibrosis. Preliminary results indicate that enhancement within the first 5 to 10 minutes is indicative of epidural fibrosis or venous plexus. The distinction between the two is not difficult because of their configuration and morphology. Herniated disk material does not enhance on early scans, but begins to show enhancement on more delayed images. This is presumably from diffusion of contrast from adjacent epidural fibrosis and/or normal venous structures.

The advantage of paramagnetic contrast agents in evaluation of the spine is obvious. Osseous and soft tissue contrast changes can be demarcated on T1W images. Gradient echo images which are strongly T1W also provide similar contrast information in shorter periods of time. Venous plexus enhancement may aid in increasing conspicuity of extradural structures, particularly the cervical spine where lateral and foraminal disease may be difficult to identify on routine MR studies.

SCIENTIFIC PAPERS

FLOW I

101

MR FLOW USING DIRECT PHASE ANGLE IMAGES

RR Price, DR Pickens, T Conturo, G Holburn, CL Partain, and AE James, Jr.
Department of Radiology, Vanderbilt University Medical Center

Constant flow along a bi-polar linear magnetic field gradient produces a shift in the phase angle of the transverse magnetization in direct proportion to the velocity component along that gradient direction. We have investigated direct phase angle images as an alternative to subtraction methods for MR angiography. Phase-angle methods eliminate subtraction artifacts and offer the possibility of obtaining quantitative flow magnitude as well as flow direction when 2-D flow encoding is utilized. Problems with the method include reduced dynamic range in the phase-angle images and flow redundancies in fast-flow conditions. The technique was initially investigated using a pulsatile phantom and then extended to animal models and human volunteers. EKG gating was used to select the velocity range over which the data could be acquired without wrap-around errors. Phase angle methods were found to produce images with usable contrast in phantom studies with pulsatile flow velocities within the physiological range. These images were correlated with information from an ultrasonic doppler flow probe and an inline flow meter. Animal and human volunteer phase angle images demonstrate flowing blood in the abdominal aorta with minimal phase errors. Subtraction of phase angle images from adjacent phases of the cardiac cycle are being investigated to correct for phase errors induced by transmitter/receiver phase inhomogeneities and other inhomogeneities which are induced by the standard imaging gradients.

Supported in part by NIH 1-RO1-33951

102

ANALYSIS OF FLOW VELOCITY PROFILES USING MRI

KA Kraft, PP Fatouros, SE Rittgers, DY Fei, P.R.S. Kishore
Dept. of Radiology and Bioengineering Program, Virginia Commonwealth Univ., Richmond, VA

Laser Doppler Velocimetry (LDV) has been used to validate MRI-derived flow velocities and to verify the accuracy of imaged fluid velocity profiles under a wide range of simulated vascular flow conditions. The flow model incorporated a paramagnetically doped aqueous dextran solution having a T1 relaxation time and viscosity similar to those of blood. This fluid was circulated at a constant rate through a 2.35 T horizontal bore magnet and was imaged under a variety of situations simulating normal and pathologic vascular conditions. The imaging sequence involved selective RF excitation of a slice perpendicular to the tube axis followed by gradient-refocused signal acquisition, with read-out along the flow direction. Fluid velocity profiles are visualized directly with this technique, and accurate velocity data may be extracted immediately from displacement measurements. Studies of developing laminar flow (entrance effects) over a range of Reynolds numbers have yielded results quantitatively in agreement with laser Doppler data. The appearance and resolution of turbulent flow due to axisymmetric stenoses have been investigated as a function of Reynolds number, degree of constriction, and displacement downstream from the stenosis. Beyond a 40% reduction in tube diameter, images clearly demonstrate jet formation, flow stagnation and reversal, regions of turbulence, and reestablishment of ordered flow distal to the constriction. Compiled velocity data (5 - 180 cm/s) measured using both MRI and LDV show quantitative correlation ($r = 0.991$). Such studies of simulated pathologic flow patterns may prove helpful in identifying specific vascular abnormalities in vivo.

103

MR ANGIOGRAPHY: APPLICATION TO CAROTID ATHEROSCLEROTIC DISEASE

S.R. Felber, P.M. Ruggieri, G.A. Laub, F. Aichner
SIEMENS MEDICAL SYSTEMS, ERLANGEN, FRG: DEPT. OF NEUROLOGY, UNIV. OF INNSBRUCK, AUSTRIA

Preliminary work has shown that MR is capable of demonstrating normal vessel anatomy. Clinical experience in imaging diseased vessels has been limited to date as MR angiographic techniques have just developed to the point of reliably visualizing normal vessels.

In an effort to assess the reliability of MR in imaging pathologic vessels, a pilot study was initiated with a series of patients who had ultrasound-proven disease of the carotid arteries. All examinations were done on a 1.5 T Magnetom. The study consisted of three parts. Phase and magnitude images were initially obtained using EKG triggering in an axial, multislice acquisition to localize the carotid arteries and obtain information regarding flow dynamics. Gradient motion refocussing and fast, gradient echo sequences were then used in a 3D data acquisition (2 mm sagittal or coronal slices) to obtain arteriogram images and serve as an additional screening examination for the presence of disease. If atherosclerotic disease was suggested in either of these two exams, a 3D isotropic data set was obtained to define the pathology more accurately. Total examination time did not exceed 40 minutes.

MR was found to be sensitive to the presence of stenosis, but tended to overestimate the degree of stenosis due to higher order motion in the post-stenotic flow. Ultrasound was certainly better able to identify ulcerating atherosclerotic plaques. MR, however, was better able to evaluate high carotid bifurcations and assess disease in the vertebral arteries.

104

AQUEDUCTAL STENOSIS: EVALUATION WITH GRADIENT ECHO ACQUISITION RAPID MR IMAGING

S.W. Atlas, M.D., A.S. Mark, M.D., E. Fram, M.D., A.J. Barkovich, M.D., D. Norman, M.D.
Department of Radiology, University of California, San Francisco

The basis of the detection of aqueductal patency on spin echo (SE) magnetic resonance (MR) imaging rests upon the recognition of aqueductal flow void due to rapidly moving cerebrospinal fluid (CSF). SE imaging has evolved into routine utilization of flow compensation techniques (such as cardiac gating or gradient manipulation) to improve image quality, which often results in absence of the aqueductal flow void, even in the normal patient. Gradient echo imaging with sequential acquisition is highly sensitive to flow and has been applied to the diagnosis and evaluation of intravascular flow with great success. Using appropriate parameters, one can also discriminate between flowing and stationary CSF with this technique.

Twenty normal volunteers (or patients scanned for unrelated reasons) were evaluated with sequentially acquired gradient echo images (GRASS) for assessment of aqueductal flow. Comparisons were made to 20 patients with aqueductal or periaqueductal lesions causing primary or secondary obstruction to flow through the aqueduct. All images used repetition time (TR) of 150 msec, echo time (TE) of 15 msec and flip angle of 50 degrees. All patients were imaged in the axial plane with both conventional SE and GRASS sequences. All long TR SE imaging was performed using flow compensation gradients (our standard head imaging regimen).

All patients with normal aqueductal flow demonstrated marked high signal intensity within the patent aqueduct on axial GRASS images which was readily discriminated from stationary CSF. GRASS imaging was highly sensitive to obstructed flow through the aqueduct, recognized by the absence of this focal hyperintensity normally present within the aqueduct, in patients with either primary or secondary aqueductal narrowing. SE imaging using flow compensation gradients did not allow clear distinction between patent and obstructed aqueductal flow. Therefore, we feel that rapid MR imaging with gradient echo acquisition may be a useful adjunct for the assessment of aqueductal patency and may be helpful in elucidating both normal and abnormal intracranial CSF dynamics.

105

CLINICAL USEFULNESS OF MR-ANGIOGRAPHIC IMAGES

F.L. de Laat
Philips Medical Systems, Best, The Netherlands

Non-invasive projective MR-angiograms can be obtained by modulus or complex subtraction of two images, which differ in signal intensity only at the locations of flowing blood.
Image acquisition can be done on standard MR-imaging hardware by interleaving two (or more) gradient-echo pulse sequences. These have different velocity sensitivities in each of the two orthogonal directions in the image plane. This type of pulse sequence allows us to acquire MR-angiograms, as well as flow velocity data related to vessel cross-sections.

The influence of choice of parameter-values and technique will be discussed in relation to angiogram quality for studies in the neck and leg and the thoracic and the abdominal aorta. Such variables include trigger delay, velocity sensitivity, modulus or complex subtraction, single or multiple heart phases, etc.

The MR-angiograms for patients showed promising correlation with conventional X-ray images (TLA or DSA).

A better understanding of vessel structure (veins, arteries) can be gained from the phase shift information in the vessel cross sections. A number of examples will be given.

106

SUPPRESSION OF ARTIFACTS DUE TO THROUGH-SLICE FLOW IN STEADY-STATE MR IMAGING

LM Eastwood, JB Murdoch
Picker International Inc., Clinical Science Center

Rapid imaging by means of steady-state field-echo pulse sequences (FAST, GRASS, FISP, etc.) is becoming increasingly popular in clinical practice. While the technique can be very valuable in eliminating motion artifacts due to breathing (as the short imaging times can allow breath holding), it has been found to be very susceptible to artifacts due to the flow of blood and CSF. Fluid flowing 'fresh' into the slice can give rise to a much larger signal than that from material which has reached MR equilibrium, and the pulsatility of the flow means that discrete 'ghost' artifacts are common. In some cases (e.g. assessment of vessel patency) this may yield useful information, but more commonly there is a danger of the artifact obscuring, or being mistaken for, pathology.

One approach that has been successful in reducing these artifacts in non-steady-state imaging is the pre-saturation of out-of-slice material (1,2). Out-of-slice magnetization can be excited by use of a computer-optimized out-of-slice selective RF pulse tailored to generate a clean slice profile while minimizing pulse length and RF power. This magnetization is dephased prior to the main pulse sequence; any material flowing into the slice of interest cannot then contribute signal. However, in steady-state sequences, in which T2-coherence maintains a signal at all times, any attempt to pre-excite out-of-slice material will set up a corresponding steady-state signal that cannot be suppressed. This signal can still be modified, however. In particular, we have demonstrated that, even in steady-state imaging, gradient manipulation may be used to time-shift the out-of-slice signal such that it is not observed during normal data acquisition. Although there is a signal-to-noise penalty associated with the time required for extra RF and gradient pulses, ghost artifacts are reduced when compared with standard steady-state sequences.

(1) RL Ehman et. al. Magnetic Resonance Imaging 5, 33. (1987)
(2) J Frahm, KD Merboldt, W Haenicke, A Haase. Magnetic Resonance in Medicine 4, 372. (1987)

107

MONITORED ECHO GATING (MEGA) FOR THE REDUCTION OF MOTION ARTIFACTS

RS Hinks
Picker International and University of Miami Radiology Dept., 1115 NW 14 ST, Miami, FL

Gating is one method of reducing the ghosting, streaking, and loss of resolution encountered when a patient moves during a scan. It is possible to use the data available in the NMR experiment itself to test whether the criteria for acceptance of data are met. This type of information can be obtained by collecting two echoes in a sequence. The image echo represents the image data and has the normally incremented phase encoding. The monitor echo has a fixed amount of phase encoding (not necessarily zero) and gives an indication of whether the conditions under which it was sampled are the same as for previous views.

To test the sensitivity of the monitor echo to changes induced by motion, a resolution phantom was imaged using a TE40 protocol which collected a monitor echo during the dephase lobe of the read gradient. The phantom was undisturbed in the first scan and was moved intermittently during the second scan (displacement = +/- 1cm). The deviation of each view of this monitor echo from a reference view was calculated by averaging views from that scan. As expected, very little deviation is seen for the data collected without motion, while large deviations are seen for the data collected during induced motion.

To test MEGA prior to imlementing it as a true gating technique, several sets of data from this phantom were collected under identical conditions with intermittent motion induced in each case. Each of these parent images was severely degraded by motion artifacts. A new image data area was then constructed view-by-view using the image data line of the scan which exhibited the least motion in the monitor echo for that view. The resulting image exhibited almost no motion artifact and had resolution identical to that obtained when no motion occurred during the scan.

This new technique is proposed as a gating method which should be most applicable in anatomical regions which are difficult to monitor using conventional techniques (such as the orbit). Combination of MEGA with other motion-suppression techniques should offer even greater insensitivity to the effects of patient motion.

108

A SHORT-TR PULSE SEQUENCE FOR MR FLUOROSCOPY

F Farzaneh, JN Lee, TA Tascyian, RC Wright, SJ Riederer
Duke University Medical Center

Using current implementations of limited flip angle pulse sequences (FLASH, FISP) a complete image can be acquired in about 2500 ms. While this is considered fast for many applications, an imaging rate of .5 images/second is too slow for observing some dynamic phenomena. To address this we are developing the method of MR Fluorosocopy. MR Fluoroscopy is a technique, similar to X-ray Fluoroscopy, which allows fast localization of pathology via true realtime imaging. Short acquisition times are obtained by reducing the TR time and the number of phase encodings of a basic FLASH sequence. For example, in a sequence with a TR of 13 msec and 32 phase encodings, a complete image may be obtained in about 400 ms, yielding imaging rates of over 2.5 images/second. The effect of a shortened TR is seen as a lowered signal to noise ratio. Similarly, a decrease in the number of phase encodings results in degraded spatial resolution. Nonetheless, in specific clinical settings the decrease in image quality is tolerable and offset by the increase in temporal resolution. We demonstrate how TR can be reduced by increase of readout bandwidth, reduction of the number of readout points, and reduction of RF and gradient pulsewidths. The minimum duration for TR is limited by theoretical and practical boundaries. For example, the gradient strengths must be increased to offset the reduction in pulsewidths. Hence, the minimum pulsewidth is determined by scanner hardware. Problems encountered when attempting to image with such short TRs are presented. The trade-offs between temporal resolution and image quality are demonstrated quantitatively and experimentally. Images acquired with this sequence are compared to standard FLASH images. Finally, the efficacy of this pulsing technique in capturing the motion of dynamic phenomena is demonstrated.

FLOW II

109

SPATIAL PRESATURATION: A CLINICAL AND TECHNICAL EVALUATION

JP Felmlee, RL Ehman, PR Julsrud
Mayo Clinic and Foundation, Rochester, MN 55905

Spatial presaturation has proven beneficial for artifact suppression in clinical magnetic resonance imaging. This technique is useful for flow artifact suppression, as a method to eliminate aliasing often associated with small fields of view, and to minimize the signal from tissues which move into the plane of section during image acquisition as a result of physiologic motion. In some cases a multi-axis implementation has been used to provide the benefit of flow artifact and tissue signal suppression within a single image acquisition.

The purpose of this study was to determine the technical parameters which optimize spatial presaturation. Quantitative flow and stationary tissue imaging experiments were conducted to determine the presaturation parameters that provide maximum flow artifact and tissue signal suppression. The following parameters were evaluated: presaturation RF amplitude, spectral content, timing within the imaging sequence, effective TR within the presaturation regions, TE, TR, presaturation region width, presaturation region to image volume gap, and image slice thickness. After the complete phantom analysis, the optimal parameters were evaluated in imaging of normal volunteers.

Although flow artifact intensity was routinely decreased by 75 percent in both partial saturation and T2 weighted images, greater benefit was found in partial saturation images. Flow artifact suppression was found to be dependent on the effective TR within the presaturation regions, but relatively insensitive to the presaturation RF amplitudes and timing within the sequence. Tissue signal intensity could be decreased by 90 percent by presaturation. Tissue signal suppression was found to be insensitive to the effective TR within the presaturation regions, but critically dependent on the presaturation RF amplitude, timing within the sequence, and tissue relaxation times. Although the presaturation requirements appear to differ for flow and tissue signal suppression, one combination of presaturation nutation angle and timing within the sequence was found to be useful for both flow and tissue signal suppression within partial saturation and T2 weighted images.

110

PRESSURE - GRADIENT IMAGING BY NMR FLOW ZEUGMATOGRAPHY

O. Nalcioglu
Department of Radiological Sciences, Division of Physics and Engineering, University of California-Irvine

Characterization of flow in the cardiovascular system usually involves the measurement of pressure, volumetric flow or time dependent velocities. The measurement of these parameters in the cardiovascular system turns out to be rather difficult since one is usually dealing with unsteady flow. Furthermore, physiological changes may also take place during, or due to, the measurements thus perturbing the system under examination.

Here, we describe a non-invasive technique for generating pressure-gradient images of flow fields using NMR flow zeugmatography in conjunction with some concepts from fluid mechanics. An accurate measurement of dynamic pressure depends, among other things, on a thorough knowledge of the response of the transducer. Ideally, a "conventional" pressure transducer should be placed in the field of measurement to avoid any possible transient disturbances. However, for physiologic measurements *in vivo*, this may not always be feasible.

The flow velocity zeugmatography technique may be used to measure $\mathbf{v}(\mathbf{r},t)$ where $\mathbf{v}$ is the velocity of the fluid at a given point ($\mathbf{r}$) in space and at time t. Once the velocity field $\mathbf{v}$ is determined using flow zeugmatography it may be related to the gradient of pressure (∇p) using the Navier-Stokes equation .

$$\partial \mathbf{v}/\partial t + (\mathbf{v}\cdot\nabla)\,\mathbf{v} = [-\nabla p + \eta \Delta \mathbf{v}]/\rho \qquad (1)$$

In equation (1), $\mathbf{v}$, the dynamic pressure p and density ρ are functions of $\mathbf{r}$ and t. The dynamic viscosity η can, in general, be a function of the same variables. In writing eq.(1) we set the hydrostatic pressure term to zero. The complicated non-linear differential equation given above describes the evolution of an incompressible viscous fluid. If one is dealing with a steady flow then eq.(1) becomes drastically simplified. In a general case when none of the terms in eq.(1) are zero it can be rearranged to yield the pressure-gradient image "∇p" defined by,

$$\nabla p = f(\mathbf{v}, \rho, \eta, \mathbf{r}, t) \qquad (2)$$

The function f given in eq.(2) can be evaluated using eq.(1). In the case of cardiovascular system we can use the known values of ρ and η along with the zeugmatographically measured $\mathbf{v}$ to compute the pressure gradient. The pressure itself can also be computed by integrating equation (2) and using the appropriate boundary conditions.

The technique described here should yield the pressure-gradient as a function of $\mathbf{r}$ and t and does not suffer from the gross oversimplification one introduces when one applies the Poiseuille's law to the cardiovascular system. The pressure-gradient imaging technique introduced here should also find useful and unique applications in fluid mechanics. Other fluid mechanical properties such as the kinetic energy could also be imaged by an extension of the ideas presented here.

111

FLOW QUANTITATION WITH A MULTI-HEARTPHASE FLOW ADJUSTABLE GRADIENT ECHO SEQUENCE.

P van Dijk,JP Groen,RG de Graaf,JML Engels,FLMAH de Laat,JHW van den Hout*, GB Cranney**.
Philips Medical Systems, Best, The Netherlands. * University Hospital, Utrecht, The Netherlands. ** Cardiac NMR Laboratory, University of Alabama in Birmingham, USA.

Flow induced spin phase changes can be used to quantitate flow (1). Flow adjustable gradients (FLAG) were incorporated in a multi- heartphase gradient echo sequence to produce phase images with user defined velocity sensitivity (phase change per unit velocity) (2). Subtraction of flow compensated and flow sensitive phase images from thin slices across vessels then provides a means to calculate average and maximum velocity figures in the vessels of interest (3). If necessary the remaining phase errors after subtraction can be corrected by a non-linear phase correction scheme (4), while masking the vessels.

In the multi-heartphase imaging mode, using TR=30ms and a flip angle of 40 degrees, flow data is obtained for 20 or more points in the cardiac cycle in 4 minutes acquisition time and about 5 minutes processing time. This procedure can be applied for construction of flow curves from the intersected vessels. These curves in turn can be used as a preview of flow velocities in time to set sensitivity and delay for an MR angiographic scan. In itself the curves are of diagnostic value for e.g. regurgitant flow in the aorta, or flow direction determination of CSF flow in Silvius' aquaduct. Integration of flow curves in the ascending aorta has also been used to calculate reliable cardiac output figures for volunteers and patients.

References.
1. van Dijk P, JCAT 8,429,1984.
2. Groen JP,van Dijk P,In den Kleef JJE, SMRM,New York,p.868,1987.
3. Nayler GL,Firmin DN,Longmore DB, JCAT 10,715,1986.
4. In den Kleef JJE,Groen JP, SMRM,New York,p.29,1987.

112

PULMONARY ARTERY BLOOD FLOW PATTERNS STUDIED BY MAGNETIC RESONANCE

HG Bogren, RH Klipstein, RH Mohiaddin, SR Underwood, DN Firmin, DG Lowell, RSO Rees, DB Longmore
The National Heart and Chest Hospitals, London, UK

Pulmonary artery flow can be studied noninvasively by cine magnetic resonance velocity mapping, and it is potentially of interest in a variety of disorders. We have studied 25 normal subjects and 3 patients with pulmonary arterial hypertension, and comparison has been made with aortic flow and with left ventricular output measured from ventricular volumes. Pulmonary artery distensibility has also been measured from changes in cross sectional area during the cycle.

There was plug flow during most of systole with a small channel of reverse flow beginning just before pulmonary valve closure. The normal two dimensional velocity profile was skewed, but the direction of skew varied between individuals and throughout the cycle. 2cm above the pulmonary valve, the dominant direction of the skew was posterior, but immediately below the bifurcation it was anterior. There was no regular pattern in 2 subjects. Pulmonary flow, aortic flow, and left ventricular stroke volume showed very close agreement ($r = 0.96$, SEE = 8ml), validating the technique and suggesting a method for the measurement of intracardiac shunting. In the patients with pulmonary hypertension, pulmonary flow was reduced and there was an earlier and more extensive channel of reverse flow. Pulmonary artery distensibility (fractional change in area) was 0.07 (normal 0.25 to 0.30).

These studies validate magnetic resonance pulmonary artery velocity mapping and they illustrate potential sources of error in Doppler flow measurements. The abnormalities in patients with pulmonary hypertension suggest that the technique may be of value in such patients, but further studies are indicated.

113

CINE MAGNETIC RESONANCE VELOCITY MAPPING IN AORTIC DISSECTION

SR Underwood, HG Bogren, RSO Rees, RH Mohiaddin, DN Firmin, RH Klipstein, DB Longmore
The National Heart & Chest Hospitals, London, UK

Magnetic resonance is valuable in the detection of aortic dissection, but using spin echo sequences a thin intimal flap may be missed because of the signal void in each lumen. Another problem arises in the differentiation of a thrombosed false lumen from one containing static blood. The field even echo rephasing sequence (FEER) gives high signal from blood and allows the intimal flap to be seen more easily. Thrombus can also be distinguished by its intermediate signal. Cine imaging and velocity encoding of the phase of the signal produces quantitative velocity maps from which the direction and magnitude of flow can be measured.

5 patients were studied and velocity mapping was used in 3. The dissection involved the ascending aorta only in 1 patient, the descending aorta only in 2, and both parts of the aorta in 2. The amplitude reconstruction using the FEER sequence showed the dissection more clearly than the spin echo images, and in one patient, abdominal and iliac involvement was only shown by the FEER sequence. The false lumen contained static blood in 2 and thrombus in 1, and in 2 of these patients it was difficult to see this in the spin echo images alone. Velocity mapping showed no flow in the false lumen in 1 patient, and in the thrombosed lumen in another. In the patient with dissection of the whole aorta, antegrade flow was seen in both lumens in systole but retrograde flow was seen in the abdominal false lumen in diastole, suggesting that the false lumen provided a significant blood supply to abdominal organs. In the two patients in whom velocity mapping was not performed, the spin echo images alone provided the required clinical information in one, but in the other it was not possible to distinguish between a dissection and an aneurysmal dilatation lined with thrombus.

The FEER sequence aids the detection of aortic dissection and provides a distinction between thrombus and static blood. Cine velocity maps produced by encoding of phase provide flow measurements in both lumens, and haemodynamic information that may be valuable to the surgeon.

114

QUANTIFICATION OF MITRAL REGURGITATION BY MRI

D.Glogar, H.Mayr, S.Globits, A.Neuhold, L.Wicke, F.Kaindl
Kardiologische Univ. Klinik Wien, Vienna, Austria

It was the purpose of the study to evaluate the potential of MRI and Cine-MRI in detection and quantification of mitral regurgitation. 25 patients with mitral regurgitation (15 with mitral valve disease and 1o with dilative cardiomyopathy) were examined in a 0.5 Tesla Phillips Gyroscan. In each patient a multiphase-multislice study in a transverse-coronal-doubleangulated projection (four-chamber equivalent) was performed. Right and left ventricular volumes, regurgitant fraction (RF) and ejection fraction (EF) were calculated using a special software-package (cardiac modul). In addition a cine study using fast flip angles (FFA) was done to visualize the regurgitant jet. MRI-data were compared to invasive measurement done by biplan angiography (EF, RF and volumina) and to noninvasive findings of 2-D-Echo-Doppler and colour-flow mapping.

Results: Good agreement of RF measurements between angiography and MRI (R=0.9); fair correlations consisted between visual analysis of angiography and MRI-RF (R=0.76), weak correlations between regurgitant mapping in FFA-MRI, Doppler-Colordoppler and Ventriculography. Doppler was sensitive in determining minor regurgitant lesions and tended to overstimate moderate regurgitation, while MRI was insensitive to minor regurgitations but accurate in moderate and severe regurgitant lesions. Particularly in patients with dilative cardiomyopathy and poor left ventricular function 2-D-Echo and colourflow mapping were unable to quantify regurgitant lesions, while MRI-RF and FFA-MRI showed good agreement with angiography.

Conclusions: MRI offers the possibility to noninvasively quantify mitral regurgitation but is of little use in evaluating minor regurgitant lesions.

115

POSTOPERATIVE ASSESSMENT OF TRANSPOSITION OF THE GREAT ARTERIES BY CINE MAGNETIC RESONANCE IMAGING

KJ Chung, RF Glass, IA Simpson, JR Hesselink, DJ Sahn
University of California, San Diego, CA

Systemic or pulmonary venous obstruction is a common complication of surgical repair of transpositon of the great arteries (TGA) by intra-atrial baffle procedure but is difficult to assess accurately using conventional noninvasive techniques. We studied the value of cine magnetic resonance imaging (MRI) in 9 patients (ages 5 months - 9 years) who had undergone an intra-atrial baffle procedure for TGA repair by either the Senning or Mustard technique. All patients under 5 years of age were studied under sedation with chloral hydrate (80-100mg/Kg) administered 20-30 minutes prior to study. Imaging was performed using a GE Signa 1.5 Tesla superconducting magnet with a 30° flip angle, echo time of 12 msec and repetition time of 22 msec. Images from 5mm or 10mm slices without interslice spacing obtained in standard planes and selected oblique planes were displayed dynamically in a cine loop format. Cardiac catheterization results were available for comparison in 8 patients. High resolution images of the venous inflows were obtained in all patients. The superior and inferior vena cavae were widely patent in 6 patients, 2 had obstruction identified in the superior vena cava and 1 patient had obstruction to both the superior and inferior vena caval limbs confirmed subsequently at cardiac catheterization and surgery. A dilated azygous system was also identified by MRI in all 3 patients with evidence of obstruction in the superior vena caval limb. Pulmonary venous inflow was also well visualized in all patients and showed evidence of obstruction in only 1 patient, substantiated by similar findings on echo/Doppler examination. Tricuspid regurgitation was seen on cine MRI in 3 patients and mitral regurgitation in 2. No patient had evidence of left ventricular outflow tract obstruction. Right ventricular ejection fraction assessed by cine MRI (range 58-81%) was within 5% of that determined by lateral plane angiography in 4 patients. In conclusion, cine MRI can provide important anatomical and functional information noninvasively in patients after surgical repair of transposition of the great arteries and is a safe, valuable alternative procedure for the serial assessment of these patients.

116

QUANTITATIVE ASSESSMENT OF FOUR-DIMENSIONAL CARDIAC NMR IMAGES

RI Pettigrew, T Noever, RL Eisner
Emory University School of Medicine, Atlanta, GA

Current dynamic NMR acquisition, analysis and display techniques provide qualitative and some quantitative evaluation of cardiac structure and global function. We show that additional quantitative regional information inherent in the images e.g. 3 dimensional (3D) end-diastolic (EDT) and end-systolic (EST) wall thickness, 3D systolic wall thickness change (WTC), 3D radial shortening (RS), 3D myocardial T2, % abnormal ventricle (%AV) based on either EDT, EST, WTC, RS, or T2, regional deviation of each parameter from normal (nl) and ventricular shape can be obtained through computer processing of the 4 dimensional (4D) cardiac data and then displayed in a compact 2D form. To extract these parameters, we have developed programs which convert endocardial and epicardial edges, obtained from spatially and temporally sequential cardiac short axis slices, into 2D parametric images--a "Bullet" plot (BP). These displays are scaled to the LV dimensions and provide geometrically accurate quantitative images of regional cardiac parameters. The value of each parameter is encoded in the display on a pixel-by-pixel basis by either color or grey scale intensity. We are generating 3D nl files for each functional parameter. Initial experience in ischemic and myopathic heart disease indicates that a set of BPs permits objective identification, quantification, and display of the precise 3D location, size and functional consequence of abnormal cardiac regions based on either abnl EDT, EST, WTC, RS, T2 or any combination of these parameters. The display of 3D systolic WTC, which is proportional to coronary perfusion, may permit identification and sizing of viable myocardium and determination of %LV scarred based on %AV. Thus BP simplifies and integrates the presentation of NMR cardiac information and provides a new objective quantitative assessment of regional structure and function.

FAST IMAGING

201

RAPID 3D SPIN-ECHO IMAGING USING LARGE FLIP ANGLE EXCITATION

JP Mugler, III, JR Brookeman
Departments of Biomedical Engineering and Radiology, University of Virginia

Most 3D techniques such as FLASH[1] employ field-echo acquisitions to collect the data. As compared to the spin echo, the field-echo data collection has a much greater sensitivity to susceptibility variations, field inhomogeneities, chemical shift, and flow. These characteristics may be an advantage or a disadvantage, depending on the imaging task at hand. The purpose of this work was to develop a spin-echo sequence with a repetition time (TR) short enough to allow the rapid acquisition of 3D spin-echo images. When TE $\ll$ TR the maximum signal for a two pulse Θ_1 - Θ_2 spin-echo sequence usually occurs for $\Theta_2 = 180°$. However, if TR/T1 is relatively small Θ_1 must be greater than 90° to achieve maximum signal. Thus, as TR is decreased, some of the accompanying signal loss can be recovered by increasing the excitation angle above 90°. It has been previously recognized that the optimum signal and contrast do not necessarily occur at $\Theta_1 = 90°$ for a Θ_1-180-echo pulse sequence.[2] The signal-to-noise ratio per unit time (SNR) versus T1 has been calculated from the Bloch equations for a 100/16 (TR/TE) 130°-180° sequence and for a 100/16 standard (90°-180°) sequence. For T1's of 0.5 and 1.0 sec, the SNR's of the former are 61 and 83 percent higher, respectively.

We have implemented a 100/16 130°-180° 3D spin-echo pulse sequence on a Siemens Magnetom 1.0T whole-body imager. This allows 16 128x256 3D images to be acquired in only 3.5 minutes. The quality of the slice profile and power deposition are prime considerations, since the sequence uses two high angle pulses. Both pulses are non-selective to achieve a uniform flip angle across the volume. With non-selective pulses, the region of sensitivity must be limited by proper choice of the imaging plane or by using a surface coil. Power deposition is not a problem using the non-selective pulses and TR = 100 ms. With a short TR, it is imperative to use a spoiler gradient that varies in strength from repetition to repetition in order to effectively dephase residual transverse magnetization.[3] Initial clinical experience with knees and ankles has been very encouraging. We use a 16 slice 256 x 256 acquisition with an in-plane resolution of 0.78 mm. The sequence requires 6.9 minutes. In this manner, we acquire high quality T1-weighted images across the whole joint with truly contiguous slices. The image quality is nearly identical to that obtained using our standard 2D SE/500/17 sequence.

1. Haase, A., J. Frahm, D. Matthaei, W. Hanicke, K. D. Merboldt. J. Magn. Reson., 67, 158, 1986.
2. Provost, TJ., R.E. Hendrick. Magn. Reson. Imaging. 4, 105, 1986.
3. Edelstein. W.A., P.A. Bottomley, H.R. Hart, L. S. Smith J. Comput. Assist. Tomogr., 7, 391, 1983.

202

TECHNIQUE FOR RAPID ROTATING-FRAME IMAGING

K.R. Metz*, J.P. Boehmer+
*Radiology Department, New England Deaconess Hospital, Harvard Medical School, 185 Pilgrim Road, Boston, MA 02215
+Department of Internal Medicine, University of Massachusetts Medical Center, 55 Lake Avenue North, Worcester, MA 01605

The rotating-frame imaging technique (Hoult, J Magn Reson 33, 183 [1979]) employs radio-frequency field (B_1) gradients to produce a spatial (x) dependence of the NMR nutation frequency: $F_1(x) = \gamma B_1(x)/2\pi$. In practice, one-dimensional spatial image data may be formed using the pulse sequence: (Preparation - n·P - FID Acquisition-Relaxation Delay)$_n$ where the rf pulse width n·P is incremented with the number of stored FID's. The image is formed using a 2D Fourier transform.

We demonstrate a much more rapid pulse technique for acquisition of rotating-frame image data:

Preparation - (P - Acquire One Point)$_n$ - Relaxation Delay

where successive points are acquired between pulses (P) of a long train. A one-dimensional Fourier transform may then be used to form the image. This approach can reduce the data acquisition time and total rf power deposition by five and three orders of magnitude, respectively. Furthermore, with suitable preparation, chemical shift information and relaxation weighting can be achieved.

203

SYNCOPATED PERIODIC EXCITATION (SPEX): FAST IMAGING WITH REDUCED SUSCEPTIBILITY ARTIFACTS

William Sattin
Picker International Inc., Clinical Science Center

Carr first demonstrated the steady-state free precession technique by applying periodic, equal and coherent rf pulses to a nuclear spin system. Haase et al. described the adaptation of this periodic string of rf pulses in the fast MR imaging technique, FLASH. This current investigation considers a related but different class of problems: the establishment of a steady-state via the application of a string of rf pulses, where there is not simple periodicity (i.e. no single interpulse period), and the rf pulses may be of different intensities. This class of problems has been designated **S**yncopated **P**eriodic **EX**citation (**SPEX**).

A particular SPEX sequence has been implemented which consists of a bundle of three rf pulses (interpulse spacing of T), where each bundle is separated by a time 2T. Actual data from this sequence is shown in the figure below. Continuous repetition of this sequence results in a steady-state echo forming at a time centered between the rf bundles. Since the echo occurs at a time when no rf is applied, it can be read out as in conventional SE imaging rather than as a gradient echo as in all contemporary steady-state based fast imaging sequences. This has the great advantage of retaining the echo's susceptibility, inhomogeneity and chemical shift refocusing properties. In particular, imaging sequences which use a gradient echo readout are troubled by image artifacts due to susceptibility variations within the patient. Additionally, SPEX offers greater flexibility in varying the time T and flip angle to alter contrast and/or acquisition time than do FLASH and CE-FAST.

Rapid head images were acquired with this SPEX sequence which displayed high GM-WM contrast and increased image quality due to the reduction of artifacts.

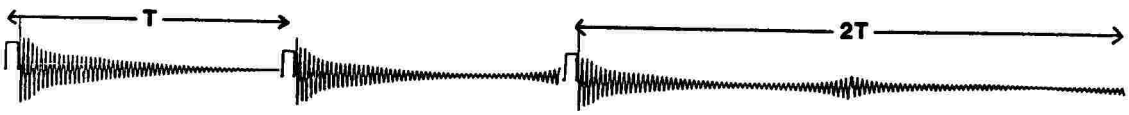

204

ON APPROACHING EQUILIBRIUM IN FAST MR IMAGING

W Sattin and JB Murdoch
Picker International Inc., Clinical Science Center

Recent advances in fast MR imaging have come about from the exploitation of steady-state NMR signals. Images with short acquisition times and useful contrast have been the result. While much effort has been put forth to comprehend how sequence parameters impact image contrast and acquisition time, less effort has been made to better understand the prerequisite to the fast image, namely, the approach to steady-state equilibrium. Depending upon relaxation times and particular sequence parameters, the time required to reach steady-state equilibrium may be on the same order as the time needed to acquire the fast image. Reducing the time required to establish a steady state is of importance in all fast imaging, but may be particularly crucial for cardiac and flow-related work. We have therefore examined, by simulation and empirical means, the effects of rf pulse shape, rf tip angle, rf phase, gradient waveforms and sequence timing upon the establishment of the steady state.

A bifurcated analysis was conducted. First, standard broadband, Gaussian, and apodized-sinc-shaped rf pulses were examined to characterize their efficiency at creating a steady state. Second, attempts were made to reduce the time required to reach the steady state by computer generating and implementing rf pulses optimally designed with this purpose as a constraint. The underlying concept was to create one set of rf pulses, gradient waveforms and sequence timing parameters that minimized the time needed to reach equilibrium, and another set which produced the desired image contrast and acquisition time. Each set was optimized for its respective function, insuring a smooth and continuous transition of the steady-state magnetization at their interface in time.

205

REAL TIME MRI

R. R. Rzedzian
Advanced NMR Systems, Inc., Woburn, MA

MR movies of the human heart in motion have been obtained in real-time with no cardiac gating. These were taken on INSTASCAN whole-body system operating at 2.0 Tesla designed and built by Advanced NMR Systems, Inc. (Woburn, MA). Each complete image was acquired in 25 milliseconds with a TE of 14 milliseconds using a new imaging technique. The technique is capable of producing images with relatively high SNR and resolution and has been used to demonstrate cardiac function and blood dynamics.

Instant imaging has recently been presented (1,2) which utilizes a 90°-180°-[acquire image] sequence, where a complete image is acquired by rapidly effecting a complete k-space trajectory in 26ms under a "conventional" spin echo envelope (elicited by the 180° RF pulse). In these images traditional T1 and T2 contrast is preserved through the use of the TR and TE parameters. By taking the [acquire image] portion of the scan and by reducing the 90° RF excitation to an α-pulse a sequence suitable for real-time imaging can be created. The new sequence consists of the following elements [α - pulse] [pre-encode][image acquire] and may be preceded by a "fat suppression pulse" and followed by an optional "coherence spoiler" pulse where necessary. The image contrast of such a sequence run in real-time is similar to that obtained by the many of the "rapid" sequences using low angle RF pulses with gradient echoes. Although, as averaging of the data over many partial acquistions is not performed in this case instant information about flow and motion can be obtained.

The technique was used with a TR of 100ms and TE of 14ms to obtain 16 ungated images in real time through the heart of an adult volunteer and spanned two complete cardiac cycles. The method has great potential applications in cardiac MRI and in the observation of non-repetitive transient phenomena especially in the investigation of flow and motion.

1. Rzedzian, RR, Pykett, IL. Radiology, 16(P), 333, 1986
2. Rzedzian, RR. A method for instant whole-body MR imaging at 2.0 tesla and system design consideration in its implementation. Soc. of Mag. Res. in Med. N.Y., July 1987.

206

MILLISECOND ABDOMINAL MR IMAGING AT 2.0T

S Saini, DD Stark, IL Pykett, RR Rzedzian, PF Hahn, J Wittenberg, JT Ferrucci
Department of Radiology, Massachusetts General Hospital and Advanced NMR Systems, Inc.

Instant Scan MR Imaging technique (1) allows image acquisition in as little as 1/25 of a second using a traditional SE pulse sequence, which has a TR value of infinity, and a TE that can be varied from 30 to 600msec. Such images exhibit pure T2 contrast and are free of motion artifacts. The images are also fat suppressed because only water protons are selectively excited. This study was undertaken to investigate the utility of this technique for detecting and characterizing lesions in the upper abdomen. The potential of using physiologic motion as a source of organ contrast (e.g., bowel vs pancreas) was also examined by acquiring multiple images in a single breath-hold using TR values of 1-2 sec.

Single slice transverse images were obtained at 2.0T using a 5mm or 10mm slice thickness in 4 normal volunteers and 17 patients. Images were evaluated for signal-to-noise (SNR) ratios, lesion-to-normal tissue, contrast-to-noise (CNR). Tissue T2 values were calculated from a monoexponential decay curve.

Images showed no degradation due to physiologic motion and showed high SNR. Lesions as small as 5mm were detected. Movie display of images obtained in a single breath-hold clearly distinguished peristalting bowel from adjoining viscera such as the pancreas. Normal liver had T2 values of 40-60msec; hemangiomas (n=8) 119-181msec; and liver metastases (n=5) 71-84msec. Fluid-containing structures such as the gallbladder, bladder, and renal cysts had T2 times of >600msec. Thus, high CNR were also present.

Due to exceptional anatomic resolution and extremely high lesion-tissue T2 dependent contrast, this technique offers a new dimension in abdominal MRI.

1. Rzedzian RR, Pykett IL. Instant images of the human heart using a new, whole body, MR imaging system. AJR 1987;149:245-250.

207

OPTIMIZATION OF GRASS IMAGING FOR ABDOMINAL MRI

R Weissleder, V Raptopoulos (*), DD Stark, R Waite (*), JT Ferrucci.
Departments of Radiology, Massachusetts General Hospital, Boston, MA and University of Massachusetts Medical Center, Worcester, MA (*)

Fast imaging with breath holding is an effective technique for reducing abdominal respiratory motion artifacts while increasing patient throughput. This study was designed to optimize gradient recalled echo (GR) imaging for abdominal MRI at 1.5 T. To compare directly contrast and signal-to-noise ratios (CNR and SNR) five normal volunteers were studied using a wide variety of spin echo (SE) (TR 300, 600, 1200, 2400, 3600 msec; TE 20, 40, 60, 80 msec) and GR (flip angle 15, 30, 45, 60, 75, and 90 degrees; TR 21, 100, and 200 msec; TE 12, 20, 30, and 40 msec) pulse sequences. Ten patients with hepatic tumors were also studied. Using SE pulse sequences the highest CNR was achieved using a T1-weighted SE 300/20 (CNR=-6.3) and a T2-weighted SE 3600/80 (CNR=+11.6). For GR pulse sequences the highest CNR was achieved using a short TR (100 msec), a short TE (12 msec) and a flip angle of 60 degrees (CNR=-11.6). With increasing TE and/or lower flip angle, spleen-liver CNR and tumor-liver CNR decreased to $|\pm 1.0|$. Comparing SE and GR pulse sequences with identical imaging parameters CNR did not vary significantly (-2.6 for the SE vs +2.7 for the GR). Background noise degrading image quality was lowest using the GR 100/12/60 pulse sequence.

208

OPTIMIZED FAST MR IMAGING OF LIVER AND SPLEEN WITH SUSPENDED RESPIRATION

J Griebel, G Laub, M Deimling, G Bongartz
Siemens AG, UB Med, STME 6, Henkestr. 127, D-8520 Erlangen, West Germany

Fast MR imaging with suspended respiration is a promising approach to minimize motion artifacts in the upper abdomen. Of primary importance in the clinical use of these new techniques is the contrast-to-noise ratio (CNR) between normal and pathological tissues. The purpose of the present study is (i) to clarify the signal behavior of normal liver and spleen using FLASH and FISP sequences, and (ii) to assess the optimal liver-to-spleen contrast achievable within the constraints of the measuring time imposed by breath holding. This contrast can serve as a figure of merit for the detection of hepatic lesions with elevation of both T1 and T2.
10 healthy volunteers underwent both FLASH and FISP MR imaging at 1.5 T (Siemens Magnetom). Scans were obtained within a breath holding interval of 15 sec. In general the following combinations of TR and TE were used : TR30/ TE10,16msec/ AC(no. of acquisitions) 4, TR120/ TE10,16msec/ AC 1. In 5 volunteers, sequences with bandwidth optimization (sampling time TS=15 msec for long TE; in all other scans: TS=7.68 msec) and/or sequences with ultrashort echo delay time (TE=6 msec) were used. The flip angle FA was varied from 5° to 90° in 15 steps.
The ROI signal intensity plots as a function of FA can be characterized by the slope of the initial increase and by the location (=Ernst angle) and the height of the maximum. Except for higher maximal intensities in FISP, the plots were similar for both sequences: for any combination of TR and TE, a steeper or at least equal initial increase and a smaller Ernst angle of the spleen was found as compared to the liver (Fig.1).

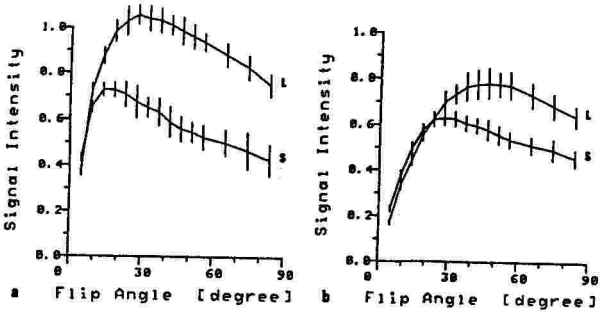

Fig.1: Roi signal intensity plots of liver (L) and spleen (S)
(a: TR 30 msec / TE 10 msec, b: TR 120 msec / TE 16 msec)

FLASH showed the best T2-weighted liver-to-spleen contrast at long TE/ small FA (TR=30 msec: 5°-10°, TR=120 msec: 7.5°-12.5° (Fig.1b)) and the optimal T1-weighted contrast at short TE/ medium to large FA (TR=30 msec: 35°-45° (Fig.1a), TR=120 msec: 60°-75°). The TR-influence on CNR's was relatively small. With all parameter settings, the T1-weighted contrast was stronger than the T2-weighted one. Significantly improved CNR's with respect to T1-weighted images could be achieved with an ultrashort TE. The measurements with bandwidth optimized sequences indicated some improvements of the T2-weighted CNR, but chemical shift artifacts increased. Except for a somewhat stronger T2 contrast, a similar contrast behavior was found in FISP images, especially with a long TR.

JOINTS

209

MRI OF THE SHOULDER WITH SURGICAL CORRELATION: A PRELIMINARY REPORT

DH Deutsch and JH Mink
Section of Magnetic Resonance, Cedars-Sinai Medical Center, Los Angeles, CA 90048

Although the MR anatomy of the shoulder has been well described, few reports have attempted to correlate the MR findings with that of surgery. MR evaluation of the shoulder presents several technical difficulties including the need for off-center imaging, oblique imaging planes and the requirement for a high degree of spatial resolution. In a retrospective analysis, we correlated results of MR findings in a small group of operated patients. In the course of evaluating our data we have developed a rapid imaging protocol and diagnostic criteria for the evaluation of shoulder disorders.

All studies were performed on a 1.5 T. MR imager (Signa, General Electric, Milwaukee, Wisc.). Since December 1986 80 shoulders suspected of rotator cuff tear or biomechanical impingement have been imaged using a variety of techniques. Our current routine employs an anteriorly placed 5½ inch surface coil and an initial off-center axial GRASS acquisition (TR 25, TE 13ms.) followed by a T1 weighted coronal oblique series (TR 700, TE 20ms., 256x128 matrix, 4 nex, 5mm interleaved) selected through the supraspinatus muscle and tendon. A third T2 weighted coronal oblique series (TR 2000, TE 20, 80ms.) is obtained if there is any question as to the integrity of the rotator cuff.

Criteria were established for rotator cuff tears as well as biomechanical impingement. MR findings were correlated with 10 operative cases. MR demonstrated rotator cuff tears in 7 patients and there was surgical confirmation in 6. The single false positive MR study demonstrated not only impingement and increased signal in the supraspinatus tendon but retraction of the muscle. The other 3 patients had surgically confirmed impingement.

Our preliminary results suggest that MR does offer the ability to localize and quantify abnormalities of the rotator cuff. In addition, MR can identify the causes of biomechanical impingement; evaluate the glenoid labrum and the integrity of the biceps tendon; and identify osteonecrosis. Therefore MR, as a single examination, can evaluate the complete spectrum of shoulder disorders.

210

OBLIQUE PLANE MR IMAGING OF THE BRACHIAL PLEXUS

AR Babaria, VM Rao, RJ Wechsler, MD Rifkin, HT Doan, MM Mishkin, CF Gonzalez
Department of Radiology, Thomas Jefferson University Hospital, Philadelphia PA 19107

Visualization of brachial plexus along its entire length is necessary, but difficult to obtain, especially in view of its complex anatomic relationship and oblique course from the lower neck, through the supraclavicular region, interscalene triangle and costoclavicular space into the axilla. CT is somewhat limited by axial imaging and streaking artifact from shoulders. MR delineates brachial plexus better than CT in the straight axial and coronal planes. To optimize the visualization of the brachial plexus, we attempted imaging in oblique axial and oblique coronal planes, parallel to the axis of the brachial plexus.

Ten normal volunteers (5 men and 5 women) were imaged using a GE 1.5 T SIGNA scanner. GRASS sequence was used in a coronal plane as the localizer using TR-25ms, TE-13ms, matrix-256x128, NEX-4, FOV-48cm, slice-10mm. The subclavian artery was recognized and oblique axial images were then obtained along the axis of the subclavian artery. Imaging parameters included TR-1600ms, TE-20ms, matrix-256x128, NEX-4, FOV-24, slice-5mm. Cardiac gating and no-phase wrap options were utilized.

Straight axials were then obtained as a localizer using TR-900ms, TE-20ms, matrix-256x128, NEX-4, FOV-48cm, slice-5mm. The subclavian artery was recognized and oblique coronal images were obtained parallel to the clavicle. Imaging parameters included TR-160ms, TE-20ms, matrix 256x128, NEX-4, FOV-24cm, slice-5mm.

The results of this study revealed that the images of brachial plexus obtained in the oblique planes were superior to the conventional axial and coronal images. In conclusion, oblique imaging is easy to perform and allowed the branches of brachial plexus to be traced as they followed the subclavian artery into the axillary fossa.

211

HIGH RESOLUTION MRI EVALUATION OF MENISCAL TEARS

F Wessbecher, S Rapoport, S McCarthy, C Pope, R Lange, P Jokl, K Lynch
Depts of Diagnostic Radiology & Orthopedic Surgery, Yale Univ. School of Medicine

Purpose: Evaluation of the sensitivity and specificity of magnetic resonance imaging in the diagnosis of meniscal tears.

Materials & Methods: One hundred fifty-four knees were evaluated for meniscal injuries using a 1.5 Tesla imager. Patients with prior meniscal surgery were excluded from the study. High resolution images were obtained using a dedicated extremity coil and 256x256 matrix. Images were obtained in the axial, sagittal and coronal planes using proton density, T1 and T2-weighted sequences. Criteria used to diagnose a meniscal tear were: a) linear or globular increased signal intensity extending to an articular surface and present on two or more contiguous sections and b) disruption of meniscal contour. Correlation with the arthroscopic findings was obtained in 48 patients (96 menisci) in whom 31 tears were identified.

Results: When only the sagittal plane was evaluated, sensitivity for diagnosis of meniscal tears was 87% and specificity 94%. When both sagittal and coronal planes were used, sensitivity was 100% and specificity 94%. Evaluation of the signal characteristics showed that only 9 of the 31 tears demonstrated high signal intensity on the T2-weighted images and did not improve specificity.

Conclusion: High resolution magnetic resonance imaging is both sensitive and specific in the diagnosis of meniscal tears and sensitivity is increased to 100% when both sagittal and coronal planes are utilized.

212

MAGNETIC RESONANCE IMAGING OF PIGMENTED VILLONODULAR SYNOVITIS

LS Steinbach, D Stoller, LW Bassett, CM Mills, G Vallier, HK Genant
University of Calif. San Francisco and Los Angeles; Diagnostic Networks Inc., SF

Magnetic resonance imaging was used to evaluate seven patients with joints affected by pigmented villonodular synovitis (PVNS). Studies were performed utilizing high-resolution thin-section multiplanar T1- and T2-weighted spin-echo images. All patients underwent arthroscopy following MR imaging. PVNS was diagnosed in all patients preoperatively on the basis of low-signal intraarticular deposits on T1- and T2-weighting, characteristic of hemosiderin deposits in hyperplastic synovium. In three patients with diffuse PVNS, there was hemosiderin deposition along the synovial reflection on an irregular Hoffa's fat pad- an early sign of synovial irritation. In another patient, a low signal mass was identified in Hoffa's fat pad on MRI which was not visible arthroscopically, but knowledge of the existence of the mass from the MR scan enabled the surgeons to find and excise the lesion. Lipid components, also produced in joints with PVNS, were seen in juxtaarticular cysts in one knee. All patients had intraarticular effusions. Three patients had large popliteal cysts filled with hemosiderin which were unsuspected prior to MR evaluation. MR imaging is useful to diagnose PVNS noninvasively in patients with monoarticular arthritis and aids in surgical planning for joints affected by PVNS.

213

1.5T MRI OF MENISCAL AND GANGLION CYSTS OF THE KNEE

DL Burk‡ MK Dalinka, E Kanal, ML Schiebler, EK Cohen, RJ Prorok, WB Gefter, HY Kressel
*Thomas Jefferson Univ. Hospital, Hospital of the Univ. of Pennsylvania, Philadelphia, PA.

Meniscal and ganglion cysts frequently present as palpable masses about the knee in locations atypical for popliteal cysts. Meniscal cysts also may be discovered incidentally on studies performed for suspected internal derangement. Twenty cystic lesions about the knee were evaluated with MRI, including 15 meniscal cysts and 5 ganglion cysts. All of the ganglion cysts and 8 of the meniscal cysts presented as palpable masses. Scans were performed at 1.5T using a transmit/receive extremity coil or a receive-only surface coil. Standard spin-echo imaging, including at least one long TR/asymmetric TE sequence, was performed in all cases. In 10 patients, gradient echo, reduced flip angle sequences were done also. Arthrographic correlation was available in 2 patients and CT scans were performed on 2 patients. Surgical correlation was obtained in 16 patients. In 2 patients the cysts ruptured spontaneously and 2 other patients were lost to followup.

Eleven meniscal cysts were located on the medial side of the knee and 4 were located on the lateral side. The ganglion cysts were located at variable sites about the knee. All meniscal cysts but none of the ganglion cysts were associated with horizontal meniscal tears. Cysts were visualized best on the long TR/TE images, but meniscal tears were seen best on the short TR/TE and long TR/short TE images. Meniscal tears and cysts were also well demonstrated on the fast scanning sequences. Septations were noted in four meniscal cysts and four ganglion cysts on the long TR/TE images. Long TR/TE images were also useful in showing connections between the cyst and joint capsule in three of the ganglion cysts. MRI is an effective, noninvasive method for the evaluation of these cystic lesions about the knee.

214

FAST RADIAL SCANNING: AN OPTIMIZED GEOMETRY FOR MR IMAGING OF THE KNEE

RL Ehman, TH Berquist, JP Felmlee
Mayo Clinic and Foundation, Rochester, MN 55905

An MR examination of the knee should clearly display menisci in their entirety, as well as permitting evaluation of the cruciate, collateral, and patellar ligaments, the articular cartilages, and periarticular tissues. We are dissatisfied with current protocols which attempt to achieve these goals using spin echo imaging in sagittal and coronal planes.

PURPOSE: To refine and evaluate a technique for imaging the knee utilizing non-coplanar, radially oriented sections, with an efficient interleaved gradient-refocused acquisition.

METHOD: The technique was optimized in volunteer studies and then tested clinically in a series of 32 patients, with a 1.5T GE imager. A gradient-recalled double echo sequence was employed (TR=400, TE1=13, TE2=35, Alpha=22 degrees, NEX=2, Views=192, FOV=16 cm). A multisection radial scan was performed for each meniscus. Scan software permitted dynamic angulation, yielding 10 double echo images of each meniscus at rotational increments of 18 degrees, with an acquisition time of just over 5 minutes for each side. A sequence with interleaved multiangulated sections was used to complete the examination by imaging the cruciates in approximately 2.5 minutes.

RESULTS: The technique provides highly detailed images of the menisci, with a geometry that is well suited for evaluating their arc-like shape. It closely matches the standard views of arthrography and pathological sectioning. Intersections between slices are only barely detectable, because of the small tip angle and the lack of a 180 degree RF pulse. The relatively long TR provides greater contrast stability and signal to noise than conventional very short TR fast scans. The second echo images are strongly T2 weighted and clearly depict the margins between hyaline cartilage and joint fluid. The clinical trials show superior performance in demonstrating meniscal tears and articular cartilage pathology, while substantially reducing examination time, compared to the conventional technique.

CONCLUSION: Fast radial-geometry scanning is an advantageous method for imaging the knee. We are currently evaluating other logical applications of this technique.

215

MR IMAGING FAT SUPPRESSION IN THE EVALUATION OF THE KNEE

SL Weiss, S Totterman, J Szumowski, RW Katzberg, JE Lovelock, J Burke, J Hornak, J Eisen
Department of Radiology, University of Rochester Medical Center, Rochester, New York

Magnetic resonance imaging appears to be an important alternative to arthrography in the evaluation of internal derangements of the knee. By eliminating the bright signal from bone marrow, subcutaneous, and surrounding tissue fat, fat suppression pulse sequences provide an expansion of the MR signal gray scale for water-containing tissues. The purpose of this study was to assess the usefulness of the chopper fat suppression pulse sequence, a modification of Dixon's method, in evaluation of the normal and abnormal knee. Both spin echo and fat suppression pulse sequences have been conducted on six healthy volunteers and 20 patients with suspected meniscal and/or anterior cruciate tears. The results of 20 patients were compared to arthrographic and/or arthroscopic findings. The fat suppression technique markedly improves visualization of the hyaline cartilage and shows promise for an improved depiction of meniscal and cruciate tears.

216

MAGNETIC RESONANCE IMAGING EVALUATION OF KNEE JOINT EFFUSION VOLUME AND DISTRIBUTION

DP Berthoty, BA Howard, MJ Mitchell, DJ Sartoris, DL Resnick
Department of Radiology, University of California, San Diego

Magnetic resonance imaging has been shown to be sensitive in the detection of joint effusions, but no guidelines currently exist for distinguishing normal from abnormal volumes and distributions of intra-articular fluid in the knee. Three cadaveric knee joint specimens were imaged with both T1 weighting and low flip angle fast scans at 1.5 Tesla after the injection of 0, 1, 2, 3, 4, 5, 10, 15, and 20 cc of Gadolinium DTPA. The specimens were positioned supine with the knee extended in a cylindrical extremity coil. The appearance of the different fluid volumes on images obtained using the two pulse sequences was established and compared to conventional radiography of specimens injected with comparable amounts of fluid. The distribution and volumes of intra-articular fluid as depicted by MRI was also compared to scans from normal volunteers and forty patients with acute knee injuries. MRI was found to be more sensitive than conventional radiography in the detection of intra-articular fluid, as well as more accurate in characterizing its distribution. Criteria were developed for normal versus pathologic quantities of fluid within the knee joint. Normal and pathologic synovial recesses of the knee articulation were also documented by MRI. The information obtained in this investigation has practical relevance to the interpretation of MRI examinations performed in the clinical setting of suspected internal knee pathology.

GENITOURINARY

217

CARCINOMA OF THE CERVIX - SURGICAL CORRELATION WITH MRI STAGING

JW Lecky, AWL Leung, A Greco, P Mason
Strickland Scanner Centre, Mt. Vernon Hospital, Northwood, Middlesex, England

Since November 1985, 338 examinations have been performed on 166 patients with cervical cancer. A Picker 0.5 Tesla superconductive magnet using spin echo sequences (SE 1100/40, SE 1200/60) and more recently STIR (IR2200/120) were used to examine the patients in sagital, coronal, and transverse planes. Thirty seven patients had Wertheim hysterectomies with pelvic lymph node dissection.

Twenty four (24) women were surgically staged 1B, MRI correctly staged 21/24. MRI problems were primarily those of lymph node (LN) detection and size. Three had LN smaller than 1 cm and these were non-malignant and the patients were correctly staged 1B. Three had benign LN of 1-1.3 cm size, but these patients were overstaged by MRI. One of these patients had incorrect MRI suggestion of rectal invasion.

Five (5) women were surgically staged 2B. MRI correctly staged only 2/5. MRI was not correct in visualizing parametrial and/or vaginal extension in 3. MRI did correctly show vaginal extension in 2 patients, but 1 of these patients had a 1.7 cm LN which was surgically benign.

Seven (7) women were surgically staged 3B. MRI correctly staged 6/7 although not always for the correct reason. MRI suggested parametrial extension and LN greater than 1 cm in 4 patients The LN contained tumor but all parametria were normal. The single patient who was understaged had microscopic evidence of tumor in a very small LN.

MRI clearly demonstrated the cervical neoplasm in all patients. The position was correct and the size description was within acceptable range compared with the surgeons and pathologists' descriptions.

Utilizing T1W sequences MRI cannot differentiate between normal, malignant, or inflammatory lymph nodes. It is understood that size alone is not a good criteria for staging purposes. The parametrium remains a difficult and uncomfortable area to assess with T2W sequence. STIR (IR 2200/120) has distinct advantages in better cervical edge detail and parametrial non-vascular information.

218

UNDESCENDED TESTES: EVALUATION WITH HIGH FIELD MR IMAGING

R. Kier, S. McCarthy, N. Rosenfield, A.T. Rosenfield, S. Rapoport, R.M. Weiss
Yale University School of Medicine

Clinically suspected undescended testes have been evaluated with ultrasound, computed tomography, testicular venography, and low field magnetic resonance (MR) imaging. The current study explores the value of high field MR imaging for undescended testes.

MR imaging at 1.5 T was performed in 20 male patients with clinically suspected undescended testes. All patients were evaluated with both T_1- and T_2-weighted pulse sequences. Axial and coronal images were obtained through the retroperitoneum and scrotum.

Undescended testes were identified as soft tissue structures in the normal course of descent of the testis. The ectopic testis was often located along the course of a linear soft tissue structure, presumably the persistent gubernaculum, which extended to the empty scrotum. In some cases, identification of the mediastinum testis was possible, confirming the diagnosis. In most cases, these ectopic testes demonstrated similar relaxation characteristics to orthotopic testes, with high signal intensity on T_2-weighted sequences. In a few cases, an undescended testis demonstrated lower signal intensity on T_2-weighted sequences, presumably due to atrophy and fibrosis.

In four patients, MR accurately localized an undescended testis in the inguinal canal, confirmed at clinical followup with subsequent testicle descent. In another patient, MR accurately localized an intra-abdominal testis, confirmed at surgery. In four patients, MR correctly predicted the absence of an undescended testis at subsequent surgical exploration. In one patient, MR failed to localize an intra-abdominal undescended testis. In another patient, a soft tissue mass in the inguinal canal, interpreted as an undescended testis, corresponded to a lymph node at surgery. Definitive clinical or surgical followup is pending in nine patients.

We conclude that high field MR is helpful in evaluation of patients with clinical suspicion of undescended testes.

219

MRI & SYNTHETIC IMAGING OF ENDOMETRIAL CARCINOMA

F.Long, L.Scoutt, S.McCarthy, R.Lange, M.Zawin, S.Chambers, J.Chambers, P.Schwartz
Yale University School of Medicine

We studied synthetic imaging to determine the optimal pulse sequences for maximizing contrast between endometrial carcinoma and the normal myometrium.

Thirteen patients with endometrial carcinoma, diagnosed by prior D&C, were studied using a 1.5T GE Signa system. Basis images representing T_1, T_2, and proton density were calculated from two imaging sequences: A short TR (one echo) and a long TR (four echoes). The basis images were used to synthesize spin echo images with TRs between 300 and 3000 msec and TEs between 25 and 100 msec. The relative contrast between tumor (T) and myometrium (M) was calculated from the signal intensity (I) measured in the images at T and M locations: relative contrast = [I(T)-I(M)/I(T)].

Surgical pathology was available in nine patients within three days of the MRI exam. Five patients had invasive disease, two patients had focal disease, while two patients had no evidence of disease at the time of surgery. In two patients MRI demonstrated such extensive disease that surgery was cancelled. Two patients had surgery postponed secondary to medical complications. In all cases of invasive and negative disease, MRI correlated with the surgical pathology.

Synthetic images demonstrated that in patients with invasive disease, increasing the TE at any TR above 300 enhanced T/M contrast. Increasing TR alone had little effect on the relative contrast. Even with synthetic imaging, only mild heterogenecity within the endometrial cavity could be demonstrated at any TR/TE values in patients with focal disease.

These results indicate that invasive endometrial CA may be detected and staged with MRI at much lower TR values than used at present, enabling faster scan times and greater patient throughput.

220

HIGH FIELD MRI OF UTERINE FIBROIDS AND COMPARISON WITH ULTRASOUND

M. Zawin, S. McCarthy, L. Scoutt, F. Comite
Yale Uiversity School of Medicine

22 women with uterine fibroids were evaluated by magnetic resonance imaging (MRI). The average age of the patient was 35 years old. A total of 45 scans were performed, 10 having concurrent ultrasound (US) examinations. MRI was obtained with a 1.5 Tesla (G.E.) system, using T_1, proton density and T_2-weghted images in the axial and sagittal plane. The MRI and US were independently read blind of the results of the other study and the results of the physical exam.

Prospective criteria for fibroids on MRI included an abnormal space-occupying mass in the uterus or cervix of low signal intensity on all pulse sequences. Vascular lesions were suspected in the presence of prominent arcuate vessels. On US, fibroids were suspected in the presence of a relatively hypoechoic mass or diffuse enlargment and inhomogeneity of the uterus.

A total of at least 60 fibroids were identified by MRI. While the majority were intramural, 13 were submucosal, 6 subserosal and 2 cervical. Vascular fibroids were present in 9 cases. In two patients where US questioned an ovarian mass, MRI documented a subserosal fibroid.

The uterus was enlarged in 19 of the 22 patients, with an average total intrauterine volume of 528 cc (the largest being 2200 cc). Accurate volumetric determination was possible in all cases by MRI but in only 4 of the 10 ultrasounds.

In a total of 44 ovaries, MRI identified 35 of the 10 patients with concurrent studies, MRI identified 18 of the 20 ovaries and US only 7.

In conclusion, MRI is not only capable of diagnosing and localizing fibroids, but is also superior to US in assessing uterine size and in visualizing the ovaries, parameters useful in following such patients for response to therapy.

221

MAGNETIC RESONANCE IMAGING DETERMINATION OF MYOMETRIAL INVASION IN ENDOMETRIAL CARCINOMA

Jesse M. Cohen, M.D., Roberto Yazigi, M.D., Paul Weatherall, M.D., Alan Munoz, M.D., Jeffrey C. Weinreb, M.D.
University of Texas Health Science Center at Dallas, Dallas, Texas

Fifteen patients with FIGO stage I biopsy confirmed endometrial adenocarcinoma underwent pre-operative pelvic magnetic resonance imaging (MRI) to evaluate the presence and depth of myometrial invasion. All patients then received primary therapy consisting of abdominal hysterectomy and bilateral salpingo-oophorectomy. Imaging findings were then compared with the uterine specimen histopathology. MRI was accurate in predicting the presence or absence of invasion in 13 of 15 cases (87%) and was able to discriminate superficial from deep invasion in 9 of 11 cases (82%). Based on our findings, we conclude that MRI appears to be an excellent technique for determining myometrial invasion, and that it may play a significant role in the pre-operative planning of a thorough search for lymphatic spread in those patients considered to be at high risk by virtue of myometrial invasion.

222

MR EVALUATION OF HEMOSIDERIN DEPOSITION IN RENAL TRANSPLANT PATIENTS

M. R. Fisher, F. Miller, S. Kupetz
Department of Radiology, Northwestern Memorial Hospital, Chicago, IL 60611

Chronic renal failure patients have multiple factors contributing to their anemia including diminished erythropoiesis, hemolysis, and gastrointestinal and chronic dialyzer blood loss. Blood transfusions are avoided unless their anemia aggravates other disorders such as coronary or cerebrovascular disease. However, for renal transplantation blood transfusions have been found necessary for optimal graft survival. Consequently, certain renal transplant patients may have associated hemosiderin deposition within their liver and spleen. The purpose of this study was to prospectively evaluate a group of patients following renal transplantation to determine whether there were signs of hemosiderosis and to correlate factors that may affect hemosiderin deposition, such as age of onset of renal failure, history and number of blood transfusion, age of transplant, and number of transplants. Nine patients who had undergone renal transplantation were evaluated. MR imaging was performed on a Philips 1.5 Tesla System operating at 0.5 Tesla.

Five patients were found to have lower signal intensity than normal within the liver and spleen on T1 weighted (T1W) sequences compatible with hemosiderin deposition compared to normals. Factors found to correlate with the findings of hemosiderin deposition were age of onset of chronic renal failure and the number of transfusions. In conclusion MR is a technique that allows demonstration of hemosiderin deposition within the liver and spleen of renal transplant patients, it provides insight into the contributing factors of hemosiderin deposition within this subgroup of patients and may play a role in the future therapeutic considerations regarding blood transfusions.

223

RENAL CORTICOMEDULLARY JUNCTION: OPTIMAL T1-WEIGHTED MR PULSE SEQUENCE

BR Baumgartner, RC Nelson, WE Torres, ME Bernardino
Emory University School of Medicine

The inability to demonstrate the renal corticomedullary junction (CMJ) on MR images has been reported in several medical renal diseases including nephritis, vascular occlusion and transplant rejection. T1-weighted spin echo pulse sequences have been advocated to demonstrate a signal difference between cortex and medulla. With the current technology allowing shorter echo time (TE), this study was undertaken to determine which of several T1-weighted spin echo (SE) and gradient echo (GE) pulse sequences is optimal for delineation of the CMJ. The MR studies were performed with a 0.5T magnet on 27 normal volunteers. Multi-slice axial images of both kidneys were obtained at each of the following pulse sequences: SE 250/20, SE 500/30, SE 900/30, GE 300/15 with an 80° flip angle and GE 300/15 with a 64° flip angle. For each patient and each sequence, operator-defined regions of interest were obtained. The signal intensity was measured from the cortex and the medulla of the left kidney on a single slice and from the background. Contrast/noice ratios were calculated from this data. In addition, the images of each sequence were independently ranked for delineation of CMJ by 3 experienced MR radiologists without knowledge of which sequence was used. While no sequence delineated the CMJ best in every patient, the average contrast/noise ratios ranked as follows: GE 300/15/80° = 3.01±0.74, GE 300/15/64° = 2.72±0.74, SE 250/20 = 2.02±0.33, SE 500/30 = 1.96±0.51, and SE 900/30 = 1.71±0.39. The subjective ranking (1 [best] to 5 [worst]) is as follows: SE 500/30 = 2.27, GE 300/15/80 = 2.52, GE 300/15/64° = 3.19, SE 900/30 = 3.24, SE 250/20 = 3.78 Although better contrast-to-noise ratios are achieved with the GE sequences and more T1-weighted SE sequences, as a practical matter this does not seem to be a significant factor when compared with the image evaluation by independent observers.

FAST IMAGING: CLINICAL

224

PULSE SEQUENCE OPTIMIZATION FOR THE KNEE: 3DFT-FISP IMAGING
EC Unger (1), MS Cohen (2), TR Brown (1)
Fox Chase Cancer Center (1), Siemens Medical Systems (2)

We developed and tested 3DFT FISP and FLASH pulse sequences and compared these sequences to T1- weighted and T2- weighted SPIN echo sequences in knee examinations of ten volunteers, and then performed the 3DFT FISP examinations on more than twenty patients. The 3DFT FISP and FLASH sequences involve a non-selective excitation technique with subsequent partitioning into slices. The resulting sequences have high signal to noise, high image quality and thin slice capability. Using this technique, 3DFT scans of the knee, with 3mm slices may be obtained in a seven minute acquisition time with a 256 x 256 matrix.

Using FLASH, cartilage and muscle appear bright, joint fluids bone marrow, tendons and ligaments are dark.

Using FISP cartilage and muscle are still bright. Joint fluid appears brilliant, brighter than cartilage. Bone marrow, tendons and ligaments still appear dark.

Comparing the contrast charecteristics of FISP and FLASH to spin echo techniques, the FISP technique was judged to have the best contrast. Using FISP we have found the following: Joint fluids appear very bright similar to a highly T2- weighted technique. Torn menisci appear as linear areas of increased signal intensity within the menisci. Loose bodies appear as dark objects surrounded by high signal intensity fluid. Avascular necrosis appears as lenticular subchondryl areas of high signal intensity within the low signal intensity bone marrow.

After evaluating the FISP, FLASH and spin echo techniques for imaging of the knee, the 3DFT FISP technique has become our technique of choice. Because of the rapid acquisition time we are able to perform a complete knee examination in under 15 minutes.

225

CORRELATIVE INTERPRETATION OF FISP, FLASH AND SE IMAGES OF THE FEMALE PELVIS
HK Brown, LP Clarke, T Dula, C Phillips, R Murtagh, P King, M. Silbiger
Anatomy and Radiology, Univ. of South Florida Medical Center

Spin-echo T1 and T2-weighted images of the uterus and adnexa have demonstrated their utility in delineating and, to some extent, differentiating normal anatomical structures and many types of pelvic masses or lesions. Fast acquisition scans such as FISP and FLASH may provide both improved signal to noise and superior contrast for some tissues or fluids.

Pelvic images were obtained using a 1.0 Tesla Siemens Magnatom and were compared to T1 and T2 weighted SE images and to gross anatomical cadaver slices. Each organ or tissue was evaluated for its relative signal intensity in the images, including FLASH and FISP at flip angles from 10^0 to 70^0. One of the most striking differences is in the contrast between muscle and fat. With a 10^0 flip angle, urine and ovaries are hyperintense to muscle which is hyperintense to fat giving the appearance of a negative image of SE T1 weighted image. The hyperintense "junctional zone" of the myometrium and its continuation of the hypointense zone of the cervical stroma are easily identified in 10^0 flip angle FISP images but there is no urine/bladder wall differentiation. As the flip angle is increased to 50^0 or 70^0 urine becomes hypointense and is well differentiated from bladder wall, while the contrast between muscle and fat is gradually reversed and the junctional zone becomes isointense with myometrium. Dense collagenous tissues such as tendons, ligaments and aponeuroses are much better defined because the contrast between them and striated muscle is much greater than that in T1 or T2 weighted images. Areolar connective tissue planes are hypointense to their surrounding muscle in FLASH images, whereas in SE T2 images they are slightly hyperintense. As in FISP images, this contrast reversal is made even more apparent by the higher intensity signal observed from skeletal muscle in FLASH images. This contrast advantage could be important in the diagnosis of musculo-skeletal diseases.

Currently. this laboratory is conducting feasibility studies for the production of tissue differentiating thematic maps by feature extraction methods applied to multiple fast scan pulse sequences.

226

FAST MR IMAGING OF SHOULDER INJURIES

G BONGARTZ, P RUGGIERI, M REISER*

SIEMENS medical engeneering group, Henkestrasse 127, D - 8520 Erlangen, FRG
*Dep. of Radiology, University of Muenster, D-4400 Muenster, FRG

The stability of the shoulder joint is maintained by the rotator cuff muscles, the glenohumeral ligaments and the fibrocartilagous glenoid labrum. Direct trauma or luxation usually cause soft tissue injuries. Among these, ruptures of the rotator cuff and labral tears (Bankart lesion) are most often found. Accurate diagnosis helps to plan correct treatment. Arthrography, arthrotomography, ultrasound and CT are either unable to visualize cartilage defects or require intraarticular contrast. Shoulder arthroscopy has not yet been established as a routine method of evaluation.
MR is well suited to joint-imaging because of multiplanar cuts and improved soft tissue differentiation. Due to its position far off the center, MRI of the the shoulder appears to be complicated. Using an Helmholtz resonator with an OFFCENTER-ZOOM technique allows excellent delineation of shoulder anatomy with short TR/TE spin echo sequences. Hyaline and fibrous cartilage, the entire rotator cuff and bony structures are readily differentiated. Traumatic tears require T2-weighted sequences with emphasis on edema and synovial fluid. Spin- echo experiments with long TR/TE are extremely time consuming and give low SNR. Gradient-echo sequences are faster, thus limiting motion artifacts, and give adequate tissue constrast when using optimized parameters for FLASH or FISP.

Our study was performed on a group of patients with various shoulder injuries. On axial and coronal views labral and bony lesions were clearly demonstrated. Tears of the rotator cuff required coronal or sagittal imaging to differentiate the rotator cuff ligaments. On T1 weighted images, only complete distortion of the glenoid labrum could be detected. Joint effusions and fractures were easily diagnosed. Rotator cuff lesions and partial labral tears gave false negative results with T1- parameters except in one case of a fresh hemorrhage into the rotator cuff causing high signal intensity. Improved T2-like contrast in gradient-echo imaging was achieved with FISP-sequences using a flip angle of 40 to optimize tissue contrast. Synovial fluid together with hyaline cartilage showed a band of bright signal, whereas fibrous cartilage remained low in intensity. Rotator cuff ruptures were identificated by foci of high signal intensity due to traumatic edema or effusion extending into the ligaments. Labral tears also were delineated by the FISP 40 sequences. Demonstration of articular fractures was possible with every sequence, although smaller cortical fractures could not be differentiated from labral detachment regardless of the sequence. With fast gradient-echos, imaging of shoulder injuries in at least 2 planes each with T1 and T2-weighting can be performed within 15 minutes.

227

3-D FLASH IMAGING OF THE CNS

VM Runge, KL Nelson, MR Traill, ML Wood
Division of Magnetic Resonance, Tufts-New England Medical Center Hospitals

3-D FLASH was evaluated in more than 50 clinical examinations of the CNS. Scan times varied between 3 and 15 minutes, with slice thickness of 0.5-2.0 mm. The flip angle was varied between 30 and 50°, depending upon TR, to achieve T1 contrast. A Mipron workstation was employed for rapid reformatting of images in any arbitrary plane desired. In all cases, conventional spin echo technique (TR/TE=0.6/17) was compared to 3-D FLASH for lesion depiction.

Analysis of grey-white contrast in patient studies revealed an improvement of 117 $\pm$ 58% (n=4) with 3-D FLASH (TR/TE/angle=0.04/12/50°), when compared to T1 weighted spin echo images. This reflected an improvement in T1 contrast with 3-D FLASH. The ability to define lesion boundaries was also improved due to the reduction in partial volume effects. Hemorrhagic lesions were better depicted with 3-D FLASH when compared to 2-D spin echo. Because of the small nearly symmetrical voxel dimensions, image reformatting was possible with little loss of detail in the direct orthogonal planes. Projection and rotation of the lesion in three dimensions was also possible. Enhancement of intracranial neoplastic lesions on 3-D FLASH was demonstrated following I.V. Gd DTPA administration. Enhancement of normal arterial and venous structures was also common on 3-D FLASH. TEs at the two ends of the spectrum, 8 and 17 msec. were preferred in order to avoid problems at fat and water interfaces due to out of phase effects at 1.0 Tesla.

3-D FLASH is advocated to replace axial T1 weighted spin echo scans in routine screening of the CNS. Scan times are comparable, being in both instances routinely less than 10 minutes. T1 contrast was superior with 3-D FLASH. Lesion depiction and detection also improved with 3-D FLASH. Use of this technique enables routine acquisition of very thin sections ($\leq$ 1 mm.) with high quality reformatted images in any arbitrary plane. The introduction of shorter TE and motion compensation sequences will result in greater T1 contrast, decreased motion artifact, and decreased magnetic susceptibility effects.

228

CLINICAL UTILIZATION OF THE TRI-RADIAL FLASH SCOUT

MR Traill, VM Runge, ML Wood, KL Nelson, DM Kaufman
Division of Magnetic Resonance, Tufts-New England Medical Center Hospitals

A tri-radial FLASH localizer scan was evaluated clinically in 10 cases.

Three orthogonal images are acquired simultaneously in 5-15 seconds using FLASH technique. The three planes can be selected to be the central sagittal, coronal, and axial slices or an arbitrary offset can be utilized for each axis. The sequence was optimized primarily for signal to noise ratio and secondarily for T1 contrast and lack of image artifacts, with TR/TE/angle=0.105/13/50°. A rectangular pixel matrix was employed to minimize scan time and maximize signal to noise. The sequence was designed to allow rapid simultaneous acquisition of scouts in the sagittal, coronal, and axial planes.

This sequence was evaluated in the head and spine. It was designed for utilization as well in the abdomen, pelvis, and extremities. The short scan time allows acquisition of breath-hold images if desired. A single vertical and horizontal interference line approximately 1 cm. in width is seen in each of the three images at the point of intersection of the three planes. This is due to the additional excitation and incomplete relaxation which occurs at these intersection points. This was not found to be detrimental in use of this technique as a localizer scan. Indeed, normal structures are seen within these dark bands with however an overall lower signal intensity.

The tri-radial scout was preferred for use as a localizer scan. Visualization was provided in three planes vs. one plane with scan time equivalent to the previously used single slice spin echo localizer. In our clinical experience, two orthogonal scout images have been required in greater than 90% of spine, abdominal, pelvis, and extremity examinations. This can now be replaced by use of a single sequence, the tri-radial scout. Image quality was also substantially improved over the short spin echo scan, which suffered from truncation lines and motion artifacts.

229

FAST 3D IMAGING OF THE CERVICAL SPINE

P.M. Ruggieri, S.R. Felber, G.A. Laub, R.U. Meissner, J. Willeit
SIEMENS MEDICAL SYSTEMS, ERLANGEN, FRG

Effective imaging of the cervical spine often requires multiplanar orthogonal and oblique orientations. The routine clinical study includes a series of examinations, whereas the 3D technique uses a single isotropic data acquisition which can then be reconstructed in any arbitrary plane.

A series of patients, who presented with neck and/or upper extremity symptoms, were examined with a 1.5 T Magnetom. A new volume coil, with a helmholtz configuration, was used in all cases. The original data sets were obtained in the sagittal orientation which consisted of 64 or 128, contiguous, 1-2 mm thick slices. Coronal, axial and oblique planes were then reconstructed. Fast gradient echo sequences, FLASH and FISP, were utilized to maintain a reasonable examination time. Short echo times not only improved the contrast in these sequences, but also reduced the artifacts inherent in spine imaging due to magnetic susceptibility and flow. Motion artifacts were more effectively suppressed by incorporating gradient motion refocussing.

The 3D examinations were diagnostic in all patients once the reconstructed axial, coronal and oblique planes were compared to the measured sagittal scans. The thin slices with high S/N, which are characteristic of the 3D technique, provided excellent delineation of the spinal anatomy and pathology. The rectangular slice profiles and multiplanar reconstructions reduced questions related to volume averaging. Nerve root compression was easily evaluated in the oblique reconstructions through the neural foramena. The use of the volume coil provided good homogeneity throughout the neck and therefore yielded additional information about the anterior soft tissues which would not be possible with a surface coil. The results of this pilot study suggest that 3D imaging may reduce overall examination time in routine cervical spine imaging as well as provide improved visualization of cervical anatomy and pathology.

230

MR DEMONSTRATION OF MULTIPLE SCLEROSIS USING FAST PROTON DENSITY IMAGING

S. Albert, N.E. Leeds, W.C. Yang
Department of Radiology, Beth Israel Medical Center, New York, N.Y.

Several attempts to use small flip angle experiments to detect multiple sclerosis (MS) lesions have been reported recently.[1,2] The results have been compared with conventional T2-weighting images and show that not all the lesions have been detected and that the S/N ratio is considerable lower than that of conventional images.

We have used small tip angle proton density imaging techniques[3] to study MS patients. The examinations have been performed at a magnetic field strength of 1.5T with a GE SIGNA system using a varient of the fast field echo pulse sequence GRASS (Gradient Recalled Acquisition in the Steady State).

The fast proton density (FPD) images demonstrate the MS lesions that have been identified with conventional proton density and T2-weighted images and have good S/N ratio.The contrast of the FPD images is mainly determined by the pulse angle.The artifacts are less evident for FPD images than for other types of fast images.

1. E.Kanal et al, Twenty-Fifth Meeting of the American Society of Neuroradiology, p193,1987.
2. R.I. Grossman et al, Sixth Annual Meeting of the Society of Magnetic Resonance in Medicine, p. 311, 1987.
3. S. Albert et al, Sixth Annual Meeting of the Society of Magnetic Resonance in Medicine, p. 913, 1987.

IMAGING TECHNIQUES

231

SCAN TIME REDUCTION USING CONJUGATE SYMMETRY AND RECALLED ECHO

GN Holland, T Provost, G DeMeester, K Denison
Picker International, NMR Division, Highland Heights, Ohio

We present a method of achieving almost a factor of four reduction in scan time, without the stringent system demands of the earlier hybrid echo-planar methods. Our technique combines the use of conjugate symmetrization to reconstruct the negative half of k-space views from the acquired positive views, and a double echo to separately acquire inner and outer phase encoding views.

The pulse sequence used consists of a standard spin echo followed by a gradient echo formed by reversing the read gradient immediately after acquisition of the spin echo signal. An additional phase encoding "offset" pulse is applied during the read gradient reversal to ensure that the data acquired from the second echo is from the outer phase encoding views. The sequence is set up so that the first phase encoding pulse corresponds to 0.5(+Gmax). The second pulse is of the same area so that the +Gmax view is encoded, and captured during the second acquisition. The total phase encoding gradient is decremented view-by-view in the normal manner to just past zero, so that all of the positive phase encoding views have been acquired, plus several of the negative views, but that inner and outer views reside in separate areas. The total number of sequence repeats is just over one quarter of that required for conventional k-space coverage.

To form an image from the acquired data, first the inner and outer phase encoding views must be combined. Care must be taken to avoid phase discontinuity where the data sets are combined by appropriate (zero and first order) phase correction. Second, a phase map is constructed from a kernel of points around kp=0 for use during the symmetrization process to correct local phase variation within the data set. Finally, after phase correction, the processing is completed by a normal 2D-FT.

Resulting images have the same spatial resolution, half the signal-to-noise ratio, but are acquired in little over one quarter of the time of the "conventional equivalent.

232

MIXED BANDWIDTH PULSE SEQUENCES FOR MRI: TECHNICAL ASPECTS

JP Mugler III, JR Brookeman
Departments of Biomedical Engineering and Radiology, University of Virginia

The length of the data sampling period, T_S, or equivalently the bandwidth per pixel, $1/T_S$, is an important parameter in optimizing the signal-to-noise (*SNR*) and contrast-to-noise (*CNR*) performance of pulse sequences.[1,2] At moderate to high field strengths, the most restrictive limitation on T_S in a well-shimmed magnet is that due to chemical shift.[2] In certain situations however, such as when imaging many areas of the brain, the chemical shift artifact is not of concern and extending T_S and thereby narrowing the bandwidth per pixel can greatly improve the *SNR* and *CNR* of heavily *T2* weighted images.

In a clinically useful double-echo sequence, it would be desireable to use a relatively short T_S (wide bandwidth) for the first echo to achieve a short minimum echo time, and a long T_S (narrow bandwidth) for the second echo to improve the *SNR* and *CNR*. In general, this approach requires lowpass filters with different bandwidths for the two echoes. It is usually not possible with present commercial imagers to vary the filter bandwidth within one sequence repetition. It is possible though, by over-sampling[3] during T_S, to use different T_S's with the *same* lowpass filter and not alias excess noise into the image. For a times two over-sampling, such that the effective field-of-view (FOV) in the readout direction is twice the desired FOV for the image, the data sampling period for the second echo can be made three times that for the first echo if the 3db point for the lowpass filter is set at $1/2 \cdot \Delta t$, where Δt is the sampling interval that would have been used for the *first* data sampling period *without* over-sampling.

This sequence has been implemented on a 1.0 T Siemens Magnetom whole-body imager. On patient images, the background noise level on the second echo is approximately 60% of that on the first echo, in good agreement with the 58% ratio predicted by theory. We have begun preliminary clinical evaluation of this sequence against a standard sequence in which the T_S's for the first and second echoes are equal.

1. RE Hendrick, *Magn Reson Imaging* **5**, 31 (1987).
2. JP Mugler III, JR Brookeman, submitted to *J Comput Assist Tomogr.*
3. ER McVeigh, RM Henkelman, MJ Bronskill, *Med Phys* **12**, 586 (1985).

233

EFFECTIVENESS OF THE SIGMA NOISE REDUCTION FILTER ON MR IMAGES

ML Wood and VM Runge
Tufts University and New England Medical Center, Boston, MA

Much of the noise in MR images is random, and consequently there is a 95.5% probability that it lies within two standard deviations of its mean value. The sigma filter(1) smooths images locally by averaging only those pixels in a neighborhood that have intensity within a predetermined range, typically two standard deviations from the center pixel. This restriction distinguishes the sigma filter from the median filter and allows edges and other fine detail to be preserved.

The sigma filter was available on a Kontron MIPRON image processing workstation (Kontron Instruments, Everett MA). The algorithm employing a 15 x 15 neighborhood took three seconds to filter a 256 x 256 pixel image. Two-dimensional and three-dimensional Fourier MR images of phantoms, heads, spines, joints, and abdomens were used for the evaluation. The filtered images were compared to similar images for which more acquisitions of data were averaged.

Tests on a resolution phantom found no measurable loss of high contrast spatial resolution even for the largest neighborhood, which was 15 x 15 pixels. The standard deviation of image intensity was reduced by at least a factor of two, and as much as five in the most uniform regions. The sigma filter similarly reduced the level of random noise in the other images. Multiple iterations using successively smaller allowable ranges for the noise demonstrated gains over a single attempt. Ghosts due to motion were partially suppressed, provided they did not have sharp edges. The evaluation concludes that the sigma filter is effective at reducing the level of noise in common MR images.

1. Lee, JS. Digital image smoothing and the sigma filter. Computer Vision, Graphics, and Image Processing. 24:255-269; 1983.

234

MR IMAGE RECONSTRUCTION USING MAXIMUM ENTROPY

RT Constable, RM Henkelman
Dept. of Med. Biophysics, University of Toronto, Canada

The Maximum Entropy Method(MEM) of image reconstruction has been used to a limited extent for several years, yet the potential benefits of the method have not been realized. The principle behind the MEM is simple: that is, of the many possible images that may be reconstructed, all of which are consistent with the data, MEM chooses the image with the least amount of information. Thus, any structure which appears in the image must have evidence for it in the data.

In the past the main criticism directed toward MEM has been the tendency for the technique to suppress only the background noise leaving the noise within the image unaltered. New approaches have been incorporated to address this problem. The effects of using prior information in the reconstruction scheme and the scaling of the logarithmic regularizer have been investigated. Also, it is found that reconstruction of shortened data sets may be performed using MEM without the introduction of truncation artifacts commonly found in Fourier Transform images.

235

SAMPLING INTERVAL IN SIMULTANEOUS SPIN ECHO AND GRADIENT REFOCUSING MRI

S Vinitski, R Prost+, DG Mitchell, MD Rifkin, DL Burk, D Levy
Thomas Jefferson Univ, Philadelphia, PA, +GE Medical Systems, Waukesha, WI

Spatial resolution and pixel SNR depend on the sampling interval, τ. Too wide or too narrow τ allows collection of the noise from the regions outside of the echo tails or only the central portion of the echo respectively. Using the methodology developed for the single echo (1); the model of susceptibility induced magnetic gradients (2); and estimating effects of the spin-lattice relaxation, we investigated the effect of sampling time, magnetic field inhomogeneity and tissue susceptibility on the spin echo (SE) and gradient refocusing (GRE) image contrast. Hydrogen imaging to determine correlation with theory was performed using a 1.5T Signa GE System. The results suggest that the optimum τ required to maximize T2 contrast in SE imaging is significantly longer (20-30 msec) than that to enhance T1 contrast (10-15 msec). Prolonged τ does not degrade the spatial resolution, provided the magnet is well shimmed and TE is long. Bo inhomogeneity degrades the T2 contrast to a greater extent than T1 contrast. The susceptibility differences result in signal attenuation of pixels representing the tissues in question, as well as propagation of signal attenuation into the neighboring pixels. Shortening of the TE and τ drastically reduces the image distortion. These findings suggest the following data acquisition strategy: after a small excitation RF pulse the GRE echo is immediately collected at the rate of about 60-80 KHz. Next, one or two 180° RF pulses produce spin echoes, which, in turn, are collected at a slow rate of about 10 KHz. As a result, simultaneous proton density (GRE) and T2 (SE) weighted images are obtained. Additionally, TR can be significantly shortened due to the use of a small excitation RF pulse (3). The imaging results are in agreement with theoretical predictions.

1. Vinitski S, Fuka M, Prost R. Magn Reson Med (in press), 1987.
2. Gasel JA, Lee KU. J Am Chem Soc 1974; 36:370-378.
3. Vinitski S, et al. IEEE Trans Nucl Sci October 1987.

236

Measurements of radiation dose distributions in irradiated gels by MRI
J.C. Gore, S. Majumdar and R.J. Schulz
Yale University School of Medicine

We have previously shown (1) that irradiation of ferrous ammonium sulphate solutions with x rays produces a detectable change in the NMR relaxation rate of the solution. The oxidation of ferrous to ferric ions by radiation decreases T_1 because ferric ions are more effective paramagnetic relaxation agents, and the change in relaxation rate increases linearly with dose. We have infused polyacrylamide gel-phantoms with ferrous ions, and imaged the dose distributions resulting from both external beams and discrete radioactive sources. Using calculated T_1 maps we have been able to derive isodose contours in three dimensions with high spatial resolution. We have measured the relaxation-rate change per gray at both 6.35 and 20 MHz and have demonstrated a sixfold increase in the sensitivity of the technique using polyacrylamide gels at the lower frequency. Diffusion of the ions in the time between irradiation and imaging has been measured by studying the edge spread function at various times. The diffusion coefficient was calculated to be 7.8 ($\pm$ 1.8) x 10^{-6} cm^2 sec. Chemical means of reducing this are being studied, as well as deconvolution techniques able to reduce blurring effects from diffusion. MRI promises to provide a convenient and accurate means of assessing complex radiation dose distributions in tissue equivalent phantoms.

1. Gore, J.C., Kang, Y.S. and Schulz, R.J.
Phys. Med. Biol. 29, 1189-1197, 1984.

MONDAY P M

237

19-FLUORINE 2-FDG NMR IMAGING OF THE BRAIN IN RAT

T Nakada*#, IL Kwee*#, BV Griffey‡, RH Griffey‡
VA Med Ctr, Martinez, CA*, Univ of Calif, Davis, CA#, Univ of New Mexico, NM‡

2-Fluoro-2-deoxy-D-glucose (2-FDG) is the most widely utilized metabolic probe to study regional glucose utilization, non-invasively, by positron emission tomography (PET). In spite of recognition of the importance of the ^{18}F 2-FDG PET studies and its relevance to every day clinical medicine, ^{18}F 2-FDG PET studies have remained essentially a research tool due to its technical complexity and resultant high cost. In this study, we obtained images of the rat head reflecting glucose utilization, similar to those of ^{18}F 2-FDG PET studies using ^{19}F 2-FDG and ^{19}F nuclear magnetic resonance (NMR) imaging.

Sprague-Dawley rats, 200-300g, were given a single oral dose of sorbinil, 25 mg/kg, one hour prior to the study to inhibit metabolism of 2-FDG into the aldose reductase sorbitol pathway. Animals were immobilized by intraperitoneal injection of inactin, 12.5 mg/kg, and placed in the RF coil constructed using the design of Alderman and Grant. After proton localizer images were obtained using a gradient recall rapid imaging sequence and a 256 x 256 data matrix, the transmitter was positioned at the resonance frequency of 2-FDG-6-phosphate and ^{19}F images were obtained using partial saturation spin echo imaging sequences with a restoring 180° pulse (TR: 600 msec, TE: 12 msec). The total time needed for data acquisition was ca. 60 min.

^{19}F images clearly demonstrated spatial heterogeneity of glucose utilization in the rat head. Significantly higher glucose utilization in the brain than surrounding tissues was observed. Although the potential adverse effects due to the high doses of 2-FDG (400 mg/kg) needed to perform the study compared to the tracer dose of ^{18}F 2-FDG PET studies preclude immediate application of this technique to quantitative glucose utilization studies, the present study shows promise for future development of glucose metabolic imaging by NMR.

238

^{19}F NMR Studies of liver oxygenation

S.Holland, R. Soto, C. Jaffe, E. Gordan, J.C. Gore
Yale University School of Medicine

Fluorine images of perfluorocarbons have previously been shown to be sensitive indicators of tissue pO_2 (1-3).We have extended such studies to investigate regional pO_2 variations in liver and their alterations with acute insults. Studies of Fluosol-DA have been performed at 2.0T. ^{19}F images of rats confirmed that within a few hours most of the ^{19}F accumulated in the liver and spleen.The paramagnetic effect of oxygen has also been investigated. ^{19}F relaxation rates were measured from images of a bottle of Fluosol as various mixtures of O_2 and N_2 were bubbled through the sample. Similar measurements were made on the livers and spleens of live, fluorinated rats by adjusting the mixture of O_2 and N_2 in the breathing gases.These measurements exhibited a linear dependence of $1/T_1$ on PO_2. Additional studies performed on the rats used a 2 cm surface coil placed over the liver. The steady state ^{19}F signal strength was recorded every 0.2 seconds and the changes that occur when blood flow to the liver is occluded have been used to assess the corresponding changes in tissue PO_2. The effects of other acute insults are also being studied. High resolution images of livers have been made with resolution of 200 um in a 1 mm slice and show promise for continuing studies of regional, in vivo oxygen tension gradients with ^{19}F NMR.

1) Clark, L.C. Jr., Acherman, J.L., Thomas, S.R. et al, Exp. Med Bio. 180, 835, 1984. 2)Fishman, J.E., Joseph, P.M., Floyd, T.F. et al, Mag. Res. Imag. 5 (4), 279, 1987. 3) Fishman, J.E., Joseph P.M., Floyd, T.F., et al Mag. Res. Imag. 5 (4), 279, 1987.

EXTREMITIES & TUMORS

239

POTENTIAL USE OF MRI FOR SKELETAL MUSCLE IN THE STUDY OF NEUROMUSCULAR DISEASES:CORRELATIVE STUDY CT,ULTRASOUND,EMG,BIOPSY.

M.NAEGELE,F.KARABENSCH,C.D.REIMERS*,D.HAHN.
UNIVERSITY OF MUNICH,DEPT.OF RADIOLOGY,DEPT.OF NEUROLOGY*,WEST GERMANY

95 patients with neuromuscular disorders were examined by MRI,CT,Ultrasound, EMG.A muscle biopsy was taken in all cases.RESULTS:MR-CT:MR shows better anatomical muscle detail and soft tissue contrast,no osseous beam artifacts, more precise evaluation of extent and severity of inflammatory reaction in a single muscle,possibility of three dimensional imaging.Both techniques are able to differntiate between affected and nonaffected muscle.They can be used for estimation of muscle atrophy and the amount of replacement of the muscle by fatty infiltration and connective tissue.They generate objective reproducible images without influence of the investigating person and give a definite mapping of pathology for an efficient muscle biopsy.

Ultrasound:The computer assisted echogeneity evaluation of Ultrasound is a cost efficient screening method,a real time examination procedure but less sensitive than MRI.

All three techniques are able to point out charakteristic pathological distribution patterns of degenerative,metabolic and inflammatory muscle disorders.

240

MR FEATURES OF BENIGN MUSCULOSKELETAL SOFT TISSUE NEOPLASMS

Paul Weatherall, M.D., Jesse Cohen, M.D., James Fleckenstein, M.D.
University of Texas Health Science Center at Dallas, Dallas, Texas

42 cases of soft tissue neoplasms were evaluated using a 0.35T magnet. They included hemangiomas (12), neurofibromas (9), AVM's (6), fibrous tumors (4), lipomas (4), ganglion tumors (4) and lymphangiomas (3). When compared to other imaging techniques including plain films, CT and angiography, MR was superior in demonstrating the location and extent of the lesions. In addition, MR provided specificity not otherwise available in a number of cases. As most benign soft tissue neoplasms are not calcified and produce few skeletal changes, plain films are of limited value. With the exception of vascular lesions, angiography shows only non-specific mass effect when benign masses are large enough to displace vessels. CT usually demonstrates any clinically symptomatic lesion, but frequently falls short of MR imaging in the categories of tumor extent and specificity. MR defined the bone and muscle extent of AVM's well and also more easily differentiated them from other vascular tumors when compared to CT. Both CT and MR can be used to diagnose lipomas. The diagnosis of fibrous lesions was possible with MR when T2 weighted images failed to show an increase in signal (and no pattern suggestive of hemorrhage). Hemangiomas, neurofibromas, and ganglion tumors were relatively bright on T1 weighted images compared to muscle, and increased in signal relative to muscle and fat on T2 weighted images. They were not easily distinguishable by MR factors alone. Hemangiomas frequently involved the skin and muscle whereas neural tumors would typically be found between muscle planes and along known neural pathways. Several plexiform neurofibromas were readily diagnosed using MR since their entire extent was easily visible.

The inversion recovery (STIR) sequence was valuable whenever used. This pulse sequence was found to be very sensitive but provided specificity only in the case of lipomatous tumors. In addition, the use of the MR STIR sequence to differentiate it from liposarcoma may prove more specific than the CT demonstrated heterogeneity. All other neoplasm became nearly white against the background of dark fat and bright grey muscle. Blood vessels and other fluids also are bright but rarely caused difficulty in interpretation.

The overall utility of MR has been high in our experience and as reported by others when used for evaluation of soft tissue neoplasms. T1 weighted spin echo and STIR sequences may be all that is necessary for tumor screening. Our experience suggests that MR should be the initial imaging procedure of choice in most cases where a soft tissue mass is or strongly suspected.

241

UTILITY OF MRI IN THE DIFFERENTIATION OF PAROSTEAL OSTEOGENIC SARCOMA FROM OSTEO- AND PERIOSTEAL CHONDROMA

OB BOYKO, DA CORY, JB VOGLER, CE SPRITZER, RJ HERFKENS DUKE UNIVERSITY MEDICAL CENTER

Parosteal osteogenic sarcoma (POS), a malignant juxtacortical tumor of bone, can be on occasion confused for benign cartilagnous tumors such as osteo- and periosteal chondroma (OC and PC). We evaluated the utility of T1-weighted spin echo sequences in distinguishing pathologically proven cases of POS (3) from OC (6) and PC (2).

Studies were performed on either a General Electric (1.5 T) superconducting magnet or a Technicare Teslacon (0.15 T) resistive magnet utilizing TR = or less than 750 msec and TE = or less than 32 msec. All cases of POS had an inhomogeneous low signal when compared to marrow fat; correlating with the histologic presence in the tumor matrix of ossified/nonossified chondroid, osseous trabeculae with spindle-cell fibrous stroma between the bone trabeculae.

All cases of OC and PC had a component of bright signal (short T1), specifically at the initial point of continuity of the underlying normal bone with the cortex and medullary space of the exostotic lesion. This bright signal correlated with the presence of fatty and/or hematopoietic marrow between the lobules of cartilage or osseous trabeculae.

In conclusion T1-weighted MR imaging serves as an adjunct to the radiographic differentiation of POS from OC/PC preoperatively, independent of magnetic field strength.

242

MRI OF BONE MARROW IN ADULT ACUTE LEUKEMIA

PY Poon, RM Henkelman, H. Messner
St. Michael's Hospital and Ontario Cancer Institute, Toronto, Canada

The bone marrow of normal volunteers, patients with active acute leukemia, in remission, and in relapse were studied by MRI. A circular surface coil, 20 cm. in diameter was placed behind the medial thirds of the iliac crests, and the sacrum with the patient in a supine position. These locations were chosen because the bone marrow aspirations were done here. A 0.15 Tesla imager with a resistive magnet was employed in this study. Interleaved spin echo and inversion recovery pulse sequences were used to obtain images from which T1 relaxation times could be calculated. Small test tubes containing copper sulphate solutions of known T1 values were placed within the field of view as references. A small number of patients also had serial MR studies before the induction therapy, at 14th and 20th day after induction, and monthly during maintenence therapy. Bone marrow aspirations were done within 2 days of the MR examinations.

The mean T1 values of control (n=5), active leukemia (n=10), remission (n=10) and relapse (n=12) were 340±27 ms, 476±86 ms, 291±26 ms and 335±35 ms.

The following graphs show the time-course of 3 patients. The status of the patients as predicted by the MR results correspond very well with the clinical and bone marrow aspiration findings.

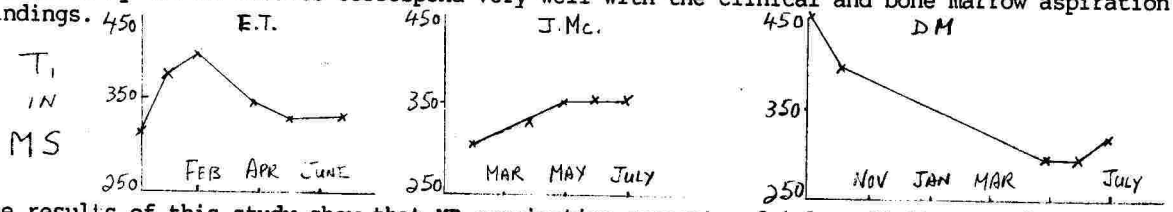

The results of this study show that MR examination separates fairly well the normal volunteers and patients in remission from patients with active leukemic disease. The serial studies are even more predicative of the change of disease status. The latter may be the most useful clinical application of MRI in acute leukemia.

243

MRI IN MELANOMA

HF Marx, PM Colletti, JK Raval, WD Boswell, C-S Zee, DCP Chen, PE Liggett, RA Kempf
University of Southern California School of Medicine

T1 relaxation time shortening secondary to paramagnetic compounds has been described in melanoma. The purpose of this paper is to evaluate short TR, short TE images of various body areas involved with melanoma.

Twenty-six body areas in 23 patients with melanoma were imaged with T1 and T2 weighted spin echo techniques. Signal intensities were evaluated for T1 shortening.

All lesions were bright on T2 images. Seven of 10 orbital melanomas, 3 of 4 melanoma brain metastases, 4 of 7 spine metastases, 0 of 3 soft tissue metastases, 0 of 2 pelvic metastases, and 2 of 2 lung metastases were bright on T1 images.

Overall, 62% of melanoma lesions were bright on T1 weighted images. While high T1 signal lesions are typical of melanoma, the absence of high signal does not exclude the diagnosis.

244

MR FINDINGS IN CARPAL AVASCULAR NECROSIS

MR Traill, VM Runge, KL Nelson, JE Kirsch
Division of Magnetic Resonance, Tufts-New England Medical Center Hospitals

Thirteen patients with wrist pain and a clinical suspicion of carpal avascular necrosis were evaluated. In all patients, both coronal T1 and T2 weighted images were obtained using standard spin echo sequences. For the T1 weighted images TR/TE=.7-.5/25 was used, and for T2 weighted images TR/TE=3.0/70-90. All images were obtained using a 13 cm. circular surface coil. Pre-acquisition zooming of the images by a factor of 2-3.5 was employed.

The criteria for diagnosing carpal AVN by MRI was a loss of the normal intense signal from the intramedullary fat on T1 weighted images. Based on this criteria, clinical history, and additional radiographic evaluation, seven patients were diagnosed as having carpal AVN and six patients were diagnosed as having wrist pain secondary to etiologies not associated with AVN.

While the findings on T1 weighted images were consistent in the patient diagnosed as having AVN, the findings on the corresponding T2 weighted images varied. Areas that were of very low signal intensity on T1 weighted images were found to correspond with a similar appearance on T2 weighted images in only 3 cases. In the remaining four cases, the area of necrosis had an intermediate signal intensity on T2 weighted images similar to or above that of adjacent normal marrow.

Pockets of joint effusion within the wrist were present on T2 weighted images in all patients examined and typically involved multiple compartments. The amount of joint fluid in patients with AVN was not greater than the patients without AVN.

The findings on T2 weighted images in patients with carpal AVN is variable and may represent significant differences in the underlying morphology. The presence of an effusion in the wrist is not a helpful secondary sign in diagnosing carpal AVN.

245

AVASCULAR NECROSIS IN SICKLE CELL ANEMIA: MR CHARACTERISTICS

VM Rao, RM Steiner, S Ballas, D Mitchell, L Burk, MD Rifkin
Department of Radiology, Thomas Jefferson University Hospital, Philadelphia, Pennsylvania

The purpose of this study was to determine: (1)if the MR appearance of avascular necrosis (AVN) in sickle cell anemia (SCA) differs from AVN in patients without hemoglobinopathy, (2)if the type of bone marrow (fatty or red marrow) in the epiphyses affects the morphologic features of AVN. MR images of 20 hips and 4 shoulders in 10 patients, with known homozygous SCA were reviewed. All images were obtained on a 1.5T superconductive magnet, using short and long TR/TE sequences. The MR appearance of AVN was classified according to that previously described.[1]

Results revealed varying patterns of epiphyseal marrow (EM). The EM in short TR/TE images showed high signal (fatty in 2 hips, 1 shoulder), low signal (hematopoietic in 11 hips), mottled with high and low signal (mixed in 4 hips, 2 shoulders), and signal absence (hemosiderosis in 2 hips). The extent of hematopoietic marrow expansion into the epiphyses may be related to the severity of the disease. AVN, with variable appearances ranging from Class A to Class D were noted in fatty as well as hematopoietic marrow. The double line sign of AVN was seen only in fatty epiphyses. Different stages of AVN were present in the same area and may be related to repeated episodes of vascular insult and necrosis. Class A AVN with central high intensity surrounded by dark rim on short TR/TE sequences was noted in 4 hips and 1 shoulder; Class C AVN in 2 hips; Class D in 2 hips, 1 shoulder and Class B in none. MR diagnosis of AVN corresponded with radiographs in every case.

Though our numbers are small, our observations suggest that the changes of AVN are more easily seen in fatty epiphyses. When SCA epiphyses demonstrate low signal intensity on short TR/TE sequence, changes of AVN may not show the same pattern as AVN in patients without hemoglobinopathies.

1. Mitchell DG, Rao VM, Dalinka M, et al: Femoral head avascular necrosis: Correlation of MR imaging, radiographic staging, radionuclide imaging and clinical findings. Radiology 1987; 162:709-715.

246

DEGENERATIVE CARTILAGE LESIONS OF THE HIP: IMPROVEMENTS IN VISUALIZATION OF EARLY ARTHRITIS WITH A NEW SWITCHED-ARRAY-COIL (SAC) IN COMBINATION WITH FAST IMAGING.

G. Bongartz, H.Requardt, J. Griebel.Siemens medical engeneering group, Henkestrasse 127, D - 8520 Erlangen, FRG

Early degenerative disease of the hip joint cannot be seen on conventional x-rays and CT because hyaline cartilage is invisible. Secondary phenomena like narrowing of the joint space and reactive sclerosis in the weight-bearing areas represent advanced stages of cartilage damage. To introduce orthopedic treatment at an early stage of hip arthrosis, direct imaging of the cartilage and of its varying appearance with degeneration is necessary. Magnetic Resonance Imaging has been shown to be reliable in soft-tissue differentiation. Improvements in resolution and SNR have been achieved by the use of a variable Helmholtz coil in a double ladder design that is able to vary the field of view during one examination without changing the patient's position. In this way it is possible to investigate both hips separately in a smaller volume, thus diminishing artifacts and increasing SNR.
T1 - weighted spin-echo sequences with short TR and TE demonstrated detailed anatomy of the hip joints and were easily done within 3 - 4 minutes. Both cartilage layers could be separated in unaffected joints by a small dark film of synovial fluid between them. The brighter signal of hyaline tissue on T2-weighted images is due to its water content. In these sequences, differentiation of both cartilage layers is impossible because of the increased signal from synovial fluid.
SE-sequences with long TR and TE are time-consuming and sensitive to various artifacts, thus having a low SNR. Similar tissue characterization and contrast can be achieved by fast gradient echo - sequences like FLASH or FISP with various flip angles. 2D and 3D studies were possible in 1 - 5 minutes with spatial and contrast resolution superior to T2-weighted SE - sequences. Development of degenerative changes in the hip-joint was examined using a 1.0 tesla Magnetom. Multidirectional images of 10 healthy volunteers and 45 patients with different stages of arthritis were compared. In some ad- vanced diseases, MR was performed prior to joint replacement. In these cases, histopathological correlation was possible. Thinning and irregularities of the hyaline cartilage was found in T1-weighted images in early arthritis, whereas signal intensity did not vary from normal. In T2-weighted sequences,focal areas of slightly lower signal likely reprensented dehydration and fibrosis of the cartilage. This was found to be an early sign of degenerative arthritis of the hip.

GASTROINTESTINAL

247

A New Multislice Gradient Echo Sequence for MRI of focal Liver Lesions

Bittner,R., Laniado,M., Sander,B.,Langer,M., Claussen,C.
Dept.of Radiology, Klin. Charlottenburg, Freie Universität Berlin

A T1-weighted multislice gradient echo sequence (MGE) was employed in 20 patients with focal liver lesions. Results were intraindividually compared with those of SE 200/16- (8 acquisitions,6.9 min/single slice) and SE 1600/35,105 sequences (1 acquisition,7 min./8 sections). MGE yielded 18 contiguous 10 mm slices (TR 306/TE 12msec,α= 90^{o}). With four acquisitions imaging for the entire liver was 5.25 min. Lesions that were shown on T1- or T2- weighted SE images were confirmed on MGE scans. Due to signal averaging motion artifact reduction of MGE was superior compared with proton- or T2-weighted images. In 12 out of 20 patients MGE yielded the highest contrast-to-noise ratio for liver lesions. In 4 cases SE 200/16 sequence displayed slightly higher contrast-to-noise ratio than MGE. In 3 out of 7 cases of hemangiomas T2-weighted images were superior with respect to contrast-to-noise ratio. Multislice capabilities of the GE technique made up a significant advantage of this heavily T1-weighted sequence especially in multifocal lesions. We conclude that the MGE sequence is a time-saving and highly effective screening technique for focal liver lesions.

248

QUANTITATIVE AND QUALITATIVE CRITERIA FOR THE DIFFERENTIAL DIAGNOSIS OF HEPATIC HEMANGIOMA AND METASTASES

E Rummeny, DD Stark, R Weissleder, S Saini, PF Hahn, JF Simeone, S Geller, J Wittenberg, JT Ferrucci
Department of Radiology, Massachusetts General Hospital, Boston

Several groups have suggested that MRI is a useful method for diagnosis of hepatic cavernous hemangioma. However, controversy exists about MRI tissue specificity and as to which pulse sequence technique(s) most accurately distinguish hepatic cavernous hemangioma from hepatic metastases. To establish criteria for the differential diagnosis of cavernous hepatic hemangioma we quantitated MR tissue characteristics and evaluated the morphologic features of 69 hemangiomas in 47 patients and 72 metastases in 51 patients. T1 and T2 weighted (T1W,T2W) SE, and gradient recalled echo (GR) images were obtained at 0.6 T. Quantitative image analysis included measurement of tumor/liver signal intensity (SI) ratios, tumor/liver contrat-to-noise (C/N) ratios, and calculation of proton density and relaxation times. Qualitative image analysis included assessment of lesion homogeneity and configuration of the lesion margin. T1W SE and GR techniques as well as the T2W SE 2400/60 pulse sequence failed to provide reliable differentiation. However, mean SI ratios for the SE 2400/120 sequence were for cavernous hemangioma and metastases, respectively, 3.6 ± 1.3 and 1.7 ± 0.7 and for the SE 2400/180 sequence were 6.0 ± 2.5 and 1.6 ± 0.7. These data were statistically significant at $p<.001$ for both pulse sequences. Furthermore, of the 98 individual patients studied, the SI ratio of metastases overlaped the hepatic cavernous hemangioma group in only 4 cases while morphologic features were diagnostic for cancer in two. Therefore, we conclude that MRI performed at 0.6 T with the SE TR 2400/TE 120 or 180 msec offers an overall accuracy of greater than 95% in the differential diagnosis of hepatic cavernous hemangioma and liver metastases.

249

MRI OF HEPATIC LYMPHOMA

R Weissleder, DD Stark DD, G Elizondo, E Rummeny, PF Hahn, S Saini, JT Ferrucci.
Department of Radiology, Massachusetts General Hospital, Boston, MA.

We studied eight patients with proven hepatic lymphoma to evaluate the potential of MRI in detecting human hepatic lymphoma. In addition, rodent models of hepatic lymphoma were studied to evaluate the potential of ferrite enhanced MRI for detection and differential diagnosis of hepatic lymphoma. Three patterns of human hepatic lymphoma could be identified by MRI. Using standard imaging pulse sequences (SE 260/14, SE 2350/120) focal hepatic lymphoma was most easily detected, diffuse hepatic lymphoma was undetectable and mixed hepatic lymphoma (focal and diffuse) was detected when solid lymphoma deposits of greater than 5 mm in diameter were present in the hepatic parenchyma. Experimental studies in rodents indicate that lymphoma-liver contrast can be increased 35 fold (increase in contrast-to-noise ratio from 0.4 to 14.1) by administration of ferrite, increasing the detectability of focal and mixed hepatic lymphoma. Diffuse lymphoma limited to periportal spaces was not detected by MRI probably because phagocytosis of ferrite by reticuloendothelial cells takes place in sinusoids and is not affected by periportal lymphoma cells.

250

IMAGE ARTIFACTS INTRODUCED BY MRI GASTROINTESTINAL CONTRAST AGENTS: MAGNITUDE, CAUSE, AND AMELIORATION

PF Hahn, DD Stark, R Weissleder, S Saini, G Elizondo, JT Ferrucci
Department of Radiology, Massachusetts General Hospital, Boston, MA

Gastrointestinal contrast agents for MRI have been developed to act as either positive or negative agents. Positive agents act by shortening the spin-lattice relaxation time (T1), producing increased signal compared to native bowel contents. Negative agents shorten the spin-spin relaxation time (T2) or reduce the proton density to decrease signal intensity. Problems include homogeneity of small bowel marking, patient tolerance, and artifacts created by the presence of magnetically active material. Additives to distend the bowel or speed passage, special imaging techniques (fast scanning), and chemical reformulation with coating or chelation have been proposed to overcome these difficulties.

Based upon previous experience with superparamagnetic iron oxide (ferrite) as a negative gastrointestinal contrast agent, we report in vitro MR spectroscopy and in vivo animal MR imaging studies comparing ferrite (T2) with paramagnetic (T1) contrast agents including ferric ammonium citrate and a gadolinium chelate (Gd-DOTA). The positive agents are indistinguishable from each other when used in animal models in a molar concentration ratio of 6 (Fe) to 1 (Gd), resulting from 6-fold greater in vitro T1 shortening effect of Gd compared to ferric iron. Motion ghost artifacts were increased in animals by the use of the positive agents and decreased with ferrite. Image distortion occurs when ferrite is present in overdose. Focal distortion can occur in individual bowel loops with otherwise satisfactory doses, an effect that can be reduced with suspending agent additives. Such focal distortion is attributed to regional concentration gradients from gravitational settling, so reduction in particle size may ultimately eliminate this effect by increasing particle buoyancy.

251

A NEW ORAL CONTRAST-AGENT IN MRI FOR THE GASTROINTESTINAL TRACT : STUDIES IN PATIENTS.

RA Maas, HJ Langkowski, MA Heller, RO Spielmann, HO Jend, FR Oesterreich, EG Buecheler
Department of Radiology, University Hospital Eppendorf, Hamburg / FRG

MRI of the upper abdomen has become feasible with the developement of rapid pulse sequences (e.g. fast-field-echo, FFE). However, further improvement of the diagnostic potentials of MRI may be achieved by the use of oral contrast agents.

This report focusses on the application of a solution - known as "astronautic solution", which is totaly absorbed in the small bowels, as an oral contrast agent in MRI, because it raises the signal intensity of the GI-tract significantly - T1 and T2 weighted. The solution contains amongst other substances iron(III)pyrophosphate and manganesesulphate at a concentration of 0.007 mg/ml and 0.0012 mg/ml respectively. These paramagnetic agents shortens the T1 and T2 relaxation times. A bright contrast enhancement between the stomach and duodenal wall (dark) and the internal volume of the bowels is achieved.

The contrast agent is non-toxic, cheap, widely used in internal medicine and has a quite moderate taste.

In-vitro phantom-measurements at various concentratins with calculation of pure T1 and T2 values were performed. In addition the findings in patients with pancreatic neoplasms (n=3) and abdominal lymphomas (n=7) are demonstrated. The increased contrast of the upper GI-tract together with FFE-imaging creates excellent distinction between gastrointestinal structures and adjacent abdominal viscera.

252

MAGNETIC IRON OXIDE: CLINICAL STUDIES

D Stark, R Weissleder, G Elizondo, P Hahn, S Saini, J Wittenberg, J Ferrucci
Department of Radiology, Massachusetts General Hospital

Iron oxide (ferrite) crystals, 50-150 nm in size, obtained from Advanced Magnetics, Inc., Cambridge, MA as AMI-25 were studied in doses ranging from 5-40 umol/kg. Twenty patients with liver cancer, lymphoma, or abscess were imaged before and after iron oxide administration using 0.3T Fonar and 0.6T Technicare systems. No symptoms, signs, or changes in laboratory tests could be attributed to the drug. Liver and spleen SNR decreased 50-90% and focal lesions were unchanged. As a result, CNR of liver cancer increased more than two-fold over what could be achieved with pulse sequence manipulation alone. Lesion conspicuity increased dramatically, smaller lesions (2-8 mm size) were detected, and more extensive disease and/or a greater number of lesions were identified in 16/20 patients. In four patients, the pre- and post-contrast images were equivalent. The most effective pulse sequence for iron oxide enhanced MRI, SE 500/30, is widely available and has the advantage of rapid patient throughput.

253

HEPATIC METASTASES: DETECTION BY FERRITE-ENHANCED MR

Y-M Tsang, DD Stark, M C-M Chen, R Weissleder, S Saini, J, Wittenberg, JT Ferrucci
Department of Radiology, Massachusetts General Hospital

Recent investigations have shown that ferrite-enhanced MR is a promising technique for hepatic cancer detection. We utilized a rat liver-tumor model to determine the relationship of contrast-to-noise ratio (CNR) to size threshold of lesion detection. Twenty-eight rats were innoculated with 500,000 cells of rat mammary carcinoma and 4-14 days later underwent non-contrast and ferrite-enhanced MR using the head coil of a 0.6T clinical MR system. The rats were scanned in the coronal plane with 21 cm field-of-view (FOV) and 4 mm slice thickness. Non-contrast SE 500/32 images were obtained. Rats were killed immediately after MR, and hepatic tumors identified at autopsy were correlated with MR image findings. CNR was measured from the non-contrast and ferrite-enhanced MR images. Non-contrast SE 500/32 CCChad the lowest CNR (1.5) and detected the fewest lesions (6/39); non-contrast SE 260/21 had CNR=5.3 and detected 14/39 lesions; ferrite-enhanced SE o hold size of detection was decreased from 4 mm by non-contrast SE 500/32 to 2 mm by ferrite-enhanced SE 500/32. Non-contrast SE 500/32 underestimated lesion size by 2 mm, whereas ferrite-enhanced SE 500/32 enabled accurate size measurement.

254

FAST MR IMAGING OF LIVER LESIONS WITH GD-DTPA

HJ Langkowski,R Maas,M Heller,HH Jend,R Spielmann,T Knepper,E.Buecheler
Department of Radiology, University Hospital of Hamburg, Germany

With a 1.5 Tesla MR imager investigations of patients with liver lesions before surgical resection are done. The investigations are performed in fast-field-echo technique (FFE, gradient echo) in approximately 8 sec for a T1- and 15 sec for a T2-weighted slice with a slice thickness of 10 mm in breathing-pause. Within this time even an ill patient can hold the breath, so that no breathing artefacts occur. The whole liver is investigated without a gap first in a T2-weighted series, in a T1-weighted without and then in a series T1-weighted after application of Gd-DTPA i.v.. The total time for the whole liver investigation is less than one hour. Furthermore most of the patients get US, CT, scintigraphy and angiography of the liver before resection of the lesions.
We have examined 51 patients, 25 patients have got a resection of the liver lesions. From these 25 patients we got the real number and size of the lesions with their histologies.

The lesions are seen best in T1-weighted images with Gd-DTPA, worse in T2-weighted and worst or not seen in T1-weighted MR images. Lesions less than 1 cm could not be seen, except in one case with liver metastases of a melanoma, which showed a good contrast and were bright in T1-weighted images without Gd-DTPA. Nearly all lesions over 3 cm in size were seen well. Between a size from 1 to 3 cm we often failed, because of less contrast to the normal liver tissue even with application of Gd-DTPA.

PERFUSION & FLOW

301

PROBLEMS IN THE CLINICAL APPLICATION OF PERFUSED FLOW VISUALISATION TO THE ABDOMEN

I R Young, G M Bydder
NMR Unit, Hammersmith Hospital, Du Cane Road, Hammersmith, London W12 OHS

It has proved practicable to apply large enough gradient pulses to develop enough sensitivity in the method of measuring flow using symmetrical pulses on either side of the 180^{b} pulse in a spin echo experiment (1) to allow visualisation of phase change due to coherent perfused flow (2). These effects are identified as being one of the potential contributors to the changes observed by Le Bihan and described by him as intra voxel incoherent motion (3). (Effects are observed in image magnitudes where some of the signal from a voxel arises from moving material and some from stationary, and where the phase of the former is shifted relative to that of the latter.)

The majority of the work thus far (2) has been done in the brain, and is relatively easier than the corresponding experiment in the abdomen for a number of reasons.

1) T2 in the normal brain is longer than in most of the normal abdomen.
2) There are relatively few motion related artifacts apart from those associated with cardiac related pulsatility.

Techniques like MAST (4), with no compensation for the velocity component, are useful, but are only partly applicable as a better strategy is to eliminate the signals from fast flowing material as completely as possible by selective saturation. Respiratory encoded phase encoding (ROPE) (5) is used to control respiratory motion, and cardiac gating to lock the experiment to a fixed time in the cardiac cycle. With all these precautions, adequate visualisation can be obtained for perfused flow patterns in abdominal tissues using phase maps. Quantification, already mentioned as a problem in the brain (2) is significantly harder in abdomen as artifact levels are significantly higher.

1) D J Bryant et al, J. Comp. Asst. Tomog., 8, 588-593 (1984)
2) I R Young et al, Proc. 6th Ann. Mtg. SMRM p863 (1987)
3) D LeBihan et al, Radiology 601, 401-407 (1986)
4) P Pattany et al, J. Comp. Asst. Tomog. 11 (in press) (1987)
5) D R Bailes et al. J. Comp. Asst. Tomog., 9 835-838 (1985)

302

PAIRED CPMG SEQUENCES FOR APPARENT DIFFUSION CONTRAST

R.V. Mulkern, R.S. Spencer, D.C. Metcalf
Dept. of Radiology, Brigham and Women's Hospital

We have used paired, interleaved CPMG sequences to create two images which, when divided, yield an image whose contrast depends only upon the apparent diffusion coefficient in a given pixel. The two magnitude-calculated images were reconstructed using back-projection from respectively, the seventh echo of a CPMG sequence with a TE of 20 ms and the first echo of a CPMG sequence with a TE of 140 ms. We used a Bruker BNT-1000 MRI unit operating at a field strength of 0.15T, with read gradient strengths of 0.23 G/cm. The slice selection process employed permits the use of hard 90^{o} and 180^{o} pulses with widths of 12.5 and 25 us respectively. This eliminates the effects of selective refocusing pulses which have recently been shown to enhance the decay of echo signal intensity beyond that due to normal T2 processes and diffusion. Further, this technique differs from those previously applied in that no diffusive probe gradients are required. The method has been tested on a variety of phantom materials including water, hot coffee and gelatin at various concentrations. Reasonable values for diffusion coefficients in the homogeneous phantoms have been obtained, although additional dephasing of the spins due to field drifts of the resistive magnet can lead to anomalously high values. We find (1) an apparent diffusion coefficient in hot coffee (cream only) of up to 1.6 x 10^{-4} cm^2/sec (reflecting the presence of both convection and diffusion); (2) a diffusion coefficient in room temperature coffee of 2.1 x 10^{-5} cm^2/sec, in excellent agreement with the accepted value for room temperature water; and (3) decreasing diffusion coefficients with increasing weight-percent gelatin. We also present pure diffusion maps of human brains and discuss methods for the improvement of signal to noise with the technique that do not require additional signal averaging.

303

PERFUSION IMAGING WITH A SINGLE MULTIECHO PULSE SEQUENCE

JR MacFall, GA Johnson, JP Karis
GE Medical Systems, Milwaukee, WI and Duke University, Durham, NC

Current models describe tissue perfusion in terms of the amount of flow occuring in small capillaries averaged over an imaging voxel. Perfusion is then measured by observing the image intensity reduction due to dephasing of spins flowing through paired pulsed gradients. A simple application of this technique actually observes flow and diffusion. Improved techniques utilize even-echo rephasing to separate these effects. Typically, however, two or more separate scans are used to acquire the required data.

A three echo multi-echo technique was developed to acquire the necessary data in a single scan. A dialyser was used to construct an appropriate phantom. Data from the phantom and human volunteers was acquired to test the sequence. Qualitatively the data shows the expected effects. However, results also show that stronger gradients than the $1G/cm^2$ used in this work seem to be required for the technique to work well with the short T_2 values (T_2 ~ 70msec) typical of humans.

304

SLOW MOTION EFFECTS IN FAST MR IMAGING

RB Buxton, D Chien, CR Fisel, TJ Brady
Dept. of Radiology, Massachusetts General Hospital, Boston MA

A new technique for assessing slow motions, such as diffusion and capillary flow, with fast imaging has been developed and tested in phantoms. In steady-state fast imaging methods (e.g., GRASS), the phase encoding gradient pulses are compensated so that a particular spin group precesses by the same angle between each RF pulse. For TR<T2, a steady-state is produced that generates significantly more signal than when the transverse magnetization is spoiled. When a GRASS pulse sequence is modified by addition of another z-gradient pulse prior to each rf pulse, small displacements of the spins between rf pulses (e.g. by diffusion or capillary motion) lead to a decrease in the MR signal that can serve as a measure of these motions. Modified GRASS images were obtained at 0.6 T with the additional gradient pulse provided by varying the duration of the slice-select gradient before the RF pulse from 1.7 to 13 msec. Results of imaging water, acetone, and egg white are shown in the figure and table. For each phantom, the signal decreased as the gradient duration increased, and the magnitude of the signal drop was correlated with the diffusion coefficient. Preliminary experiments in a porous bed phantom designed to mimic capillary flow showed a decrease in signal between stationary and slow flowing (< 1.0 mm/s) water. This technique may prove useful in assessing tissue perfusion and diffusion.

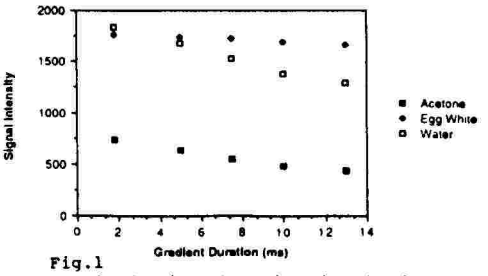

Fig.1
Graph showing drop in signal with increasing gradient duration.

	D ($10^{-5}cm^2/s$)	Maximum Signal Drop
Acetone	4.6	43%
Water	2.4	34%
Egg White	1.7	6%

305

BLOOD FLOW EFFECTS IN DIFFUSION IMAGING
D Chien, PG Okunieff, RB Buxton, BR Rosen, TJ Brady.
Massachusetts General Hospital, Boston.

Experiments were performed to measure the effects of tissue perfusion on MR images designed to be sensitive to small scale motions. Our objectives were: 1) to quantitatively measure the diffusion coefficient D in the murine fibrosarcoma tumor in mice, 2) to determine the effects of blood flow on measurements of D in this model, 3) to exclude the effects of temperature between normal and non-perfused states, 4) to calculate the blood volume fraction in the tumor by a simple model.

Spontaneous C3Hf murine fibrosarcomas implanted in the hind foot of C3Hf/ Sed mice were imaged in a 0.6T Technicare clinical imager. A diffusion sensitive SE (TR=500 msec, TE=180 msec) sequence was used, in which the duration of the read gradient was varied both before and after the 180 pulse. Diffusion maps were generated on a pixel by pixel basis. Images were acquired A) during anesthesia, B) immediately post sacrifice with barbiturate overdose, with temperature control, and C) following equilibration to room temperature.

Preliminary data (n=5) showed that the measured D decreased by approximately 10%, when blood flow effects were removed (comparing A and B) while the temperature difference caused the D to differ by 25%, in agreement with the known variation in D with temperature. Using a simple two compartment model of the vascular and extravascular spaces of the tissue, the measured 10% decrease in the apparent D between the tumors with and without flow is consistent with a vascular volume of approximately 6%, in reasonable agreement with other estimates.

These results demonstrate that perfusion has a measurable effect on diffusion imaging. This is a necessary first step in developing techniques to distinguish between capillary flow and molecular diffusion, and to directly image perfusion.

306

CLINICAL RESULTS OF MR FLUOROSCOPY

JN Lee, T Tascyian, RC Wright, F Farzaneh, SJ Riederer
Duke University Medical Center

Initial clinical results of magnetic resonance (MR) fluoroscopy are presented and discussed. This method is similar to x-ray fluoroscopy in that it produces high imaging rates at reduced spatial resolution and signal-to-noise. A limited number of phase encodings is repeatedly acquired using limited flip angles (LFA) to produce a sequence of MR images. These images can be separated in time by as little as one TR interval; that is, when a new phase encoding is acquired, it replaces the data previously recorded for that phase encoding, and the image is reconstructed again. Although the interval between successive images may be as small as TR , the lag time for a complete image is still dictated by the number of phase encodings; 40 phase encodings with TR=15 msec will produce a completely new image every 600 msec.

In this presentation clinical studies will be shown to demonstrate practical uses for MR fluoroscopy . One of these is the ability to quickly scan through the patient to locate the slice of interest before acquiring the more time consuming diagnostic images. The patient can be mechanically moved while the data is being acquired, or the slice of interest can be electronically scanned through a given volume.

Another possible use is the interactive rotation of the slice of interest for oblique angle imaging. By changing the imaging angle during an MR fluoroscopy pulse sequence the result can be displayed immediately, without stopping to reset the angle. Since it is not currently possible to change gradient values during a scan, the effect was simulated by having the patient rotate and tilt their head during data acquisition.

These examples show that the high imaging rate of MR fluoroscopy can be a valuable tool for quickly locating slices of interest in MR imaging.

307

BIPOLAR PHASE COMPENSATED TECHNIQUES TO SUPRESS MOTION ARTIFACT

EC Unger (1), J McGlone (2)
Fox Chase Cancer Center(1), Siemens Medical Systems(2)

We have implemented and tested bipolar techniques to improve motion artifact on SPIN echo imaging. A bipolar gradient was applied in the read-out (i.e. frequency encoding) axis to re-phase spins which had been de-phased by motion. Bipolar sequences were developed for T1-weighted (short TR/short TE) and T2- weighted double echo (long TR/short TE/ long TE) sequences. We compared the image quality from bipolar sequences with non-gaited and gaited standard SPIN echo techniques and also non-gaited and gaited bipolar techniques. Non-gaited bipolar techniques resulted in improved image quality in the spine and abdomen relative to either non-gaited or gaited standard SPIN echo techniques. Gaited bipolar techniques resulted in slight further improvement in image quality relative to non-gaited bipolar techniques. When bipolar techniques were used CSF consistently appeared bright and the cord was easily differentiated from CSF. Motion artifact was consistently improved on bipolar relative to SPIN echo techniques.

There are certain limitations in the implementation of the bipolar sequences because an additional gradient pulse is required, this limits the minimum echo time which can be obtained on either single or multi echo sequences. Because an additional gradient pulse is required this also limits the maximum zoom factor or minimum field of view which can be obtained. At the present time, on a double echo sequence, with a minimum TE of 35msec the minimum field of view is approximately 25 cm.

Bipolar techniques provide a practical approach to suppressing motion artifacts and improving anatomic visualization and contrast. We have found these sequences to be quite useful, and are now the sequences of choice at our institution for spine and abdominal imaging.

308

PULMONARY ARTERY BANDING IN INFANTS AND CHILDREN: NONINVASIVE ASSESSMENT OF CINE MAGNETIC RESONANCE IMAGING

IA Simpson, KJ Chung, JB Powell, DJ Sahn, DP Berthoty, JR Hesselink
University of California, San Diego

Noninvasive assessment of pulmonary artery (PA) banding in infants and children can be difficult and evaluation by cardiac catheterization and angiography is often required. Cine Magnetic Resonance Imaging (MRI) now provides dynamic functional information, in addition to precise anatomical detail and is of potential value in the assessment of these patients. We performed conventional ECG-gated and cine MRI using a GE Signa 1.5 Tesla superconducting magnet in 6 infants and children with PA banding, ages 9-36 months under sedation with chloral hydrate (80-100mg/Kg). All patients were studied within the 24cm round coil for high resolution imaging. MRI was performed in sagittal and rotated coronal views with 5mm slice thickness without interslice spacing. Flow enhanced imaging in the cine mode was obtained by gradient recalled acquisition in steady state (GRASS) scanning with a 30° flip angle and 22 msec repetition time. All patients underwent cardiac catheterization for comparison. High resolution images of the PA band position and anatomy were obtained in all patients using conventional ECG-gated MRI and the measured PA band diameter (mean 3.32mm ± SD 0.92mm) correlated well with the pressure gradient across the PA band at catheterization (mean 55 ± SD 9 mmHg, r= -0.94). Flow through and distal to the PA band was visualized in all patients by cine MRI and was always associated with a significant systolic and early diastolic flow void distal to the banding, indicating satisfactory banding and the presence of high velocity flow, confirmed as always > 3.0 m/sec by continuous wave Doppler examination. The size of the distal PA's and the presence of satisfactory flow in the distal PA were well visualized in all patients on cine MRI, confirmed at angiography in all cases. In conclusion, the dynamic spatial and temporal flow information at and distal to the PA band, in addition to high resolution anatomical detail provided by the combination of conventional ECG-gated and cine MRI now allows accurate assessment of pulmonary artery banding to be obtained noninvasively and will provide valuable assistance in the timing and planning of surgery in these patients.

309

ELIMINATION OF MNHPTA IN RENAL COMPROMISED RABBITS

F Leone, H Galanty, R Hooley, D Kukafka, D McDonald, D Sonenblick, G Wolf
Pittsburgh NMR Institute, Pittsburgh, PA 15213

The chelate MnHPTA has proven useful as a paramagnetic contrast agent for MR imaging of animals. This compound is primarily eliminated via the hepatobiliary tract with small amount excreted by the kidney. Potential patients for MRI include subjects with one of these elimination routes compromised.

Three groups of adult male NZW rabbits (2.5 kg) were utilized to simulate potential patients: 1. Normal untreated controls, 2. Normal rabbits injected with MnHPTA 3. Rabbits with experimentally induced acute renal failure (ARF) plus MnHPTA. To induce ARF, both ureters of the experimental animals were ligated 24 hours prior to the study. Five millimete thick T1 weighted images were obtained in a 1.5T GE Signa system using TR 400, TE 20, NSA 2. Images were obtained prior to and at times 1 min, 6 min, and 15 min after an IV bolus of 20 uM/kg MnHPTA. The MnHPTA was supplied by Mallinkrodt Inc. All the rabbits were euthanized b pentobarbital overdose at T = 15 min in order to halt the biological process and obtain tissu samples for T1 and T2 determinations on RADX Proton Spin Analyzers. Intensity values were recorded over time using the available Signa software.

In vitro analysis of tissues from animals sacrificed at 15 minutes showed that proton relaxation rates of rabbit liver in the ARF group were significantly increased over those of normal rabbit liver after injection of MnHPTA. However, the renal cortex and medulla showed no significant enhancement of relaxation rate as compared to untreated rabbit cortex and medulla. In vivo, the kidney showed a nephrogram at 1 minute in the ARF animals but rapidly decreased in intensity over time. Intensities of normal rabbit cortex and medulla with MnHPT remained significantly elevated. The difference in renal response reflects the marked reduction in glomerular clearance of MnHPTA in rabbits with ARF. On the other hand, ARF livers accumulated so much MnHPTA that short T2 reduced actual image intensity.

This data suggests that in rabbits with renal compromise, the hepatic uptake of MnHPTA is enhanced. With filtration compromised, renal MnHPTA clearance is reduced and remains in the systemic circulation to be sequesterd by the liver.

HEAD

310

MRI FOR EVALUATION OF ENLARGED OPTIC NERVE

B Azar-Kia, M Mafee, MH Naheedy, M Fine
Department of Radiology, Loyola University Medical Center and University of Illinois

The purpose of this presentation is to discuss the value of MRI in cases of an enlarged optic nerve. Before the advent of MRI, CT was the best method of evaluation for optic nerve pathology. However, differentiation of lesions involving the optic nerve could not be easily made by CT scanning. MRI has assumed a greater role in assessment of optic nerve lesions. We have used 1.5 tesla GE signa unit for our studies.

The most common causes of enlarged optic nerve are glioma and meningioma. Gliomas show high intensity signal on T_2 weighted images along with an irregular and tortuous enlarged optic nerve. Meningioma usually has low signal intensity on T_1 and T_2 weighted images, showing uniformly enlarged optic nerve. Optic neuritis other than high signal intensity on T_2 weighted images may show evidence of multiple sclerotic changes in the brain tissue. Cases of sarcoidosis have shown similar features as meningiomas. However, sarcoid usually extends into the suprasellar cistern and pituitary fossa. Associated systemic symptoms are of value for differentiation. Enlargement of the optic nerve due to widening of the subarachnoid space around the optic nerve is easily recognizable by low intensity of CSF on T_1 and high signal intensity on T_2 weighted images. These cases show normal size optic nerve through the CSF. These cases include increased intracranial pressure due to intracranial mass lesions and pseudotumor cerebri. We have also seen asymptomatic unilateral or bilateral enlarged optic nerve, the result of widening of the subarachnoid space around the optic nerve giving a false impression of enlarged optic nerve. These cases referred to us after eye examination for correction of eye glasses showed changes in the optic disc. Follow up on these cases failed to demonstrate any abnormality. We believe that this could be a normal variation of the size of the subarachnoid space around the optic nerve.

311

VISUAL PATHWAY GLIOMAS IN NEUROFIBROMATOSIS PATIENTS: MR CHARACTERISTICS

C.F. Dowd, M.D., S.W. Atlas, M.D., W.F. Hoyt, M.D., A.J. Barkovich, M.D., D. Norman, M.D.
Departments of Radiology & Ophthalmology, University of California, San Francisco

Approximately one-third of patients with neurofibromatosis (NF) have visual pathway gliomas. CT data suggests that less than one-fourth of these lesions extend into the retrochiasmatic visual pathways. Twelve patients (ages 5 to 27 years) with NF and optic chiasm gliomas were evaluated with spin echo magnetic resonance (MR) imaging at 1.5T. Clinical neuro-ophthalmologic status was correlated with MR abnormalities.

Long TR sequences demonstrated chiasm masses to be high signal intensity in 11/12 cases and, in one case, markedly hypointense on the long TR/TE image. Two-thirds of cases showed extension of high intensity posteriorly into the optic tracts, which was usually bilateral and into the geniculate nuclei. Optic tract lesions were patchy, and usually without mass effect. The abnormal intensity spared the retrogeniculate optic radiations in 11/12 cases. Optic nerve enlargement was common and bilateral in 50% of abnormal cases. Enlarged optic nerves were distinctly different from involved chiasm or optic tracts, in that these masses were relatively low intensity on long TR images (i.e. isointense to normal white matter and normal optic nerves). Clinical signs/symptoms were not indicative of the extent of MR abnormality.

In our series, contrary to CT experience, the majority of patients demonstrated retrochiasmatic visual pathway involvement in association with their chiasm gliomas. Interestingly, optic radiations were almost always spared, suggesting that the clinical and histologic benignancy of these lesions may correlate with their lack of aggressive extension. Alternatively, the geniculate region, although frequently involved with this low grade lesion, somehow limits extension posteriorly into the occipital lobes. Furthermore, the difference in the signal intensity patterns of the involved optic nerves and the chiasm/optic tracts raises the likely possibility that although these lesions are within the same neuroanatomic pathway, they are two entirely different pathologic processes. A significant portion of these retrochiasmatic lesions may represent secondary demyelination or gliosis rather than actual tumor. MR more fully characterizes this frequently occurring, but poorly understood lesion and may offer insight into the pathophysiologic mechanisms involved in its natural history.

312

PARRY-ROMBERG SYNDROME: VALUE OF MR IMAGING

G Elizondo, M Dieste (*), R Weissleder, LE Todd (*), DD Stark.
Department of Radiology, Massachusetts General Hospital, Boston and MR Unit, University Hospital of Monterrey, N.L., Mexico (*)

The Parry-Romberg syndrome is characterized by a unilateral progressive atrophy of facial skin, subcutaneous fat, connective tissue, and occasionally muscle and bone beginning in the first or second decade of life. CNS anomalies at the level of basal ganglia, disturbances in embriogenesis, and trauma have been attributed as etiologic factors. A total of 5 patients with Parry-Romberg syndrome were studied by MRI using a 0.3 T permanent magnet (FONAR, Melville, NY). T1 weighted (SE 500/28) and T2 weighted (SE 2000/84) images were obtained in transverse and coronal planes. All patients showed unilateral atrophy of subcutaneous fat, superficial facial and masseter muscles, and parotid and submandibular glands. Compensatory ipsilateral and contralateral hypertrophy of medial pterygoid muscle was also present in all cases. Ipsilateral atrophy of the tongue was present in two cases, unilateral orbital fat atrophy in two cases, and unilateral mandibular dysplastic bone in one case. CNS anomalies could not be identified in any case. MRI is a useful imaging modality to assess the extent of unilateral facial atrophy, and reconstructive surgery can be planed more accurately. Furthermore, CNS abnormalities can be investigated or excluded.

313

THE MUSCLES OF MASTICATION: MR IMAGING.
KP Schellhas, HM Fritts, KB Heithoff
All doctors in private practice.

Normal muscles of mastication and pathologic muscle changes may be demonstrated with magnetic resonance (MR) imaging. Lesions of the masseter, temporalis, anterior belly of the digastric and lateral pterygoid muscles may occur in conjunction with central nervous system (CNS) disease, following trauma, in generalized neuromuscular and inflammatory disorders, and accompanying temporomandibular joint (TMJ) disease. MR changes associated with disuse and denervation of the masticatory muscle group are presented. Atrophy and fibrosis of the superior belly of the lateral pterygoid muscle is conjunction with mechanical internal derangements of the TMJ is presented. A spectrum of pathologic lesions involving each of the masticator muscles is shown. Case material was selected from MR studies of the brain, maxillofacial region, and surface coil studies of the TMJ during a twelve month period, employing a 1.5 T magnet (General Electric, Milwaukee, Wisconsin). The authors conclude that MR is a valuable tool for studying lesions involving the muscles of mastication.

314

INTERNAL DERANGEMENTS OF THE TEMPOROMANDIBULAR JOINT: MR STAGING.
KP Schellhas, CH Wilkes, JC Block, MR Omlie, EG Manoles
All doctors in private practice (Dr. Wilkes: President of American Society of TMJ Surgeons).

Internal derangements of the temporomandibular joint (TMJ) can be clearly defined and successfully staged with surface coil MR. Either T1-weighted or partial flip angle sagittal MR imaging techniques may be employed to demonstrate specific meniscus changes associated with early-, intermediate-, and late-stage internal derangements. Early-stage disease is defined as simple anterior meniscus displacement without either morphologic alteration in meniscus shape or change in intrinsic signal intensity in the absence of degenerative bony pathology. Intermediate-stage disease is characterized by meniscus displacement and deformity, with or without meniscus reduction relative to the manidublar condyle, with or without intrinsic meniscus signal changes, without perforation or osteoarthritis. Intermediate stage derangements are separated into early-intermediate and late-intermediate-stage, depending upon the presence or absence of meniscus reduction relative to the mandibular condyle. Early late-stage disease is defined by perforation of the meniscus or disc attachments without osteoarthritis. Advanced late-stage derangements are characterized by meniscus displacement, deformity, perforation and osteoarthritis.

Cases selected for illustration were selected from 740 TMJ studies performed in 452 patients (aged 11 to 78 years) during a nine month period. Surgical results are available for correlation in over 150 cases from the series to date and in all of the cases presented. The presence of an altered meniscus signal may indicate a meniscal tear or myxomatous degeneration of meniscus fibrocartilage in conjunction with fibrillary changes and separation of collagen fibers, which is important information for preoperative staging, prognosis and surgical planning. Pathologic changes within the attached pterygoid muscles are also presented as valuable ancillary findings which may accompany internal derangements in each stage. The authors conclude that surface coil MR is the procedure of choice in most circumstances for staging of internal derangements of the TMJ.

315

MRI TUMOR MARGINS IN LOW GRADE ASTROCYTIC TUMORS

RA Clasen, DC Bergen
Depts. of Pathology and Neurology, Rush Medical College, Chicago, IL

Eleven surgical specimens of resected low grade tumors of the astrocytic series were studied. Eight of these were obtained from patients undergoing surgery for intractable epilepsy. The other three were patients with adult-onset seizures who were operated upon primarily for brain tumors. The fixed specimens were sectioned in the plane of the MRI and gross photographs were obtained of the cut surfaces. Microscopic slides were prepared from all of the surfaces. The extent of the tumor, defined histologically, was drawn on the photographs and these were compared to the MRI obtained prior to surgery. The images were produced from both 0.5 and 1.5 Tesla magnets. The spin-echo sequence was used. Six tumors were completely resected. In five of these there was no histologically recognizable edema and the extent of the tumor closely matched the MRI abnormality. In one the tumor was undergoing malignant transformation. The site of the transformation was seen on the rho weighed but not the T_2 image. In the tumor with edema, the T_2 was shorter than the edema. Five tumors were incompletely excised. In three of these, not associated with edema, the anterior, lateral and posterior margins were identified. These corresponded to the MRI. One tumor was associated with edema which could not be differentiated on MRI. This was the only patient in this series which showed isolated tumor cells in the adjacent white matter. The fifth case was not visualized on MRI. This tumor contained excessive amounts of iron which could have had a paramagnetic effect on the MRI. In two additional patients, a large portion of the frontal and temporal lobes was resected and biopsies obtained from the cut surfaces. These showed grade 2 astrocytomas. The resected specimens, from areas which were normal on MRI, showed neither edema nor isolated tumor cells. It is concluded that MRI accurately defines the tumor in most instances but that it is not always possible to differentiate tumor from edema when this is present. Infiltration of isolated tumor cells into adjacent brain is an uncommon event in low grade astrocytomas.

316

CLINICAL UTILIZATION OF A TRIPLE ECHO MULTISLICE SPIN ECHO SEQUENCE

KL Nelson, VM Runge, J Kirsch, MR Traill, ML Wood
Division of Magnetic Resonance, Tufts-New England Medical Center Hospitals

Nineteen patient examinations were performed using a triple echo multislice motion compensated spin echo sequence.

A triple echo multislice technique was developed to evaluate the clinical utility of an additional more heavy T2 weighted scan in the examination of the CNS. Within one sequence, three echoes were acquired with TEs of 24, 70, and 140 msec. Utilizing a TR=3.0 sec, this allowed for acquisition of 15 slices with each echo, resulting in 45 images of the brain from one pulse sequence. Low bandwidth technique was used with each echo. The second and third echoes also utilized refocusing gradients. Refocusing was performed in the readout and phase encoding direction for TE=70 msec. and in the phase encoding direction only with the 140 msec. echo. The correction was first order in each instance. In two patients with multiple sclerosis, this sequence was compared to a routine double echo multislice technique with TR/TE=3.0/28,70. This sequence did not employ either low bandwidth or motion compensation techniques.

The third echo with TE=140 msec. was degraded in a minority of cases due to artifacts from CSF pulsation. Use of such heavy T2 weighting provided improved delineation of necrotic lesions and abnormal iron deposition. An additional important finding was the utility of a third echo for confirmation of lesions observed on either the first or second echoes. No substantial improvement was however noted in detection of multiple sclerosis plaques. The first echo with TE=24 msec. produced a high signal to noise ratio and high spatial resolution image. The second and third echoes both provided T2 information. Lesion detection improved markedly in the posterior fossa because of motion compensation and high SNR.

Use of a triple echo multislice spin echo technique improved reader confidence in identification of CNS abnormalities. Such a sequence may also find specific application in examination of the infant brain, where T2s are normally prolonged. Adequate motion compensation techniques are critical for high image quality with very long TEs, such as the 140 msec. echo.

317

Fast MRI with a Heavily T2-Weighted PSIF Sequence
B Sander, W Schörner, R Bittner, R Felix
Dept. of Radiology, Klinikum Charlottenburg, Freie Universität Berlin

The interest in the clinical application of rapid steady-state free precession (SSFP) sequences is still growing. Although T1- and proton density weighted SSFP sequences have already proved their clinical relevance T2-weighted SSFP sequences could not compete with conventional spin echo (SE) sequences up to now due to insufficient sensitivity and low signal-to-noise ratio. The purpose of our study is to evaluate the diagnostic value of the new T2-weighted SSFP sequence called PSIF. PSIF is a gradient echo technique and simply a time reversed version of FISP (Fast Imaging with Steady Precession). With PSIF technique signal intensity is mainly based on the steady-state of transverse magnetization which yields highly T2-weighted images.

MRI was performed on a 0.5 Tesla Siemens Magnetom. We examined 40 patients (32 intracranial lesions, 4 spinal chord lesions and 4 liver lesions) with PSIF (TR 40 msec, TE 24 msec, flip angle 90°, matrix 256 X 256, single slice, acquisition time = 42 sec) and multi echo technique (TR 1600 msec, TE 30 to 240 msec).

T2-weighted PSIF images and multi echo images were compared with respect to lesion detection, image contrast and image quality. With both multi echo and PSIF technique all lesions could be depicted. Image contrast of PSIF was comparable to multi echo images with a TE of 180 msec. However, image quality of PSIF images was decreased due to lower signal-to-noise ratio and artifacts due to suszeptibility and proton motion.

In conclusion PSIF is a very fast and sensitive method to detect lesions with prolonged T2-relaxation time.

RELAXATION IN TISSUES

318

CORRELATION OF NISSL, MYELIN, AND IRON STAINS AND MRI OF THE NORMAL SPINAL CORD
AJ Curtin, DW Chakeres, M Finneran, C Boesel, A Yates, E Flint
Departments of Radiology and Pathology, Ohio State University College of Medicine, Columbus, Ohio

The goal of this study is to better understand the magnetic resonance imaging (MRI) appearance of the normal spinal cord. The image contrast does not conform to most histiologic sections and the signal intensities of gray and white matter are different than that seen in the brain.

High resolution axial magnetic resonance images and histiologic stains (iron, myelin, and Nissl) were correlated. All of the images were made with a 1.5 Tesla General Electric Signa system. Spin echo TR 600 TE 20 msec and true proton density (TR 1000, TE 12, flip angle 22 degrees gradient refocused echo at a steady state) images of normal volunteers and a cadaver spinal cord were completed.

The short TR TE images demonstrated low signal areas within the cord including the anterior, posterior columns and the central lateral columns. The proton density images more accurately displayed the gray matter structures as high signal regions.

The iron stains did not correlate well with the images. The myelin stains correlated well with the proton density images. The regions which did not stain with Nissl were dark on the short TR TE images.

We conclude that the Nissl stain correlates with the short TR TE images. The non staining areas are dense nerve tracks without cell bodies similar to the medial lemniscus and generate little signal on all pulse sequences like a ligament. The proton density images most directly correlate with the myelin stains only.

319

T1 ELONGATION IN MOUSE TUMOR TREATED WITH rH-TNF

K Nagano, Y Ueshima, K Goto, T Yamamoto, M Hagiwara, N Iriguchi, J Oh-ishi,H Hayashi,Y Ichikawa
Asahi Chemical Industry Co.,Ltd.

The influence of rH-TNF (recombinant human tumor necrosis factor) administration on the T1 images and the related T1 values of tumors was investigated with a 0.1T MRI (Asahi Mark-J), as the presence of edema, which is generally known to cause T1 elongation, has been demonstrated histologically around the boundary mouse tumors during necrosis induced by rH-TNF.

T1 images (Tr=2000msec, Td=500msec) were obtained using AFP as the inversion pulse, for BALB/c mice bearing transplanted Meth-A sarcoma or Colon 26 carcinoma. T1 imaging just before and 4hr (Meth-A) or 2hr (Colon 26) after administration of rH-TNF at 10,000 U/mouse showed the occurrence of T1 elongation in all tumors following rH-TNF administration, while no significant T1 elongation was observed under similar conditions in mice receiving only rH-TNF-free vehicle (0.1% gelatin-PBS buffer).

Investigation of the time course and dose dependency of changes in the T1 image for Meth-A tumors showed the T1 value to increase markedly during the second hour after administration of rH-TNF at 3,000 or 30,000 U/mouse, but to remain unchanged for tumors in mice receiving vehicle only or rH-TNF at 300 U/mouse, as indicated in the figure.

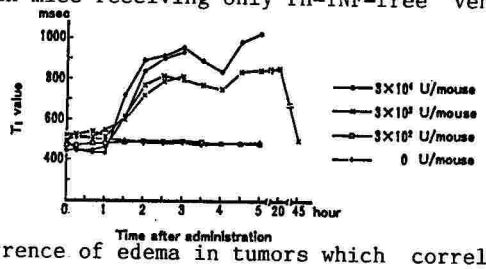

Histological study of sacrifices showed the occurrence of edema in tumors which correlated with the increased T1 values.

The occurence of edema and the resulting T1 elongation may be attributable to damage in tumor blood vessels induced by rH-TNF. The results suggest that a similar occurrence of edema in human cancers, if present, might allow the utilization of MRI for correlation between animal models and clinical studies, and for early evaluation of the antitumor efficacy of rH-TNF in human patients.

320

FOLLOW-UP-STUDY OF BONE TUMORS DURING CHEMOTHERAPY BY T1 AND T2 RELAXATION TIMES.

RA Maas, HJ Langkowski, MA Heller, RO Spielmann, HO Jend, TH Knepper, GU Delling, EG Buecheler
Department of Radiology, University Hospital Eppendorf, Hamburg / FRG

MRI offers accurate information about the morphology of bone tumors concerning tumor localisation, size and volume. The high tissue contrast depicts clearly the extention of the bone marrow alteration and the involvement of the surrounding soft tissues. Compared to CT, MRI gives less information about pathological changes of the calcified bone structures, but this does not minimize it's diagnostic potential significantly, because the tumor can be imaged in coronal, sagittal, axial or even angulated planes and this offers the surgeon a precise overview about the tumor morphology.

A second aspect of MRI is the capability to characterize the tumor tissue by relaxation times T1 and T2. These parameters seem to allow statements about the tissue quality and the fluid content. In vivo studies of bone tumors were performed to find a correlation between T1 and T2 and the distribution of necrotic or vital areas within the neoplasm.

In order to study the influence of antineoplastic chemotherapy on the relaxation times, 8 patients (6 osteosarcomas and 2 Ewing's sarcomas) underwent a follow-up-study for a 2 to 5 months period. MRI was performed 3 to 5 times before, during and after chemotherapy. 27 mixed sequences (alternating SE and IR sequences) during the last 10 months were used to measure T1 and T2 within the tumor. In all patients T2 values increased of about 15 to 30% throughout the imaged section of the tumor. On the other hand T1 values showed a different behaviour : in the majority an increase of 10 to 30% was found, but in 2 cases only parts of the tumor showed an increase of T1 whereas in other areas no change or a decrease was observed. The follow-up is documented graphically. After surgery a histopathological mapping of the resected tumor was performed. The corresponding areas of tumor vitality or necrosis or cystic structures were compared with the measured MRI relaxation times in the same plane. Up to now the value of MRI in predicting responders and non-responders during chemotherapy is not yet fully established.

321

NMR RELAXATION TIME FREQUENCY DEPENDENCE OF IMMATURE RAT TISSUES

M.A.Foster, J.E.Rimmington and J.R.Mallard
Department of Biomedical Physics, University of Aberdeen, Aberdeen, UK

During maturation T1 and T2 relaxation times of most tissues fall coinciding with reduction in water content. We report the frequency dependence of relaxation during maturation. White brain, liver, spleen and skeletal muscle were obtained from Sprague Dawley rats between 3 and 36 days after birth. Approximately 0.5g of tissue was used from a single organ or by pooling from several animals. Graph points are an average of four samples obtained from four or more animals. Samples were examined at 29-31C with a Bruker CXP100 spectrometer operating from 2 to 90 MHz. Graph points for one age are not from the same sample because of time constraints.
Results from muscle and white brain are shown. Muscle has a greater spread of 1/T1 at low than at high frequencies, frequency dependence increasing regularly with age. White brain shows a jump in frequency dependence between days 13 and 21 coinciding with the main phase of myelination. Spleen has marked frequency dependence but this shows almost no change in with age, nor is there a marked change in relaxation time with age. Liver produces a variable picture, corresponding to variability of maturation changes previously reported. In conclusion, age-dependent changes in frequency dependence of T1 are observed for certain tissues. When these are examined in light of earlier studies they appear to correlate with biochemical and structural changes in the tissue and tissue water content.

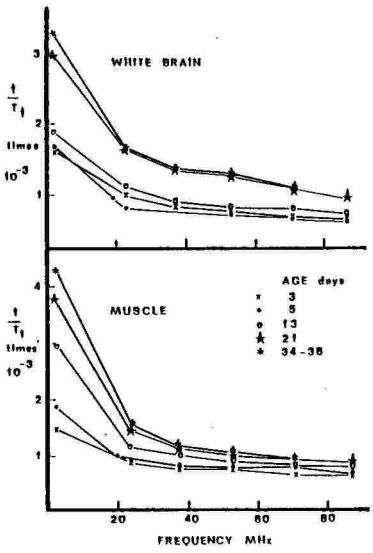

322

TISSUE CONTRAST IN BOTH "FID" AND "ECHO" STEADY-STATE MR IMAGING

LM Eastwood, RE Hendrick, K Jerjian
Picker International Inc. and University of Colorado School of Medicine

The use of steady-state field-echo techniques (FAST, GRASS, FISP) is growing rapidly in clinical MRI. This necessitates a thorough understanding of tissue contrast in the resultant images and its dependence on sequence parameters such as TR, TE and RF flip angle. Previous published papers (1,2) have attempted to describe this contrast based on simple (non-imaging) theory of steady-state signals. While this model does correctly indicate certain trends, such as the increase in T2 contrast with reduction in RF flip angle, more detailed analysis shows it to fail. In particular, the two studies referred to assume the use or absence, respectively, of phase-alternation for the RF pulses and predict very different tissue contrast. In practice, such phase-alternation of the RF pulses has no effect on tissue contrast when using a well constructed steady-state field-echo sequence.

Full analysis of contrast in steady-state imaging requires allowance for the dephasing effects of gradients (3). This fuller model is also required to explain the strong T2 weighting in the "echo", rather than "FID", steady-state imaging of the "contrast-enhanced FAST" technique. In each case, allowance is made for 2N.pi read-gradient dephase across each pixel during TR, with zero dephase between the signal peak and either the preceding or the following RF pulse. The resultant equations cannot be solved analytically, but numerical integration has been used to show the good agreement between the theory and both "phantom" and clinical studies.

(1) TG Perkins, FW Wehrli. Magnetic Resonance Imaging 4, 465. (1986)
(2) RE Hendrick, JB Kneeland, DD Stark. Magnetic Resonance Imaging 5, 117. (1987)
(3) ML Gyngell, Ph.D. Thesis (University of Nottingham, England). (1987)

323

A NEW SEQUENCE TO ENHANCE T2 CONTRAST AT SHORT REPETITION TIMES

G Johnson, DH Miller, PS Tofts, DG MacManus
NMR Research Group, Institute of Neurology, Queen Square, London.

We have developed a new sequence (FRESE - Fast REcovery Spin Echo) which reduces the T1 dependence of spin echo (SE) images and hence emphasises T2 differences. Contrast is thus enhanced at short repetition times. The sequence uses two RF pulses separated by an interval τ to form an echo (which compensates for static field inhomogeneity) at 2τ, i.e. α-τ-β-τ-collect. The nutation angles of the two pulses are chosen to give a positive value of longitudinal magnetisation after the second pulse so enhancing recovery.

Equations describing the behaviour of the magnetisation have been derived. These equations show the following: FRESE T2 dependence is very similar to that of conventional SE sequences; recovery is relatively inefficient unless $\tau \ll TR$; at short TR's echo amplitude is a function of frequency offset unless $\beta = 180^\circ$; provided $\tau \ll TR$ optimum signal is obtained with $\cos(\alpha+\beta) = \exp(-TR/T1)$. The following FRESE parameters may then be optimal: $\cos\alpha \approx -\exp(-TR/T1)$; $\beta = 180^\circ$; 2τ (= TE) = 60-120 ms (similar to conventional SE sequences); $TR > 5\tau$.

We have imaged multiple sclerosis patients at 0.5 T with FRESE sequences with parameters around our provisional estimates of the optimum. FRESE images with TR = 500 ms, TE $\approx$ 100 ms, $\alpha \approx 130^\circ$ and $\beta = 180^\circ$ give comparable contrast to conventional "T2 weighted" spin echo sequences (e.g. SE2000/60) but are collected in a quarter of the time.

324

MATERIAL-SELECTIVE PROJECTION IMAGING IN MR

G.A. Wright, T.J. Brosnan, A. Macovski, D.G. Nishimura
Department of Electrical Engineering, Stanford University, Stanford, CA, 94305

With larger fields of view and shorter acquisition times, projection images have several advantages over cross-sectional images, particularly for screening. Their major drawback is poor conspicuity due to overlapping structures. However, MRI is well-suited to overcoming this difficulty through material cancellation. In an MR projection image, a pixel represents the sum of material thicknesses along the projection each weighted by a non-linear function of material-specific parameters such as ρ, T_1, and T_2, and user-selected imaging parameters. By acquiring a set of images with different material-dependent weightings and combining them linearly, projection images of individual materials can be produced.[1]

We have examined the feasibility of this concept experimentally and have developed practical methods of implementation. In initial studies, we acquired three T_2-weighted projection images of a test tube phantom (in which overlapping test tubes contained solutions with T_2 = 36, 59, and 85 ms respectively) using a standard multiple spin-echo sequence. Assuming the ith material in the jth image is weighted by $e^{-TE_j/T_{2i}}$, we successfully produced projection images of each material using linear combinations of the original images. In this study, noise in the resultant image was the primary limiting factor. However, in repeating this procedure for body images (human leg), we also suffered poor material cancellation due to material inhomogeneities and the non-monoexponential decay of various materials, particularly lipids.

We address these difficulties as follows. For a given volume, we acquire N ($N >$ number of materials to be cancelled) cross-sectional images of a single slice in the xy plane, each with different T_1 and/or T_2 weightings. For each of these images, a corresponding projection image (projected in y) is acquired. In a cross-sectional image, a user indicates image regions containing materials to be cancelled or isolated. Using the linear least squares estimate, we determine the linear combination of the N cross-sectional images so that resultant pixels containing cancelled material are close to zero while those containing desired material are close to one. To produce the selective projection image, we take the same linear combination of the corresponding projection images. This method directly determines the combination of the N images which maximizes the contrast-to-noise ratio in the final image, allowing for both noise and variability of material characteristics across different volume elements while bypassing estimation of material-dependent parameters.

Reference: 1. A. Macovski, IEEE Trans. on Medical Imaging, MI-1(1):42-47, 1982.

325

CALCULATION OF "SURVEY" PROTOCOLS FOR MR IMAGING

Elliot R. McVeigh, Michael J. Bronskill and R. Mark Henkelman
Department of Medical Biophysics, University of Toronto

Using MR imaging to screen patients for lesions of unknown type in different organ systems presents an interesting problem in pulse sequence optimization. For this case, the values of T1,T2,N(H),... in the lesion are unknown, and the background tissue in which the lesion may be located is also unknown. Therefore, the protocol used must provide sensitivity over a broad region of tissue parameter space (T1,T2,N(H)...), and this sensitivity must be isotropic. This condition implies that a multi-sequence protocol must be used, such as a T1-weighted, T2-weighted, N(H)-weighted image triplet.

At a point $\mathbf{r}_o$ in tissue parameter space, the sensitivity can be evaluated by calculating the probability of distinguishing $\mathbf{r}_o$ from all other points. The probability of distinguishing $\mathbf{r}_o$ from a neighbouring point $\mathbf{r}$ is given by $P(\mathbf{r}_o,\mathbf{r}) = 0.5(1+\mathrm{erf}(\Delta S(\mathbf{r}_o,\mathbf{r})/2\sigma))$, where ΔS is the Euclidean distance between $\mathbf{r}_o$ and $\mathbf{r}$ in the n-dimensional signal space of an n-sequence protocol. For independent trials, the probability of distinguishing $\mathbf{r}_o$ from all neighbouring points is proportional to the product of the individual probabilities. Therefore, if one maximizes the function $F(\mathbf{r}_o)=\int \ln(P(\mathbf{r}_o,\mathbf{r}))d\mathbf{r}$, (where the integral is over all tissue parameter space), the total probability will be maximized. Extension to the domain of interest is accomplished by a similar integration over $\mathbf{r}_o$.

This optimization method can compute the trade-offs between sensitivity in different directions, and over a whole domain of interest. The images of the derived optimal protocol form the best basis set for synthesizing images, allowing sensitivity in many directions to be defined by the diagnostician.

SPECTROSCOPY

326

A FAST CHEMICAL SHIFT IMAGING SEQUENCE

G Johnson, PS Tofts
NMR Research Group, Institute of Neurology, Queen Square, London, UK.

We have developed a fast chemical shift imaging technique (MULCH - MUlti-Line CHemical shift imaging) which is more efficient than localisation techniques (LT's) such as SPARS or ISIS and is much faster than multidimensional Fourier transform (MDFT) chemical shift imaging.

The method involves: saturating all spins outside a plane; selectively exciting individual lines of spins within the plane; phase encoding along each line; sampling the FID without gradients; interleaving interrogation of multiple lines (in a method analogous to multislice imaging).

The method is more efficient than LT's in that information from many voxels can be collected simultaneously. The number of voxels depends on the ratio of T1 (which determines repetition time) over T2* (which determines sampling time) and the number of signal averages (Nav) required for adequate signal to noise ratio (SNR). An array of Nav x (T1/T2*) spectra can be acquired by MULCH in the time LT's require for one voxel. SNR and spectral resolution are equivalent.

Imaging time for an array of N x N spectra using MDFT techniques on a plane is approximately $2N^2T1$ (assuming TR = 2T1). Imaging time using MULCH is 2NT2* (assuming data collection for 2T2*). Consequently MULCH is faster than MDFT by a factor NT1/T2*.

A 64 x 64 array of spectra with 5 Hz resolution could be obtained with MULCH in 17 minutes. In our initial experiments we have obtained spectra with good spectral and spatial resolution from bottles of hexane immersed in water.

327

MULTIPLE QUANTUM IMAGING: A NEW FORM OF TISSUE CONTRAST

DN Kennedy, BR Rosen, JD Pearlman
Dept Nuc Engin, MIT Cambrige Ma, Dept of Radiology and Cardiology, Mass. Gen. Hosp. Boston, Ma

Tissue characterization can be accomplished by the use of multiple quantum imaging techniques. In particular, the image intensity of the single, double and triple quantum images yields information about the spin-coupled fraction of the sample. The scalar-coupled fraction of a tissue directely reflects the the type of lipids present. This information can be useful in the differentiation of various disease states.

The following pulse sequence is capable of generating all orders of quantum transitions:

$$90_x - t_p - 180_y - t_p - 90_x - t_e - 90_x - t_d - \text{OBS}$$

The various orders of quantum transitions can be separated in time during the detection period by the application of a magnetic field gradient during the evolution period. The gradient echos of the various orders of transitions will occur during the detection period at equally spaced intervals of the initial gradient. From these discrete echos, any order transition can be imaged by appropriately timed data acquisition.

We demonstrate the imaging of these various transition orders on phantoms of lactate and ethanol. The multiple quantum signal intensity is independant of water and is demonstrated to be directely proportional to the concentration of the spin-coupled material. The water supression offered by this technique makes it a useful adjunct in water-supressed metabolic chemical shift imaging. In addition to water supression, multiple quantum imaging offers specific information about the chemical composition of the lipids present in any tissue, allowing better evaluation of disease state. Applications of this technique include characterization of lipid state in atherosclerotic plaque as well as lactate quantification in metabolic imaging of stroke models.

328

Spectroscopic Imaging with Double Quantum Filter and Water Referencing

Peter Webb, Daniel Spielman, Albert Macovski : Department of Electrical Engineering, Stanford University

To produce a spectroscopic image the problems of main field inhomogeneity and low concentrations of metabolites of interest must be overcome. Our data processing method [1] (water referencing, parametric least squares estimation), reduces ΔB_0 requirements to uniformity across a voxel, rather than across the entire volume, by spatially localizing then using the water signal as a local demodulator for each volume element. We extend this without losing robustness by using a double quantum filter to preferentially excite coupled species. The use of a DQ filter as a suppression technique [2][3] offers the following advantages:

- it is immune to the effect of ΔB_0, unlike presaturation, selective excitation and other chemical shift selective techniques.
- in addition to suppressing the water signal, the DQ filter is effective in reducing the intensity of the lipid resonances which overlap the lactate methyl line, as they are only partially coupled. Lipid signals may be further reduced by using selective pulses, which takes advantage of the difference between the chemical shift of the coupling partners of the lipid methyl group compared to those of the lactate methyl.
- the suppression effect is intrinsic; that is, we do not need to rely on subtraction of two acquisitions, but rather can prevent the signal from uncoupled protons from ever being received by using gradients to control the phase of two spin coherence. This is of *vital* importance as one must consider the dynamic range of the acquisition system (especially when applying imaging gradients to the signal and thus further reducing its intensity) as well as the inherent unreliability of subtraction *in vivo*.

Results A DQ filter sequence was implemented on a GE Signa 1.5 T imaging system: water suppression by more than a factor of 100 was easily achieved. Further reduction was possible by phase cycling. Even so, the signal level of lactate at physiological concentrations (< 10mM) is dominated by water, and thus an image cannot be directly produced. Instead the excitation sequence is combined with a 3DFT localization, and after spatial transformation, water referenced spectral estimation is performed on each of the localized time signals to produce the lactate image. The double quantum filter thus extends the robustness of our spectral estimator to the excitation/suppression phase of the sequence.

References

(1) Spielman, D. et al. *SMRM-VI.* (2) Dumoulin, C. et al. *Mag. Res. Med* 3,1986. (3) Szeverenyi, N. et al. *J. CAT*, 10(3),1986.

329

LOCALISED 31P SPECTROSCOPY IN-VIVO PHASE ENCODING NMR TECHNIQUES

D J Bryant, I J Cox, A G Collins, R R Harman, A S Hall, S Khenia, I R Young, G M Bydder
Picker Research Lab, GEC Research Ltd., East Lane, Wembley, London HA9 7PP, England

We have used three dimensional phase encoding NMR techniques to obtain an array of phosphorus-31 spectra, each localised to a voxel of dimensions 2-4cm in each direction. The positions of the voxels were determined by low resolution (2mm) proton imaging. Spectra show tissue heterogeneity of normal and pathological tissues, and are specific to individual organs.

Spectra were obtained from a Picker Prototype 1.6T spectroscopy research system. A saddle-shaped transmitter coil was used. Various receiver coils were used, including a surface coil and a closely coupled head shaped coil.

The phase encoding technique employed has been previously described (1,2). The amplitudes of three phase encoding gradients (in x, y, z directions) were incremented through 8 individual values. Total acquisition time, using two data collects for each permutation of gradient valus, was 17 minutes. The resulting resolution metabolite maps (using relative peak heights or peak areas).

In the data set obtained from the liver of the normal volunteer signal was distinguishable in 76 voxels, limited by the sensitive volume of the receiver coil. Metabolite maps of PCr/Pi and PDE/PCr showed that liver and skeletal muscle could be distinguished. Abnormalities in the phosphomonester maps were observed for the diseased liver of two patients.

This method of 31P spectroscopic imaging allowed variations in normal metabolism across the head to be mapped. Metabolite maps of patients presenting cerebral tumours have been obtained.

While the metabolite maps are necessarily of low spatial resolution, since the minimum voxel size is limited by the inherant low sensitivity of 31P MRS, we anticipate this method of 31P spectroscopic imaging will improve the specificity of 31P MRS and enhance our understanding of tissue heterogeneity.

1 Brown T R et al Proc. Natl. Acad. Sci. USA 1982; 79: 3523-6
2 Maudsley A A et al, J. Mag. Res. 1983; 51: 147-52

330

SELECTIVE PULSES DESIGNED FOR SPECTROSCOPY (SPUDS)

JB Murdoch
Picker International, Clinical Science Center

The same computer-optimization techniques and programs that have been used to generate narrowband RF pulse shapes for multi-slice imaging (1) can also be employed in the design of volume-selective pulses for in vivo spectroscopy.

For volume localization using the eight-acquisition ISIS sequence (2), one needs cleanly slicing 180° inversion pulses that, for surface coil use, should be insensitive to the overall RF level. We have therefore created a number of optimized selective-inversion RF-inhomogeneity-stabilized (OSIRIS) pulse shapes. These phase-modulated waveforms are generated by independently varying approximately 100 pulse amplitude steps. Alternatively (and more quickly), one can tailor the hyperbolic secant pulse (3) to specific experimental conditions by optimizing only three dimensionless parameters. These describe the degree of phase modulation, the point at which the function is truncated, and the overall RF scaling (1).

For presaturation of magnetization outside a given region, we have also optimized the volume-selective pulses of Aue et al. (4). The resulting bimodal out-of-slice saturation (BOSS) pulse shapes are purely amplitude modulated and can be either symmetric or asymmetric; the latter have lower peak RF amplitude. BOSS pulses can in addition be used for suppression of bi-directional flow artifacts in FAST or MAST imaging.

1. JB Murdoch, AH Lent, and MR Kritzer, J. Magn. Reson. (in press).
2. RJ Ordidge, A Connelly, and JAB Lohman, J. Magn. Reson. 66, 283 (1986).
3. MS Silver, RI Joseph, and DI Hoult, J. Magn. Reson. 59, 347 (1984).
4. WP Aue, S Muller, TA Cross, and J Seelig, J. Magn. Reson. 56, 350 (1984).

331

INEPT SPECTROSCOPY USING SURFACE COILS

D G Norris[1], N Schuff[2] and D Leibfritz[1].
Universität Bremen[1] and Bruker Medizintechnik[2], West Germany.

A number of schemes have been suggested recently to obtain 90° excitation, and 180° refocussing pulses, that are insensitive to large variations in the strength of B_1, using the principle of AFP (1,2). These pulses are sensitive to off-resonance effects which makes them unsuitable for frequency selective excitation, but spectroscopy using a surface coil both for transmission and detection is possible.

When used in conjunction with a suitable inversion pulse, these pulses allow the enhancement of ^{13}C spectra by means of polarisation transfer techniques such as INEPT (3). The INEPT sequence was implemented on a Bruker 4.7T, 30cm bore BIOSPEC-BMT system using a double tuned surface coil placed in close proximity to a sample of DMSO, having natural abundance ^{13}C (1.1%). The spectra obtained are shown in the figure. Further investigations will concentrate on the feasibility of in-vivo studies.

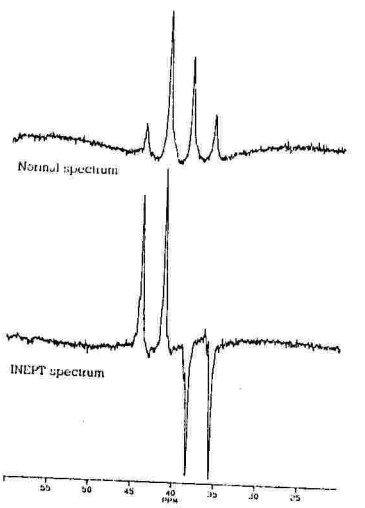

(1) K. Urgurbil et. al. J. Magn. Reson. **72**; 177-185 (1987). (2) M. R. Bendall et. al. Magn. Reson. in Med. **4**; 493-499 (1987). (3) G. A. Morris and R. Freeman J. Am. Chem. Soc. **101**; 760-762 (1979).

332

MONITORING MURINE TUMOR BY ^{31}P MRS: INFLUENCE OF PENTOBARBITAL ANESTHESIA AND OXYGEN BREATHING

E Rummeny, P Okunieff, TJ Brady, H Suit, and LJ Neuringer[1]
Massachusetts General Hospital, Boston, and [1]Massachusetts Institute of Technology, Cambridge

Anesthesia is frequently used for in vivo studies. It can sensitize tumors to radiation, can affect tumor metabolism, and may influence ^{31}P MRS high energy phosphate profiles. In this study we investigated: 1) the effects of pentobarbital anesthesia (PB) and 2) the combined effects of PB and oxygen (O_2) breathing on murine tumors.

Methods: 16 C_3Hf Sed mice were studied on a 8.5 T spectrometer using a single turn 1.4 cm surface coil. Two C_3H tumor histologies [MCaIV (n=5), FSaII (n=11)] were used. Tumors were implanted into the hind foot dorsum to eliminate spectral contaminations from nearby tissues. All animals were unanesthesized and air breathing for acquisition of the baseline spectrum. A repeat spectrum was obtained after 20-30 minutes of 100% O_2 breathing. Then PB (0.05mg/g) was administered intraperitoneally (ip) with continued O_2 breathing and a third spectrum was obtained 5 minutes later. Air breathing was then resumed, and five minutes preceeding the fourth spectrum an additional "boost" dose of PB (0.025mg/g, ip) was given.

Results: Effects of anesthesia: In air breathing unanesthetized animals, with tumors less than 250mm^3, the average PCr/Pi was 1.12±.09 for FSaII (n=6) and 0.86±.12 for MCaIV (n=3). With PB the PCr/Pi was 1.01±.14 (FSaII) and 0.71±.21 (MCaIV). Corresponding values for tumors greater than 250mm^3 were 0.32±.07 for FSaII (n=5) and 0.39±.07 for MCaIV (n=2) before PB vs. 0.46±1.4 and 0.16±.05 after PB. Seven of 16 animals had individual PCr/Pi changes >50% despite no significant changes in the average of the cohort.

Effects of oxygen breathing: MCaIV and FSaII tumors with initial PCr/Pi ratios less than 0.7 showed greater relative changes in PCr/Pi ratios after O_2 breathing. The effect of O_2 on the PCr/Pi ratios was independent on PB and histology, but individual variability was still present.

Conclusions: 1) PB anesthesia had no significant effect on PCr/Pi ratios when examing the average in a cohort. Individual tumors however did have significant changes. 2) The response to oxygen breathing on the PCr/Pi was greater for tumors with ratios less than 0.7, suggesting an oxygen limited metabolism in tumors with initially low PCr/Pi ratios.

333

SELECTIVE EFFECTS OF INSULIN-INDUCED HYPOGLYCEMIA AND RHODAMINE-123 ON TUMOR ENERGY METABOLISM

J.M. Arbeit, B.J. Toy, G.S. Karczmar, & M.W. Weiner
Magnetic Resonance Unit, VA Medical Center, University of California, San Francisco, CA

It is well established that cancers *in situ* have increased reliance on glycolysis for energy metabolism. Previous efforts to inhibit glycolysis were toxic because of the brain's utilization of glucose. The goal of the present experiments was: 1) to provide the brain with the alternate substrates beta hydroxybutyrate and acetoacetate by inducing ketosis; 2) to determine the response of tumor energy metabolism to inhibition of glycolysis or respiration produced by insulin hypoglycemia, rhodamine-123 (a mitochondrial inhibitor), or the combination of these agents, using ^{31}phosphate magnetic resonance spectroscopy. Control spectra were obtained from male Fisher F344 rats with a MCA sarcoma on a 2.0 T NMR spectrometer at 34.6 MHz using surface coils. Regular insulin (I), 125u/kg, rhodamine-123 (Rh-123), 6 mg/kg, or both were injected i.p., and spectra were acquired for 180 min. Tumor ATP fell to 52 ± 11% after I (n = 6), 30 ± 7% after Rh-123 (n = 4), and 11 ± 5% after I + Rh-123 (n = 4), ($p < 0.05$). Brain ATP remained at 103 ± 6% after I (n = 6) at 104 ± 5% after I + Rh-123 (n = 4). These data show that tumor ATP decreased modestly as a result of the decreased substrate availability produced by insulin hypoglycemia. Inhibition of tumor glycolysis and respiration by I + Rh-123 depressed tumor ATP levels by 90% without interfering with CNS metabolism. These findings demonstrate that the combined use of agents which acutely inhibit glycolysis and respiration dramatically impair tumor energy metabolism without affecting normal tissue. The results may suggest a new approach to cancer therapy.

HEART

334

DYNAMIC CARDIAC MRI TO ASSESS VIABLE VS SCARRED MYOCARDIUM: COMPARISON WITH SPECT TL-201

J Ziffer, RI Pettigrew
Emory University School of Medicine

In patients with coronary artery disease, the identification of viable myocardium vs scar in a particular vascular distribution could determine if therapeutic intervention is indicated. To evaluate the potential role of dynamic cardiac MRI in distinguishing viable myocardium from scar, we examined 31 discrete abnormal myocardial segments defined by conventional stress TL-201 SPECT (TL) in 18 patients. The TL images were interpreted based on principally 3 stress-redistribution patterns: 1)No redistribution at 4-24 hr = scar, 2)partial redistribution = ischemic (viable) myocardium + scar, and 3)complete redistribution = ischemic (viable) myocardium only. MRI dynamic short axis images were obtained with a dual spin echo technique, and long axis images were obtained with a fast gradient echo technique. Myocardial segments were categorized into 3 groups based on end-diastolic wall thickness (EDT), systolic wall thickness increase (ΔWT), and wall motion (WM): 1)Decreased EDT with no ΔWT = scar, 2)decreased EDT or WM with some ΔWT = scar + viable and 3)normal EDT and ΔWT = viable.

Of 16 segments interpreted as scar on TL, 9/16 had scar but 7/16 were viable by MRI. In these 7, MRI demonstrated likely causes of false positive TL abnormalities including hypertrophy, valvular disease, or attenuation by elevated diaphragm, pericardial effusion or fat pad. Of 9 segments interpreted as scar + viable myocardium on TL, 5/9 had the same interpretations on MRI, but in 4/9 MRI showed no evidence of scar, with probable causes of TL false positives. All 6 segments interpreted as purely ischemic were interpreted as viable by MRI.

Thus when TL demonstrated redistribution, MRI confirmed viability, however, when TL redistribution was incomplete, there was a high incidence of false positive scar interpretations by TL. We conclude that MRI may be a more definitive study for identifying scar and viable myocardium in a particular vascular distribution and therefore, may be of significant value for determining if intervention is indicated.

335

MR IMAGING OF THE PERICARDIUM: COMPARISON OF SPIN-ECHO AND CINE TECHNIQUES

SR Nokes, RJ Herfkens, JA Kisslo, CE Spritzer
Department of Radiology, Magnetic Resonance Imaging Section, Duke University Medical Center

Thirty patients with pericardial effusions who were examined with both spin-echo (SE) and CINE MR techniques were retrospectively reviewed to ascertain which method better evaluates pericardial fluid. Twenty of these patients had correlative echocardiography within one week of the MR study. Twenty patients without pericardial effusion examined with both techniques served as controls. The studies were blindly reviewed by two experienced MR physicians to assess the detectability, quantification, and characterization of pericardial effusions. While both techniques adequately demonstrated enlargement of the pericardial space, CINE MR, due to its higher contrast sensitivity and dynamic capability, gave more information, particularly in differentiating pericardial thickening from effusion. The study suggests that CINE MR should be the MR method of choice for evaluating pericardial effusions.

336

MAGNETIC RESONANCE IMAGING OF CARDIAC SARCOIDOSIS

SR Underwood, FM Prigent, RSO Rees, RH Mohiaddin, HG Bogren, DN Firmin, RH Klipstein, DG Lowell, DB Longmore
The National Heart & Chest Hospitals, London, and University of Miami Medical School, Miami

Cardiac involvement in sarcoidosis is frequently occult but its detection is important because it may present as sudden death. Diagnosis is usually based upon evidence of cardiac abnormality in the presence of known sarcoidosis, but even myocardial biopsy can be unreliable. We have studied 9 patients with proven or suspected cardiac sarcoidosis by magnetic resonance imaging and have demonstrated myocardial and pericardial abnormalities.

1 patient was previously diagnosed by cardiac biopsy, and in the others the diagnosis was made from proven involvement of another organ with evidence of rhythm disturbance or heart failure. There was histological evidence in 4 patients and a positive Kveim test in 5. Spin echo (TE 40ms and 120ms), field echo (cine imaging), and inversion recovery (TI 100ms for fat suppression) sequences were used although not every sequence was used in every patient. The images were scored by two observers independently for areas of high signal within the myocardium and differences were resolved by consensus. Areas of high signal were seen in 7 of the 9 patients, most commonly in the proximal septum, the posterolateral wall and in the right atrioventricular groove. The fat suppression sequence was used to demonstrate that high signal was not due to epicardial fat. Using the longer spin echo sequence, the abnormalities were more obvious. Pericardial thickening and effusion were seen in two patients and the cine field echo sequence allowed distinction of the two. In 1 patient, no cardiac abnormality was seen although there were multiple masses in both lung fields and the diagnosis was altered to multiple metastases from an unidentified malignancy.

Magnetic resonance imaging is able to demonstrate myocardial and pericardial abnormalities in cardiac sarcoidosis. Further studies are warranted to compare its sensitivity with other techniques such as echocardiography and thallium scintigraphy and to investigate the specificity of abnormalities.

337

THE ACCURACY OF CINE MRI CARDIAC VOLUME DETERMINATIONS: PHANTOM VERIFICATION

AJ Evans, RJ Herfkens, RA Blinder, CE Spritzer, RB Meese, LW Hedlund
Department of Radiology, Magnetic Resonance Imaging Section, Duke University Medical Center

CINE MRI is a new, noninvasive means of evaluating cardiovascular function. Recent reports have stated that MR can accurately quantify important clinical parameters such as ejection fraction, stroke volume, and systolic and diastolic volumes. For verification, these studies have compared values from MR measurements to published normal values or compared right to left sided volumes. These methods are useful, but cannot be used to define with precision the ability of MR to make measurements of dynamic volume changes. We use a dynamic cardiac phantom as "gold standard" to evaluate more accurately the ability of MR to determine volume changes. This phantom consisted of a proloid elliptical ventricle that pumped fluid through a simulated aorta at physiologic volumes and velocities, and generated concentric wall motions similar to those seen in the left ventricle.

All imaging was done in the body coil of a 1.5 T GE magnet with a gradient refocused acquisition in the steady state (GRASS), TR = 25 msec, TE = 13 msec, flip angle 30°.

We obtained good agreement between volume changes measured in the phantom and volume changes measured by MR. Percent error in end diastolic volumes was 7%, in end systolic volumes 6%, in stroke volumes 8%, and in ejection fractions 2%.

CINE MRI is a noninvasive technique that gives accurate anatomic information as well as dynamic functional information. This technique appears to have similar accuracy to other clinical modalities that measure cardiac volumes.

338

DIAGNOSTIC IMPACT OF MRI IN CONGENITAL HEART DISEASE OF ADULTS

H.Mayr, D.Glogar, S.Globits, A.Neuhold, D.Tscholakoff, H.Imhof, F.Kaindl
Kardiologische Univ. Klinik Wien, Vienna, Austria

It was the purpose of this study to evaluate the diagnostic impact of MRI in congenital heart disease in adults. 62 patients (34 men, 28 women, mean age 34±11 years) with congenital heart disease were examined using a 0.5 Tesla Phillips Gyroscan or a 1.5 Tesla Siemens Magnetom. All patients were invasively evaluated by right- and leftheart-catheterization as well as by 2-D-Echo, Doppler and Colorflow-mapping. Patients diagnosis were the following: Atrial septal defect (ASD)-18, ventricular septal defect (VSD)-8, tetralogy of Fallot - 1o, trilogy of Fallot - 3, transposition of great vessels - 7, double outlet right ventricle - 5, different complex disorders - 1o. Method MRI: In each patient 9 to 15 tomographic slices (8 to 1o mm thick) were collected in 3 planes (transverse, sagittal and coronal). In patients with shunts a multislice multiphase study was done in a coronal-transverse-doubleangulated projection (four chamber equivalent). Right- and left ventricular volumes and ejection fraction were calculated as well as shunt volumes. In addition a cine-MRI-Study with fast flip angles (FFA) was done to visualize shunt flow. Results: While 2-D and Doppler sonography was in good agreement with the results of invasive studies allowing estimation of severity of the shunt lesion as well as chamber size and hypertrophy, MRI had specific advantages over both methods. In patients with ASD, MRI was of great value to demonstrate the location of the shunt and to quantify noninvasively shunt volumes (MRI vs catheterization: R=0.91). In VSD, MRI was superior in demonstrating the topographic position of the great vessels and allowed to differenciate between big septal defects and single ventricle. In small shunt lesions Doppler- and Colorflow-mapping were more sensitive. In trilogy and tetralogy of Fallot, MRI was superior to sonography for evaluation of right- and leftventricular outflowtract, visualisation of pulmonary stenosis and of pulmonary vessels. MRI was comparable to Dopplersonography in quantitation of pulmonary stenosis. In complex congenital diseases MRI allows excellent visualisation of anatomic structures, abnormal venous returns and demonstration of abnormal vessels in the mediastinum. In conclusion MRI should be considered as an additional procedure to fully visualize and diagnose complex congenital heart disease in adults.

339

IMAGE GUIDED PHOSPHORUS 31 SPECTROSCOPY OF THE HUMAN HEART

S Schaefer, J Gober, M Valenza, GS Karczmar, G Matson, B Massie, MW Weiner
Magnetic Resonance Unit VAMC and Univ of California, San Francisco

31P nuclear magnetic resonance spectroscopy (31P MRS) can determine the status of high energy phosphates in vivo. However, successful use of 31P MRS in the human heart requires precise tissue localization. Previous investigations have relied on the B1 profiles of surface coils to define the lateral borders of the volume of interest (VOI), thus making it difficult to avoid contamination from the right ventricle and skeletal muscle. To correct this problem, we used ISIS, a Bo technique which allows 3-dimensional localization of the VOI. We performed proton magnetic resonance imaging (MRI) to select the VOI for the ISIS experiment. 31P MRS was used to determine normal values of phosphocreatine (PCr) and adenosine triphosphate (ATP) in the human left ventricle. Studies were performed on 8 normal subjects using a Phillips Gyroscan imaging and spectroscopy unit operating at 1.5 Tesla. Using MRI, the VOI was chosen to encompass the antero-apical region of the left ventricle. 31P MRS was performed with a 9 centimeter single turn surface coil placed on the chest. Signal acquisition was gated to the ECG and 1000-1200 repetitions were averaged. Average time for acquisition of each spectra was 35 min (range 27 to 46 min). Spectra were obtained over a mean volume of 80 cc (range 56 to 103 cc). Cardiac muscle comprised approximately 57% of the VOI. Peaks for PCr and ATP were clearly resolved on all spectra. The ratio of peak heights of PCr to gamma ATP was 1.46 $\pm$ 0.44. All spectra had prominent peaks in the phosphomonoester region, presumably due to 2,3 DPG of blood. In conclusion, these experiments demonstrate the feasibility of image guided, localized 31P MRS of the human heart. This technique should prove useful for the study of metabolic disturbances in cardiac disease.

340

MRI IN THE PREOPERATIVE EVALUATION OF PATIENTS WITH TETRALOGY OF FALLOT

Mirowitz SA, Gutierrez FR
Mallinckrodt Institute of Radiology, Washington University School of Medicine

The undertaking of a definitive repair procedure in patients with Tetralogy of Fallot requires accurate definition of all anatomic structures. In particular, the morphology of the central pulmonary vasculature must be clearly demonstrated. This has frequently necessitated serial cardiac catheterizations while awaiting attainment of adequate pulmonary artery size to allow for successful repair. We have examined twenty patients with Tetralogy of Fallot with gated MR imaging in order to assess the value of this technique in preoperativ evaluation. Sizes and shapes of the atria and ventricles were noted with particular emphasis on the right ventricular outflow tract. Size and location of intracardiac defects and presence and patency of palliative systemic to pulmonary shunts (13) was analyzed. The main and central pulmonary arteries were evaluated regarding size, shape, confluence of central branches, areas of stenosis, and presence of collateral supply. The results were then compared to findings obtained at catheterization (14), echocardiography (14) and surgery (9). MR was found to be a good noninvasive imaging tool in preoperative evaluation of patients with Tetralogy of Fallot, and was especially useful in defining the anatomy and architecture of the central pulmonary arteries. Our findings suggest that in the future MR may add significant information to, and in some cases possibly obviate the need for catheterization in the routine evaluation of patients awaiting definitive repair of Tetralogy of Fallot.

PULSE SEQUENCES

341

STATISTICAL DECISION ANALYSIS TO DETERMINE OPTIMAL MRI PROTOCOLS

Elliot R. McVeigh, Michael J. Bronskill and R. Mark Henkelman
Department of Medical Biophysics, University of Toronto

The ability of NMR to characterize and distinguish individual tissues by quantitative methods derives from differences in the NMR parameters of these tissues. Optimization of MRI protocols for specific clinical problems must, therefore, begin with appropriate measurements of NMR parameters in the tissues relevant to the problem. These measurements must include estimates of the correlations and biological variability in the NMR parameters. The figure of merit for the optimization should be an estimate of the ability to distinguish the modelled tissues from one another based on the MR signal characteristics. Simply maximizing the signal-difference-to-noise ratio between two tissues modelled by discrete values of NMR parameters does not treat adequately the problem of consistently distinguishing tissues in a patient population.

In order to address this problem we model each tissue with a probability density function (PDF) in the tissue parameter space (T1,T2,N(H)...). The separation of the tissues in this space can be calculated using statistical decision analysis. This separation establishes the upper bound for the performance capabilities of any NMR technique in distinguishing these tissues based on signal strengths. The optimal MRI protocol is the one that provides the best decision boundary between the tissue PDFs.

In order to incorporate the image noise into the calculation, the tissue PDFs are mapped with the protocol to signal PDFs. These signal PDFs are broadened by convolution with a distribution modelling the noise. After this, a decision boundary in the signal space is found which minimizes a risk function.

342

USE OF THE STIR SEQUENCE TO DIFFERENTIATE BETWEEN EXTRA-CRANIAL FATTY AND HEMORRHAGIC LESIONS.

M. R. Fisher
Department of Radiology, Northwestern Memorial Hospital, Chicago, IL 60611

Differentiation of fatty from subacute hemorrhagic lesions within the body is often difficult on standard spin echo imaging. These lesions have bright signal intensity on a T1 weighted (T1W) sequence. Often the clinical history or location of the mass lead to the correct diagnosis. Many times the answer is not so readily obtainable. Specialized techniques such as the chemical shift sequence designed by Dixon (although not routinely available), may aid in this differentiation. The purpose of this study was to evaluate the use of the short time of inversion recovery sequence (STIR) to differentiate fat from subacute hemorrhage. Seven patients with high intensity lesions on standard spin echo (SE) T1W sequence were evaluated with the STIR sequence. Surgical confirmation was available in two patients and clinical correlation in the other five. MR imaging was performed on a Philips 1.5T System operating at 0.5T. Pulse sequences used were: SE T1W TR 500-750, TE 30 ms and STIR: TR 1000-1200, TI 100, TE 30 msec. In all patients the STIR sequence allowed a definitive diagnosis into either the hemorrhagic or fatty lesion category. On the STIR sequence the fatty lesions were low intensity while the hemorrhagic lesions were of bright signal intensity. On the STIR sequence, which utilizes a TI of 100 msec, the signal intensity of fat is suppressed. This is the time of inversion most suitable to eliminate the fat signal. Use of the STIR sequence is recommended for the diagnostic dilemma of differentiating fat from hemorrhagic lesions.

343

PULSE SEQUENCE OPTIMIZATION FOR STIR INVERSION RECOVERY SEQUENCES

EC Unger (1), J McGlone[1](2), M Silver (3)
Fox Chase Cancer Center[1], Siemens Medical Systems[2]

STIR (short TAU inversion recovery) sequences use a short inversion time to cancel the signal from fat by setting the inversion time equal to the cross over time of fat. Signal from fat essentially disappears. Because the signal of fat is supressed problems with chemical shift are ameleorated. To improve the signal to noise in the STIR sequence we tested various sequences and developed low bandwidth versions of STIR sequences. Because of fat suppression in STIR it is possible to extend the duration of acquisition time as is done in low bandwidth techniques without increasing chemical shift. We also implemented rectangular pulses developed by one of the authors which permitted us to obtain contiguous slices with high image quality. The resulting STIR sequence, which we have developed, has high signal to noise and contiguous capability. We have used this sequence in over fifty examinations, and have found it useful for evaluating the soft tissues and marrow. Compared to spin echo sequences the STIR sequence has higher contrast and less problems with chemical shift.

344

MRI OF JOINTS: EVALUATION OF SHORT TI INVERSION RECOVERY PULSE SEQUENCE
DJ Schnapf, S Sen, JA Frank, PA Eagle, RK Drum, AR Michetti,
York Imaging Ctr/Georgetown Univ School of Medicine/National Inst of Health

MRI is proving to be an acurate and noninvasive technique to evaluate a variety of joints of the body. The short TI inversion recovery (STIR) pulse sequence has several unique advantages: first, there is a suppression of the fat signal and increased contrast between normal and pathologic tissue; secondly, there is less phase induced noise due to motion from subcutaneous fat. Next, the synergistic effects of prolonged T1, T2, and spin density are additive and this is a major practical advantage of the STIR sequence. Finally, there is at least a 25% reduction in imaging time when compared to T2 spin echo sequences, while still preserving sensitivity to detection. The purpose of the study was to evaluate the role of STIR and compare it with other, more conventional pulse sequences.

In this study we evaluated 100 joints. The majority of the joints were temporomandibular joints and knees, but also evaluated were hips and ankles. Images were obtained on both a Thomson-CGR, and Picker MR scanners operating at 0.5 tesla. The STIR sequence consisted of a TR 1500 msec, TE 26 msec, and TI 100 msec. In addition, patients in the study were also assessed with conventional T1 and T2 spin echo (SE) and gradient echo images. The majority of the gradient echo images were T1 weighted, but we have also included in our evaluation T2 weighted images utilizing variable flip angles.

The study was divided into two sections: first, to evaluate anatomic structures such as, articular cartilage, cortex, marrow, menisci, and ligaments; secondly, we have evaluated the images for their diagnostic quality and compared pulse sequences for diagnostic accuracy. Images were also reviewed with appropriate non-radiologic specialists to access their use of the varied images and pulse sequences in clinical application.

Results show that the STIR sequence is extremely accurate in detecting fluid, neoplasia, inflammation, and edema. We believe STIR can replace T2 spin echo sequences in joint imaging. Our series demonstrates a high degree of diagnostic accuracy of both T1 weighted spin echo and gradient echo studies. Our results demonstrate that STIR is equally accurate, but because of the unique properites of STIR, there were fewer equivocal cases. We believe that STIR is a valuable imaging parameter to use when evaluating joints by MRI.

345

OPTIMIZING LONG TR/TE IMAGES OF THE UPPER ABDOMEN AT 1.5 TESLA
DG Mitchell, S Vinitski, DL Burk, D Levy, MD Rifkin
Thomas Jefferson University Hospital, Philadelphia, Pennsylvania

In an attempt to determine the optimal T2 weighted imaging method of the upper abdomen with a 1.5T Signa System, we evaluated the effect of the number of echoes on image contrast and motion-induced artifact, and compared two different strategies for reducing motion-induced artifact. Fifteen subjects, 8 patients (5 with liver lesions) and 7 volunteers had MRI and were studied with at least two different sequences with identical parameters, except for a different series of refocusing pulses and/or a different method of motion-artifact reduction. These sequences included single echo, asymmetric (TE=20,80) and symmetric (TE=40,80) double echo and quadruple echo techniques. Comparisons were also made between respiratory sorted phase encoding (RSPE) and nulling of the gradient's first moment (NGFM), using both single and symmetric double echo techniques. Image contrast and severity of motion-induced artifact was measured via blind examination by three independent MRI radiologists and calculation of signal-difference and signal-difference-to-noise ratios, and of the intensity of motion-induced "ghost artifact". Respiratory artifact was best separated from vascular artifact by noting ghosts from the high intensity gallbladder. Increasing the number of echoes decreased the signal differences between tissues. When NGFM was not used, symmetric double and quadruple echo images had the least severe motion-induced artifact. Single echo images had superior tissue contrast, but because of severe artifact on portions of the image, symmetric double echo images were considered more reliable. The asymmetric double echo technique gave consistently poor results. NGFM was more effective than RSPE in reducing vascular and respiratory artifact. Even-echo rephasing in symmetric double-echo images greatly reduced artifact in RSPE images but had only minimal effect in NGFM images. Intrahepatic vascular structures had high signal intensity with NGFM. All liver lesions were either unchanged or more obvious with NGFM. NGFM is a powerful motion reducing technique (and is beneficial in spite of the resulting high signal of intrahepatic vessels).

346

T1*T2 IMAGES: A METHOD OF CONTRAST ENHANCEMENT IN LIVER MRI

CE Spritzer, RA Blinder, ME Baker, JR MacFall, RJ Herfkens
Department of Radiology, Magnetic Resonance Imaging Section, Duke University Medical Center

Most liver tumors have prolonged T1 and T2 relaxation times, therefore, an image where the pixel values equal the tissue's T1 value multiplied by the T2 value should theoretically improve lesion contrast. To test this hypothesis, we generated T1 times T2 images (T1*T2) in cases of documented liver pathology and evalauted the technique for lesion detectability, lesion contrast, and potential problems.

Two spin echo sequences of the liver were obtained on a 1.5 T imager using TR/TE = 500/25 and 2000-2500/25/80 holding transmitter power and receiver gain constant. Computed T1 and T2 images (pixel value = T1 or T2), were generated by a least squares two point fit, scaled by a factor of 0.1 and multiplied together to produce the T1*T2 image.

Sixteen documented liver lesions in 15 patients were studied. All lesions were detected on T1*T2 images. The mean liver T1 and T2 values were 632 and 32, and mean tumor T1 and T2 values were 1257 and 63. T1*T2 values for liver had a mean of 205 $\pm$ 72, T1*T2 values for tumor had a mean of 1287 $\pm$ 793. Calculated contrast values for tumor vs liver exceeded the contrast on routine MR images. T1*T2 images markedly highlighted pathology. In contrast, normal liver, fat and muscle demonstrated relatively low pixel values. Problems encountered included misregistration of data sets and pixel saturation in one case each.

T1*T2 images have the potential to increase tumor to liver contrast.

SPINE

401

ENHANCED T2-WEIGHTED 1T CERVICAL SPINE IMAGING USING GRADIENT MOTION REFOCUSING COMBINED WITH RECTANGULAR RF PULSES AND OPTIMIZED EKG SYNCHRONIZATION

SA Gronemeyer[+], FJ Wippold II[¥], RM Derler[+], MS Silver[§], NC Henselmans[*]
Siemens Medical Systems, St Louis MO[+], Iselin NJ[§], and Erlangen W Germany[*]
Department of Radiology, Christian Hospital, St Louis MO[¥]

EKG triggering is often used on high field MR imagers to improve CNS T2-weighted imaging by reducing pulsatile CSF flow artifacts.[1] Gradient motion refocusing has been introduced to further reduce CSF flow artifacting[2]. Rectangular 90° and 180° RF pulses[3] have recently been developed to improve slice profile; this reduces the cross talk between adjacent slices which reduces image contrast.

EKG triggering techniques collect data after the R Wave. If a large number of slices are acquired, the later slices spill over into later R waves without being triggered to them, resulting in CSF artifacting in these later slices. We have developed a simple software method for optimized EKG synchronization which samples all slices between R waves without increasing imaging time. We have combined optimized EKG synchronization with gradient motion refocusing and rectangular RF pulses. Evaluation of this combined technique in Helmholtz coil imaging of the cervical spine at 1T will be presented.

[1] JL Sherman and CM Citrin, American Journal of Neuroradiolgy 7:3-6, 1986.
[2] EM Haacke, et al, Proc Society of Magnetic Resonance in Medicine, 1055, 1986.
[3] F Loaiza, et al, Health Care Instrumentation 1:188-194, 1986.

402

THE 'PSEUDO-CENTRAL' CANAL: GIBBS PHENOMENON AND MRI OF THE SPINE

E Kanal, FW Wehrli, R Prorok
Pittsburgh NMR Institute

It was empirically noted on may sagittal examinations of especially the cervical spine that a linear structure of increased signal intensity was frequently identified vertically oriented within the spinal cord on long TR and TE spin echo images or on gradient recalled imaging techniques emphasizing T2* or relative proton density (RPD) information. Axial images on these patients invariably failed to confirm the presence of such a central structure within the cord. This signal pattern has been hypothesized as resulting from various etiologies, including central canal to central gray matter to phase shifted signal secondary to pulsatile CSF flow. It was noted, however, that such a signal pattern was much more commonly identified when 128 phase encoding steps (N_p) were utilized for data acquisition, and rarely if ever being seen when N_p=256. Ten volunteers and ten patients were prospectively examined with varying N_p as well as interchanging the directions of the phase and frequency encoding gradients. Long TR and TE spin echo as well as GRASS imaging techniques were utilized. The results confirm the artifactual nature of this signal pattern. These are felt to be secondary to truncation artifact ('Gibbs phenomenon') of the low sampling studies. As such a signal pattern may be occasionally confused with true parenchymal pathology such as a syrinx, recognition of such artifacts may prove quite valuable for avoiding inaccuracies of diagnostic evaluation of the images in which they are found.

403

: MR-Anatomic Correlation of Fetal Lumbosacral Spine and Spinal Cord.
: E. Leon Kier, M.D., C. Camputaro, R.T.
: Yale University School of Medicine

The correlation of anatomic material and diagnostic imaging techniques have resulted in major advances in neuroradiology. Ultrasound, computed tomography and magnetic resonance imaging are increasingly used in the diagnosis and treatment of lower spine and neural tube abnormalities of the premature infant.

Anatomic-diagnostic imaging techniques correlation for developing spinal cord has been handicapped by the lack of anatomic material. For at least sixty years the literature contains no dissected specimens of the fetal cord, and the normal developmental changes described in the literature are based on diagramatic material from the early part of this century.

Over the past several years techniques for the dissection and photography of the formalin fixed fetal spine and spinal cord have been gradually developed.

MR of formalin fixed fetal specimens of various ages have now been performed prior to dissection. This presentation will demonstrate the normal developmental changes of the lumbosacral spine and lower spinal cord that can be visualized by MR imaging techniques.

The effects of developmental changes in regards to the differential growth of the spine and cord, tethered cord theories and neural tube abnormalities will be described.

404

MR IMAGING AT 0,5 TESLA IN 34 CASES OF ARTERIO-VENOUS MALFORMATION OF THE SPINAL CORD

F. GELBERT, E. ASSOULINE, D. REIZINE, M.C. RICHE, D. DORMONT, J.J. MERLAND

Service de Neuroradiologie, Hôpital Lariboisière, Paris

Between May 1986 and Septembre 1987, MR imaging was performed in 35 patients with angiographycally proven arterio-venous malformations (AVM) of the spinal cord.

All examinations were performed with a CGR Magniscan 5000 using surface coils. Average time of examination was 45 to 60 minutes. There were 19 males and 15 females (21 intramedullary AVM, 6 perimedullary fistulas and 7 dural A.V. fistulas with perimedullary drainage). After embolisation follow-up MR study was performed in 5 patients.

Our results confirm the value of MR in spinal cord AVM in demonstrating and differenciating the different types of spinal cord AVM and their associated lesions.

405

MR IMAGING IN THE EVALUATION OF SPINAL DYSRAPHISM & CONGENITAL SCOLIOSIS.

G.J. Beers, S.R. Koch, G.G. Wagner, J.R. Johnson, E.J. Arpin, R.T. Holt, E.A.Amin.
University of Louisville

30 patients with congenital scoliosis or other spinal abnormalities were studied with 0.5T or 1.5T Philips MR imagers. MRI proved useful at delineating tethered cords, lipomas, and diastematomyelia as well as associated syringohydromyelia and Chiari malformations. A spinal cord astrocytoma was discovered in one asymptomatic patient. Incidental pathology such as renal and splenic cysts, absent kidney, orbital hypoplasia, and cortical heterotopia were noted in some patients.

Various problems and pitfalls were encountered. It was not practical to image some patients thoroughly in one session. Although sagittal images with or without coronal images sufficed in many cases, additional axial images were often necessary to distinguish diastematomyelia from syringohydromyelia. Ghosting artifacts mimicked thickened fila on some sagittal images. Diagnosing tethered cords was often hindered by difficulties in designating lumbar vertebrae numerically even in patients without osseous segmentation abnormalities. These problems not withstanding, MRI evaluation of these patients proved to be useful and practical.

406

MRI OF ANTERIOR LUMBAR DISC EXTRUSION

J. R. Jinkins, M.D., A. R. Whittemore, M.D., Ph.D., W. G. Bradley, M.D., Ph.D.
Huntington Medical Research Institutes, Pasadena, CA

Extruded lumbar intervertebral discs have traditionally been categorized as posterior or postero-lateral in location. A detailed retrospective review of 250 MRI examinations of the lumbar spine utilizing low and high field imagers has revealed a total of 236 extrusions with 29% directed anteriorly, 14.5% centrally, and 56.5% extruding posteriorly.

The clinical state of radiating pain accompanying posterior extrusions has been well described, however the uncomplicated ADE may also be associated with a definite clinical syndrome, which includes both local and referred symptoms without specific lumbosacral root involvement. Out of the 250 subjects presenting with low back pain in this series, 28 or 11.2% revealed isolated ADE as their only extrusive abnormality. The anatomic basis for the generation of pain within the disc and paradiscal structures rests with afferent sensory fibers from two primary sources: 1) posterolateral neural branches emanating from the somatic ventral ramus of the spinal root, and 2) neural rami projecting directly to the paravertebal autonomic neural plexus. Thus, the conscious perception of pain originating in the vertebral column, although complex, has definite peripheral pathways explainable on the basis of this dual innervation. The directional differentiation of lumbar disc extrusions utilizing MRI, together with a clarification of the accompanying clinical syndromes should contribute to the further elucidation of the specific cause and treatment of acute and chronic low back pain engendered by these distinct organic lesions.

407

INTERVERTEBRAL DISC DEGENERATION IN YOUNG ADULTS:
CORRELATION TO LUMBAR INSTABILITY

Hannu Paajanen MD, Minna Erkintalo BM, Seppo Dahlström MD,
Martti Kormano MD

We have prospectively performed lumbar MRI and functional x-ray examination to 60 low back pain patients (age 18 - 20 years old). Sagittal spinal T1 and T2 weighted images were obtained using 0.02 Tesla system (Acutscan, Instrumentarium, Finland). Forty volunteers at the same age without pain symptoms were imaged as controls. Lumbar radiography included the anterior and posterior bending images to diagnose the segmental instability in the lumbar region. In the low back pain group 60 % of the patients had disc degeneration revealed by MRI (but not seen on x-ray films). In the control group the corresponding value was about 30 %. Segmental instability was diagnostized in 35 % of the patients. The discs which were involved in the instabile segments were not always degenerated as assessed by MRI.
Conclusions: Young adults which have low back pain have about two times more early disc degeneration than the controls at the same age. Segmental instability does not always damage the related discs.

VESSELS

408

MR CAN MEASURE FLOW CHANGES USING GD-DTPA AND INDICATOR DILUTION CURVES

PL Davis, GL Wolf, JS Gillen
Pittsburgh NMR Institute, Dept. of Radiology, University of Pittsburgh, Pittsburgh, PA

To determine if MR can accurately measure flow at the capillary level, we assembled a flow phantom with flow rates approximating capillary flow velocities. Gd-DTPA was then injected into the phantom perfusate as a bolus. The change in MR intensity was measured using FLASH, and a modified line scan technique on a GE 1.5 Tesla Signa imager. The modified line scan technique enabled data points to be obtained every 1.5 seconds. At capillary flow rates, this sampling frequency generated well defined time-activity indicator dilution curves. Combining the equations relating relaxation times, relaxation rate effects of paramagnetic agents and the FLASH intensity equation, we were able to calculate the relative concentration of Gd-DTPA in the phantom at any time from the measured MR intensity.

If Gd-DTPA concentration can be accurately measured, it should be possible to obtain accurate correlation between measured flow rates and certain integrals of the Gd-DTPA concentration over time using indicator dilution methods described by Zierler(1). To test the technique, the flow velocity was varied from .35 cm/sec to .70 cm/sec, and the injected amount of Gd-DTPA was varied by a factor of 10. Excellent correlation was obtained as the concentration was varied (correlation coefficient=.97) and the flow rate was varied (correlation coefficient=.96).

In conclusion, using a capillary flow phantom with Gd-DTPA as the indicator and MRI as the detector, flow at rates similar to tissue perfusion was accurately measured in vitro.

Reference: Zierler KL. Theoretical basis of indicator-dilution methods for measuring flow and volume. Circ Res 1962:10;393-407.

409

IMAGING INTRACEREBRAL VESSELS WITH GRADIENT MOTION REFOCUSSING SEQUENCES

P.M. Ruggieri, G. Laub, S.R. Felber
SIEMENS MEDICAL SYSTEMS, ERLANGEN; FRG

Preliminary studies have shown that it is possible to image extracranial vessels with MR angiography and these same techniques can be used to visualize the intracranial vessels. Our efforts have been directed towards the cerebral vasculature of greatest clinical significance which is that at the base of the brain. This is generally the site of aneurysms and, in the case of an acute subarachnoid hemorrhage, these vessels are frequently in spasm.

Gradient motion refocussing has been the most successful technique to date for vascular MR imaging. This technique is most effective when incorporated into fast gradient echo sequences such as FLASH and FISP. Initial work has shown that optimal enhancement is obtained when the sequences are optimized using low flip angles (approx. 20°), long TR's (40 ms), and short TE's (12-14 ms). A 3D data acquisition permits further improvements in visualization of the vessels as there is reduced phase dispersion due to velocity in the thinner partitions; vascular anatomy is better defined; and there is less signal loss due to variations in magnetic susceptibility form the subjacent sinuses at the skull base.

The multidirectional flow and variable orientation of the vessels at the base of the brain limited vessel enhancement. If the excited planar volume in the 3D acquisition was oriented axially, vessel visualization was much improved. This phenomenon is likely attributed to paradoxial enhancement and increased efficacy of the gradient motion refocussing.

This combination of imaging techniques provided 1 mm isotropic resolution of these intracranial vessels. Branches of the middle cerebral artery were well seen as far periphally as the sylvian fissure. When the data sets were processed with the ray projection technique, reconstructions in multiple projections were possible to better visualize the complex array of vessels in this region.

410

CINE MAGNETIC RESONANCE IMAGING OF RIGHT VENTRICULAR OUTFLOW TRACT ANATOMY IN CONGENITAL HEART DISEASE: OPTIMAL IMAGING BY ANGULAR ROTATION.

KJ Chung, IA Simpson, DJ Sahn, JR Hesselink
University of California, San Diego

Anatomical and functional assessment of the right ventricular outflow tract is important in many congenital heart lesions, but can be difficult using conventional noninvasive techniques. The combination of dynamic flow enhanced information and anatomical detail make cine magnetic resonance imaging (MRI) an attractive technique for the assessment of these patients but the complex geometry of the right ventricular outflow tract make this difficult using standard imaging planes. We used oblique plane imaging to study 30 infants and children (ages 5 months - 14 years) with a variety of congenital heart lesions. Twelve patients had tetralogy of Fallot (studied either pre- or postoperatively), 8 had transposition of the great arteries repaired by an intra-atrial baffle procedure, 6 had undergone pulmonary artery banding and 4 a Fontan procedure. Cine MRI was performed using a GE Signa 1.5 Tesla superconducting magnet and fast scan images from 5mm or 10mm slices obtained using a flip angle of 30°, repetition time of 21 msec, echo time of 12 msec displayed in a dynamic cine loop format. Narrowing of the outflow tract and main pulmonary artery were seen in all preoperative patients with tetralogy of Fallot, and postoperatively, a widened outflow tract with pulmonary regurgitation seen as a diastolic signal void. In transposition, the outflow tract and pulmonary arteries were well visualized and there was no evidence of outflow tract obstruction. In the 4 patients with a Fontan procedure, free swirling flow was visualized from the right atrium to pulmonary artery with a stenosis at the pulmonary artery insertion seen in one patient. The position and anatomy of the pulmonary artery band was well visualized in all 6 patients and the diameter of the band correlated well with the pressure gradient measured at cardiac catheterization (r= -0.94). Lucent jets of high velocity (> 3.0 m/sec on continuous wave Doppler) were identified distal to the band in all patients. In conclusion, oblique cine MRI imaging enhances the evaluation of anatomy and flow in the the right ventricular outflow tract and pulmonary arteries providing a safe, accurate and easily applicable technique for the serial assessment of congenital heart disease.

411

AORTIC FLOW PATTERNS IN HEALTH AND DISEASE STUDIED BY MAGNETIC RESONANCE VELOCITY MAPPING

HG Bogren, RH Klipstein, RH Mohiaddin, SR Underwood, DN Firmin, DG Lowell,
RSO Rees, DB Longmore
The National Heart and Chest Hospitals, London, UK

Aortic flow patterns are related to myocardial function and to the nature of the arterial system. We have used cine magnetic resonance velocity mapping to study the patterns in 25 normal subjects and 7 patients with coronary artery disease. Antegrade and retrograde flow were imaged at two levels: the level of the bifurcation of the pulmonary artery, and the junction of the sinuses of Valsalva and the ascending aorta.

The normal pattern was plug flow at the level of the pulmonary artery bifurcation, with a reverse channel beginning in late systole and continuing throughout diastole along the posterior left wall. Maximal forward flow started along the left wall of the aorta in early systole rotating around posteriorly to end up along the right wall in diastole. The total amount of retrograde flow at the level of the pulmonary artery bifurcation was 6.4% of forward flow (range 2-14%). Peak systolic flow at the sinuses of Valsalva rotated in a similar fashion, however the reverse flow was split. The majority was directed into the left coronary sinus and the minority to the right coronary sinus. No reverse flow entered the noncoronary sinus. In the patients with coronary artery disease, 4 had very low volumes of reverse flow (1%) while 3 had normal volumes. In these 3 patients, however, it was directed abnormally into the noncoronary sinus.

It is concluded that in normals, the reverse aortic flow is related to coronary artery flow and that the coronary arteries have their functional origin quite distally in the aorta. The reverse flow may also serve to close the aortic valve. Patients with coronary artery disease have abnormalities of aortic flow that may either be a cause or a consequence of disease. The relationship of aortic flow to coronary artery anatomy in health and disease and to aortic compliance, which is known to be altered in disease, will be fruitful areas for further investigation.

412

MAGNETIC RESONANCE MEASUREMENT OF AORTIC COMPLIANCE IN HEALTH AND DISEASE

RH Mohiaddin, SR Underwood, HG Bogren, DN Firmin, RH Klipstein, DG Lowell,
RSO Rees, DB Longmore
The National Heart & Chest Hospitals, London, UK

Compliance is the change in volume per unit change in pressure and it is a measure of distensibility. Arterial compliance alters with age and disease, but its clinical significance is unknown because it is difficult to measure. In this study we establish the normal variation of aortic compliance with age and we investigate compliance in athletes and in patients with coronary artery disease.

30 normal subjects were studied (age 16 to 83), 6 trained athletes, and 9 patients with coronary artery disease without previous infarction. Spin echo images were acquired at end diastole and end systole in three oblique planes perpendicular to the mid points of the ascending aorta, the aortic arch, and the descending thoracic aorta. The change in area of the aorta between diastole and systole was measured and compliance was derived using the pulse pressure measured with a sphygmomanometer. Total arterial compliance was also measured from the left ventricular stroke volume determined by biplane area-length measurements.

Mean ($\pm$SD ml/mm Hg) ascending aortic compliance in the normal subjects aged less than 50 (0.040 ± 0.010) was greater than the arch (0.024 ± 0.011, $p < 0.001$), which was in turn greater than the descending aorta (0.018 ± 0.008, $p < 0.05$). Compliance fell linearly with age up to the age of 50 ($r = -0.93$), so that over 50, there were lesser differences between the ascending and descending aorta. In the athletes, compliance was significantly higher than normal ($p < 0.001$), and in the patients aged less than 50, it was significantly lower ($p < 0.001$). Total arterial compliance also fell with age in the normal subjects, although there was more variation and it was more difficult to separate the athletes and the patients.

In conclusion, normal aortic compliance falls with age and the ascending aorta is the most compliant region. Athletes have very high compliance and patients with coronary artery disease very low compliance. The significance of these findings for the assessment of fitness and the detection of disease remains to be established.

413

EVALUATION OF THE THORACIC AORTA WITH MRI

AS Gomes, JF Lois
Department of Radiology, UCLA Medical Center

A group of seventy one patients with a suspected abnormality of the thoracic aorta underwent ECG gated MRI using spin echo technique in axial and sagittal oblique projections. Sagittal oblique imaging planes were obtained using an electronic curser. Thirty five patients were evaluated for an acquired aortic lesion, 36 patients for a congenital abnormality. In the group with a suspected acquired abnormality, MRI clearly showed aortic width, and delineated the presence of true and false aneurysms and dissections. It was superior to CT and echocardiography for screening and obviated arteriography in 23 of 35 patients (66%). In the group with congenital abnormalities, MRI accurately diagnosed the lesion in 33/36 (92%) while 2-D echocardiography was accurate in 19/29 (66%). Lesions diagnosed with MRI included coarctation of aorta, right aortic arch, double aortic arch, truncus arteriosus, patent ductus arteriosus, and aorticopulmonary window. We have found ECG gated MRI useful in the evaluation of the thoracic aorta and have found it to be a reliable alternative for arteriography in many cases.

414

INFERIOR VENA CAVA (IVC) TUMOR THROMBUS IN RETROPERITONEAL MALIGNANCIES: ASSESSMENT BY MRI

JK Raval, TR Pritchett, PM Colletti, WD Boswell, JM Halls
University of Southern California School of Medicine

The IVC may be involved by tumor thrombus from various retroperitoneal malignancies. Our purpose was to study the accuracy of MRI in assessing the superior extent of tumor thrombus prior to surgery since the operative approach depends on the level of involvement.

Eight patients with suspected IVC involvement from a retroperitoneal tumor were evaluated on an 0.5 T MR scanner pre-operatively. T1 weighted (8/8) and T2 weighted (6/8) scans were obtained in at least one of coronal, sagittal, or axial planes. The following IVC tumor level grading system was used:

Level I: IVC involved only in infrahepatic portion.
Level II: Intrahepatic IVC involved without right atrial involvement.
Level III: Right atrium involved.

Surgical proof was obtained in each case. Six patients had renal cell carcinoma (2 level I, 3 level II, 1 level III). Two patients had adrenocortical carcinoma (1 level II, 1 level III). The superior extent of tumor thrombus was accurately depicted by MRI in seven patients. In one patient with adrenocortical carcinoma - level III, MRI showed it to be a level II, however, EKG gating was not available for that case. T1 weighted images showed much better detail than T2 weighted images.

Thus, MRI can be used in assessing the superior extent of IVC tumor thrombus.

415

LUXURY PERFUSION IN CEREBRAL INFARCTS: COMPARISON OF CT, MRI AND SPECT

H Henkes, M Cordes, W Schörner, R Felix
Radiological Department, Klinikum Rudolf Virchow, Freie Universität Berlin

Thirty patients with clinically confirmed cerebral infarctions at various stages were examined by contrast enhanced CT and Gd-DTPA enhanced MRI. Regional cerebral blood flow (rCBF) and regional cerebral blood volume (rCBV) were measured by SPECT. Results from CT, MRI and SPECT were compared with respect to location and size of infarcted areas. Diagnosis of infarction could be made up with CT in all cases. However, MRI revealed more extended lesions and showed precise topographic relationship of the infarcted area to anatomic structures. After i.v. application of Gd-DTPA disruption of the blood brain barrier (BBB) could be demonstrated as a circumscribed accumulation of the contrast medium in area of recent cerebral infarction.
Corresponding to these findings, SPECT demonstrated an increased rCBF and rCBV in the areas with disrupted BBB; a reduced rCBF and rCBV was detected only exceptionally. As our preliminary results show, the use of Gd-DTPA clearly depicts areas with disrupted BBB by MRI. A luxury perfusion with increased rCBF and rCBV can be detected by SPECT.

MR OPERATIONS

416

MRI SITING AND CLINICAL EXPERIENCES WITH THE OXFORD ACTIVE-SHIELD MAGNET

M. F. Murphy, D. E. Andrews, P. Hobday
Oxford Instruments Group

The Oxford ACTIVE-SHIELD magnet is an innovative, reduced-fringe field superconducting magnet. It provides a practical and cost-effective solution to the MRI siting problem. The ACTIVE-SHIELD magnet is one which employs a unique geometry utilizing superconducting counter running coils to cancel the field at distances remote from the magnet origin. The shielding is performed electrically within the cryostat itself. It does not employ conventional steel shielding techniques. The result is a reduction in the five gauss volume, the recommended safety limit, by a factor of twenty. The ACTIVE-SHIELD design has been applied to field strengths up to 1.5 Tesla. The current status of the 0.5 Tesla, 1.0 Tesla and 1.5 Tesla ACTIVE-SHIELD development programs will be presented, as well as a summary of the siting and clinical experiences to date.

417

COMPARISON OF MAGNETIC RESONANCE IMAGING (MRI) AND SPECTROSCOPY (MRS) AT 1.5 AND 2.0 T

G. Matson, M. Boska, G. Karczmar, D. Twieg, D. Adams, J. Buchanan, M. Healy, C. Anderson, and M.W. Weiner
Magnetic Resonance Unit, VA Medical Center, University of California, San Francisco

Clinical application of MRS is limited by sensitivity and spatial resolution. In theory, the signal/noise and spectral resolution of MRS can be improved by increasing field strength. In contrast, MRI image quality may be significantly reduced at higher field. The goal of the present experiments was to directly compare MRI and MRS on phantoms, and the heads and bodies of human subjects at 1.5 and 2.0 T using the same MRI/MRS system. All experiments were performed on a Philips Gyroscan MRI/MRS system. MRI of brain and body tissues was performed at 1.5 T with standard resonators. At 2.0 T, MRI on the body was performed with a specially built bird cage coil. MRI was performed on the head with a home-built coil. Preliminary results suggest that substantial improvement of sensitivity (signal/noise) and spectral resolution of ^{31}P and ^{1}H MRS was achieved at 2.0 T compared to 1.5 T. Surprisingly, MRI image quality was only slightly reduced at 2.0 T compared to 1.5 T and remains acceptable for clinical studies. Therefore, the results obtained thus far suggest that the gains achieved by increasing field strength from 1.5 to 2.0 T for MRS are not substantially offset by losses of image quality. In conclusion, 2.0 T appears to offer some advantage over 1.5 T for studies combining MRI and MRS for clinical investigation.

418

SPECIFICATION OF MAGNET QUALITY BY FIELD GRADIENTS

I R Young, D J Bryant, G M Bydder, I J Cox
NMR Unit, Hammersmith Hospital, Du Cane Road, London W12 OHS, UK

The method used in determining the quality of magnets for whole body imaging and spectroscopy is essentially the same as that used in non-localised high resolution NMR, in that it involves a statement of the field deviation from a mean over the required volume. Localisation in imaging and, now, localised spectroscopy (1, 2) implies a re-assessment, and it is shown that defining a maximum field gradient is to be preferred (ie, rather than specifying the field quality as being, for example, ±20ppm over 40cm DSV, a better definition is a maximum vector field gradient of 1ppm/cm. over 40cm DSV). The impact of local gradient fields arises through the reduction in T_2^*, which enters the signal-to-nose ratio expression in two ways in gradient re-called echo and FID experiments. It determines the signal which is available at the peak of the echo, or FID when data acquisition can begin, and it is a measure of the length of time for which it is useful to acquire data (and so of the bandwidth of the experiment). Particularly in rapid imaging where T1 >>TR these effects can have a dramatic effect on the performance of machines. For example, in fields with a gradient of 1ppm/cm, assuming using as model grey matter in the brain, the external signal-to-noise ratio obtainable in an imaging experiment with a TR of 100msec TE of 30msec, 8mm slice width and 256 x 256 image matrix is about the same at 0.1T and 1.5T with a performance peak at about 0.5T. Reducing the slice width (at constant field gradient) or decreasing the gradient (at constant slice width) results in a substantial relative improvement at higher field. In body imaging the situation is a little less unfavourable since the intrinsic T2 of most body tissues is shorter than those of brain tissues. The effects of field gradient have been shown both in phantoms and in vivo, with much less loss of signal-to-noise as the voxel volume is reduced than would be expected (5).

1) D J Bryant et al, Proc. 5th Ann. Mtg. SMRM, New York p156 (1987). 2) P A Bottomley et al, Works-in-Progress, 6th Ann. Mtg. SMRM, New York p8 (1987). 3) A Abragam, The Principles of Nuclear Magnetism, Clarenden Press, Oxford (1961). 4) J Frahm, Mag. Reson. Med., 3 (2) 321-327 (1986). 5) A G Collins et al, Proc. 6th Ann. Mtg. SMRM, New York p946 (1987)

419

LINEARITY OPTIMIZATION IN SADDLE-COIL GRADIENT SYSTEMS

B. Ozdemirel , O. Nalcioglu
Department of Radiological Sciences, Division of Physics and Engineering, University of California - Irvine

Saddle-coil gradient systems, also called Golay type gradient coils are widely used as a part of the MRI equipment. The construction of this type of gradient systems is easier and they do not restrict the sample access . The coil design investigated in this abstract is based on a configuration of four symmetrically arranged saddle-coils which are divided into a number of circular arc segments with different axial separations. We assume that an equal amount of current is carried by each segment, while a single circular arc at the far end of the coil works as the return path for all segments. We developed a computer program which minimizes the gradient field linearity error in a volume specified by the user to find the optimum configuration of the circular arc segments. The program calculates the axial component of the magnetic field generated by the segments by numeric integration of the Ampere's Law for a current element. The magnetic field calculation is performed at a number of equally separated points in one quadrant of a central equilateral volume. The average field gradient in the y-direction that gives the smallest squared error for a field distribution symmetric with respect to the horizontal axis is obtained by,

$G_y = \Sigma\Sigma\Sigma y_j B_z(x_i,y_j,z_k) / \Sigma y_j^2$ and the squared error is $\varepsilon = \Sigma\Sigma\Sigma [G_y y_j - B_z(x_i,y_j,z_k)]^2$

where B_z is the axial component of the field, and x_i, y_j, z_k are the coordinates of the field calculation points.

The program searches for the optimum axial distances from the coil center and radial angle for the circular arc current segments and the current return path. One of these configuration parameters is modified at every minimization step to give a smaller squared error. The step size of the variations are initially chosen by the user. The program reduces the step size for a parameter to half its value when further error minimization is no longer possible. Execution of the program is terminated when all the step sizes are reduced below practically significant limits.The optimum configuration for a four segment saddle-coil is shown in Figure. 1. For this configuration the maximum calculated linearity error was found to be less than 1.0 % in a central cylindrical volume of R/3 radius and R/3 length, where R is the radius of the saddle-coil system. In a similar volume of R/2 radius and R/2 length the maximum linearity error is 4.0 %.

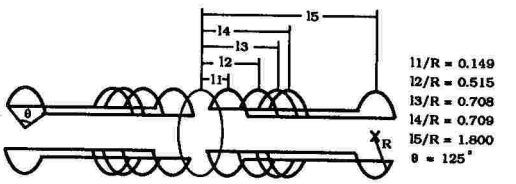

Figure 1. Optimum Configuration For A Four Segment Saddle-coil

420

TEMPERATURE RESPONSES DURING CLINICAL MRI: IS THE RECOMMENDED EXPOSURE FOR RADIOFREQUENCY RADIATION TOO CONSERVATIVE?

FG Shellock, JV Crues*
Cedars-Sinai Medical Center, Los Angeles, CA;*Santa Barbara Cottage Hospital, Santa Barbara, CA

Because of the thermogenic qualities of radiofrequency (RF) radiation, the National Radiological Protection Board (NRPB) of the United Kingdom has recommended that exposure to RF fields during magnetic resonance imaging (MRI) should not cause a rise in body temperature of more than 1° C as shown by skin and rectal temperatures. It was presumed that this slight temperature change would be ensured by limiting the RF exposure to a whole body average specific absorption rate (SAR) of 0.4 W/kg (similar to that recommended by the U.S. Food and Drug Administration).

To determine the temperature responses of patients undergoing MRI at RF radiation exposures up to an SAR of 0.4 W/kg (average SAR-0.3 W/kg), we measured body (sublingual pocket) and skin temperatures in 14 patients immediately before and after examinations performed with a 1.5 T/64 MHz MRI system (General Electric Co.). Room temperature was 23±1° C, relative humidity was 45±5%, and air flow within the bore was less than 0.1 L/min. There were statistically significant ($p<0.01$) increases in both body (36.6 to 36.7° C, largest change-0.5° C) and skin (31.8 to 33.2° C, largest change-3.5° C) temperatures. Although none of the patients had changes in body temperature of greater than 1° C, 7 patients (50%) had skin temperature changes that exceeded the NRPB safety recommendations, despite the fact that they were imaged below an SAR of 0.4 W/kg. Nevertheless, these patients did not experience any adverse temperature-related sequelae. Since heating during MRI occurs predominantly on the periphery and skin temperature may vary by as much as 10 degrees (depending on a variety of factors) without any serious physiologic consequences, it appears as though the NRPB guidelines are inappropriate and may be too conservative with respect to the skin temperature criterion.

421

DUAL SURFACE COILS FOR MR IMAGING: CAPABILITY, ADVANTAGES, AND APPLICATIONS

(1) M. R. Fisher, (2) E. B. Boskamp, E. Russell, F. Steinberg, J. Levy
(1) Northwestern University Medical School, Chicago, IL, (2) Philips Medical Systems, Netherlands

In the usual clinical application of MR only one surface coil per body region can be applied at a time. The purpose of this study was to assess the capability, advantages, and applications of dual surface coil imaging. MR imaging was performed on a Philips 1.5T System operating at 0.5T. Dual surface coil imaging is possible because two surface coil connections are provided with this imager and there is electronic decoupling using PIN diodes that allow flexible positioning of surface coils. A series of coil pairs were evaluated: 40 X 10 cm and 14 cm for lumbar and thoracic spine imaging; 16 x 45 cm and 8 cm for orbit, internal auditory canal, temporal bone, temporomandibular joints and shoulders; 11 x 32 cm and 8 cm for wrist and elbows; or two 8 cm coils for each temporomandibular joint. We were able to employ, if necessary two different fields of view (FOV) with each combination. Coils were positioned at the onset of the exam and then used sequentially without changing patient positioning. Results show that there was no interference between the two surface coils. Since two different FOVs were used the signal to noise ratio (SNR) and spatial resolution matched the area of interest; patients did not require repositioning for each coil acquistion; the larger coil of the pair provided a screening study while the smaller coil provided a high resolution study of the area of interest; and patient through-put increased. In conclusion, the flexibility provided by the PIN diode decoupling technique allowed the use of overlapping surface coils which improved SNR and spatial resolution for the area of interest and allowed a screening study with an optimal SNR.

422

CLINICAL RELEVANCE OF AUTOMATIC SURFACE COIL INTENSITY CORRECTION

F. Zanella, G.J. Dijkstra, M. Fuderer
Department of Radiology, Univ. of Cologne; Philips Medical Systems, Best

Surface coils in MR imaging have the advantage of a high signal to-noise-ratio in the region near to the surface coil. Their disadvantage is a considerable sensitivity fall-off for tissues at larger distances. As a consequence, regions at moderate distances of the coil suffer from severe contrast losses. Clinically, this is particularly disadvantageous when the object of interest lies at this moderate depth (e.g. optic nerve, spinal canal). This interferes with accurate diagnosis. It is desirable that contrast is chiefly determined only by T1 and T2 differences and not affected by such a sensitivity fall-off. This can be achieved by applying homomorphic filtering (1). This post-processing method estimates the inhomogeneity from the surface coil image itself, hence no reference calculations or measurements are needed. This robust correction method is independent of variations in surface coil characteristics as coil position, dimension, shape and coil quality. The correction method is fully operational in a clinical environment using circular, rectangular and wrap-around surface coils. Corrected images of orbit and spine show considerable contrast improvement at depth. Contrast is achieved virtually identical to that obtained using a head or body coil. The method proves to give good results for all surface coils. Patient throughput is not affected, because the filtering demands no operator interaction and processing time is only about 2 seconds per image. Clinical results with surface coil images show that homomorphic filtering facilitates diagnosis.

References

1) M. Fuderer, A. van Est and G.J. Dijkstra. "Surface coil intensity correction using homomorphic filtering", Abstracts of SMRM, 6, p.266, 1987.

423

IMPROVED ORBITAL IMAGING BY MULTISLICE, SINGLE SCAN, CHEMICAL SHIFT IMAGING

RS Hinks, RM Quencer
Picker International and University of Miami Radiology Dept., 1115 NW 14 ST, Miami, FL

Since water and fat have resonant frequencies which differ by the difference in their chemical shift, the slices of fat and water which result from a slice-selective RF pulse are physically offset from each other by a fixed ratio equal to the chemical shift divided by the RF pulse bandwidth. If these slices are offset from each other by more than half a slice thickness, it is possible to selectively refocus only water (or fat, if desired) by reversing the direction of the slice selection gradient and hence reversing the relative positions of the fat and water slices.

This technique offers several advantages over other methods of chemical shift imaging. Since only the water (or fat) signal is refocussed to form a spin echo, there is no need for acquiring multiple sequences or for post-processing. Since all of the RF pulses are slice selective, this technique is easily implemented as a multislice sequence. As well, since only the single resonance forms an echo, there is no chemical shift artifact. This allows the use of long sampling times with the associated benefits of increased signal-to-noise. Finally, the technique is widely applicable and may be used with T1 or T2-weighted scans or with virtually any sequence which uses two slice-selective RF pulses.

We have implemented this multislice chemical shift imaging technique at 1.5 T (Picker) and have applied it to imaging of the orbit. Fat-suppressed images were obtained on normal volunteers and on several patients with orbital pathology. Orbital fat was effectively suppressed and the entire length of the optic nerve including that portion of the nerve in the orbital apex was clearly demonstrated. Intraorbital vessels and muscles are more clearly seen with this fat suppression technique than with standard T1 and T2 sequences. In patients with orbital abnormalities we were able to more easily detect and/or define intra and extraconal lesions including those involving the optic nerve. Our results indicate that this may be an improved method of orbital MR imaging.

424

STATIC AND DYNAMIC MRI OF BOTH TEMPOROMANDIBULAR JOINTS USING DUAL SURFACE COILS AT 1.5 TESLA

BD Pressman, FG Shellock, W Faulkner+, DG Mills+, J Prost*, N Campagnas*, F Wehrli*
Cedars-Sinai Medical Center, Los Angeles, CA; +Diagnostic Imaging Consultants, Chattanooga, TN; *General Electric Company, Milwaukee, WI.

Magnetic resonance imaging (MRI) using surface coils has proved to be an excellent method for diagnosing internal derangements and other disorders of the temporomandibular joint (TMJ). Two problems associated with utilizing this imaging technique are the time required to examine both TMJs (which is a necessity due to the high incidence of bilateral pathology) and the difficulty of identifying movement-related abnormalities. In order to resolve these problems, we used dual surface coils to simultaneously examine both TMJs with static and "dynamic" MRI techniques.

MRI was performed using a 1.5 T scanner (GE Signa System) with two standard 3" receive-only surface coils. Graphic prescription software (version 3.0) enabled us to obtain only the slices of interest in an obliqued-sagittal plane. High-resolution T1 weighted images were acquired with the patient's mouth in closed and opened positions. Dynamic MRI was accomplished using a device that opened the mouth at 2-4 mm increments, from a partially closed to a maximally opened position. Lower-resolution T1 weighted images were acquired at each degree of opening. These images were viewed using a "paging" format that provided a representation of passive motion. The entire examination took approximately 40 minutes.

Normal volunteers and symptomatic patients were studied. Static images displayed superb anatomical detail allowing for the delineation of the shape of the condyle, condylar fossa and articular eminence as well as the shape and position of the meniscus. Deformity and dislocation of the meniscus were optimally demonstrated. The dynamic display showed the point of reduction of a meniscal dislocation and could be correlated with the clinical "click". In hypermobile joints, the point of excessive motion was clearly defined. Simultaneous acquisition of images from both sides allowed direct comparison at different points of mouth opening and resulted in an increased understanding of the dynamics of the two sides. This was found to be useful in those cases in which there was bilateral symmetry in the closed and opened mouth positions, but asymmetry (and, therefore, a rotational abnormality) at the intermediate positions.

BRAIN

425

NON-SPECIFICITY OF THE ABSENCE OF THE POSTERIOR PITUITARY "BRIGHT SPOT" AT 1.5 TESLA

OB BOYKO, WJ MEISLER, JT CURNES, ER HEINZ, WT DJANG
Duke University Medical Center, Department of Radiology

A high intensity signal on Tl-weighted images from the posterior pituitary gland is a normal finding in the neonate (Wolpert et al.) as well as the adult (Kucharczyk et al.). Further work (Kucharczyk et al.) suggests that this "bright spot" represents intracellular lipid droplets in pituicytes.

We observed the absence of this signal at 1.5 T in a child with acute idiopathic diabetes insipidus (DI). The absence of this signal was also noted in three patients (2 pediatric aged) with past histories of whole brain radiation but no clinical history of DI at the time of imaging.

From our preliminary findings, the absence of the posterior pituitary "bright spot" can be associated with a disturbance of the hypothalamic neurohypophyseal secretory process (such as DI) but is not specific for it. The presence or absence of this signal and its clinical correlative significance will also be discussed.

426

PINEAL REGION TUMORS: COMPARISON OF CT AND MRI

H Henkes, W Schörner, R Felix
Radiological Department, Klinikum Rudolf Virchow, Freie Universität Berlin

The diagnostic value of CT and MRI in lesions of pinealis region was compared. The study included 14 patients, 8 females and 6 males. Diagnoses were subependymoma (2x), astrocytoma (2x), ependymoblastoma (1x), arachnoidal-cyst (1x) and pineocytoma (1x); 7 cases were without histological confirmation. Plane and contrast enhanced CT scans were compared with T_1- and T_2-weighted MR-images (SE 400/35, SE 1600/35,70), Siemens Magnetom 0.5 T.

We collated CT and MRI with respect to diagnostic sensitivity, topographic attachment and tissue characterization. Prospective evaluation of CT scans showed tumors of pinealis region in 8 cases. Retrospectively discrete signs of space-occupying processes could be detected in 4 more cases. In contrast MRI revealed lesions in 14 patients, histologically confirmed in 7 of them. In all cases, topographic assessment was superior with MRI than CT, especially attachment of tumor and surrounding structures like lamina quadrigemina in mediosagital planes. With respect to tissue-characterization CT showed tumor calcification and contrast enhancement whereas MRI provided superior information concerning the differentiation of liquid and solid tumor-compartments (especially multi-echo sequences). According to our experience MRI should be the first imaging technique because of its better sensitivity and topographic assessment. In case of pinealis-tumor detection by MRI, CT should be performed in addition to increase specificity.

427

MRI OF CALLOSAL DYSGENESIS

J. R. Jinkins, A. R. Whittemore, J. S. Tsruda, W. G. Bradley
Huntington Medical Research Institutes, Pasadena, CA

INTRODUCTION: The direct multiplanar imaging of MRI lends itself ideally to the evaluation of callosal dysgenesis (CD) together with the important associated hemispheric findings. Older classification systems including simply agenesis and partial agenesis were found to be inadequate for the precise description of the spectrum of developmental callosal anomalies. MRI illustrates patterns which allow a categorization of morphologic forms of CD based upon the embryogenesis of the telencephalon.
METHODS: The study consisted of a retrospective review of 12 subjects with CD. Patterns were sought in the morphology of the corpus callosum (CC) and the cerebral hemispheres which revealed a predictable relationship to embryonic development both in regard to the decussation of the CC as well as the formation of the cortex responsible for projection of the callosal fibers.
RESULTS: MRI enabled the differentiation of three distinct categories of dysgenesis. In agenesis the CC was completely absent. In hypogenesis the CC was variably curtailed in development due to primary factors or factors related to organic obstruction (i.e., lipomatous neural tube inclusion). In hypoplasia the CC was completely formed although focally or generally small in size and associated with prominent dysgenesis of the hemispheric cerebral cortex.
CONCLUSION: Normal embryogenesis of the telencephalon dictates the final structural morphology of the CC. This depends upon the uncomplicated closure of the neural tube, the formation and maintenance of the inductive bed of the massa comissuralis throughout decussation, and the proper migration and lamination of the elements of the cerebral cortex. Interference with, or interruption of any one or combination of these parameters may result in CD of varying expression. Thus, the basis of CD reflects its origins in essential failure of decussation induction, interrupted decussation, and/or partial failure of commissural fiber projection secondary to primary cortical dysgenesis.

428

MRI OF THE HYPOGLOSSAL CANAL

Shapiro M, Desser T, Sasaki C and Cross R
Yale University School of Medicine

The 12th cranial nerve exits from the ventrolateral sulcus of the medulla as two separate bundles which enter the hypoglossalcanal (between the jugular tubercle superiorly and the occipital condyle inferiorly). Within the hypoglossalcanal proper the two separate bundles fuse into one discrete nerve. The primary function of the 12th cranial nerve is motor supply to muscles of the tongue.

A retrospective study of 125 MRI examinations was performed in order to delineate the normal dimensions, anatomic variations of the optimal viewing plane of the hypoglossal canal. 60 studies in the axial projection (T1 and/or PD weighted, 3-5 mm sections), 60 studies in the coronal projection (T1 weighted, 3 mm), and 25 studies in the sagittal plane (T1 and/or PD, 3-5 mm) were obtained. From this retrospective analysis, data concerning the optimal plane, normal dimensions and anatomic variations (including compartmentalization of the canal into two sections by a bony spicule)were reviewed.

Demonstrations of pathology involving the canal will include an unusual 12th nerve neuroma (large cystic component) chordoma, meningioma, paraganglioma of the jugular foramen and metastatic disease.

MRI, because of superb signal disparity between fat and muscle, readily demonstrates the effects of denervation on muscles of the tongue with loss of colume of and increase in signal intensity (fatty degeneration).

429

MAGNETIC RESONANCE IMAGING OF COLLOID CYSTS

E Kanal, LD Lunsford, FL Thaete, AJ Martinez
Pittsburgh NMR Institute

Nine third ventricular colloid cysts were studied by single and multiple echo multiplanar spin echo 1.5T MRI. The cysts varied in diameter from 5-20 mm. The signal patterns from this tumor were found to be quite variable as compared to white matter, ranging from isointense to markedly hyperintense on short TR and TE techniques and hyperintense to near complete absence of signal on long TR and TE studies. Absence of signals on late echoes was attributed at least in part to a solid, waxy matrix found during surgical intervention of one particular tumor exhibiting this signal pattern. Paramagnetic ion deposition and secondary T2 shortening may be another possible etiologic factor. We have also found several cysts containing focal areas of both intense as well as near absence of signal on late echoes, reinforcing a prior report of a similar MR appearance. A literature review revealed a total of eight colloid cysts studied by MR reported to date. Although a "characteristic" appearance (increased signal intensity on all sequences) has been described, our results suggest that the appearance is quite variable, and depends at least in part on the underlying matrix and cyst composition.

430

MR IMAGING OF PROGRESSIVE MULTIFOCAL LEUKOENCEPHALOPATHY IN AIDS

A.S. Mark, M.D., S.W. Atlas, M.D., W. Olsen, M.D., D.R. Newton, M.D., D. Norman, M.D.
Department of Radiology, University of California, San Francisco

Progressive multifocal leukoencephalopathy (PML) is a rare fatal neurological disease of severely immunocompromised adults thought to be secondary to reactivation of a latent Papovavirus infection. CT and pathologic literature state that most lesions occur in the parieto-occipital white matter. More recently, PML has been reported to occur in patients with acquired immune deficiency syndrome (AIDS). The purpose of this paper was to review the magnetic resonance (MR) imaging findings in patients with AIDS and PML.

Eight patients with AIDS and pathologically proven PML were evaluated with spin echo MR using both short repetition time (TR)/short echo time (TE) and long TR/long TE sequences. Contrast enhanced CT's were available for comparison in six of the eight patients.

Focal lesions were clearly identified on all patients as high intensity on long TR scans. Three cases demonstrated high intensity hemorrhage on short TR/TE scans, and two cases demonstrated intralesional heterogeneity with central low intensity foci on long TR scans. Six of eight patients had multiple lesions. The predominant lesions involved the gray matter in seven of eight patients, and in two patients the gray matter was exclusively involved. Lesions were scattered throughout the brain, but most commonly were supratentorial.

In summary, contrary to the CT and pathologic literature concerning PML in non-AIDS patients, PML in patients with AIDS usually affects the gray matter and is commonly hemorrhagic. In this sub-group of PML patients, no prediliction for the parieto-occiptal region was identifiable. Furthermore, although previously thought to be essentially a non-hemorrhagic white matter lesion, it appears that PML cannot be confidently differentiated from other intracerebral lesions found in AIDS patients on the basis of MR characteristics.

431

MR OF CNS IN AIDS WITH PATHOLOGIC CORRELATION

DB Berthoty, MR Grafe, GA Press, JH Hesselink, CA Wiley
Divisions of Magnetic Resonance and Neuropathology, University of California, San Diego

To better define the sensitivity and specificity of MR in the diagnosis of CNS lesions in AIDS, we correlated MR scan (1.5-T) results with pathological examination in 10 post-mortem formalin-fixed specimens. All brain specimens were obtained from patients with AIDS encephalopathy. Using spin-echo pulse sequences, the entire brain above the cervical cord was imaged with 5 mm thick, interleaved, proton density, and T2 weighted sequences. The infratentorial region was additionally imaged perpendicular to the brain stem to match the thorough neuropathologic examination that followed.

Infarctions associated with cytomegalovirus (CMV) infection were seen as hyperintense foci within the basal ganglia, brainstem, and cerebellum on T2 weighted MR images. Most of the cytomegalic cells proved to be of glial or neuronal lineage; others were of endothelial origin. The latter finding suggests that some infarctions may be secondary to CMV infection of endothelial cells. Similar, but smaller lesions were discovered at pathology that were not detected by MR. These lesions consisted of microglial nodules, many of which were centered around cytomegalic cells. Our data indicates that MR can detect CMV lesions that have progressed to small infarctions. MR may be relatively insensitive in the detection of earlier manifestations of CMV infection, including microglial nodules.

432

THE ROLE OF ISOMORPHIC GLIOSIS IN INCREASING THE APPARRENT SIZE OF DEEP WHITE MATTER INFARCTS

William G. Bradley, MD, PhD; Vaughn G. Marshall, MD, Roy H. Rhodes, MD, PhD
Huntington Medical Research Institutes

Patchy periventricular abnormalities were described in the elderly in the very early days of clinical MRI (1). These were initially attributed to deep white matter infarcts, presumably on a hypertensive basis (which would make them a form of Binswanger's Disease or subcortical arteriosclerotic encephalopathy). Continuing experience has revealed the relatively ubiquitous nature of these lesions (i.e., 30% of patients over age 60) in nonhypertensive patients and suggested an etiology of decreasing perfusion.

To determine the exact nature of these lesions, 14 postmortem, formalin-fixed brains were scanned by MRI and perivenricular white matter lesions subjected to detailed histopathologic evaluation. Routine stains (hematoxylin and eosin, Luxol fast blue, Congo red) as well as special immuno stains (glial fibrillary acidic protein [GFAP], immunoglobulin G [IgG], and albumin) were used. In all cases, a central small region of cavitation and necrosis was noted, which is, by definition, a deep white matter infarct. Surrounding the central lesion were reactive astrocytes which were aligned along white matter tracts. This is known as "isomorphic gliosis". Reactive astrocytes were most concentrated near the central lesion but could be found several centimeters from the infarct, generally in the direction of the lateral ventricles. Reactive, swollen astrocytes contained increased water and protein due to inherent injury (GFAP) or to uptake of serum proteins from prior blood brain barrier breakdown (i.e., IgG and albumin). Increased hydration layer water environment increases the intensity of such lesions on T2-weighted images and makes the lesions appear much larger than the central small infarct which, in most cases, appears to be an asymptomatic result of decreasing cerebral perfusion.

Reference

1. Bradley WG, Waluch V, Brant-Zawadzki M, et al. "Patchy, perientricular white matter lesions in the elderly: a common observation during NMR imaging". Noninvasive Medical Imaging Vol 1, 1:35-41; 1984.

CONTRAST AGENTS

433

FREQUENCY DEPENDENCE OF RAT RELAXATION TIMES IN THE PRESENCE OF GADOLINIUM-DTPA

J. Ewen Rimmington, MA Foster and JR Mallard
Department of Biomedical Physics, University of Aberdeen, U.K.

The effect of Gd-DTPA on proton T1 and T2 of rat tissues has been studied as a function of frequency. Liver, spleen, muscle, kidney cortex and abdominal fat were obtained from rats two hours after 1ml inter-peritoneal injection of .5mM Gd-DTPA . T1 and T2 were compared with those from age and sex matched controls. A Bruker CXP-100 spectrometer was used at 29-31°C and 4.7 to 90MHz. All T2 data were multiexponential and were fitted to two components.

Doping with Gd-DTPA reduced both components of T2 in all tissues (liver illustrated in upper figure), being most effective in kidney cortex and least in fat and muscle. For each tissue component magnitudes were the same in both control and doped animals (+/-7%). In all cases except muscle there was a decrease in overall size of the slow component by as much half as the frequency increased from 4.7 to 90MHz. This suggests component association with NMR dispersion rather than physical compartments.

The lower figure shows 1/T1 at 4.7, 40 and 90MHz. Kidney cortex T1 became multiexponential with Gd-DTPA. Doping reduces T1 (increases 1/T1) in all tissues but has little effect on frequency dependence except for kidney cortex. In this the slow component decreased by a factor of 5 - 15 compared with the single control value as the frequency INCREASED, while the fast component decreased by a factor of 100.

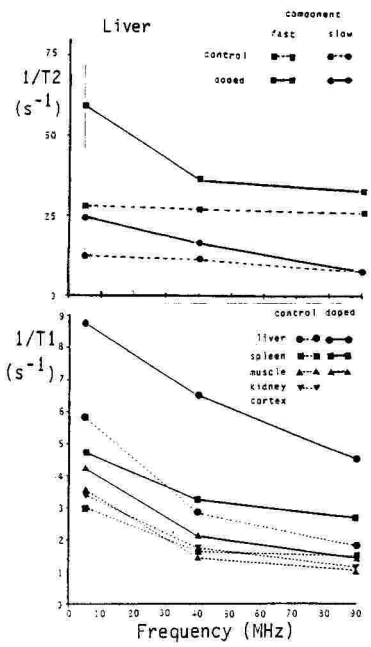

434

DYNAMIC CONTRAST ENHANCED MRI OF THE LIVER

CL Partain, JA Clanton, M McCurdy, G Holburn, and R Price
Department of Radiology, Vanderbilt University Medical Center

The pharmacokinetics of gadolinium DTPA was evaluated in an animal model for liver toxicity using 100 gram Fischer 344 rats. Forty rats were exposed to a chronic PO ingestion of axo dye, an hepatocarcinogenic agent, together with an equal number of control rats. Quantitative measures of liver toxicity included intensity changes before contrast in comparison with time intensity curves after the intraperitoneal or intravenous injection of gadolinium DTPA. Pathological correlation was provided by histological studies. Significant toxic effects in the liver in-vivo seem to correlate well with abnormal increased intensity on T2 weighted MRI images before contrast enhancement and with changes to the character of the time intensity curves using dynamic contrast enhanced MRI. Injection dose levels of gadolinium DTPA were 0.1 mmol/kg.--images were obtained every minute for 30 minutes after injection. Abnormal changes in time intensity curves included increased peak level and decreased rate of excretion from the liver. Future studies will involve improved MRI pharmaceuticals designed to be concentrated by the hepatocyte and/or the reticuloendothelial system of the liver. It is concluded that time intensity curves in multiple organs including the liver may further enhance the sensitivity and specificity of MRI diagnostic applications in multiple disease processes.

435

GADOLINIUM ENHANCED MRI IN PEDIATRIC PATIENTS WITH MASSES IN THE BRAIN AND SPINAL CORD

CL Partain, TA Powers, MP Freeman, RH Robertson, JA Clanton, JA Patton, and HT Whalen
Department of Radiology, Vanderbilt University Medical Center

Twenty pediatric patients with a variety of lesions of the brain and spinal cord were studied with and without gadolinium DTPA enhancement. Correlative interpretation was made with appropriate images in CT and angiography. Increased levels of conspicuity were visualized in every mass lesion in comparison with unenhanced MR and with CT. After informed and written consent was obtained from the parents and in appropriate cases from the children, T1 and T2 weighted precontrast MRI scans were performed using spin echo 500/30 and spin echo 2000/90-45 pulse sequences. After injection of 0.1 mmol per kg of gadolinium DTPA intravenously post contrast MRI scans included spin echo 500/30 less than 10 minutes after injection, then echo 2000/90-45 less than 30 minutes after injection. No significant adverse reactions were observed in these 20 patients. In order to monitor the possibility of adverse side effects, blood chemistry and hemotologic indices were measured before contrast injection and at 2-4 hours and 24 hours after injection. Transient evaluations in serum iron were seen in virtually every case, felt to be insignificant clinically, and possibly related to the gadolinium injection. Mild hypotension described in other centers was not experienced in our 20 patients. This study is part of a multi-center trial involving a total of 6 medical centers and childrens' hospitals in the United States. It is our judgment that gadolinium enhancement plays a significant role in diagnosing very small lesions in the brain and central nervous system establishing the presence and extent of abnormal CNS masses. The exact role of external contrast enhancement in comparison with the inherent contrast available from fast pulse sequences is under evaluation.

436

GADOLINIUM-DTPA IN THE EVALUATION OF INTRAMEDULLARY DISEASE OF THE SPINE

Gordon Sze, M.D.

George Krol, M.D.

Memorial Sloan-Kettering Cancer Center

and

Cornell University Medical College

Twelve patients with proved intramedullary disease were examined before and after the administration of gadolinium-DTPA. Six patients had primary tumors of the cord; two had thrombosed vascular malformations of the cord; two had multiple sclerosis with involvement of the cord; one had metastasis to the cord; and one had a benign syrinx. 3 mm. sagittal and 5 mm. axial scans were performed. Long TR scans employed cardiac gating.

Six of the twelve patients showed regions of enhancement. These six all consisted of patients with tumors. Six of the twelve patients showed no enhancement. These cases involved patients with thrombosed vascular malformations, benign syrinx, multiple sclerosis, and one case of presumed astrocytoma. In our series, gadolinium-DTPA did not help in detection of lesions. However, the delineation and characterization of pathology was improved. Enhancement was very helpful in: 1) Surgical planning and biopsy. 2) Grading of tumor; 3) Differentiating benign from neoplastic syrinx. Even lack of enhancement provided additional information, for example in suggesting the non-neoplastic origins of intra-cord hematomas. Because of these benefits, gadolinium-DTPA will probably be used routinely in the MR evaluation of intramedullary lesions.

437

PLAIN AND GADOLINIUM-DTPA ENHANCED MULTISLICE GRADIENT-ECHO IMAGES FOR EVALUATION OF INTRACRANIAL TUMORS

W Kornmesser, W Schoerner, B Sander, M Laniado, R Felix
Dep. of Radiology, Klinikum Charlottenburg, Freie Universität Berlin

In 34 patients with a variety of intracranial tumors examined by MRI (Siemens Magnetom 0.5T) plain and Gd-DTPA enhanced gradient-echo sequences were employed in addition to conventional spin-echo (SE) sequences. The diagnoses included meningeomas, gliomas, pituitary adenomas, parasitosis and miscellaneous tumors. The gradient-echo technique was employed as a multislice sequence (15 contiguous slices) by selective excitation of one slice every 21 ms. The effective TR for each slice was 315 ms (TE 14 ms). With single signal acquisition imaging time was 83 sec (matrix 256x256). Gradient-echo images were compared with SE images (TR 400 ms, TE 30 ms, 2 acquisitions, 3,4 min imaging time/4 slices). With both techniques high quality diagnostic images were obtained before and after Gd-DTPA injection. Delineation of enhancing tumor tissue was identical. Grey/white matter contrast was higher on gradient-echo images, whereas signal-to-noise ratio was slightly lower compared to SE-images. Both techniques provided comparable anatomic resolution. Artifacts from metal incorpration (dental filling, cerebrofluid valves, metal splinters after surgery) were larger with the gradient-echo technique. However, diagnostic information was not reduced in any of our investigations.

In enhancing brain tumors multislice gradient-echo techniques offer a promising approach to increase patient throughput.

438

GD-DTPA MRI: Differentiation Of Scar And Recurrent Disk Herniation

T Knepper,M Heller,HH Jend,HJ Langkowski,R Spielmann,FU Oesterreich,R Maas
Department of Radiology, University-Hospital of Hamburg

Up to 30% of patients who have had lumbar surgery for herniated disk have unsatisfactory results. High resolution CT using iv contrast agents answers in only 65% whether or not it is caused by scars, recurrent or persistent disk herniation. MRI seems to offer a solution to this problem.

The MR-examinations were performed with a 1.5 T Gyroscan S 15 in sagittal and transversal planes in multiple slice technique. We used intravenous Gadolinium-DPTA for differentiating the vascularized scar from the avascular disk material. First,we performed T-1 and T-2 weighted images in the transversal plane, then we injected Gadolinium-DTPA and performed T-1 weighted planes again.

Up to now 30 patients were examined between 2 month and 5 years after surgery. In 20 cases the postoperative problems were caused mainly by scars,only in 2 cases by recurrent or persistant disk herniation and in 8 cases by a combination of scar and disk herniation.

Our results indicate that MRI using Gadolinium DTPA is helpful for differentiating scar and disk herniation.

439

HEBATOBILIARY CONTRAST AGENT FOR HEPATIC MR: TISSUE SPECIFIC BIODISTRIBUTION OF Mn-S095

Y-M Tsang, M Chen, G Elizondo, D Stark, S Rocklage*, S Quay*, S Saini, J Ferrucci
Department of Radiology, Massachusetts General Hospital, and Salutar, Inc.

The time-response and dose-response of S095 in normal rats was studied in vitro by measuring T1 and T2 changes of tissue samples of liver, kidney, blood, and muscle using a Bruker 20 MHz spectrometer. Parallel in vivo MR image data were obtained by measuring signal-to-noise ratio (SNR) changes of the liver imaged with a 0.6T clinical MR imaging system and a head coil using a SE 250/21 pulse sequence. Tumor-liver contrast-to-noise ratios (CNR) were studied using rats with mammary adenocarcinoma implanted in the liver. Thirty minutes after intravenous injection of 0.05 mmol/kg S095, liver T1 and T2 were reduced by 75% and 38%, respectively. On MR images, 52%, 65%, and 70% increases in SNR were noted at 30 minutes after I.V. injection of 0.025, 0.05, and 0.1 mmol/kg S095. Liver enhancement peaked at 30 minutes and persisted until 90 minutes after S095 administration. Selective biodistribution of S095 to liver and rapid clearance from the blood pool and tumor resulted in increased tumor-liver CNR and increased tumor conspicuity.

440

GASTROINTESTINAL CONTRAST ENHANCEMENT IN MRI: FIRST CLINICAL EXPERIENCE WITH GADOLINIUM-DTPA

W Kornmesser, C Claussen, S Kaminsky, M Laniado, B Hamm, R Felix
Dep. of Radiology, Klinikum Charlottenburg, Freie Universität Berlin

20 healthy male volunteers and 31 patients with abdominal pathologies were investigated by MRI prior to and after oral administration of gadolinium-DTPA (Gd-DTPA, Schering AG). 10 ml/kg of a .001 molar Gd-DTPA solution containing mannitol were administered after precontrast images had been obtained. Spin-echo sequences (TR 200-2000 ms, TE 16-70 ms) and a multislice gradient-echo sequence (TR 315 ms, TE 14 ms, 15 slices) were employed. In 15 patients glucagon was IV injected to reduce peristalsis after administration of Gd-DTPA.

Contrast enhancement of the GI-tract was observed in all studies with all sequences applied. In keeping with the results of experimental studies in dogs highest contrast of enhanced GI-tract versus adjacent tissues including abdominal fat was achieved on T2-weighted images. In 16 of 20 healthy volunteers delineation of the pancreas was significantly improved on postcontrast images. In 28 of 31 patients differentiation of GI-tract from both parenchymal organs and pathology was better compared to unenhanced images. Apart from minor signs of GI-tract discomfort no side effects were observed. A variety of serum parameters measured pre- and postcontrast showed no changes.

Our preluminary results suggest that oral administration of Gd-DTPA is a promising approach toward improvement in abdominal MRI.

441

GADOLINIUM-DTPA LIPOSOMES AS POTENTIAL MRI CONTRAST AGENTS

EC UNGER (1), PR CULLIS (2), CP TILCOCK (2)
Fox Chase Cancer Center (1), University of British Columbia (2)

We synthesized unilamellar vesicles with diameters between 0.1 to 0.4 microns using the freeze thaw extrusion method to encapsulate Gadolinium-DTPA (Gd-DTPA). ^{14}C inulin and ^{153}Gd-DTPA were used as tracer to determine encapsulation ratios. Dialysis or chromotography was used to remove unbound Gd-DTPA. Encapsulation efficiency was as high a 37% for the 0.4 micron vesicles. Vesicles purified by dialysis had a concentration of approximately 0.15 molar Gadolinium-DTPA. In vitro solutions of Gd-DTPA liposomes were scanned at 1.5 Tesla in phantoms prepared in normal saline, whole human blood, and agar gelatin. Gadolinium-DTPA liposomes caused a concentration dependent increase in signal intensity on Tl- weighted pulse sequences with maximal signal intensity observed at an approximately 5 millimolar concentration Gd-DTPA. Free Gd-DTPA, prepared in similar phantoms, caused maximal signal intensity at an approximately five fold lower concentration of 1 millimolar Gd-DTPA. In vitro stability of Gd-DTPA liposomes was tested by dialysis and after 48 hours essentially 100% of Gd-DTPA was retained within the vesicles.

Scans of rats, pre and post-contrast, after intravenous injections of Gd-DTPA liposomes showed prolonged intra-vascular enhancement and increased signal intensity in the liver. Comparison scans of rats after intravenous injections of Gd-DTPA showed increased signal intensity in the kidneys and urinary bladder, but no sustained intra-vascular contrast enhancement, nor appreciable change in signal intensity of the liver. Rats tolerated intravenous injections of liposomes well without signs of acute or delayed toxicity.

Liposomes prepared by the freeze thaw extrusion method are stable in vitro and appear to be well tolerated in vivo. Paramagnetic liposomes have potential as a contrast agent for evaluating the vascular system, organ or tumor perfusion and also to potentially improve detection of malignancy in the liver and spleen.

CLINICAL SPECTROSCOPY

442

CLINICAL APPLICATIONS OF PROTON CHEMICAL SHIFT IMAGING AT 1.5 T.

R.L. Kamman Ph.D., E.L. Mooyaart, MD, Ph.D.
Dept. of Magnetic Resonance, University Hospital Groningen, The Netherlands

Several methods have been developed to acquire images depicting separately the water and fat distribution of a single slice MR image. One of these methods was developed by Dixon and is based on interleaved scanning of water plus fat and water minus fat image profiles. Additional post-processing including phase correction and image addition and substraction results in the desired fat and water images.

To evaluate the use of this technique in clinical applications, fat/water images were obtained in 40 patients in whom pathological conditions containing fatty tissue were suspected.

Measurements were performed on a 1.5 T. Philips Gyroscan system using a single slice single echo (TE=30 msec) technique. A phase correction algorithm was applied based on a piecewise-linear phase error estimation.

Initially studies were performed on water and fat containing phantoms followed by routinely fat/water image acquisition on patients. The chemical shift images were compared with routinely made spin echo images and clinical and histological data.

Chemical shift imaging provided additional information in tissue characterization of pathological tissue, moreover this technique was very useful to enhance contrast between pathological and fatty tissue.

443

ANALYSIS OF HUMAN FAT BY H-1MR SPECTROSCOPY IN VIVO

M Bàràny, E Abraham, PN Venkatasubramanian, E Mok, DG Spigos
Col. of Medicine, Univ. of Illinois and Cook County Hospital Chicago, IL 60612

Various human tissues contain neutral fat that may be quantified and analyzed for its composition by H-1MR spectroscopy. Our investigation focused on the tissues of normal and diseased leg.

H-1 spectra were recorded on a GE Signa MR scanner at 63.86 MHz, with the H-1 dual coil, 8-in. transmitter and 3-in. receiver. Coronal slices, 10 mm, were selected from the gastrocnemius or quadriceps muscles, the subcutaneous fat, or the tibia of the leg.

The fat content of the muscle was quantified relative to that of the water by integrating the area of the fat and water resonances in spectra recorded with the SPECFID pulse program of GE. Normal human muscle contained 5-7% fat relative to 100% water. In primary muscular diseases the fat content was increased up to 50%. In secondary muscular diseases the fat content remained under 25%. However, in arthrogryposis multiplex congenita, a disease of the joints, the fat content of the muscle was elevated to 150% and above.

For analysis of the composition of fat, the various H-1 resonances of the fatty acyl chains were amplified by suppressing the tissue water with the SPECSUP2 pulse program of GE. Chemical shifts were referenced to the center of the field, set to 4.77 ppm. In the normal muscle spectra, the resonance from the $-(CH_2)_n-$ protons, 1.2-1.3 ppm, was the most pronounced. Other resonances were: $-COCH_2C\underline{H}_2-$, 1.6-1.7 ppm, and $-COC\underline{H}_2$, 2.3-2.4 ppm. In the diseased muscle spectra additional resonances were: $=CHC\underline{H}_2-$, 1.9-2.1 ppm, $=CHC\underline{H}_2CH=$, 2.7-2.8 ppm, and $-CH=C\underline{H}$, 5.3-6.0 ppm. In arthrogryposis multiplex congenita the H-1 spectra of gastrocnemius muscle, tibia bone marrow, and subcutaneous fat were compared. The major resonances were at 1.47 and 1.67 ppm in muscle, at 1.73 and 1.91 ppm in bone marrow, and at 1.29 ppm in subcutaneous fat.

We estimated the distribution of saturated and unsaturated fat in the tissues by integration of the area of the fatty acyl chain resonances. Thus, fat analysis by H-1MR may help in elucidating biochemical pathways in disease processes. (Supported by MDA and CTR).

444

EXAMINATION OF HUMAN BRAIN PATHOLOGIES BY WATER-SUPPRESSED IMAGE-LOCALIZED 1H MR SPECTROSCOPY

D. Balériaux *, J. W. Berkelbach v.d. Sprenkel $, J. A. den Hollander &, P. R. Luyten &, P. C. van Rijen $, C. Segebarth *, and C. A. F. Tulleken $
* Hôpital Erasme, Brussels, Belgium; $ Department of Neurosurgery, University Hospital Utrecht, The Netherlands; & Philips Medical Systems, Best, The Netherlands.

Recent progress in spectroscopic localization techniques has made it possible to observe metabolites in the human brain by means of water suppressed 1H MR spectroscopy [1]. Here we wish to report on 1H MR spectroscopic examination of patients with intracranial tumors, or with cerebral infarction.

Water suppressed localized 1H MR spectra of the human brain were obtained on a 1.5 tesla Philips whole body imager, using the regular head coil. 1H MR images were used to select the area of interest for spectroscopy. Localized 1H MR spectra were obtained by means of SPARS, or by stimulated echo's; water suppression was done using 1331 selective excitation, or by DANTE presaturation. Measurements were done for different echo times (TE). Spectral editing was performed in order to differentiate lactic acid from lipid resonances. Spectroscopic imaging was applied to obtain in one single measurement spectra from a large number of volumes.

Water suppressed 1H MR spectra from the normal human brain, show resonances from N-acetyl aspartate (NAA), creatine and phosphocreatine (Cr), and phosphocholine (Cho), and a small resonance from lactate (~ 0.5 - 1.0 mM). Six patients with low grade gliomas were examined. Each of these tumors showed broad resonances in the spectral range of 0.5 - 1.5 ppm, absent in the normal brain. These resonances, presumably from lipids, have a long T2 relaxation time (up to 350 ms). There is a considerable variation between different tumors. Spectroscopic imaging revealed spectroscopic heterogeneity through the tumors.

1H MR spectra were also obtained from patients with cerebral infarction. In a patient with subtotal occlusion of the right carotid artery an increased lactate level was observed in a region next to the infarct. This region showed only minor abnormalities in the MR image. After bypass surgery the lactate level decreased. The infarcted region showed lipid resonances, and decreased NAA and Cho/Cr signals.

[1] Luyten P.R., and den Hollander J.A., Radiology, 161, 795, 1986

445

Alteration of Phosphate Levels in Neonates During Seizure
B. Chen, RSK Young, J.C. Gore

Alterations of brain energy state of a developing brain in prolonged seizures were investigated using in vivo and in vitro 31P-NMR. Such data are important in understanding the metabolic ramifications of seizure in neonates, and to the medical management of epilepsy. Neonatal dogs were anesthetized with halothane (0.5-3.0%) and the animal was mechanically ventilated with 30% oxygen mixed with 70% nitrous oxide for analgesia and then paralyzed with pancuronium bromide. Flurothyl-induced seizures were compared with controls and the results showed a continuous decrease of phosphocreatine during 60 minutes of concomitant seizure. A marked increase of inorganic phosphate and a consistent decrease of PCr/Pi ratio were observed. However, brain cellular ATP pools were maintained relatively constant. Administration of diazepam (0.2 mg/kg I.V.) during flurothyl seizure inactivates paroxysmal activity. Inorganic phosphate and phosphocreatine respectively recovered to control levels. Our results indicate that brain injury produced by seizure may not be associated with the metabolic high energy state of the brain.

446

H-1MR SPECTROSCOPY OF HUMAN HEART IN VIVO
M Bàràny, E Mok, PN Venkatasubramanian, BG Langer
Col. of Medicine, Univ. of Illinois and Cook County Hospital, Chicago, IL 60612

High resolution H-1MR spectra were recorded on the heart of six volunteers using the GE Signa MR scanner at 63.86 MHz, with the body coil as transmitter and the 5-in. coil as receiver. High quality cardiac images were acquired using the same coils and with the ECG triggering on. For spectroscopy, coronal slices, 10 mm thick, were selected about 30 mm beneath the internal chest wall.

The main problem of water-suppressed H-1 heart spectroscopy is the adjustment of field homogeneity because of the motion of cardiac muscle. Our volunteers were in the prone position and the cardiac gating was turned on for shimming. We desensitized the remote shim control knobs to achieve an optimum adjustment of the water peak. Nevertheless, 5-10 min. were required to obtain a line-width of 0.25-0.40 ppm.

Water-suppressed slice-selective H-1 spectra were recorded with the SPECSUP2 pulse program of GE. With the cardiac gating on, this program utilizes a large spectral-width which reduces the resolution of the resonances. We turned off the cardiac gating and used the following parameters: 650 Hz spectral-width, 3 sec TR, 25 msec TE/2, and 3.5 msec interpulse interval. Approximately 200 transients were accumulated to average out motional artifacts. Chemical shifts were referenced to the center of the field, set to the water frequency, 4.77 ppm.

The following H-1 resonances were visible in the heart spectra (tentative assignments are made in terms of ppm): $-CH_3$ of acetate (1.86), β-CH_2 of GLU and GLN (2.07), γ-CH_2 of GLN (2.43), $\equiv\overset{+}{N}CH_2$ of β-alanine in carnosine (2.66), PCr and Cr (3.02), S-CH_2 of taurine (3.22), $\equiv\overset{+}{N}$-CH_2 of taurine (3.42), CH=CH of fumarate (6.51), C4-H of histidine in carnosine (7.01), and ring protons of amino acids (7.25-7.58). In addition resonances from both saturated and unsaturated fatty acids were observed in the aliphatic and aromatic part of the spectra. These data show the potential of H-1MR to analyze metabolites in live human heart. (Supported by MDA and CTR).

447

EFFECTS OF HYDRALAZINE ON TUMOR METABOLISM USING ^{31}P MRS

P Okunieff, F Kallinowski, E Rummeny, P Vaupel, HD Suit
Massachusetts General Hospital, Dept. Radiation Medicine, Boston, MA.

The effect of the vasodilator hydralazine (HYD) on in-vivo tumor metabolism was studied by ^{31}P MRS. Tumors were isotransplants of a murine fibrosarcoma (FSaII) implanted in the hind foot dorsum. Tumors were 30-200mm^3 in volume. HYD was delivered via intraperitoneal catheter. Drug doses were 0.25, 0.5, 1, 2, and 10 mg/kg. MRS was performed at 145.6 MHz for ^{31}P using a 1.4cm diameter surface coil. Pulse parameters included a 60° tip angle, a 2 sec relaxation delay, and 128 averaged FID per spectrum. The phosphocreatine to inorganic phosphate peak height ratio (PCr/Pi) measured by MRS was used to evaluate tumor metabolism. In separate experiments, mean systemic blood pressure was measured via intracarotid catheter using the same HYD doses.

Results: HYD doses of 0.25 mg/kg had no significant effect on blood pressure, but may have resulted in an increased cardiac output due to decreased afterload. At 0.25 mg/kg there was an increase in PCr/Pi in 5 of 6 animals ($p<.05$). Doses of 2 and 10 mg/kg HYD caused hypotension (60-70mmHg mean arterial). This was associated with a three fold decrement in PCr/Pi (PCr/Pi(control) = 1.2, PCr/Pi(10mg/kg HYD) = .4, $p<.01$).

Conclusion: The metabolic response of individual tumors to vasoactive drugs can be examined by MRS. Information obtained by MRS indirectly reflects tumor oxygenation and perfusion, and may therefore be useful for optimization of therapy.

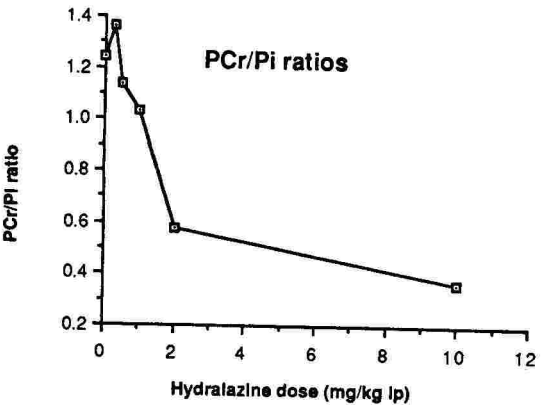

448

In-vivo ^{19}F magnetic resonance study of 5-FU kinetics in human liver

Semmler,W.,P. Bachert-Baumann,G. Gademann,P. Schlag[x],F. Gückel, W. Lorenz, G. v. Kaick, German Cancer Research Center, Institute of Nuclear Medicine, Im Neuenheimer Feld, D-6900 Heidelberg 1,[x]University of Heidelberg, Department of Surgery, W.-Germany

5-Fluorouracil (5-FU) is used as a cytostatic drug in the treatment of various tumors. 5-FU is either metabolized to 5-fluorouridine-5'-monophosphate (FUMP) and its desoxy analog or via the detoxifying pathway to α-fluoro-β-alanine (FBAL) in the liver. For unknown reasons the therapy is successful in less than 30% of the patients. In order to improve FU therapy, information concerning in-vivo metabolism of 5-FU in normal tissue and tumor is required. First ^{19}F-MR studies in humans have been performed by Wolf et al. in a whole-body MR scanner. ^{19}F-spectroscopy was performed in our 1.5-Tesla whole-body MR system (MAGNETOM) with a 12 cm surface coil applied to the patient's liver region. A selective catheter was positioned in the arteria hepatica and 1.0 g/m² 5-FU was injected. The spectral intensities of 5-FU and FBAL were evaluated by least-square fits. Different half-life times $t_{1/2}$ for 5-FU (decay) and FBAL (increase) could be observed depending whether the patient has been pretreated with 5-FU ($t_{1/2}$ approx. 20 min) or not ($t_{1/2}$ approx. 75 min). In conclusion, we have shown that the 5-FU kinetics in patients can be monitored in a whole-body MR system. This may help to optimize chemotherapy with 5-FU.

449

Correlation of X-ray diffraction and proton NMR measurements of myelin associated fluid spaces.

D Zamaroczy, FA Jolesz, DA Kirschner*
Department of Radiology, Harvard Medical School and Brigham and Women's Hospital
Department of Neuropathology, Harvard Medical School and Department of Neuroscience
Children's Hospital Medical Center*

The periodic nature of myelin and the presence of water spaces between the cytoplasmic and extracellular surfaces of the apposed membranes are revealed by X-ray diffraction. We manipulated the size of intramyelinic water compartments by inducing nerve swelling. We then correlated the changes of myelin periodicity with the T2 and percent fractional sizes (A) of three compartments revealed by multiexponential decomposition of T2 decay. Rabbit sciatic nerves were soaked for 24 hours in saline solutions with identical ionic strength but differing pH. The results are presented in the Table:

	pH 3	pH 6	pH 9
Period in Angstroms	169	229	248
T2 (msec)	164 ±18	130 ± 8	89 ±30
T2 (1)	42 ± 4	40 ± 2	34 ± 3
T2 (2)	161 ±12	135 ± 6	122 ± 8
T2 (3)	516 ±76	489 ±52	475 ±50
A1 (%)	20	29	36
A2 (%)	62	49	49
A3 (%)	18	22	15

The results show increasing periodicity of the myelin with higher pH values and corresponding reduction of the overall T2 and the T2s of the first two components. The changes in the size of the first compartment are well correlated with the X-ray diffraction data. The larger size of this compartment and the faster relaxation rate of the second one at the basic pH most likely related to the water penetration between myelin membranes.

AUTHOR INDEX